Impact of diagenesis on seismic properties of siliciclastic rocks

Anders Dræge

Thesis submitted to the University of Bergen towards the fulfilment of the requirements for the Ph.D. degree.

Department of Earth Science and
Centre for Integrated Petroleum Research
University of Bergen
February 28, 2006.

Contents

A scientist is supposed to have a complete and thorough knowledge, at first hand, of some subjects and, therefore, is usually expected not to write on any topic of which he is not a master. This is regarded as a matter of noblesse oblige. (...) I can see no other escape from this dilemma (less our true aim be lost for ever) than that some of us should venture to embark on a synthesis of facts and theories, albeit with second-hand and incomplete knowledge of some of them - and at the risk of making fools of ourselves. So much for my apology.

Erwing Schrödinger 1944, What is life? Cambridge University Press

Preface

This Ph.D. thesis counts four papers written in the period from February 2003 to February 2006. The papers will be referred to numerically as 1-4. This introduction will give a short description of the themes and principles studied in the papers. I will also try to illuminate the thread between the different papers.

The work with all papers is done at the Centre for Integrated Petroleum Research (CIPR) at the University of Bergen. Contemporary I was affiliated to the Department of Earth Science (DES) at University of Bergen. The project was financed by Det norske vitenskaps akademi (VISTA). The project leader was Professor Tor Arne Johansen at CIPR and DES with co-supervisor Dr. Ivar Brevik from Statoil. Division head in Statoil was Dr. Per Arne Bjørkum. The title of this project was defined by Professor Tor Arne Johansen and Dr. Ivar Brevik.

Paper 1 was presented at the 74th SEG conference in Denver 2004, and is published in Petroleum Geoscience, volume 12, pp. 49-57, 2006. Paper 2 was presented at the 67th EAGE conference in Madrid, 2005 and is accepted for publication in Petroleum Geoscience, while paper 3 was presented at the 75th SEG conference in Houston, and is submitted to Petroleum Geoscience. Another presentation held at the 75th SEG conference is included in abstract F. Paper 4 is in preparation for submition to Geophysical Prospecting.

I wish to thank all my co-workers for pleasant and fruitful technical discussions, as well as social non-technical discussions. Erling has saved me a lot of computational problems, by always helping me out on short notice. The teabreaks with Remy and varying "guest tea-drinkers" will be greatly missed. So will the football trainings organized by the always enthusiastic Edin. I will further express my gratitude to the team of petroleum geophycisists here at CIPR; Bent Ole, Morten, Tor Arne and Remy, for sharing their knowledge with me, and giving me ideas and suggestions. I will give a special thank to my thesis

1 Introduction

The objective for this Ph.D. thesis is to increase understanding of the interplay between geological processes and seismic rock properties. The approach has been to first study geological processes, and then develop rock physics models that were meant to account for the geology. Therefore a detailed insight in both rock physics and diagenetic mineralogical processes has been necessary.

Sedimentary rocks are commonly built up by micro-size grains, with geometries and arrangements that influence the macroscopic rock properties. Rock physics modelling aims to relate large-scale rock properties like seismic velocities to small-scale rock properties like pore-shape, texture and distribution. This connection is necessary, because the scale-size of the microscopic rock properties is considerably smaller than seismic wavelengths recorded on the surface. Hence, seismic waves only register the large-scale or effective properties of a composite rock. The effective elastic properties of a rock are dependent on the elasticity of the constituents, the distributions and shapes of the constituents, the geometrical properties of the pores and the relative proportions of each constituent. If the heterogeneous microstructure has certain preferred orientations of non-spherical constituents, the average response on the macroscopic level will be anisotropic, which means that large scale properties are dependent on the direction of wave propagation. A theoretical rock physical model should honour all these effects, to give a realistic description of the rock.

Geological mineral reactions are commonly considered exponential related to temperature and linearly related to time (Bjørkum and Nadeau, 1998). Mineralogical reactions are constrained to certain temperature intervals. These intervals are dependent on time and the mineral stability, which in turn is dependent on rock mineralogy, fluid composition and permeability (accessibility of reactants). Many approximations are suggested for temperature intervals in which various mineral reactions occur, for instance by Bjørlykke and

Brendsdal (1986), Walderhaug (1996) and Bjørkum and Nadeau (1998). These temperature intervals are mainly based on observations, and can be used as rules of thumb when performing simple mineralogical modelling versus increased temperature.

Chemical reactions become important controls on permeability and porosity at temperatures greater than 60 °C in sedimentary rocks (Bjørkum and Nadeau, 1998). Above this temperature, and independent of depth and sedimentation rate, fluid pressure and migration are driven by thermally controlled mineral reactions. Three diagenetic processes are important for porosity evolution versus increased temperature and depth (Bjørkum et al., 1998): Mechanical compaction (reorientation, repacking and deformation), chemical compaction (reduces bulk volume by dissolution of loadbearing minerals) and precipitation of cement. Some of these processes can further depend on mineralogy/constituent properties, texture, pressure, pore fluid composition, permeability, temperature and burial history.

Paper 1 of this Ph.D. thesis is concerned about estimating the effective anisotropic rock properties in shales ($\geq$ 50 % clay minerals in framework) during diagenesis. Theories for the transition from mechanical to chemical compaction are presented together with a rock physics model for cemented shales. By combining this with a rock physics model for mechanical compacted shales, we presented a model for predicting anisotropic shale properties from deposition to deep burial and cementation.

Paper 2 focused on the geology of sandstones ($\geq$ 50 % quartz in framework) during diagenesis, and how this is related to large-scale seismic rock properties. A composite rock physics model was developed to estimate effective rock properties in rocks with varying distributions, and also simultaneous occurrences of various distributions. The strategy presented included classification of all minerals involved due to four distribution classes. This classification is based on mineral observations from a number of authors like Jones et al. (2000), Khidir and Catuneanu (2002), Storvoll et al. (2002), Anjos et al. (2003), Rossi

et al. (2003) and Ketzer et al. (2003). Mineralogical reactions can alter the distribution pattern, constituent properties, volume relations, porosity and permeability in the rock. It is shown that many of these processes have pronounced influence on seismic velocities, even if porosity is held constant. An analysis of the reflection coefficients in sands exposed to different diagenetic processes, showed that diagenetic changes can constitute significant reflectors in the seismic.

The relationship between velocity-depth (temperature) gradients and geological processes was the theme of paper 3. Nine different scenarios were studied, all related to fluvial and shelfal depositional environments. Models and strategies applied were adopted from paper 1 and 2, to present a method applicable on all siliciclastic rocks during diagenesis. We analyzed how mineral reactions (with entailed distribution changes), porosity, porebridging and seismic isolation of pores influenced the velocities and velocity-depth gradients for scenarios with different mineralogical compositions and reactions. A "seismic diagenetic fingerprint" for each succession of mineralogical reactions were derived. The fingerprints were based upon the first derivative of functions that were fitted to the velocity-depth curves, and could be directly related to geological processes in the rocks.

In paper 4 the rock physics models from paper 2 were inverted, to derive porosity (P), lithology (L) and pore fluid (F) in a case with known elastic properties and density in an isotropic rock. In addition to the PLF parameters (porosity, lithology and fluid), the method aims to reveal information about the microstructure in the rock. The principle is that the assumptions about microstructure implied by the rock physics model that best describe a data set, are indicative of the microstructure of the rock. The inversion method was applied on a well-log, and predictions of PLF parameters and mineral distributions were presented. Further, an example of how data uncertainties can influence the precision of the inversion was shown.

During this Ph.D. degree I have had to focus on both rock physics and geology. My geological background was pretty poor before the start of this study, so I have been specially engaged with learning geological processes during diagenesis. The mineralogical modelling performed in paper 2 and partly 3 are simplified compared to mineral reactions in real rocks. In addition, all the rock physics models applied rely on assumptions and simplifications of the real world. But the strategies and principles presented are independent on both rock physics models and accuracy of the mineralogical modelling. One could easily exchange or modify the rock physics model with an alternative one, and follow the same modelling strategy. Similarly, a skilled and experienced geologist could probably perform a more detailed and consistent mineralogical modelling, to increase the accuracy of the mineralogical input to the rock physics modelling.

2 Diagenetic processes in shales

Clay minerals are commonly elongated, e.g. Hornby et al. (1994) and Worden and Morad (2003). At deposition, the minerals are more or less randomly oriented, leading to very high porosities (water content) from 70 - 90 % (Blatt et al., 1980). After deposition, shales are rapidly compacted, due to gravity forces. Reorientation and alignment of the elongated framework grains allow a denser packing. Shales without calcite or quartz cement are subjected to mechanical compaction to a burial depth of 2 - 3 km (Bjørlykke and Høeg, 1997), where porosity is expected to be between 5 - 15 % (Katsube and Williamson, 1994). From 60 °C smectite starts to become unstable, and react with a potassium source (commonly K-feldspar) to illite and quartz. Illitization of kaolinite is started when the smectite to illite reaction terminates (Walderhaug et al., 2002), which will be at ca 120°C (Bjørkum et al., 1998). Kaolinite reacts with a potassium source (K-feldspar) and produce illite and quartz cement. Pervasive or complete illitization of kaolinite is expected at about 130°C (Worden and Morad, 2003), unless kaolinite transforms to the more stable kaolin mineral dickite. Then pervasive or complete illitization will be delayed until temperature exceeds 150°C. The smectite to illite reaction and illitization of kaolinite are the two major mineral reactions expected during shale diagenesis. These reactions can be responsible for reducing shale porosities from around 20 % to values close to zero if K-feldspar or other potassium sources are present (Walderhaug et al., 2002). They also found that porosity-depth trends can be strongly non-linear, and depend on shale mineralogy (e.g. smectite and K-feldspar content) and temperature history. I have used the porosity-depth model of Ramm and Bjørlykke (1994) to approach shale porosities during diagenesis. This model expresses the shale porosity as an exponential function, mainly dependent on depositional porosity, clay content and depth.

3 Diagenetic processes in sandstones

Diagenesis of sandstones can be more complex than in shales, since more mineralogical reactions commonly are involved. Diagenetic processes always moves towards increased textural and geochemical equilibrium for the minerals, in the environment they exist. Diagenetic processes right after deposition are controlled by the overall physical, biological and geochemical characteristics of the depositional system (Worden and Burley, 2003). The stability of the deposited minerals depends on source rock mineralogy, time, temperature (climate) and which processes that have weathered the minerals. At large burial depths, dissolution, diffusion and precipitation of quartz cement are considered to be the dominant diagenetic processes (Bjørkum, 1996), unless grain coating cement prevents precipitation of quartz on the grain surfaces. Although the depositional mineralogy gives indications about mineralogical evolution during diagenesis, the constituents of a subsiding volume of sandstone should not be considered in isolation. An integration of the processes in the whole sediment column is required to fully understand burial diagenetic processes in a given sand body (Worden and Burley, 2003). They also presented a geochemical rule of thumb: Geochemical processes speed up with increasing temperature, with an approximately doubling of the rate for every 10 °C rise in temperature. This is applied in paper 2 and 3 when mineralogical reactions go to completion. The most common mineral cements that precipitate in sandstones are quartz cement, cement of carbonate minerals and a variety of aluminosilicate clay minerals like kaolinite, illite and smectite (Worden and Burley, 2003). Other cements that should be mentioned are anhydrite, gypsum, pyrite, feldspars, zeolites, haematite, apatite and Ti-rich minerals (e.g. sphene).

Primmer et al. (1997) grouped sandstones into three diagenetic groups, due to detrital mineralogy; 1) quartzose- and lithic sandstones dominated by polycrystalline quartz, 2) K-feldspar dominated arkoses and lithic sandstones dominated by granittic rock fragments

and 3) plagioclase-dominated arkoses and lithic sandstones dominated by basaltic mudstone and metamorphic rock fragments. These groups were considered to be dominated by specific diagenetic properties: 1) Quartz cements with subordinate clay cements like kaolinite and illite, 2) abundant clay cement (kaolinite and illite) and some quartz cement, and 3) abundant clay cement (smectite, chlorite and illite), zeolite, carbonate and local quartz cement.

There are five dominant clay minerals in sandstones (Worden and Morad, 2003); kaolin, illite, chlorite, smectite and mixed layer varieties like illite/smectite and chlorite/smectite. Some of the most common mineral reactions in sandstones involve these minerals in addition to some feldspatic minerals and quartz:

- Illitization of kaolinite

- Illitization or chloritization of smectite

- Dickitization of kaolinite

- Albitization of feldspars

- Dissolution, diffusion and precipitation of quartz cement

I have used the porosity-depth model of Ramm and Bjørlykke (1994) to approach sandstone porosities during diagenesis. When quartz cementation initiates this model expresses the porosity as a linear function with higher porosity loss rate than rocks without quartz cement. Before incipient quartz cementation, the modelled porosity decreases as an exponential function, mainly dependent on depositional porosity, clay content and depth.

4   Rock physics models

Rock physics models can be divided into three main groups (Avseth et al., 2005); theoretical, heuristic and empirical models. This section will briefly go through the groups, with special emphasis on models applied in this thesis. Theoretical models are primarily continuum mechanics approximations of the elastic, viscoelastic or poroelastic properties of rocks. Biot (1956) formulated an expression for mechanical behavior of porous rocks with viscous pore-fluids. The Biot theory is an extension of the Gassmann (1951) theory for fluid filled rocks, which is only valid for low (ideally zero) frequency. Other theoretical models are the "squirt model" of Mavko and Nur (1975) and the "Bisq" model of Dvorkin and Nur (1993).

The elastic models include 1) inclusion models, 2) contact models, 3) computational models, 4) bounds and 5) transformations. Inclusion models approximate the rock as an elastic block of mineral perturbed by holes (porosity), and various attempts have been made to account for the scattering effect of each inclusion. These models are often referred to as inclusion models (Avseth et al., 2005). Inclusion models generally require the volume fraction of the constituents, physical properties (included shape) of the constituents and geometric information about how the constituents are arranged relative to each other. The models do commonly not depend on pressure and normal/tangential contact stiffness. The applied inclusion models in this thesis are Self Consistent Approximation (Willis, 1977), Differential Effective Medium theory (Nishizawa, 1982) and a Combined Effective Medium Theory (CEMT) (Sheng, 1990, 1991; Hornby et al., 1994), which is a combination of SCA and DEM. The formulation of SCA and DEM are given in appendix B and C, respectively. These models rely on a volume averaging procedure described in appendix A.

The SCA model treats constituents as connected phases if they are represented at approximately 40 % or more in the composite rock. A two phase material thus contains two

13

connected phases when the constituent concentrations lie within the interval 40 - 60 %. The elastic field (relation between applied stress and the average strain) for each inclusion is determined approximately using a single inclusion placed in a host having the elastic properties of the yet unknown effective medium. This is assumed to be an approximation that accounts for interaction between inclusions.

The DEM theory models composite media by a stepwise addition in concentration of one phase, with a corresponding reduction of other phases. For each step, new effective properties are calculated and used as background medium, in which constituents are added. The DEM has the property that any constituent that is connected before the calculations, remain connected when the constituent concentrations change. Therefore the combination of SCA and DEM (CEMT) is used to model porous composites with two connected phases over the entire range of relative concentrations. New constituents added to the effective medium will be treated as isolated inclusions by DEM.

Contact models often consider rocks as consisting of packing of spheres in the framework. The effective elastic properties of the packing depend on normal and tangential contact stiffness of a two particle combination. For a random sphere packing, effective bulk and shear moduli can be expressed through porosity, average number of contacts per sphere, sphere radius and normal and tangential stresses (Mavko et al., 1998). In our study we have used the combination of Hertz-Mindlin (Mindlin, 1949) contact theory and Hashin and Shtrikman (1963) lower bound (HMHS) as described by Dvorkin and Nur (1996), for compaction of uncemented sandstones. The formulations of these theories are shown in appendix D.

The contact cementation theory of Dvorkin and Nur (1996) uses the same principles to express the effective stiffness of an aggregate of contact cemented spheres. Effective bulk and shear moduli then become a function of the physical properties of the constituents,

number of grain contacts, porosity at which cementation initiates, and two parameters which are proportional to the normal and shear stiffness. They depend on the constituent properties and amount of contact cement. The complete sets of equations are shown in appendix E.

Computational models have not been applied in this thesis, and will not be described here. Bounds are describing upper and/or lower limits of elastic behaviour in a composite medium. The Voigt (1928) upper bound, Reuss (1929) lower bound and Hashin and Shtrikman (1963) upper and lower bounds make assumptions about the geometric distributions of the constituents in the composite, and estimate the elasicity limits. The Hill (1952) average is simply the arithmetic averarge of the Voigt upper and Reuss lower bound (also called the Voigt-Reuss-Hill average): $M_{vrh} = (M_v + M_r)/2$, where $M_v = \Sigma f_i M_i$ and $1/M_r = \Sigma f_i/M_i$. The terms f_i and M_i are the volume fraction and modulus of the ith component, respectively. The Hill averarge is used to estimate the effective elastic moduli of a rock in terms of its constituents and pore space, or to average between different rock physics models in the border areas of model validity. This is done in this thesis, for instance between sandstone models and shale models when the clay mineral concentration is between 45-55 % of the solid framework.

The Gassmann (1951) model for fluid substitution is probably the most famous transformation model. The Gassmann theories estimate the elastic properties at one fluid state, and predict the properties at another fluid state, and assumes zero viscocity. A similar model for rocks with viscous fluids was presented as the Bound Averaging Method (BAM) (Marion and Nur, 1991). The method is used to estimate effective bulk and shear modulus in a rock with pore-filling materials with non-zero shear stiffness. The model requires the same input as the Gassmann (1951) model: $K_{sat} = K_{dry} \frac{1-(K_{dry}/K_m)A}{\phi/K_f+(1-\phi)/K_m}$, and $\mu_{sat} = \mu_{dry}$. The subscripts sat, dry, m and f denote the properties for the saturated rock, dry rock, framework material and fluid, respectively. If the ratio is assumed to be much smaller than

one (typically on the order of 0.05), an approximate value for A is given by $A_{vr} \approx 1 + \phi$, when A is calculated by using the Voigt-Reuss bounds. Another transformation model was derived by Mavko et al. (1995). They suggested a geometry-independent transformation model that used hydrostatic velocity versus pressure data to predict stress-induced anisotropy.

Empirical rock physics models are expressions of trends generalized from observations and measurements. Numerous different suggestions have been made to empirically link different rock physics properties, like P- and S-wave (V_p and V_s) (Castagna et al., 1985; Wang, 2000b), V_p, V_s and clay content (Han et al., 1986), V_p and porosity (Raymer and Gardner, 1980) and V_p and density (Birch, 1968; Gardner et al., 1974). Empirical relations commonly have limited validity, since they focus on the relations between a few physical parameters, while excluding other potentially essential parameters. Nevertheless, they are very important for deriving unknown parameters from known parameters in cases with insufficient information.

Heuristic models can be considered "pseudo theoretical" models. The probably best known heuristic model is the Wyllie et al. (1956) time average, which relates velocity to porosity, $1/V = \phi/V_{fluid} + (1 - \phi)/V_{mineral}$. The time average is equivalent to a straight-ray, zero-wavelength approximation, neither of which makes any sense when modelling wavelengths that are very long relative to grains and pores. The Wyllie equation can in some cases be useful to describe clean, consolidated water-saturated rocks, but are not a theoretical justifiable model (Avseth et al., 2005).

In addition to the groups of rock physics models presented, models can be combined within groups, like the inclusion models SCA and DEM, or within different groups, like contact models and transformation theories like Gassmann. The resulting combined models can be called hybrid approaches. Sometimes models are combined to approach an extension of

the model validity area, for instance by using DEM, which is a high frequency model, to calculate dry rock properties, and then use Gassmann, which is a low frequency model, to estimate the overall rock properties with fluid in the pores. In cracked rocks, this approach can not be considered a low frequency theory, since the crack dimensions are assumed to be much smaller than a wavelength (Mavko et al., 1998).

5 Interplay between geology and effective elastic rock properties

After deposition shallow sediments are compacted due to gravitational forces (mechanical compaction). The compaction is a function of effective overburden stress and stress history (i.e. loading-unloading-reloading cycles) if little carbonate cement or other cementing agents are present (Bjørlykke and Høeg, 1997). Mechanical compaction can lead to crushing of grains, altered grain shapes and grain contacts. We use a pressure dependent rock physics model (HMHS) when estimating effective properties of mechanically compacted sandstones. The contact areas between grains increase with increased pressure. Crushing of grains is not considered to alter the grain shape in the modelling, since the HMHS theory requires spherical framework grains.

During diagenesis mineral reactions occur because the minerals attempt to reach equilibrium in the environment they exist. There are several reasons why mineral reactions have large implication on the overall elastic properties in the rock. The physical properties of various minerals commonly differ, leading to new component properties in the composite rock. The volume of solids in chemical reactions is also expected to change. The volume relations can be estimated, given the stoichiometrically balanced (balanced due to number of atoms) reactions, atomic composition (molar masses) and the densities of the constituents. During diagenesis, most of the mineral reactions lead to less volume of solids, thus shrinking the solid rock. Dissolution of minerals that become thermodynamically unstable allows a closer packing of the framework grains (chemical compaction). The precipitation of minerals (cements) around or at the expense of the clastic grains, changes the porosity and gives the sediments 'true cohesion' becoming stronger and more brittle in their behaviour (Bjørlykke and Høeg, 1997).

Different minerals can cement rocks in various ways. Some minerals like illite and kaolinite precipitate as pore-filling cements, and contribute little to the overall rock stiffness until they create contacts across pores (pore-bridging). Pore-bridging cements are expected to increase the overall elasticity significantly. We follow Sams and Andrea (2001) and use the SCA model to estimate the effective properties of the mixture of pore fluid and pore-filling cements. When the cement concentration exceeds approximately 40 % of the pore volume, the SCA returns non-zero shear stiffness for the mixture of pore fluid and cement. The cement limit for pore-bridging is assumed to coincide with the limit for positive shear stiffness in the effective pore fluid.

Minerals like quartz and calcite commonly precipitate in the grain contact area, while smectite and chlorite are evenly distributed on the grain surface. Hence mineral transitions can alter the distribution pattern in a rock. If e.g. soft framework clay dissolves and precipitates as pore-filling cement, stiffness increase is expected from chemical compaction, increased fluid stiffness and from reduced amount of loadbearing soft clays.

When the amount of cement reaches the interval 50 - 75 % of the intergranular volume, it is assumed that pore connectivity alters from seismic permeable to seismic isolated. Seismic isolation of pores is an expression introduced to separate from isolation over geological time. It means that no squirt flow occurs due to pressure changes induced by seismic waves, but the rock can still allow fluid flow over geological time. Increasingly seismic isolation of pores are expected to elevate the overall rock stiffness, and is modelled by changing from a rock physics model that consider pores as connected, to models that consider pores to be seismic isolated. In the transition interval with 50 - 75 % cement, we use the Hill (1952) average with increasingly weight on the model with seismic isolated pores, to obtain a smooth transition. The interval for seismic isolation should be considered an adjustable parameter, since we do not have any scientific evidence for the limits used. The seismic isolation process is comparable to the process of increasing frequency in laboratory velocity

measurements. For low frequencies (pore shape and fluid dependent), the fluid is able to flow freely enough to reach pressure equilibrium within the timeframe of half a wavelength (Wang, 2000a). Increasing frequencies decrease the wavelength, and at a certain frequency the fluid mobility is reduced. This entails an increased pressure buildup in the pores, when a wave penetrates the rock. The decreased fluid mobility increases the overall rock stiffness, and the velocities increase. Seismic isolation of pores are also considered to decrease fluid mobility when it occur.

A   Volume averaging techniques

The derivations in appendix A - C are based on the paper of Hornby et al. (1994). Consider a volume V of heterogeneous material, where V is large compared to the scale of the heterogeneities and small compared to the wavelength of an acoustic wave. The average stress within V is defined as

$$\langle \sigma_{ij} \rangle = \frac{1}{V} \int_V \sigma_{ij} dV. \tag{1}$$

Suppose that a static average stress field is imposed such that

$$\frac{\partial \sigma_{ik}(\mathbf{x})}{\partial x_k} = 0, \tag{2}$$

where a summation over repeated indices is understood. We then have

$$\langle \sigma_{ij} \rangle = \frac{1}{V} \int_S x_j \sigma_{ik} n_k dS, \tag{3}$$

where S is the boundary of V and $\mathbf{n}$ the outward normal to S. We may therefore impose any average stress by using suitable surface tractions $\mathbf{t}$. For instance, if we put

$$t_i = \sigma_{ij}^0 n_j, \tag{4}$$

at each point of S, where σ_{ij}^0 are constants, then

$$\langle \sigma_{ij} \rangle = \sigma_{ij}^0. \tag{5}$$

The average strain is

$$\langle \epsilon_{ij} \rangle = \frac{1}{V} \int_V \epsilon_{ij} dV = \frac{1}{2V} \int_S (u_i n_j + u_j n_i) dS, \tag{6}$$

and this can be measured or imposed on the surface S.

Since this is a linear problem the displacements must be a linear function of the imposed stress which means, if we use the tractions given by Equation 4, a linear function of σ_{ij}^0. Substituting into Equation 6, we get the linear relation

$$\langle \epsilon_{ij} \rangle = S_{ijkl} \sigma_{ijkl}^0 = S_{ijkl} \langle \sigma_{kl} \rangle, \tag{7}$$

where S_{ijkl} are identified as the elastic compliances of the effective material we want to estimate.

For a model structure consisting of inclusions embedded in a homogeneous matrix, expressions for the effective elastic moduli have been obtained by writing Equation 1 as

$$\langle \boldsymbol{\sigma} \rangle = \sum_{i=0}^{n} v_i \boldsymbol{\sigma}^i, \tag{8}$$

where $v_i = V_i/V$,

$$\boldsymbol{\sigma}^i = \frac{1}{V_i} \int_{V_i} \boldsymbol{\sigma} dV, \tag{9}$$

and V_i is the volume occupied by the i-th inclusion, or set of inclusions of similar material. The matrix material is included in the sum as $i = 0$. On the assumption that the materials of the matrix and inclusions are homogeneous, Equation 8 becomes

$$\langle \boldsymbol{\sigma} \rangle = \sum_{i=0}^{n} v_i \mathbf{C}^i \boldsymbol{\epsilon}^i, \tag{10}$$

where $\mathbf{C}^0$ is the stiffness tensor for the i-th material, and

$$\boldsymbol{\epsilon}^i = \frac{1}{V_i} \int_{V_i} \boldsymbol{\epsilon} dV. \tag{11}$$

22

Combining equations 7 - 11, we get:

$$(\mathbf{I} - \mathbf{C}^0\mathbf{S}^*)\langle\boldsymbol{\sigma}\rangle = \sum_{i=1}^{n} v_i(\mathbf{C}^i - \mathbf{C}^0)\boldsymbol{\epsilon}_i, \tag{12}$$

where $\mathbf{S}^*$ is the effective compliance tensor ($\boldsymbol{\epsilon} = \mathbf{S}^*\boldsymbol{\sigma}$) and $\mathbf{I}$ is the fourth rank unit tensor.

If an average stress $\langle\boldsymbol{\sigma}\rangle = \boldsymbol{\sigma}^0$ is imposed on a representative volume V by the use of tractions $t_i = \sigma_{ij}^0 n_j$ as given in Equation 4, the linearity of the problem means that there exists a tensor $\mathbf{K}^i$ such that

$$\boldsymbol{\epsilon} = \mathbf{K}^i\boldsymbol{\sigma}^0 = \mathbf{K}^i\langle\boldsymbol{\sigma}\rangle, 1 \leq i \leq n. \tag{13}$$

Substituting into Equation 12, we get

$$(\mathbf{I} - \mathbf{C}^0\mathbf{S}^*)\langle\boldsymbol{\sigma}\rangle = \left\{\sum_{i=1}^{n} v_i(\mathbf{C}^i - \mathbf{C}^0)\mathbf{K}^i\right\}\langle\boldsymbol{\sigma}\rangle. \tag{14}$$

Since $\langle\boldsymbol{\sigma}\rangle$ is arbitrary, it follows that

$$\mathbf{I} - \mathbf{C}^0\mathbf{S}^* = \sum_{i=1}^{n} v_i(\mathbf{C}^i - \mathbf{C}^0)\mathbf{K}^i, \tag{15}$$

or

$$\mathbf{S}^* = \mathbf{S}^0 - \sum_{i=1}^{n} v_i(\mathbf{S}^0\mathbf{C}^i - \mathbf{I})\mathbf{K}^i, \tag{16}$$

where $\mathbf{S}^0$ is the compliance tensor for the matrix material. This equation is the foundation for the derivation of the self consistent approach as well as the differential effective medium theory.

B Self consistent approach

In this approach, the elastic field for each inclusion, and therefore the tensor $\mathbf{K}^i$ is determined approximately using a single inclusion placed in a host having the elastic properties of the yet to be determined effective medium. For the approximation of $\mathbf{K}^i$ obtained, we use the notation $\mathbf{K}^{*i}$. In addition, if we wish to treat all the constituents equally, as we do in the case of porous solids with connected fluid and solid phases, we replace the matrix material in the model with the effective material; i.e. we set $\mathbf{C}^0 = \mathbf{C}^{SCA}$. Then Equation 15 becomes:

$$\sum_{i=1}^{n} v^i (\mathbf{C}^i - \mathbf{C}^{SCA}) \mathbf{K}^{*i} = 0, \tag{1}$$

where $\mathbf{K}^{*i}$ depends on the solution for $\mathbf{C}^{SCA}$. By rearranging the equation, we get:

$$\sum_{i=1}^{n} v^i \mathbf{C}^i \mathbf{K}^{*i} = \mathbf{C}^{SCA} \sum_{i=1}^{n} v^i \mathbf{K}^{*i} \tag{2}$$

and

$$\mathbf{C}^{SCA} = \sum_{i=1}^{n} v^i (\mathbf{C}^i \mathbf{K}^{*i} \left\{ \sum_{p=1}^{n} v^p \mathbf{K}^{*p} \right\}. \tag{3}$$

This expression may be solved iteratively, by setting an initial value for $\mathbf{C}^{SCA}$, computing $\mathbf{K}^{*i}$, then reevaluating $\mathbf{C}^{SCA}$. It can be shown (Hornby et al., 1994) that the K-tensor can be expressed as:

$$\mathbf{K} = [\mathbf{C}(\mathbf{I} + \widehat{\mathbf{G}}(\mathbf{C'} - \mathbf{C}))]^{-1}, \tag{4}$$

where I is the identity matrix and $\widehat{\mathbf{G}}$ is a fourth-rank tensor calculated from the response of a single inclusion embedded in an unbounded matrix of the effective material, and is discussed in e.g. Jakobsen et al. (2000). $\mathbf{C'}$ is the stiffness tensor for an inclusion embedded in the effective medium with stiffness tensor $\mathbf{C}$. By combining Equation 3 with 4, we obtain

the SCA result for the elastic effective stiffness tensor:

$$\mathbf{C}^{SCA} = \sum_{i=1}^{n} v^i \mathbf{C}^i (\mathbf{I} + \widehat{\mathbf{G}}(\mathbf{C}^i - \mathbf{C}))^{-1} \left\{ \sum_{p=1}^{n} v^p [\mathbf{I} + \widehat{\mathbf{G}}(\mathbf{C}^p - \mathbf{C})]^{-1} \right\}. \tag{5}$$

C   Differential effective medium model

The differential effective medium (DEM) model can be used to introduce new constituents or changing the relative concentrations in a mixture of materials. The calculations are performed by successive operations of adding an infinitesimal subvolume of host material. At each successive increment of component n, the previous step is taken as the host material. We note that the actual change in the concentration, v_n, of the n-th component is $\Delta v_n/(1 - v_n)$. To compute the properties of the new effective material, we return to Equation 16 in appendix A, reformulated as a differential equation. For included material $\mathbf{C}^i$ and effective properties of the media at concentrations v given by $\mathbf{S}^*(v)$, Equation 16 gives:

$$\mathbf{S}^*(v + \Delta v) = \mathbf{S}^*(v) - \frac{\Delta v}{(1 - \Delta v)}(\mathbf{S}^*(v)\mathbf{C}^i - \mathbf{I})\mathbf{K}^i(v + \Delta v), \tag{1}$$

where $\mathbf{K}^i$ is computed for the included material $\mathbf{C}^i$ in the effective material with elastic stiffnesses $\mathbf{C}^*(v + \Delta v)$. By rearranging we have, to first order in Δv:

$$\frac{\mathbf{C}^*(v + \Delta v) - \mathbf{C}^*(v)}{\Delta v} = \frac{1}{(1 - v)}(\mathbf{C}^i - \mathbf{C}^*(v))\mathbf{K}^i(v + \Delta v)\mathbf{C}^*(v + \Delta v), \tag{2}$$

and finally, as $\Delta v \longrightarrow 0$, we have an expression for $\mathbf{C}^*(v)$ in the DEM approximation for anisotropic composites:

$$\frac{d}{dv}(\mathbf{C}^{DEM}(v) = \frac{1}{(1 - v)}(\mathbf{C}^i - \mathbf{C}^{DEM}(v))\mathbf{K}^i(v)\mathbf{C}^{DEM}(v). \tag{3}$$

Inserting Equation 4 for the $\mathbf{K}$-tensor and simplifying, the final DEM equation for anisotropic composites is:

$$\frac{d}{dv}(\mathbf{C}^{DEM}(v) = \frac{1}{(1 - v)}(\mathbf{C}^i - \mathbf{C}^{DEM}(v))[\mathbf{I} + \widehat{\mathbf{G}}(\mathbf{C}^i - \mathbf{C}^{DEM}(v))]^{-1}. \tag{4}$$

D   The combined Hertz-Mindlin - Hashin-Shtrikman model

The formulas and derivations in this part is adopted from Mavko et al. (1998) and Dvorkin and Nur (1996). In the Hertz model of normal compression of two identical spheres, the radius of the contact area, a, and the normal displacement, δ, are:

$$a = \left[\frac{3FR}{8G}(1 - \mathrm{v})\right]^{\frac{1}{3}}, \quad \delta = \frac{a^2}{R}, \tag{1}$$

where G and v are the shear modulus and Poisson's ratio for the grain material, respectively., R is the radius of a particle. If a hydrostatic confining pressure P is applied to a random identical sphere packing, a confining force acting between two particles is

$$F = \frac{4\pi R^2 P}{C(1 - \phi)}, \tag{2}$$

where C is the coordination number (average number of contacts per grain). Then

$$a = R\left[\frac{3\pi(1 - \mathrm{v})}{2C(1 - \phi)G}P\right]^{\frac{1}{3}}. \tag{3}$$

The normal stiffness (S_n) becomes:

$$S_n = \frac{4Ga}{1 - \mathrm{v}}. \tag{4}$$

The effective bulk modulus (K_{eff}) of a dry random identical sphere packing then is:

$$K_{HM} = \left[\frac{C^2(1 - \phi)^2 G^2}{18\pi^2(1 - \mathrm{v})^2}P\right]^{\frac{1}{3}}. \tag{5}$$

Mindlin (1949) shows that if the spheres are first pressed together and a tangential force is

applied *afterward*, the shear and normal stiffnesses are (the latter as in the Hertz solution):

$$S_\tau = \frac{8aG}{2 - \text{v}}, \ \ S_n = \frac{4aG}{1 - \text{v}}. \tag{6}$$

The effective shear modulus of a dry random identical sphere packing then is:

$$G_{HM} = \frac{5 - 4\text{v}}{5(2 - 4\text{v})} \left[\frac{3C^2(1 - \phi)^2 G^2}{2\pi^2(1 - \text{v})^2} P \right]^{\frac{1}{3}}. \tag{7}$$

In the Mindlin formulas above, it is assumed that there is no slip at the contact surface between two particles.

Hashin and Shtrikman (1963) formulated upper and lower elastic bounds of a mixture of two constituents, when geometrical considerations are unknown:

$$K^{HS\pm} = K_1 \frac{f_2}{(K_2 - K_1)^{-1} + f_1(K_1 + \frac{4}{3}G_1)^{-1}}, \tag{8}$$

$$G^{HS\pm} = G_1 \frac{f_2}{(G_2 - G_1)^{-1} + \frac{2f_1(K_1 + 2G_1)}{5G_1(K_1 + \frac{4}{3}G_1)}}, \tag{9}$$

where K, G and f are bulk modulus, shear modulus and volume fractions of medium 1 or 2. Upper and lower bounds are calculated by interchanging which material is termed 1 and 2. Generally, the expressions give the upper bound when the stiffest material is termed 1, and the lower bound when the softest material is termed 1 in Equation 8 and 9. Dvorkin and Nur (1996) proposed a heuristic modified Hashin-Shtrikman lower bound based on the original Hashin and Shtrikman (1963) lower bound:

$$K_{eff} = \left[\frac{\phi/\phi_0}{K_{HM}^2 + \frac{4}{3}G_{HM}} + \frac{1 - \phi/\phi_0}{K + \frac{4}{3}G_{HM}} \right]^{-1} - \frac{4}{3}G_{HM}, \tag{10}$$

$$G_{eff} = \left[\frac{\phi/\phi_0}{G_{HM} + \frac{G_{HM}}{6}\left(\frac{9K_{HM}+8G_{HM}}{K_{HM}+2G_{HM}}\right)} + \frac{1-\phi/\phi_0}{G + \frac{G_{HM}}{6}\left(\frac{9K_{HM}+8G_{HM}}{K_{HM}+2G_{HM}}\right)} \right]^{-1} - \quad (11)$$

$$\frac{G_{HM}}{6}\left(\frac{9K_{HM}+8G_{HM}}{K_{HM}+2G_{HM}}\right),$$

where K and G are the grain bulk modulus and shear modulus, respectively. This model connects two end members - one has zero porosity and the modulus of the solid phase, and the other has critical porosity and a pressure dependent modulus as given by the Hertz-Mindlin theory.

E   Contact cementation theory

The derivations and figures that follows are taken from Dvorkin et al. (1994) and Dvorkin and Nur (1996). The effective elastic properties of a random packing of identical spherical particles can be expressed through its porosity ϕ, coordination number C, (average number of contacts per sphere), the radius of a particle R, and the normal (S_n) and tangential (S_τ) stiffnesses of a two-sphere combination. The normal and shear stiffnesses are defined as the ratios of a corresponding force increment to the displacement of the sphere center relative to the contact region (Figure 1):

$$S_n = \frac{\partial F}{\partial \delta} \, , \ S_\tau = \frac{\partial T}{\partial \tau} \, .$$ (1)

Effective bulk (K_{eff}) and shear moduli (G_{eff}) are:

$$K_{eff} = \frac{C(1-\phi)}{12\pi R} S_n \, , \ G_{eff} = \frac{C(1-\phi)}{20\pi R}(S_n + \frac{3}{2}S_\tau) \, .$$ (2)

The problem is to derive an expression for the normal and tangential stiffnesses of a cemented package of identical spheres. Normal displacements v, of the surface of an elastic grain due to a concentrated force P, can be expressed in the (x, y, z) coordinate system (Figure 2):

$$v(x, y) = \frac{1 - \text{v}}{2\pi G} \frac{P}{r}, \ r = \sqrt{x^2 + y^2} \, .$$ (3)

v and G are the Poisson's ratio and shear modulus of the grain, respectively. We assume that the contact region on the surface of the sphere is a circle of radius a (Figure 3b). It can then be shown that normal stresses $p(r)$ are related to normal displacements $v(r)$ as

follows:

$$v(r) = \frac{1 - \mathrm{v}}{\pi G} \int_0^\pi d\varphi \int_0^{r\cos\varphi + \sqrt{a^2 - r^2 \sin^2 \varphi}} \times p\left(\sqrt{r^2 + s^2 - 2rs\cos\varphi}\right) ds, \qquad (4)$$

where integration is conducted inside the circle $|r| < a$, Figure 4.

The displacement of the center of the spherical grain relative to the median plane of the cement layer δ can be related to the displacements V of the surface of the cement layer and v of the surface of the grain (Figure 3b-d) as

$$\delta = v(r) - V(r). \qquad (5)$$

Dvorkin et al. (1991) showed that a thin cement layer subjected to normal and shear load can be approximately treated as an elastic foundation. Therefore normal stresses p acting upon the surface of the grain, are related to the displacements V of the surface of the cement layer as

$$p(r) = -\frac{2G_c(1 - \mathrm{v}_c)}{1 - 2\mathrm{v}_c} \frac{V(r)}{h(r)}, \qquad (6)$$

where G_c and v_c are the shear modulus and Poisson's ratio of the cement, and h is half-thickness of the cemented layer. In this derivation we use the expression for h as follows:

$$h(r) = R\left[\varepsilon + \frac{1}{2}\left(\frac{r}{R}\right)^2\right], \quad \varepsilon = \frac{h(0)}{R}. \qquad (7)$$

If we assume that shear stresses at the grain surface do not significantly influence the normal deformation, Equations 4 - 7 can be combined into the following integral equation:

$$\delta + V(r) = -\Lambda \int_0^\pi d\varphi \int_0^{r\cos\varphi + \sqrt{a^2 - r^2 \sin^2 \varphi}} \times \frac{V\left(\sqrt{r^2 + s^2 - 2rs\cos\varphi}\right)}{R\left[\varepsilon + \frac{1}{2}\left(\frac{r^2}{R^2} + \frac{s^2}{R^2} - \frac{2rs}{R^2}\cos\varphi\right)\right]} ds, \qquad (8)$$

$$\Lambda = \frac{2G_c}{\pi G} \frac{(1 - \mathrm{v})(1 - \mathrm{v}_c)}{1 - 2\mathrm{v}_c}.$$

The constant δ here can be determined from the resulting compressional force F:

$$F = \int_0^a p(r) 2\pi r \, dr = -\frac{4\pi G_c(1 - \mathrm{v}_c)}{1 - 2\mathrm{v}_c} \int_0^a \frac{V(r)r}{h(r)} dr \,. \tag{9}$$

By normalizing the equations, and using 1, we arrive at the following scheme of determining normal stiffness S_n:

1) Find an as yet unknown function $H(t)$ from the integral equation

$$\Delta_0 + H(t) = -\Lambda \int_0^\pi d\varphi \int_0^{t \cos \varphi + \sqrt{\alpha^2 - t^2 \sin^2 \varphi}} \times \frac{H\left(\sqrt{t^2 + s^2 - 2ts \cos \varphi}\right)}{\varepsilon + \frac{1}{2}\left(t^2 + s^2 - 2ts \cos \varphi\right)} ds \,, \tag{10}$$

where $\alpha = a/R$, and Δ_0 is an arbitrary chosen non-zero constant.

2) Calculate the integral

$$\int_0^\alpha \frac{H(t)t \, dt}{\varepsilon + \frac{t^2}{2}} = k \,. \tag{11}$$

3) Find normal stiffness S_n as:

$$S_n = -\frac{4\pi R G_c(1 - \mathrm{v}_c)}{1 - 2\mathrm{v}_c} \frac{k}{\Delta_0} \,. \tag{12}$$

This expression can be inserted into the expression for K_{eff} in Equation 2 to obtain effective bulk modulus of a random sphere packing of porosity ϕ and coordination number C:

$$K_{eff} = \frac{G_c(1 - \mathrm{v}_c)}{1 - 2\mathrm{v}_c} \frac{C(1 - \phi)}{3(1 + \varepsilon)} \left(-\frac{k}{\Delta_0}\right) \,, \tag{13}$$

where ε is proportional to the minimal thickness of the cement layer (at r=0), and $\varepsilon = 0$ for the case where grains have direct point contacts.

The approach for solving the problem of tangential deformation of two cemented grains with the relative displacement 2τ in the x direction is similar to the one used for the normal deformation problem. We assume that the contact region is small compared to the grain, and therefore the formulas for an elastic half-space can be used to relate stresses on the grain surface to its displacements. A concentrated tangential force Q_x, when applied to an elastic half-space, produces the following displacements on the surface:

$$u = \frac{Q_x}{4\pi G} \frac{1}{r} \left[\left(1 + \frac{x^2}{r^2} \right) + (1 - 2v) \left(1 - \frac{x^2}{r^2} \right) \right],$$
(14)

$$w = \frac{Q_x v}{2\pi G} \frac{xy}{r^3} \ , \quad v = \frac{Q_x (1 - 2v)}{4\pi G} \frac{x}{r^2} \ , \quad r^2 = x^2 + y^2$$

at z=0. A tangential deformation of a two-grain combination in the x direction will produce displacements in the cement layer in both x and y direction. Similar to Equation 4, the following integral equations can be obtained to relate tangential stresses q_x and q_y distributed in the circle of radius a, to the corresponding displacements u and w:

$$u(r, \theta) = \frac{1}{2\pi G} \int_0^{2\pi} d\varphi \int_0^{L(r,\theta,\varphi)} \times \left[q_x(r_c, \theta_c)(1 - v\, sin^2\varphi) - q_y(r_c, \theta_c)v\, sin\,\varphi\, cos\,\varphi) \right] ds,$$

$$v(r, \theta) = \frac{1}{2\pi G} \int_0^{2\pi} d\varphi \int_0^{L(r,\theta,\varphi)} \times \left[q_y(r_c, \theta_c)(1 - v\, cos^2\varphi) - q_x(r_c, \theta_c)v\, sin\,\varphi\, cos\,\varphi) \right] ds,$$
(15)

$$L(r, \theta, \varphi) = a \left[\sqrt{1 - \left(\frac{r}{a} \right)^2 sin^2(\theta + \varphi)} + \frac{r}{a} cos(\theta + \varphi) \right], \quad r_c = \sqrt{r^2 + s^2 - 2rs\, cos(\theta + \varphi)},$$

$$\theta_c = arctan \left(\frac{r\, sin\theta + s\, sin\varphi}{r\, cos\theta + s\, cos\varphi} \right), \quad r = \sqrt{x^2 + y^2}, \quad \theta = arctan \left(\frac{y}{x} \right).$$

33

The domain of integration is shown in Figure 5. As for the normal deformation, the following compatibility equations can be written for the tangential displacements of the cement and the grain:

$$\tau = u(r,\theta) - U(r,\theta)\,, \ \ w(r,\theta) = W(r,\theta), \tag{16}$$

where U and W are the tangential displacements of the surface of the cement layer in the x and y directions, respectively, and τ is the tangential displacement of the center of the grain along the x direction. We now assume that a cement layer can be treated as an elastic foundation, when deforming in shear:

$$q_x(r,\theta) = -G_c\frac{U(r,\theta)}{h(r,\theta)}, \ \ q_y(r,\theta) = -G_c\frac{W(r,\theta)}{h(r,\theta)}. \tag{17}$$

We can now transform 15 into the following system of two integral equations:

$$\tau + U(r,\theta) = -\frac{G_c}{2\pi G}\int_0^{2\pi} d\varphi \int_0^{L(r,\theta,\varphi)} \times \left[\frac{U(r_c,\theta_c)}{h(r_c)}(1 - \mathrm{v}\,sin^2\varphi) - \frac{W(r_c,\theta_c)}{h(r_c)}\mathrm{v}\,sin\,\varphi\,cos\,\varphi\right]ds, \tag{18}$$

$$W(r,\theta) = \frac{G_c}{2\pi G}\int_0^{2\pi} d\varphi \int_0^{L(r,\theta,\varphi)} \times \left[\frac{W(r_c,\theta_c)}{h(r_c)}(1 - \mathrm{v}\,cos^2\varphi) - \frac{U(r_c,\theta_c)}{h(r_c)}\mathrm{v}\,sin\,\varphi\,cos\,\varphi\right]ds\,. \tag{19}$$

For the case of two spherical grains in contact, h is given by 7. In these equations, the constant τ can be determined from the resulting tangential force T:

$$T = \int_0^a \int_0^{2\pi} q_x(r,\theta)r\,d\theta\,dr = -G_c\int_0^a \int_0^{2\pi} \frac{U(r,\theta)r}{h(r)}d\theta\,dr\,. \tag{20}$$

The resulting tangential stiffness can be found from 1.

We can simplify Equation 18, and reduce it to one integral equation, to derive a simplified solution for the tangential stiffness. It can be showed that the total error of neglecting

displacement w does not exceed 6.25 % (Dvorkin et al., 1994). The reduced and simplified Equation 18 then becomes:

$$\tau + U(r) = -\Lambda_\tau \int_0^\pi d\varphi \int_0^{r\cos\varphi + \sqrt{a^2 - r^2 \sin^2\varphi}} \times \frac{U\left(\sqrt{r^2 + s^2 - 2rs\cos\varphi}\right)\left(1 - v\,\sin^2\varphi\right)}{R\left[\varepsilon + \frac{1}{2}\left(\frac{r^2}{R^2} + \frac{s^2}{R^2} - \frac{2rs}{R^2}\cos\varphi\right)\right]} ds,$$

(21)

$$\Lambda_\tau = \frac{G_c}{\pi G}\,.$$

The constant τ can be determined from the resulting tangential force T:

$$T = \int_0^a q_x(r) 2\pi r\,dr = -2\pi G_c \int_0^a \frac{U(r)r}{R\left[\varepsilon + \frac{r^2}{2R^2}\right]}\,dr\,.$$

(22)

After normalizing the above equations for tangential deformation, we obtain the following scheme for determining tangential stiffness S_τ of a two grain combination:

1) Find an as yet unknown function $H(t)$ from the integral equation

$$\Delta_0 + H(t) = -\Lambda_\tau \int_0^\pi d\varphi \int_0^{t\cos\varphi + \sqrt{\alpha^2 - t^2 \sin^2\varphi}} \times \frac{H\left(\sqrt{t^2 + s^2 - 2ts\cos\varphi}\right)\left(1 - v\,\sin^2\varphi\right)}{\varepsilon + \frac{1}{2}\left(t^2 + s^2 - 2ts\cos\varphi\right)}\,ds\,,$$

(23)

where $\alpha = a/R$, and Δ_0 is an arbitrary chosen non-zero constant.

2) Calculate the integral

$$\int_0^\alpha \frac{H(t)t\,dt}{\varepsilon + \frac{t^2}{2}} = k\,.$$

(24)

3) Find tangential stiffness S_τ as:

$$S_\tau = -2\pi R G_c \frac{k}{\Delta_0}\,.$$

(25)

Equation 2 now gives the following final expression for the effective shear modulus of a

random sphere packing of porosity ϕ and coordinate number C:

$$G_{eff} = \frac{3}{5}K_{eff} + G_c\frac{3C(1-\phi)}{20(1+\varepsilon)}\left(-\frac{k}{\Delta_0}\right),\tag{26}$$

where K_{eff} can be found from previous derivations.

The parameters S_n and S_τ are proportional to the normal and shear stiffness, respectively, of a cemented two-grain combination. They depend on the amount of the contact cement and on the properties of the cement and the grains. The amount of contact cement can be expressed through the ratio α of the radius of the cement layer (a) to the grain radius (R) as $\alpha = a/R$. By assuming that porosity reduction in sands is caused by cementation only, and by adopting certain schemes of cement deposition, we can relate parameter α to the current porosity of cemented sand (ϕ). Scheme 1 is where all cement is deposited at grain contacts (Figure 6A):

$$\alpha = 2\left[\frac{\phi_0 - \phi}{3C(1-\phi_0)}\right]^{0.25} = 2\left[\frac{S\phi_0}{3C(1-\phi_0)}\right]^{0.25},\tag{27}$$

where S is the fraction of cement due to intergranular volume and ϕ_0 is the porosity at which cementation initiates. Scheme 2 estimates α when all cement is deposited evenly on the grain surface (Figure 6B):

$$\alpha = \left[\frac{2(\phi_0 - \phi)}{3(1-\phi_0)}\right]^{0.5} = \left[\frac{2S\phi_0}{3(1-\phi_0)}\right]^{0.5}.\tag{28}$$

These results can be applied in the three steps procedures of estimating S_n and S_τ.
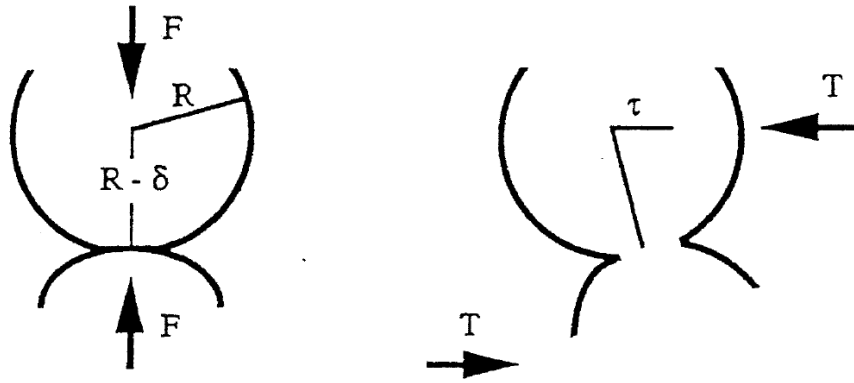
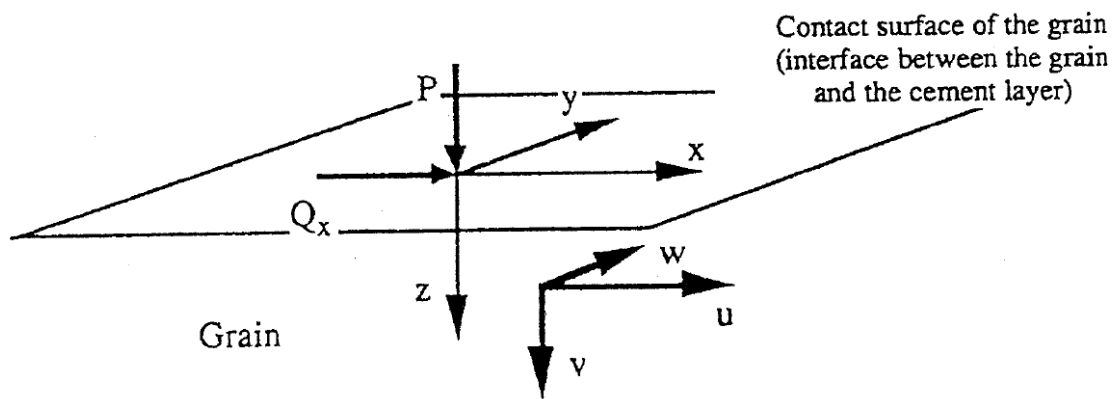Figure 1: Normal and shear deformation of a two grain combination.

Figure 2: Concentrated forces acting upon the surface of an elastic half-space. A cemented contact region between two grains is assumed to be small compared to the grain. On the basis of this assumption, displacements of the surface of the grain are related to stresses through the formulas for an elastic half-space.
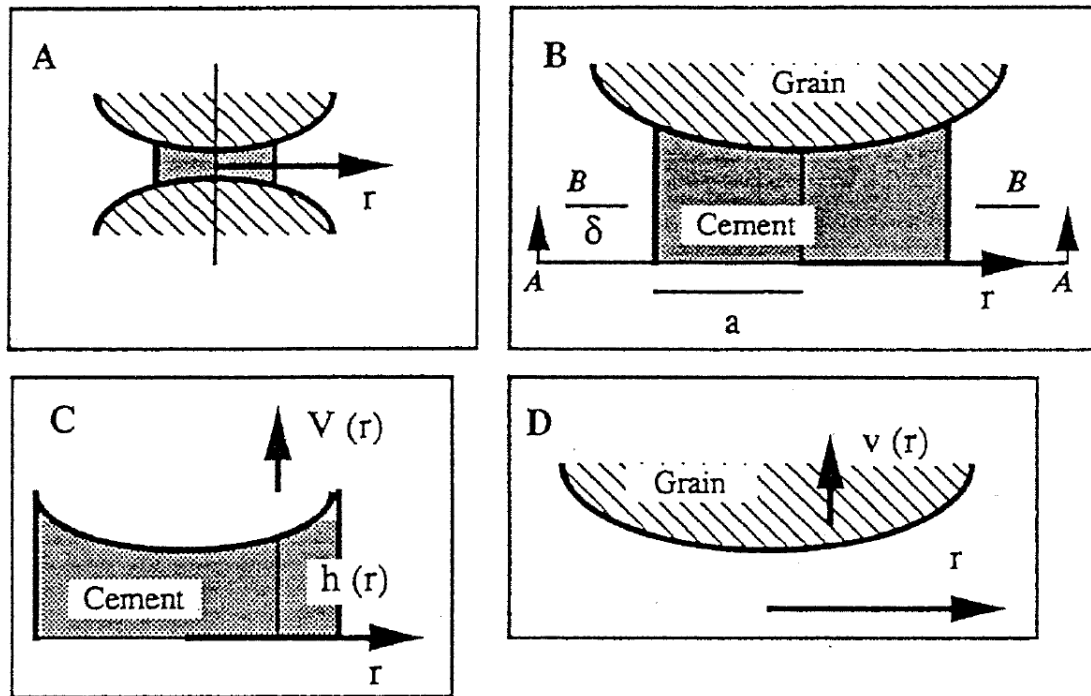
Figure 3: A cemented contact region between two spherical grains: A) The cement forms an axisymmetrical thin layer. B) Normal deformation of the grain and the cement - δ is the displacement of the center of the sphere relative to the median plane of the cement layer AA (this plane moves into position BB). C) Normal axisymmetrical displacement of the cement layer. D) Normal axisymmetrical displacement of the surface of the grain.
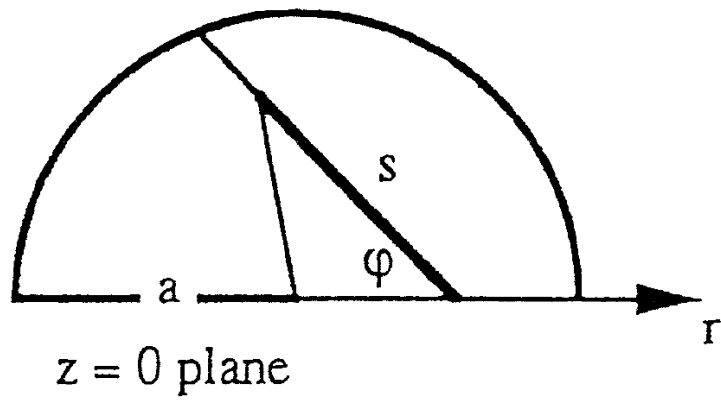
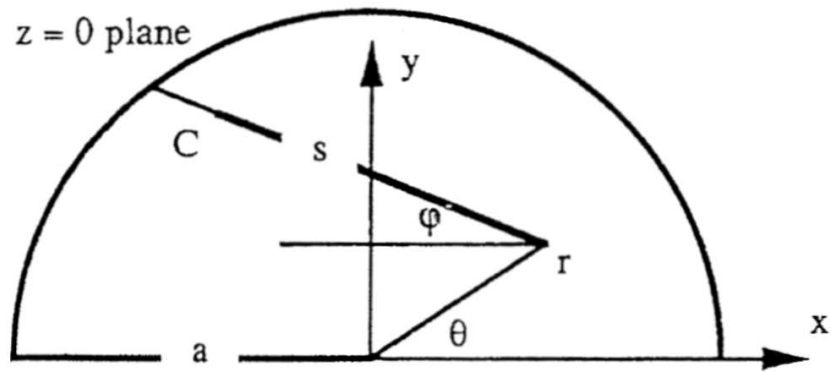Figure 4: The region of contact on the grain surface $|r| < a$ in the plane $z = 0$.
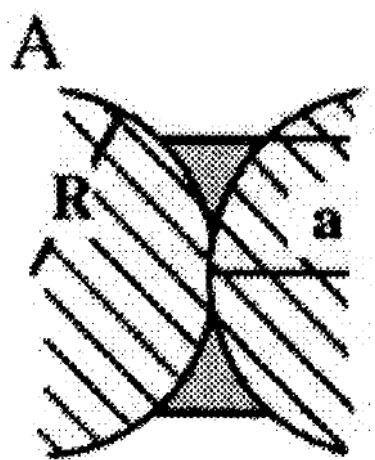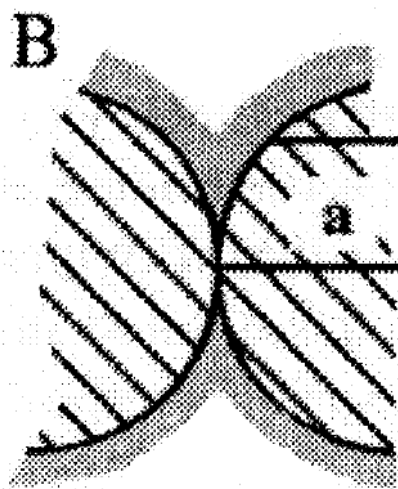
Figure 5: The domain of integration in the $z = 0$ plane used in Equation 15.

Figure 6: Cemented grains. A) Scheme 1 - all cement is in the contact. B) Scheme 2 - graincoating and contact cementing cement.

F SEG Conference, Houston, 2005

A strategy for using mineralogy as input to rock physics modelling of sandstones

Anders Dræge[1,2], Tor Arne Johansen[1,2] and Ivar Brevik[3]
[1] *Department of Earth Science, University of Bergen, Norway*
[2] *Centre for Integrated Petroleum Research, University of Bergen, Norway*
[3] *Statoil Research Centre, Rotvoll, 7005 Trondheim, Norway*

Summary

The overall rock stiffnesses are dependent on the distribution of the constituents. Thus information about which constituents are loadbearing, dispersed in pore fluid or contact cementing is necessary to perform a reliable modelling of the seismic properties. We suggest a classification of distribution-properties for various common minerals in sandstones. Further, we present a rock physics model that aims to incorporate various concurrent mineral distributions. We use the rock physics model together with the mineral classification to model P and S wave velocities in core plugs with known mineralogy. Finally we compare our model with log velocities from two wells. Our model reproduces the velocities well, even in sands with complex cementation.

Introduction

Gal et al. (1999) stated that the elastic moduli of shaly sandstones strongly depend on both volume and position of clay. Thus two different sandstones with the same clay volume, might have significantly differences in stiffnesses due to clay distribution. Sams and Andrea (2001) defined four different distributions of clay; between grain contacts, framework clay (structural), in the pore space as dispersed clay (pore-filling or grain coating) and clay lamination. Neither did they model contact cement explicitly, nor did they study the effects of more than one simultaneous distribution of clay, like structural and dispersed.

We define four different types of distributions of components other than framework quartz. Further, we assume that each mineral type has its preferred distribution. Mineralogy analysis performed by a number of researchers support this assumption. The coupling of mineralogy to distribution, allows us to use mineralogy as an additional parameter when performing rock physics modelling. Thus we are able to make predictions about the effects of fluctuating mineral concentrations, and various cement conditions.

Model description

In order to perform rock physics modelling, we have de-
fined four types of distributions for cement and loadbearing non-quartz constituents in sandstones; **i)** cement that lies in the grain contacts and stabilizes contacts between matrix grains, **ii)** pore-filling cement that contribute little to the overall rock stiffnesses until they become pore-bridging when presented at approximately 40 % or more in the pores, **iii)** graincoating and pore lining cement, that envelop the framework grains, but does not carry load in the framework grain-grain contacts, **iv a)** replacive clay or clay clasts which act as a part of the loadbearing framework and **iv b)** graincoating clay cement that prevent contact between the framework grains, and thus are loadbearing. When the cement concentrations reach certain levels, contact cement will turn into grain coating, and pore-filling cement will evolve to pore bridging. Figure 1 shows illustrations of the distributions for different stages in the diagenesis.
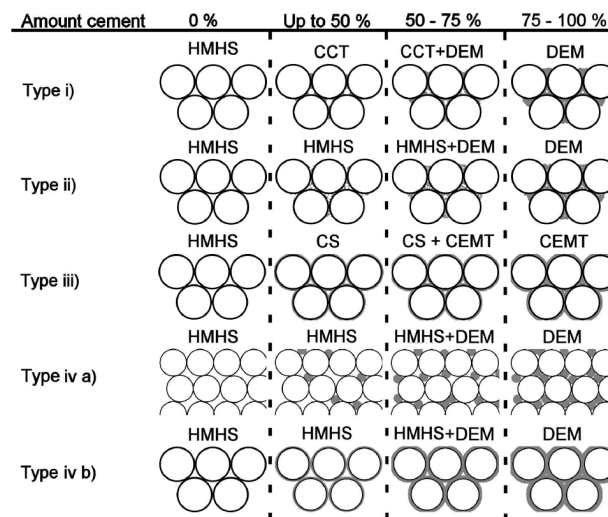
Fig. 1: The figure shows the modelling steps for the different inclusion types. White circles are framework grains, while grey indicate cement or inclusions. HMHS, CEMT, CCT, DEM and CS are rock physics models which are described in the text. The cement volume is relative to total available pore volume. When the cement volume increases, the porosity decreases correspondingly. We apply different models in cases with low and high degree of cementation, to account for connected pores in uncemented sands and isolated pores in highly cemented sands.

The text above each stage indicates the rock physics

model applied in the modelling. Permeable rocks with distribution type **ii)** and **iv a,b)** are modelled with the combined theories of Hertz-Mindlin (HM) (Mindlin, 1949) and Hashin and Shtrickman (1963) (HS) lower bound, like described in Dvorkin and Nur (1996). This combined model (HMHS) connects two end members; one has zero porosity and the modulus of the solid phase, and the other has critical porosity and a pressure dependent modulus as given by the Hertz-Mindlin theory.

The DEM (Differential Effective Medium, Nishizawa (1982)) is used to model isolated inclusions when the permeability gets low. The CEMT (Combined Effective Medium Theory) model is applied to approach connected phases in a composite medium. The CEMT consists of two steps, where the first step make use of the Self Consistent Approach (SCA, Willis (1977)) to yield a mix of equal and connected volumes of two constituents. Secondly, the DEM is used to model the effective stiffnesses at desired concentrations.

We apply the contact cement theory (CCT) of Dvorkin et al. (1999) to model the first stages of type **i)** cement. CCT provides the effective elastic properties of an aggregate of spheres, where the spheres are in direct point contact, and cement fills the space around the contacts. CCT cannot be used to estimate the elastic constants of an aggregate where cement fills the entire pore space or large portions of it (Dvorkin et al., 1999), therefore we combine it with DEM for high cement concentrations.

The coated sphere (CS) model we have applied, corresponds to the scheme 2 cement in Dvorkin and Nur (1996). This model treats the cement as evenly deposited on the grain surface, which leads to coated framework grains. We combine it with CEMT to approximate connected phases of cement and framework when the cement concentration gets high.

We apply the Bound Average Model (Marion and Nur, 1991) to model the effects of fluid saturation in permeable sandstones. The DEM is applied for modelling the fluid effects in none-permeable rocks. When the rock starts to loose its permeability we consider the process to be heterogeneous, which means that at the same time, some areas in the rock will maintain higher permeability, while others approach impermeable. In transitions from uncemented to cemented rock, and from permeable to impermeable rock, we apply the Hill (1952) average between the different models, to obtain smooth transitions.

Figure 2 shows modelled bulk and shear moduli for the different models. We have used the same cement in all models, to compare the different paths from uncemented to completely cemented rocks. It is clear that different distributions can produce significantly different rock stiffnesses, also at equal cement concentrations. The CCT model returns highest stiffnesses, but the differences decrease at low porosities. Type **iii)** inclusions are considered to be connected at high concentrations, while type **i)** and **ii)** are considered to be isolated at all concentrations. Therefore the latter types converge, while type **iii)** returns lower moduli, when porosity approaches zero.
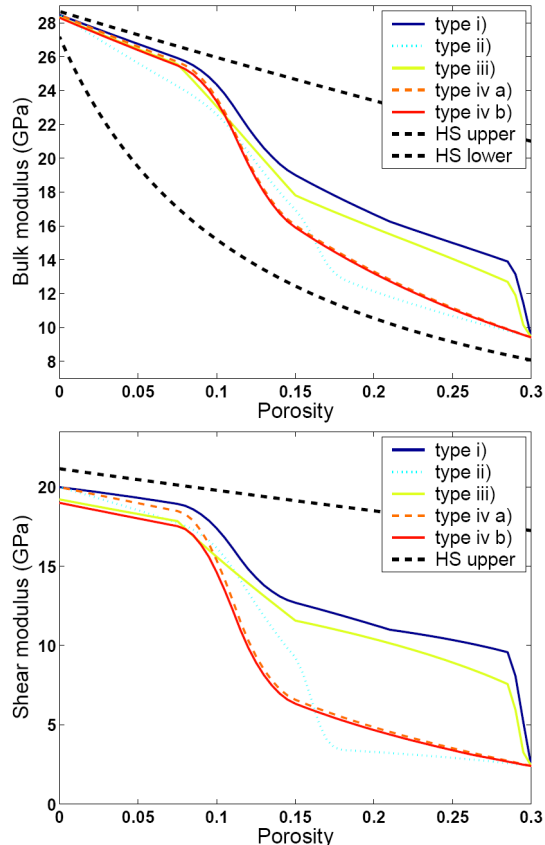

Fig. 2: The Figure show the effect of different distributions on elastic moduli. Stippled lines represent the upper and lower Hashin and Shtrikman (1963) (HS) bonds. Cement concentration is increasing from 0-30% while the porosity decreases correspondingly. We have used the mixed clay as cement, and brine as pore fluid in all modellings.

Mineral	Type
Quartz cement, calcite, siderite, ankerite	**i)**
Kaolinite, illite, pyrite and heavy minerals	**ii)**
Chlorite, A albite, A smectite	**iii)**
K-feldspar, clay clasts, plagioclase clasts,	**iv a)**
Chert clasts, muscovite clasts, biotite clasts	**iv a)**
D smectite, detrital clay coating	**iv b)**

Table 1: Suggested classification of some common minerals in sandstones. A and D denote authigenic and detrital respectively.

Mineral classification

In Table 1 we suggest a classification of clay minerals according to the four classes of distributions, so that imple-

mentation to rock physics modelling becomes convenient. Normally a cemented sandstone will contain mixtures of these distributions, so we combine the rock physics models for the different distributions to obtain the final results. The classification is based on observations, in addition to the work of Walderhaug (2000) which studied 40 thin sections from the two wells presented in this paper.

Results

The mineral properties used in this study are adopted from Mavko et al. (1998) (quartz, plagioclase, albite, muscovite, pyrite, biotite, hematite, siderite, ankerite, calcite and mixed clay), Vanorio et al. (2003) (kaolinite and smectite) and Wang et al. (2001) (illite and chlorite). We have assigned the properties from the so called "average feldspar" to plagioclase. Hematite is representing heavy minerals in the further modelling. The ankerite and detrital clay properties are adopted from dolomite and smectite respectively.

We have used the mineralogical study of Walderhaug (2000) together with our cement model, and compared with recorded velocities in dry core plugs. There are 18 core plugs from the same depths as the thin sections. The data are from two wells, A and B, and from four different sands from the Brent formation; Tarbert, Ness, Etive and Rannoch. The framework grains are subjected to widespread coatings of clay minerals, quartz, feldspar and carbonate at various degrees. Extensive clay coating prevents quartz-quartz contacts and precipitation of quartz cement in some areas. This leads to compartmentisation of the rock, with some soft compartments with clay coatings, and some stiffer compartments with quartz cementation. The seismic velocities are thus lower than we expect for a plain quartz cemented sandstone.

We do not have any information about the relative volumes of coating minerals, only the sum of coating minerals, so we have choosen values that seem reasonable. All the plugs are considered to be permeable. The most important minerals and amount of clay coatings can be seen in Table 2. Plugs 1-15 are from well B and 16-18 from A. Plugs 1-4 and 16 are from Tarbert, 5-9 and 17-18 are from Ness, 10-13 are from Etive and 14-15 are from Rannoch.

The modelling results can be seen in Figure 3. The P-wave velocities (V_p) deviate in average 152.2 m/s (4.1 %) from the measured (V_p). S-wave velocities (V_s) deviate up to 450 m/s, and on average 173.0 m/s (7.6 %). The thin sections, which make the foundation of our mineralogical input, represent just a fraction of the length of the core plugs. Thus inhomogenieties in the core plugs might entail different mineralogies and distributions than observed. The largest deviations of the predicted V_s coincide with deviating trends from the linear V_p/V_s ratio. Our model predicts a fairly constant ratio around 1.5, while the plug measurements indicate some strong deviations. The velocities in the plugs from the Rannoch sand seem to be the hardest to reproduce, while the matches for Tarbert sand are very well.

Plug	Q frw	Q cem	D clay	Cl coat
1/2	53.3/50.3	5.3/3.3	3.7/7.3	50.0/27.5
3/4	50.7/49.3	9.7/3.0	4.7/15.7	37.5/37.5
5/6	41.7/45.7	14.7/9.7	8.0/8.0	40.0/33.0
7/8	55.7/47.0	5.3/10.0	8.3/8.0	42.5/40.0
9/10	40.7/50.8	14.7/1.0	4.0/19.3	40.0/20.0
11/12	57.7/55.3	5.7/6.0	6.0/6.3	32.0/30.0
13/14	54.7/35.0	9.3/12.7	2.3/4.3	40.0/40.0
15/16	36.3/56.0	18.0/4.3	4.0/7.7	32.8/60.0
17/18	57.7/45.3	18.0/20.7	4.3/3.7	37.5/32.0

Table 2: The concentrations of the most important minerals in the different plugs. Q is quartz, D denotes detrital. The concentrations are given as percentage of the total rock volume. Cl coat is the percentage volume of the rock that is enveloped by clay coatings.
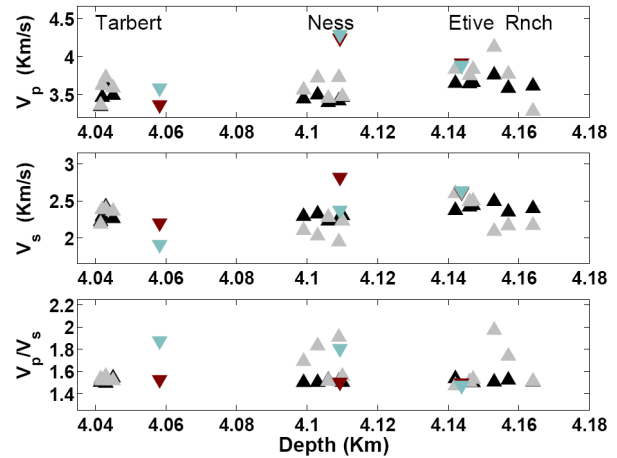

Fig. 3: Comparison between modelled and recorded velocities for dry core plugs. The dark triangles (red and black) are modelled data, while the bright ones (blue and grey) are recorded. The red and blue triangles are from well A, while the black and grey are from B. The sands occurred in different depths in the different wells, so the last coloured sample belong to the Ness sand.

	Q frw	Q cem	D clay	Cl coat
Tarb	53.0/50.0	6.0/5.0	8.5/8.0	52.5/50
Ness	55.0/50.0	13.0/10.0	5.0/6.0	47.5/45
Etive	55.0/55.0	10.0/6.5	4.0/7.0	32.5/37.5
Rnch	45.0/45.0	14.0/14.0	3.0/4.0	27.5/32.5

Table 3: The concentrations of the most important minerals in the different sands. The left and right values belong to well A and B respectively. Q is quartz, D denotes detrital. The concentrations are given as percentage of the total rock volume.

When comparing with well logs, we divide the logs according to the four different sands present. We keep the mineralogy and amount of clay coating equal in each sand. The mineralogies are derived from the core plugs in the corresponding sands. In addition we use the clay content,

A strategy for using mineralogy as input to rock physics modelling of sandstones

porosity, fluid properties, water saturation, and density from log recordings as input in our model. In well A the gas-water contact (GWC) is present at 4163,5 mRKB, while the studied sands of B are all gas/brine saturated. The concentrations of the most important minerals, and amount of clay coatings are given in Table 3. Figure 4 shows the log versus the modelled velocities. The average absolute V_p and V_s deviations are 183.4 m/s and 190.1 m/s in well A respectively, and correspondingly 160.5 m/s and 98.5 m/s in well B. We have used the same number of grain contacts (n = 8.5) and critical porosity (ϕ_0 = 0.36) for all the sands. Adjusting these parameters to each sand, would probably result in better fits.
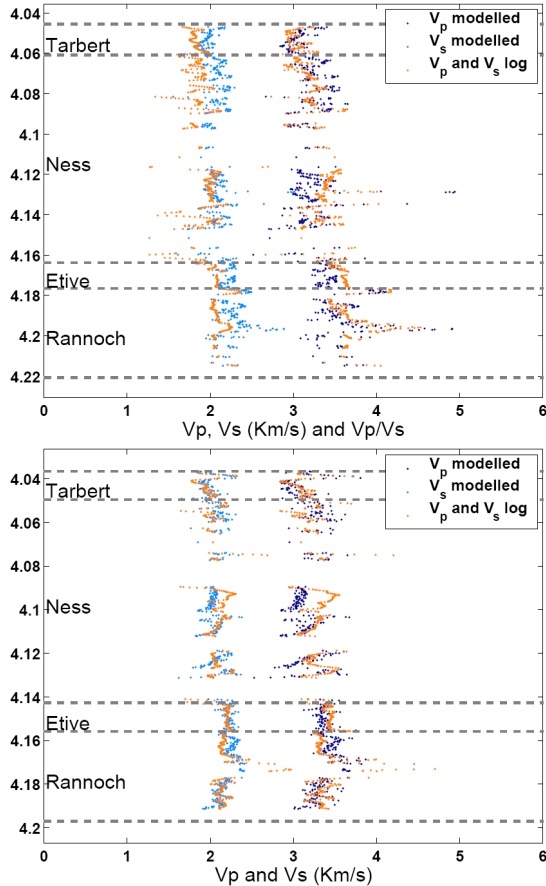

Fig. 4: Log velocities versus modelled velocities. Only sandstones with maximum 30 % clay content are considered in the modelling.

Conclusions

We have defined four distribution types for cement and inclusions in sandstones. By assigning common minerals to the different types, mineral concentration becomes an additional parameter to include in rock physics modelling. This way we account for differences in distributions that could be neglected by considering the rock as only consisting of framework with one homogeneous cement. Our model can also be combined with empirical knowledge of the mineralogy of different depositional settings, to make predictions about expected seismic rock properties. Further, since knowledge about the mineralogy will guide the modelling, we can perform inversion on the rock physics model to reveal which kind of cementation the rock is subjected to, and then try to analyze the mineralogy.

References

Dvorkin, J., and Nur, A., 1996, Elasticity of high-porosity sandstones: Theory for two North Sea data sets: Geophysics, **61**, no. 5, 1363–1370.

Dvorkin, J., Berryman, J., and Nur, A., 1999, Elastic moduli of cemented sphere packs: Mechanics of Materials, **31**, 461–469.

Gal, D., Dvorkin, J., and Nur, A., 1999, Elastic-Wave Velocities in Sandstones with Non-Loadbearing Clay: Geoph. Res. Let., pages 939–942.

Hashin, Z., and Shtrikman, S., 1963, A variational approach to the theory of the elastic behaviour of multiphase materials: J. Mech. Phys. Solids, **11**, 127–140.

Hill, R., 1952, The elastic behavior of crystalline aggregate: Proc. Phys. Soc. London, **A65**, 349–354.

Marion, D., and Nur, A., 1991, Pore-filling material and its effect on velocity in rocks: Geophysics, **56**, 225–230.

Mavko, G., Mukerji, T., and Dvorkin, J., 1998, The Rock Physics Handbook: Tools for seismic analysis in porous media: Cambridge University Press.

Mindlin, R. D., 1949, Compliance of elastic bodies in contact: J. Appl. Mech., **16**, 259–268.

Nishizawa, O., 1982, Seismic velocity anisotropy in a medium containing oriented cracks – transversely isotropic case: J. Phys. Earth, pages 331–347.

Sams, M. S., and Andrea, M., 2001, The effect of clay distribution on the elastic properties of sandstones: Geophysical Prospecting, **49**, 128–150.

Vanorio, T., Prasad, M., and Nur, A., 2003, Elastic properties of dry clay mineral aggregates, suspensions and sandstones: Geophys. J. Int., **155**, 319–326.

Walderhaug, O., 2000, Modeling Quartz Cementation and Porosity in Middle Jurassic Brent Group Sandstones of the Kvitebjørn Field, Northern NORTH Sea: AAPG Bulletin, **84**, no. 9, 1325–1339.

Wang, Z., Wang, H., and Cates, M. E., 2001, Elastic properties of solid clays: Geophysics, **66**, 428–440.

Willis, J. R., 1977, Bounds and self-consistent estimates for the overall properties of anisotropic composites: JMPS, **25**, 185–202.

References

ANJOS, S. M. C., DE ROS, L. F., AND SILVA, C. M. A. (2003). Chlorite authigenesis and porosity preservation in the Upper Cretaceous marine sandstones of the Santos Basin, offshore eastern Brazil. *International Association of Sedimentologists, Special Publication*, **34**, 291–316.

AVSETH, P. A., MUKERJI, T., AND MAVKO, G. (2005). *Quantitative Seismic Interpretation: Applying Rock Physics Tools to Reduce Interpretation Risk* (First edition). Cambridge University Press, Cambridge, UK.

BIOT, M. A. (1956). Theory of propagation of elastic waves in a fluid saturated, porous solid. I. Low-frequency range.. *J. Acoust. Soc. Am.*, **28**, 168–178.

BIRCH, F. (1968). On the possibility of large changes in the earth's volume. *Physics of the Earth and Planetary Interiors*, **1**, 141–147.

BJØRKUM, OELKERS, E., A., P., AND NADEAU, P. H. (1998). Porosity prediction in quartzose sandstones as a function of time, temperature, depth, stylolite frequency and hydrocarbon saturation. *AAPG Bulletin*, **82**, 637–648.

BJØRKUM, P. A. (1996). How important is pressure in causing dissolution of quartz in sandstones?. *Journal of Sedimentary Research*, **A76**, 147–154.

BJØRKUM, P. A. AND NADEAU, P. H. (1998). Temperature controlled porosity/permeabillity reduction, fluid migration and petroleum exploration in sedimentary basins. *Australian Petroleum Production and Exploration Association Journal*, **38**, 453–465.

BJØRLYKKE, K. AND BRENDSDAL, A. (1986). Diagenesis of the Brent sandstone in the Statfjord field, North Sea. *In: Role of Organic Matter in Sediment Diagenesis,*

Society of Economic Paleontologists and Mineralogists, Special Publication, D. L. Gautier, (ed.), **38**, 157–166.

BJØRLYKKE, K. AND HØEG, K. (1997). Effects of burial diagenesis on stresses, compaction and fluid flow in sedimentary basins. *Marine and Petroleum Geology*, **14**(3), 267–276.

BLATT, H., MIDDLETON, G., AND MURRAY, R. (1980). *Origin of sedimentary rocks* (Second edition). Prentice Hall.

CASTAGNA, J. P., BATZLE, M. L., AND EASTWOOD, R. L. (1985). Relationship between compressional-wave and shear-wave velocities in clastic silicate rocks. *Geophysics*, **50**(2), 571–581.

DVORKIN, J., MAVKO, G., AND HEZHU, Y. (1994). Effective properties of cemented granular materials. *Mechanics of Materials*, **18**, 351–366.

DVORKIN, J., MAVKO, G., AND NUR, A. (1991). The effect of cementation on the elastic properties of granular material. *Mechanics of Materials*, **12**, 207–217.

DVORKIN, J. AND NUR, A. (1993). Dynamic poroelasticity: a unified model with the squirt and the biot mechanisms. *Geophysics*, **58**, 524–533.

DVORKIN, J. AND NUR, A. (1996). Elasticity of high-porosity sandstones: Theory for two North Sea data sets. *Geophysics*, **61**(5), 1363–1370.

GARDNER, G. H. F., GARDNER, L. W., AND GREGORY, A. R. (1974). Formation velocity and density - The diagnostic basics for stratigraphic traps. *Geophysics*, **39**(6), 770–780.

GASSMANN, F. (1951). Über die elastisität der poröser medien. *Vierteljahrschrift der Naturforschenden Gesellshaft in Zürich*, **96**, 1–23.

HAN, D., NUR, A., AND MORGAN, D. (1986). Effects of porosity and clay content on wave velocities in sandstones. *Geophysics*, **51**(11), 2093–2105.

HASHIN, Z. AND SHTRIKMAN, S. (1963). A variational approach to the theory of the elastic behaviour of multiphase materials. *Journal of the Mechanics and Physics of Solids*, **11**, 127–140.

HILL, R. (1952). The elastic behavior of crystalline aggregate. *Proceedings of the Physical Society of London*, **A65**, 349–354.

HORNBY, B. E., SCHWARTZ, L. M., AND HUDSON, J. (1994). Anisotropic effective-medium modelling of the elastic properties of shales. *Geophysics*, **59**(10), 1570–1583.

JAKOBSEN, M., HUDSON, J. A., MINSHULL, T. A., AND SINGH, S. C. (2000). Elastic properties of hydrate-bearing sediments using effective medium theory. *Journal of geophysical research*, **105**(B1), 561–577.

JONES, B., RENAUT, R., AND ROSEN, M. R. (2000). Stromatolites Forming in Acidic Hot-Spring Waters, North Island, New Zealand. *PALAIOS*, **15**(5), 450–475.

KATSUBE, T. J. AND WILLIAMSON, M. A. (1994). Effects of diagenesis on shale nano-pore structure and implications for sealing capacity. *Clay Minerals*, **29**(4), 451–461.

KETZER, J. M., MORAD, S., AND AMOROSI, A. (2003). Predictive diagenetic clay-mineral distribution in siliciclastic rocks with a sequence stratigraphic framework. *International Association of Sedimentologists Special Publication*, **34**, 43–61.

KHIDIR, A. AND CATUNEANU, O. (2002). Sedimentology and diagenesis of the Scollard sandstones in South Sentral Alberta. *Bulletin of Canadian Petroleum Geology*, **51**(1), 45–69.

MARION, D. AND NUR, A. (1991). Pore-filling material and its effect on velocity in rocks. *Geophysics*, **56**, 225–230.

MAVKO, G., MUKERJI, T., AND DVORKIN, J. (1998). *The Rock Physics Handbook: Tools for seismic analysis in porous media*. Cambridge University Press, Cambridge, UK.

MAVKO, G. M. AND NUR, A. (1975). Melt squirt in the astenosphere. *Journal of Geophysical Research*, **80**, 1444–1448.

MAVKO, G., MUKERJI, T., AND GODFREY, N. (1995). Predicting stress-induced velocity anisotropi in rocks. *Geophysics*, **60**(4), 1081–1087.

MINDLIN, R. D. (1949). Compliance of elastic bodies in contact. *Journal of applied mechanics*, **16**, 259–268.

NISHIZAWA, O. (1982). Seismic velocity anisotropy in a medium containing oriented cracks – transversely isotropic case. *Journal of Physics of the Earth*, 331–347.

PRIMMER, T. J., CADE, C. A., AND EVANS, I. J. E. A. (1997). Global patterns in sandstone diagenesis: application to reservoir quality prediction for petroleum exploration. *AAPG, Memoir*, **69**, 61–78.

RAMM, M. AND BJØRLYKKE, K. (1994). Porosity/depth trends in reservoir sandstones: Assessing the quantitative effects of varying pore-pressure, temperature history and mineralogy, Norwegian Shelf data. *Clay minerals*, **29**, 475–490.

RAYMER, L. L. HUNT, E. R. AND GARDNER, J. S. (1980). An improved sonic transit time-to-porosity transform. *In: Transactions of the SPWLA twenty-first annual logging symposium*, **21**, P1–P13.

REUSS, A. (1929). Berechtungder fliessgrense von mischkristallen auf grund der plastizitatbedingung fur ein kristalle. *Zeitschrift fur Angewandte Mathematik aus Mechanik*, **9**, 49–58.

ROSSI, C., KALIN, O., ARRIBAS, J., LA IGLESIA, A., AND BARTRINA, T. (2003). Effect of Authigenic Grain-Coating Chlorite on the Resistivity and Reservoir Quality of the Lower Carboniferous RKF Sandstones (Rhourde El Krouf Field, Berkin Basin, Algeria. *AAPG, International Conference & Exhibition, 21-24 September, Barcelona*, A81.

SAMS, M. S. AND ANDREA, M. (2001). The effect of clay distribution on the elastic properties of sandstones. *Geophysical Prospecting*, **49**, 128–150.

SHENG, P. (1990). Effective-medium theory of sedimentary rocks. *Physical Review*, **B41**(7), 4507–4512.

SHENG, P. (1991). Consistent modelling of the electrical and elastic properties of sedimentary rocks. *Geophysics*, **56**, 1236–1243.

STORVOLL, V., BJØRLYKKE, K., KARLSEN, D., AND SAIGAL, G. (2002). Porosity preservation in reservoir sandstones due to grain coating illite: a study of the Jurassic Garn formation from the Kristin and Lavrans field, offshore Mid-Norway. *Marine and Petroleum Geology*, **19**(6), 767–781.

VOIGT, W. (1928). *Lehrbuch der Kristallphysik*. Teubner.

WALDERHAUG, O. (1996). Kinetic modelling of quartz cementation and porosity loss in deeply buried sandstone reservoirs. *AAPG Bulletin*, **80**, 731–745.

WALDERHAUG, O., H., N. P., AND BJØRKUM, P. A. (2002). A quantitative model of mineral diagenesis, porosity reduction and permeability decrease in shales. *Internal research report, STATOIL.*

WANG, Z. (2000a). The Gassmann equation revisited: Comparing laboratory data with Gassmann's prediction. *In: Wang, Z. and Nur, A. (eds.), Seismic and acoustic velocities in reservoir rocks, (3): Recent developments: Society of Exploration Geophysicists, 8–23.*

WANG, Z. (2000b). Velocity relationships in granular rocks. *In: Seismic and Acoustic Velocities in Reservoir Rocks, Rescent Developments, SEG Reprint Series, 3, 377–383.*

WILLIS, J. R. (1977). Bounds and self-consistent estimates for the overall properties of anisotropic composites. *Journal of the Mechanics and Physics of Solids*, **25**, 185–202.

WORDEN, R. H. AND BURLEY, S. D. (2003). Sandstone diagenesis: the evolution of sand to stone. *In S. D. Burley and R. H. Worden, (eds.), Sandstone Diagenesis - Recent and Ancient. Shannon, Reprint Series Vol. 4, International Association of Sedimentologists, 3–44.*

WORDEN, R. H. AND MORAD, S. (2003). Clay minerals in sandstones: controls on formation, distribution and evolution. *International Association of Sedimentologists Special Publication*, **34**, 3–41.

WYLLIE, M. R. J., GREGORY, A. R., AND GARDNER, L. W. (1956). Elastic wave velocities in heterogneous and porous media. *Geophysics*, **21**(1), 41–69.

6 Paper 1

Rock physics modelling of shale diagenesis

Rock physics modelling of shale diagenesis

Anders Dræge, Morten Jakobsen and Tor Arne Johansen

Centre for Integrated Petroleum Research, University of Bergen and Department of Earth Science, University of Bergen, Allegaten 41, 5007 Bergen, Norway

ABSTRACT: A model for estimating the effective anisotropic properties of cemented shales is presented. The model is based on two mathematical methods for estimation of effective properties of a composite medium; a self-consistent approximation and a differential effective medium model. In combination these theories allow approximation of a shale with connected clay minerals and cement, and disconnected pores and quartz grains, which can be compared with the conditions in a real cemented shale. A strategy is also presented for estimation of stiffnesses in the transition zone from mechanical compaction to chemical compaction dominated diagenesis. Combining these theories with a shale compaction theory, enables modelling of the effective elastic stiffnesses for shales from deposition and mechanical compaction to deep burial and chemical compaction/cementing. Results from the model were compared with velocity data from three wells, showing good fit for velocity predictions, following the main velocity trends with increased temperature and depth.

KEYWORDS: *shale, diagenesis, anisotropy, velocity, cementation, rock physics*

INTRODUCTION

Shales play an important role in fluid flow and wave propagation because of their low permeability and anisotropic microstructure. When they overlie hydrocarbon reservoirs, shales can be effective seals. Since shales make up most of the overburden of many of the worlds hydrocarbon-bearing reservoirs, quantitative information about the velocity anisotropy of shales is typically needed for the calibration of amplitude versus offset (AVO) measurements, imaging and processing purposes. The model described in this paper provides a range of stiffnesses from soft and compliant shales that are dominated by mechanical compaction, to hard and rigid shales dominated by chemical compaction/cementation. This paper refers to shale as a sedimentary rock with 50% or more clay minerals in the framework.

Cement in shales can consist of dissolved clay minerals that precipitate as more stable clay minerals and quartz. Calcite cement can precipitate at shallower depths. Cementation stabilizes the rock and inhibits/ceases mechanical compaction. Temperature is commonly the key factor in dissolution and precipitation of clay minerals, since increased temperatures make some of the minerals unstable. At 60–80°C smectite can react to form illite and quartz (Bjørlykke & Aagaard 1992). Bjørlykke & Aagaard (1992) also reported that smectite can dissolve and precipitate as chlorite or corrensite, depending on the mineralogy. Bjørkum & Nadeau (1998) asserted that the dissolution/precipitation processes are linearly dependent on time, and exponentially dependent on temperature. A mineral reaction that exemplified this behaviour was the transformation of kaolinite and K-feldspar to illite, which initiates at around 120°C. Chemical reactions and cementation will take place in sandstones as well, though the initiation temperature and reactants might differ. Dvorkin *et al.* (1994, 1999) and Dvorkin & Nur (1996) presented models for estimating the effective

isotropic properties of cemented sandstones. They treated the rock as an isotropic material with spherical matrix grains, in contrast with the anisotropic shale model presented in this paper.

The study of Bjørkum & Nadeau (1998) indicated that illite precipitation in shales at temperatures of 80–100°C reduces the already low permeability by several orders of magnitude. They asserted that dissolution/precipitation processes can continue mainly independently of fluid pressure and effective stress. The lower limit to which mechanical compaction can reduce the permeability of clay-rich sediments can be estimated to approximately 10^{-6} D (Chen & Nur 1994), but Bethke *et al.* (1988) had already shown that lower permeabilities were needed to maintain high overpressures over geological time. Thus, it is natural to relate further permeability reductions to chemical reactions inside the shale, which is also supported by the observations of Nadeau *et al.* (2002).

The cementation processes can be considered as a transition from 'soft' mudstones and shales to hard and rigid rocks. Theories that describe effective shale properties as a function of mechanical deformation (e.g. Ruud *et al.* 2003) are unlikely to provide a good prediction for the effective properties of cemented shales, since chemical processes and mechanical mechanisms are believed to have distinct effects on both porosity loss and grain–grain contacts. The transition from mechanical compaction-dominated diagenesis in shales, to cementation-dominated diagenesis is illustrated in Figure 1a. The same figure also introduces another modelling problem: the transition from one regime to another is unlikely to be abrupt. Some mechanical compaction is expected in the first stage of cementation, since a certain amount of cement is required to stabilize the rock sufficiently to resist the overburden. Figure 1b demonstrates this by decomposing the porosity loss in the transition zone (TZ) into porosity loss
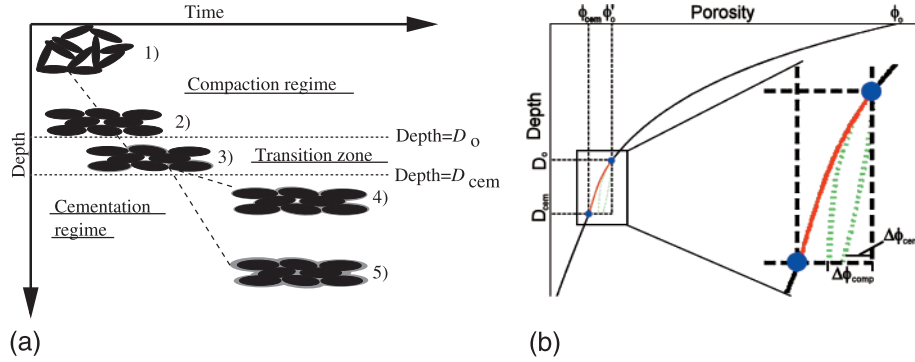
Fig. 1. (**a**) Clay minerals are orientated randomly at deposition (1), but reorientate to a sub-parallel alignment and lose most of their porosity due to mechanical compaction (2). Scattered cementation will create strong bonds in some of the grain contacts in the transition zone (3). The cementation rate increases exponentially with temperature (depth), so a slow rate of burial in the cementation regime leads to lower degree of cementation (4) than a rapid subsidence (5) at the same period of time. D_o and D_{cem} denote the depths at the top and bottom of the transition zone (TZ), respectively. (**b**) A hypothetical porosity–depth curve. In the TZ the sum of the effects of mechanical compaction ($\Delta\varphi_{comp}$) and cementation ($\Delta\varphi_{cem}$) constitute the total porosity loss. φ_o, φ'_o and φ_{cem} denote the initial porosity, the porosity at which cementation starts and the porosity at which mechanical compaction ceases, respectively. The contribution to porosity loss decreases for the mechanical compaction and increases for cementation when the depth in TZ increases.
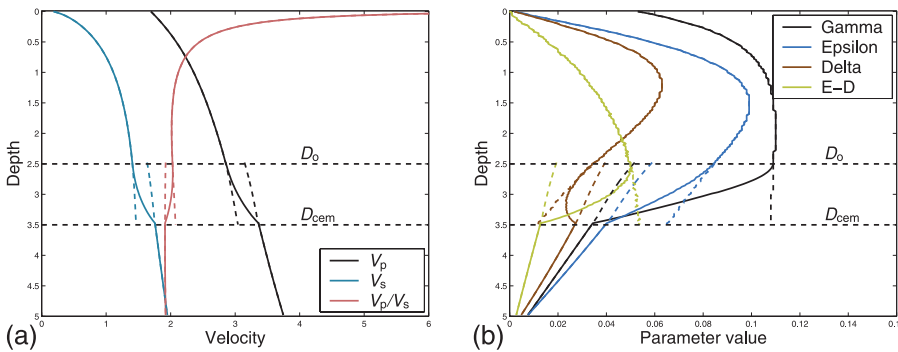

Fig. 2. (**a**) V_p, V_s and the V_p/V_s ratio with depth. Depths are in km; velocities are in km s^{-1}; (**b**) the Thomsen anisotropy parameters. The stippled lines are the elongations of the compaction and cementation trends into the TZ. The porosity in both (a) and (b) follows the same pattern as in Figure 1.

related to mechanical and chemical compaction. Figure 2 shows depth trends for vertical P-wave velocity (V_p), vertical S-wave velocity (V_s) and Thomsen anisotropy parameters, obtained from the models presented in this paper. The results are for a hypothetical shale which follows the porosity–depth pattern shown in Figure 1b. Clearly, the evolution paths of the properties vary between the different stages of diagenesis. The parameter–depth trends alter in the TZ for all parameters, but most significantly for the anisotropy parameters.

This paper presents a model for estimation of the effect of cementation on the effective elastic properties in a shale (cementation model). A strategy for estimating the effective rock properties in the transition from mechanical compaction-dominated to cementation-dominated diagenesis in shales is also introduced. First, some geometrical considerations about cemented shales are presented, followed by a description of the cementation model. Then the focus shifts to the relationship between mechanical and chemical compaction in the TZ. Further, it is demonstrated how stiffnesses and vertical velocities may vary as the shale loses its porosity by mechanical compaction and cementation. The model predictions are tested by comparison with observed vertical velocities from three wells.

CEMENTATION MODEL

Highly compacted shales have low porosity and permeability; however, severely overpressured shales can be undercompacted for a given depth. Cement will entail further permeability reduction, which makes the pores practically unconnected (see Fig. 1). Thus, after a certain amount of cement has precipitated,

the rock is treated as though it consists of continuous phases of clay minerals in the framework and cement in the pore space. It is assumed that when the cement has stabilized the shale enough to prevent further mechanical compaction, the cement can be considered a connected phase. The term 'inclusion' is used on both silt-size quartz particles and fluid-filled pores. In the cementation model, these inclusions are treated as isolated and non-communicating. The flattening of the constituents is defined by the pore aspect ratio, α which is the ratio between the shortest and longest axis of a spheroid. Following Jakobsen et al. (2000, 2001), the cement and pore shapes are considered to have the same aspect ratio as the clay minerals, which is constant with increasing depth and cementation. The shape of the cement minerals compared with matrix clay minerals is decisive for the effect of cementation. In the cementation model the same aspect ratio is assigned to the cement and matrix clay minerals, although grain size and surface area might differ. This makes the cementation model less dependent on cement volume for a given porosity, as long as the shale is pervasively cemented.

The three-step procedure of Hornby et al. (1994) is applied, together with the theories of Jakobsen et al. (2000, 2001) to estimate the effective stiffnesses of the cemented shale. The shale is considered to be an aggregate of building blocks, where the clay minerals in each block are fully aligned, but the orientations of the building blocks vary due to an orientation distribution function (ODF) that will be discussed later. Figure 3 illustrates the five-step modelling procedure. The first step makes use of the self-consistent approach (SCA) (Willis 1977). The basic idea of SCA is that the composite medium itself is
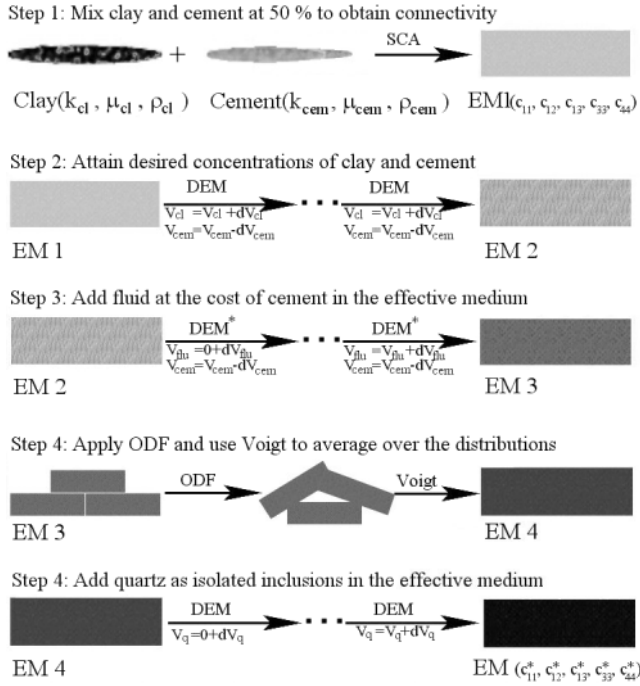
Fig. 3. Illustration of the five steps used to model the stiffness in a cemented shale. SCA, DEM and DEM* are explained more thoroughly in the text. k, μ and ρ denote bulk modulus, shear modulus and density, respectively. The indices cl, cem, flu and q denote clay, cement, fluid and quartz, respectively. Vi (i=cl, cem, flu, q) is the concentration of the different constituents. c_{11}–c_{44} are the stiffnesses of the transversely isotropic medium. ODF, orientation distribution function.

embedded in a homogeneous background medium of yet unknown effective elastic properties. The scattering effect of a wave that travels through this composite medium will be zero, due to destructive interference, if the composite properties of the background medium are those of the effective medium. A consequence of modelling with the SCA model, is that a phase represented by approximately 40% or more (shape dependent) in a composite medium, will constitute a connected phase, opposite to isolated inclusions of lower concentrations (Hornby *et al.* 1994; Jakobsen *et al.* 2000).

Step two utilizes differential effective medium theory (DEM) (Nishizawa 1982) to estimate the effective properties of the two-phase medium at the desired concentrations. The DEM approach utilizes the principle of porosity growth (Cheng 1978) to extend the results of Kuster & Toksöz (1974) to be valid at high porosities. Mechanical interactions between inclusions are modelled by a gradual adding/removing of inclusions to/from the background medium, followed by a calculation of the new effective properties in the medium with new concentrations. The background medium for each small alteration in inclusion concentrations is represented by the effective properties of the last calculation. When the desired concentrations of inclusions are reached, the effective properties of the composite are obtained. As for the SCA model, this model accounts for the effect of interactions of the individual inclusions. But the DEM model has the ability of preserving connectivity status when the concentrations of the constituents change. Thus, connected phases will remain connected when the concentrations change, and vice versa for unconnected phases. New constituents added to the composite media by using DEM, will be added as unconnected inclusions. Variation in the concentration of one of the components will affect all the other concentrations.

If a new phase is introduced in the composite material by reducing the concentration of only one of the constituents, leaving the others unchanged, a modified version of DEM, denoted DEM*, can be applied (Jakobsen *et al.* 2000). The change dC in the effective stiffness tensor C resulting from an increase dv_1, of one material and corresponding reduction dv_2, of material two can be written (Jakobsen *et al.* 2000):

$$dC = \frac{dv_1}{1 - v_1}(C_1 - C)Q_1 - \frac{dv_2}{1 - v_2}(C_2 - C)Q_2 \qquad (1)$$

where Q_i (i=1, 2) is a tensor given by:

$$Q_i = [I + P(C)(C_i - C)]^{-1}.$$

C_1 is the stiffness tensor of the material whose concentration increases with dv_1, and C_2 is correspondingly the stiffness tensor of the material whose concentration decreases with dv_2. I is the identity tensor and v_i denotes the volume concentration of medium i. P is a fourth-rank tensor calculated from the response of a single inclusion embedded in an unbounded matrix of the effective material, and is discussed in Jakobsen *et al.* (2000).

Step 3 uses equation (1) to calculate the effective stiffnesses as fluid (porosity) is introduced to the building block as isolated inclusions at the cost of cement concentration only. This will imitate the reverse cementation process, where cement replaces fluid in the pores. The operation requires that the resulting cement content in step 2 also includes the fluid concentration, since the cement content is reduced further in step 3.

The properties of one single building block of a quartz-free shale with connected clay minerals and cement and isolated pores have now been estimated. Sedimentary materials are commonly complex, with clay mineral orientations that deviate from the fully aligned orientation. Step four assumes that the clay minerals are fully aligned locally, but that the alignment axis varies from place to place. This is modelled by varying the orientations of the building blocks. If the effective properties and the orientations of the building blocks are known, one can estimate the effective stiffnesses of an aggregate of building blocks, which in this case constitute the cemented shale. Johansen *et al.* (2004) studied ODFs for the building blocks of shales. They found that the ODF resulting from vertical mechanical compaction of an initially isotropic (randomly orientated) pure shale can be described as:

$$W_c(\Theta) = \frac{1}{8\pi^2}\frac{c^2}{(\cos^2(\Theta) + c^2\sin^2(\Theta))^{3/2}}, \qquad (2)$$

where Θ is the angle between the short axis of the penny-shaped clay platelets and the vertical axis, and c is the mechanical compaction. c can be expressed by porosity due to mechanical compaction φ_t and critical porosity φ_0:

$$c = \frac{1 - \varphi_t}{1 - \varphi_0}. \qquad (3)$$

Critical porosity for shales can be expressed as a function of quartz content (Ruud *et al.* 2003):

$$\varphi_0 = \frac{1 - v}{\dfrac{1}{0.80} - v} \;, v \leq 0.50, \qquad (4)$$

where $v = \dfrac{v_q}{v_q + v_c}$, v_q and v_c denote the solid fractions of quartz and clay in the shale, respectively ($v_q + v_c = 1 - \varphi$) and 0.80 is the

critical porosity assigned to pure shale. Equation (3) includes only porosity loss that is due to mechanical compaction, since no further alignment of clay minerals is expected as a function of chemical compaction. Estimation of φ_t will be discussed later. The compaction is assumed to take place in the vertical direction only, thus the compacted medium will be vertically transversely isotropic.

Ruud *et al.* (2003) presented a quartz volume-dependent ODF for shales that incorporates the ODF for shales in equation (2). The ODF for a completely random and isotropic medium can be written: $W_i = \frac{1}{8\pi^2}$. The effect of (near-spherical) quartz grains entails an increased randomness in the clay mineral orientation, since the clay must drape around the larger and rounder quartz grains. Thus, the ODF of a shale with quartz inclusions can be approximated by a weighted average of the ODF for pure shale, and the ODF of an isotropic medium:

$$W(\Theta) = v_q W_i + v_c W_c(\Theta). \tag{5}$$

v_c and v_q are normalized to the solid part of the rock volume.

The Voigt (1928) average, which is the upper bound of effective stiffnesses of a mixture, is applied to average over the distribution of building blocks since the latter are considered to be cemented in the boundaries to neighbouring building blocks. A convenient averaging scheme was developed by Morris (1969) and adapted by Sayers (1994). Thus, step four estimates the effective anisotropic stiffnesses of a shale with varying orientations of the building blocks.

The fifth step applies DEM to add isolated quartz inclusions to the building blocks, as shown in the last step of Figure 3. Thus, the effective anisotropic stiffnesses for a shale with connected clay minerals and cement, isolated inclusions of fluid and quartz, and with an estimated internal orientation geometry, is obtained.

ESTIMATION OF COMPACTION AND ODF IN THE TRANSITION ZONE

Equation (2) indicates that the level of mechanical compaction (*c*) has great influence on the orientation of the building blocks. Mechanical compaction will still be effective in a limited depth interval after initiation of cementation. However, the influence of cementation will gradually increase from the depth of initiating cementation, D_o, to a depth D_{cem}, where the rock is strong enough to resist the pressure from the overburden. Then, porosity loss will be dependent on cementation processes alone.

Let φ_o, $\Delta\varphi_{comp}$ and $\Delta\varphi_{cem}$ denote the porosity at depth D_o, and the accumulated positive porosity change due to mechanical compaction and cementation in the TZ respectively, as illustrated in Figure 1. The sum of $\Delta\varphi_{comp}$ and $\Delta\varphi_{cem}$ thus expresses the total porosity changes in the TZ. The porosity loss in shales is related to quartz content (e.g. Ramm & Bjørlykke 1994), so the porosity loss should be estimated for different quartz contents.

The temperature increase with depth is normally considered as a linear function. Thus, since the rate of cement precipitation in a shale is increasing exponentially with temperature, it will also increase exponentially with depth, provided that all the reactants are present at sufficient concentrations.

A weight K_φ must be defined such that when multiplied with the total porosity loss in the TZ, it gives the porosity loss that is due to cementation alone. K_φ should reflect the exponential increase of cement precipitation rate with increasing temperature/depth, by letting the influence of cementation be weak in the first stage of the TZ, while the influence should
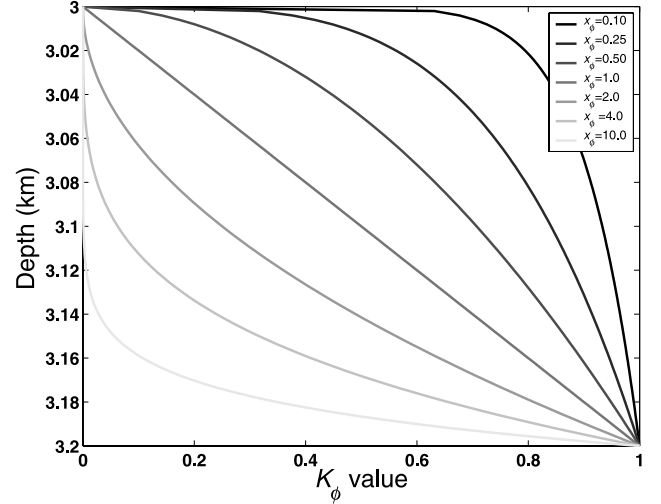

Fig. 4. Different paths from mechanical compaction- ($K_\varphi(1)=0$) to cementation- ($K_\varphi(n)=1$) dominated shales. In this example D_o and D_{cem} are 3.0 km and 3.2 km, respectively.

increase more rapidly near D_{cem}. An appropriate weight with these properties can be written:

$$K_\varphi = [0,dk,2dk,...,ndk]^{x_\varphi}, \tag{6}$$

where the array $[0,dk,2dk,...,ndk]$ is linear and increases with dk in each step. x_φ controls the local dependency of porosity loss on increasing cementation and must be a positive number. Figure 4 shows how the different values of x_φ lead to different paths from completely mechanical compaction-dominated ($K_\varphi(1)=0$) to completely cementation-dominated ($K_\varphi(n)=1$) shales, in the depth interval 3.0–3.2 km. High positive values of x_φ entail an initial slow increase in cementation-related porosity loss, while a value of $x_\varphi=1$ corresponds with a linear transition between the influence of mechanical compaction and cementation on the porosity loss. x_φ is dependent on burial rate and temperature–depth ratio, because these parameters affect the rate of cementation. dk can be chosen due to the desired resolution of the modelling. The lower the value of dk, the smaller the intervals into which TZ is divided. It is crucial that the last element in K_φ equals one, thus the number of elements, *n*, must equal $1/dk$, see equation (6). The depths D, that correspond with the weights can be written as:

$$D = D_0 + K_\varphi^{1/x_\varphi}(D_{cem} - D_0). \tag{7}$$

Since the first and last weights are zero and one, respectively, D will increase linearly from D_o to D_{cem} in *n* steps. The porosity loss due to cementation is now expressed as:

$$\Delta\varphi_{cem} = K_\varphi\Delta\varphi. \tag{8}$$

Since $\Delta\varphi=\Delta\varphi_{cem}+\Delta\varphi_{comp}$:

$$\Delta\varphi_{comp} = (1 - K_\varphi)\Delta\varphi. \tag{9}$$

The total porosity loss in TZ due to mechanical compaction, φ_t, then becomes:

$$\varphi_t = (\varphi_0 - \varphi_0')\Delta\varphi_{comp}, \tag{10}$$

which, combined with equation (3), provides the overall mechanical compaction *c* of the rock. Including the mechanical

Table 1. *Parameters used in the modelling*

	k GPa	μ GPa	ρ g cm^{-3}	α
Clay 1	21.0	7.0	2.60	0.15
Clay 2	25.0	9.0	2.55	0.15
Quartz	37.0	44.0	2.65	1.00
Cement	30.0	12.0	2.62	0.15
Brine	2.96	0.00	1.03	—

The properties k, μ, ρ and α denote the bulk modulus, shear modulus, density and aspect ratio, respectively.

compaction that occurs in the TZ, includes the continuous alignment of the building blocks in the modelling. The alignment is expressed by the compaction-dependent ODFs in equations (2) and (5).

MODELLING OF STIFFNESSES IN THE TRANSITION FROM MECHANICAL COMPACTION-DOMINATED TO CEMENTATION-DOMINATED REGIME

Before cementation the shales are soft and compliant. But, as cementation initiates, the cement will bind the grains together in stronger bonds (Bjørlykke & Høeg 1997). The first cement will thus lead to a significant increase in the overall stiffnesses of the shale. Further cementation will still increase the stiffnesses, but not at the same rate as the initiating cement.

The modelling of stiffnesses in the TZ is a four-step procedure. The first step is to apply the shale compaction model of Ruud *et al.* (2003) in the interval D_o–D_cem to estimate the effective properties of a shale with no cement, but otherwise the exact same component properties as the cemented shale. This modelling obtains the stiffnesses in a hypothetical case, where the cementation does not influence the stiffening of the rock. The next step models the partly cemented shale in the interval D_o–D_cem as if it were independent of mechanical compaction, by following the steps in the cementation model. Thus, we obtain the stiffnesses of a shale with a connected cement phase (e.g. illite), and where porosity loss is due to chemical compaction alone.

The third step is to apply a weight on the same form as in equation (6), which controls the ratio of the influence of mechanical compaction and cementation on stiffnesses in the TZ. For estimation of stiffnesses, let K_c and x_c correspond to K_φ and x_φ in equation (6). Thus, K_c and x_c control how fast the cementation will dominate the stiffness increase in a partly cemented shale. K_c should reflect the strong effect the first cement has on the shale. The lower the positive value of x_c, the faster the model will treat cementation as the dominating mechanism for increasing stiffnesses (see Fig. 4). x_c is related to
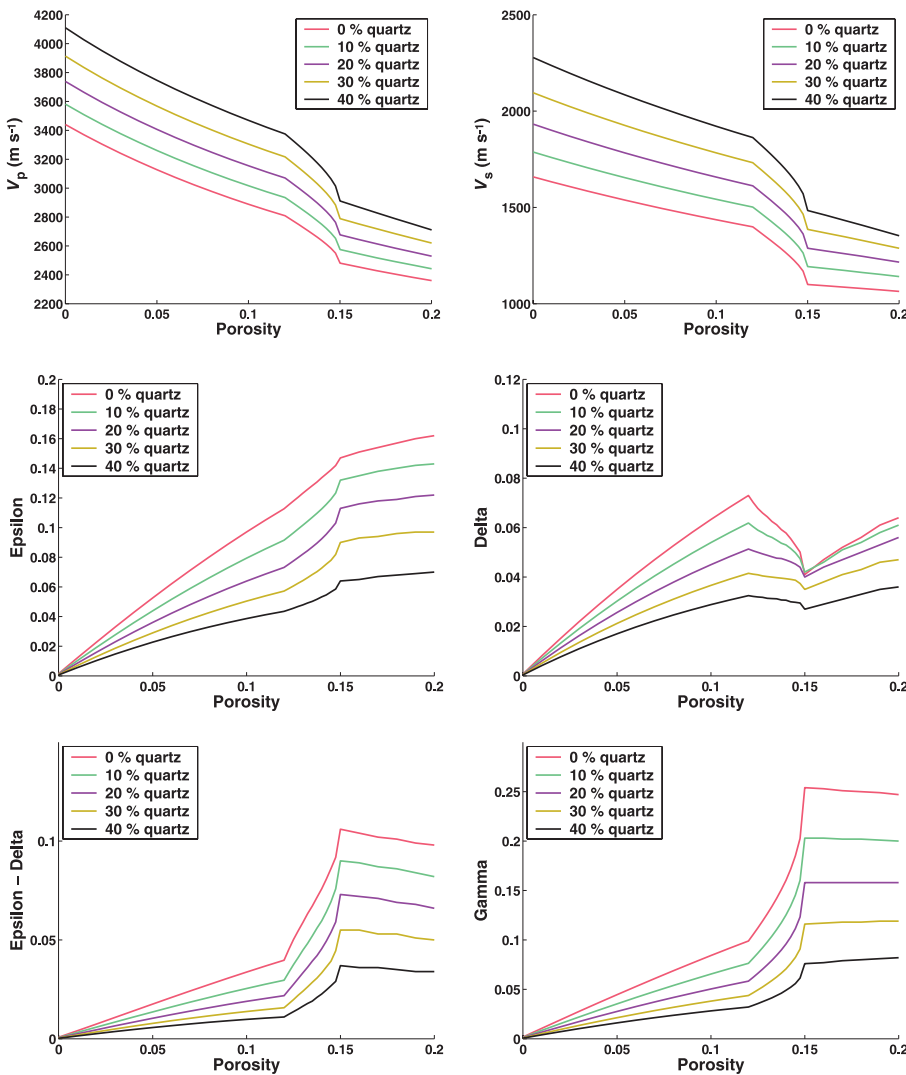

Fig. 5. Modelled vertical V_p and V_s and Thomsen anisotropy parameters as they vary with mechanical compaction- and cementation-related porosity loss and quartz concentration. Porosity is a fraction of rock volume.
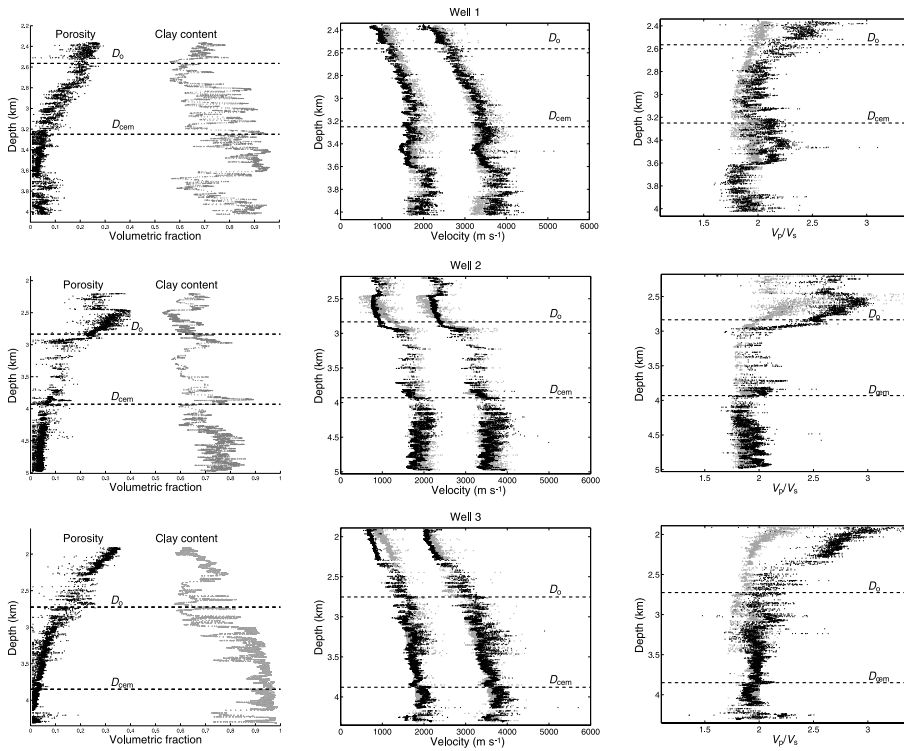
Fig. 6. Modelled velocity data (grey) compared with log velocity data recorded in three different wells (black). The clay content is normalized to the matrix volume, while the porosity is normalized to the total rock. The log recordings with less than 50% clay in the matrix are excluded from the figures and the modelling. In all wells D_o and D_{cem} are at 60°C and 100°C, respectively.

x_φ since the amount of precipitated cement affects the influence of cementation on both porosity and stiffnesses. But unlike x_φ, the value of x_c is also dependent on the way the first cement precipitates. If all the initiating cement precipitates in the contact areas of the framework grains, or bridges the pores, the stiffnesses will increase rapidly, and x_c will have a lower value than if cement precipitated in the pore space between the contacts. The weight $(1 - K_c)$ is assigned to the compaction-related stiffnesses. K_c increases from 0 at D_o to 1 at D_{cem}, which makes the influence of compaction diminish through TZ, and cease at D_{cem}.

The final step in this procedure is to use the stiffnesses for the uncemented and cemented shale together with K_c, and apply the Voigt–Reuss–Hill (VRH) average (Hill 1952) to estimate the effective rock properties for the depths in the TZ. The average tensor thus represents the overall stiffnesses of the partly cemented shale, in the transition to a state where no further compaction occurs.

RESULTS

Porosity loss and mechanical compaction

The following examples model the influence of cement content on the effective properties in an anisotropic cemented shale.

Table 2. *Results from modelling velocities in well 1, well 2 and well 3*

	Well 1 V_p/V_s	Well 2 V_p/V_s	Well 3 V_p/V_s
Mechanical compaction	150.2/242.1	105.4/178.4	168.5/318.9
Transition zone	98.3/110.1	168.7/217.3	114.1/93.5
Cementation	172.7/159.4	126.7/111.0	130.4/132.2
Whole log	144.1/153.3	129.6/150.8	132.8/164.5
Percent deviation	4.4%/9.5%	4.1%/9.9%	4.2%/10.6%

Columns 2–4 show the absolute P- and S-wave velocity deviation from the log velocities. The overall V_p/V_s ratio in wells 1–3 deviated 7.8%, 9.6% and 16.8%, respectively.

The starting point in the modelling is a hypothetical shale where the porosity is reduced from 20% to 15% (depth = D_o) by mechanical compaction. The TZ is defined to occur from 15% to 12%. Reduction of the porosity from 15% to 12% corresponds with the depth interval D_o–D_{cem}, where mechanical compaction and cementation processes both occur. Further porosity reduction below D_{cem} is considered to be due to cementation processes alone. For simplicity, it is assumed that the precipitation of cement accounts for half of the porosity loss, and chemical compaction as a result of dissolved framework causes the other half, i.e. the shale is considered a closed dissolution/precipitation chemical system for cementation.

The values of x_φ and x_c are related to 2 and 1/2, respectively. The total mechanical compaction is modelled by using equations (8)–(10) and (3) and defines the input to equation (2). Porosity reduction due to mechanical compaction dominates the shallow part of the TZ, while cementation dominates the deeper part.

Vertical velocities and elastic stiffnesses

Table 1 shows the parameters used in the modelling; the clay properties of clay 1 were used. Clay 1 parameters were adopted from Tosaya (1982) and clay 2 parameters from Han *et al.* (1986). Figure 5 shows modelled V_p and V_s for decreasing porosities/increasing depth. As expected, the velocities increase with increasing quartz content and decreasing porosity. The velocity increase is markedly larger in the TZ than in the cementation regime. This reflects the choice of x_c, which determines that the first cement is considered to strengthen the contacts between the grains and/or bridge the pores. The effect of further cementation in an already cemented shale will be smaller, as seen in Figure 5.

The modelled Thomsen's anisotropy parameters are given in the same figure. The ε and γ plots show that the anisotropy decreases with increasing quartz content in the shale. Quartz content is decisive for the anisotropy behaviour as cementation
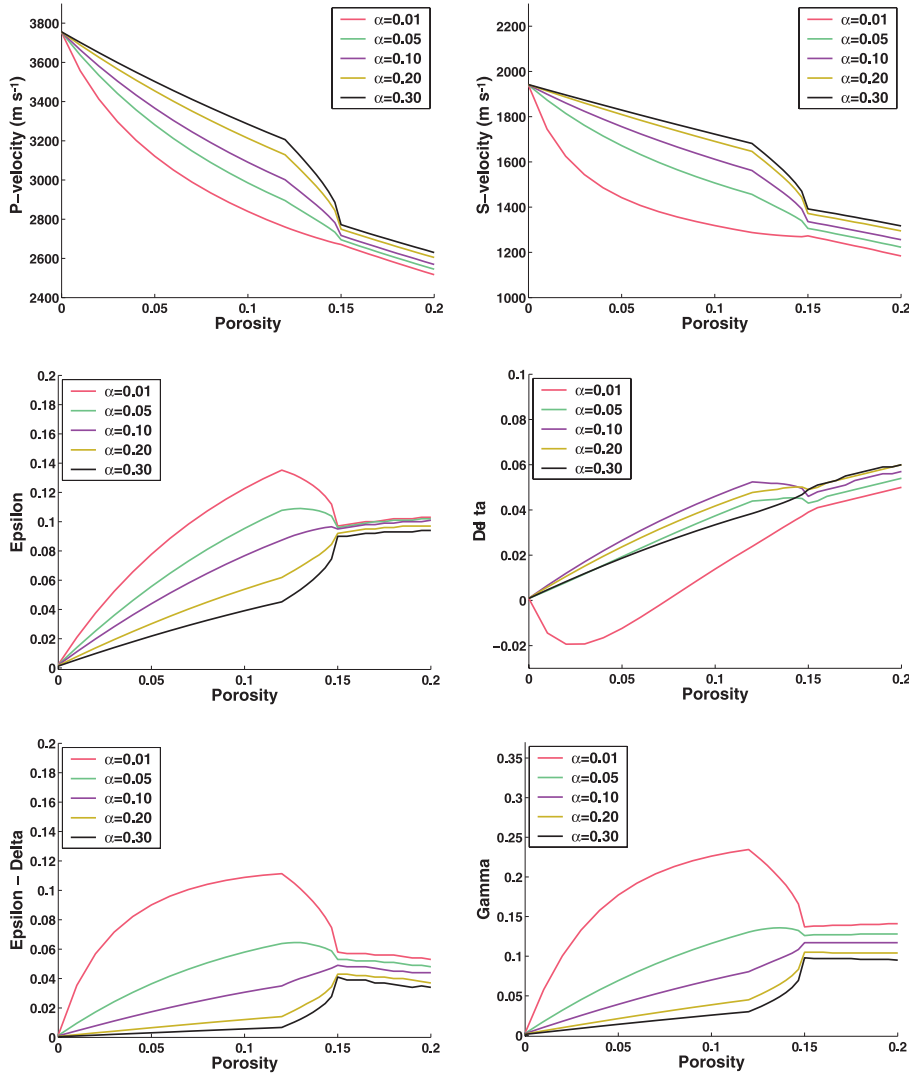
Fig. 7. Modelled effective properties of a cemented shale with varying constituent aspect ratio (α). Porosity is a fraction of rock volume.

starts. ε decreases most for shales with around 20% quartz content, while γ decreases most for quartz-free shales, when the shale enters the TZ. The plots show that the cementation model predicts lower γ dependency of quartz content than does the compaction model. This is partly due to the two different ways these models handle the aspect ratio of the pores. The compaction model of Ruud *et al.* (2003) suggests that a decreases continuously during mechanical compaction, while the cementation model uses a constant pore aspect ratio for all porosities. In the cementation regime, the modelled ε and γ anisotropy decreases most for shales with low quartz content.

The δ-plot shows that the δ values increase when cementation starts. The increase is most pronounced for shales with low quartz contents. But with further cementation, the δ values decrease smoothly towards zero. All the constituents in Table 1 are considered isotropic as they are, but the shape (a) of the grains and inclusions induce the anisotropy in the composite media.

Modelling real data

The model has been compared with vertical P- and S-wave velocities of shales recorded in three wells. Anisotropy data were unavailable, so there is no real control data to support predicted anisotropy–depth trends. The wells penetrate horizontal shales vertically. The brine properties, densities,

porosities and clay contents from the logs are used as input in the modelling. Wells 1 and 3 are modelled with clay 1, while clay 2 gives the best fit for well 2. To estimate cement concentrations, the porosity–depth curves for different quartz contents are first approached by second-order curve fitting. Theories shown previously are used to estimate how much of the porosity loss in the TZ is due to cementing. At depths deeper than D_{cem} it is assumed that all porosity loss is due to cementation processes and, as before, half of the porosity loss is dedicated to cement precipitation. D_{o} and D_{cem} are set to depths corresponding to 60°C and 100°C, respectively. Table 1 shows the properties of the constituents used in the modelling. The same values for the TZ parameters (2.0 and 1/2) for x_{φ} and x_{c}, have been applied for all wells.

Figure 6 and Table 2 shows that the modelled V_{p} and V_{s} mimic the log-recorded velocities quite well. At some intervals the velocities deviate 200–300 m s^{-1} on average from the log velocities, and a few places even more. But all modelling follows the main trends of the recorded velocities with increased mechanical compaction and cementation. The largest deviations occur in the uncemented part, especially for V_{s}, which seems to be modelled too high. It has been observed previously (Ruud *et al.* 2003) that the mechanical compaction model has a tendency to predict too high S-wave velocities. Velocities in the TZ are modelled very well for all wells. The
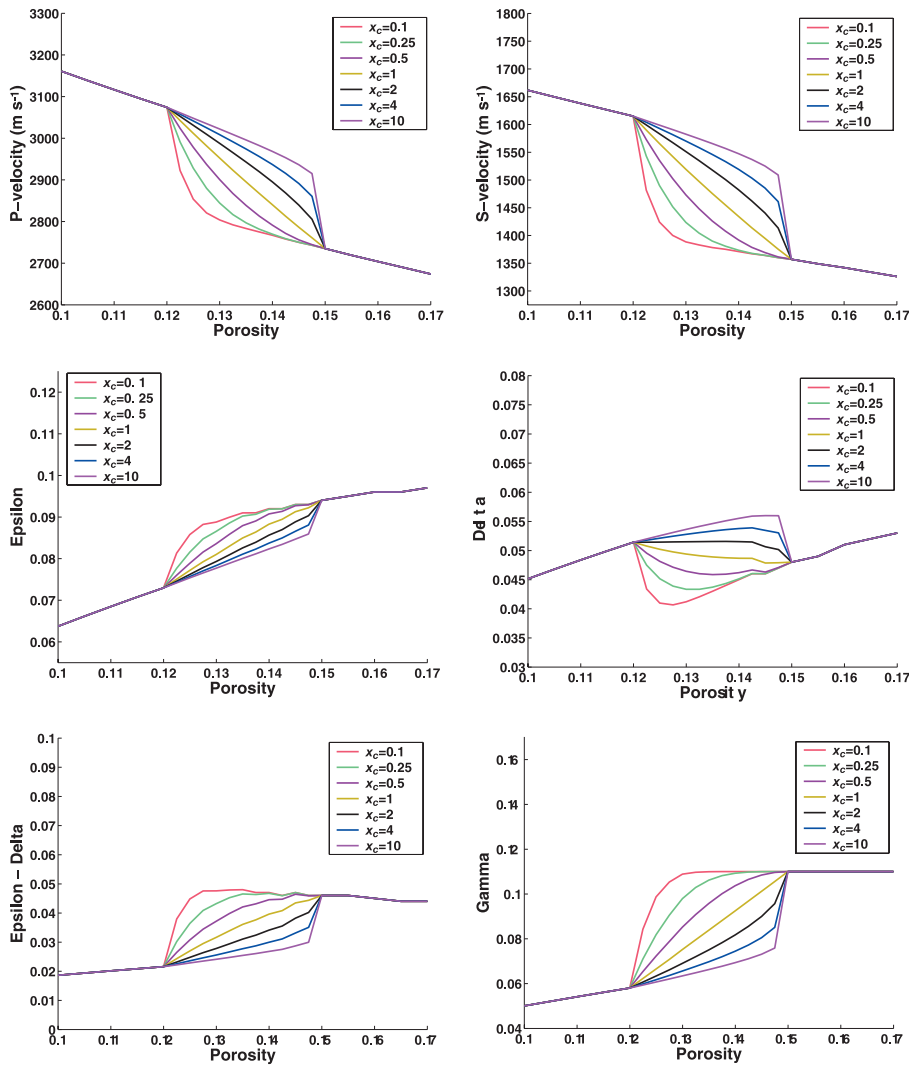
Fig. 8. Different modelled paths between mechanical compaction regime and cementation regime, as a function of x_c. Outside the TZ (12–15% porosity) all the graphs coincide. Porosity is a fraction of rock volume.

cementation model also produces modelled velocities which mainly coincide with the log data.

DISCUSSION

In order to study quartz cementation in sandstones, there exist models for estimating cement volumes mainly as a function of temperature. One such model has been presented by Walderhaug (1996). A similar model for shales and clay cementation could be combined easily with the modelling strategy presented in this paper. Conversely, the theories for compaction and cementation in the TZ can be applied in rock physics modelling of cemented sandstones.

The chemical reaction rates in shales are dependent mainly on temperature, and they appear to be less time dependent than those in sandstones (Bjørkum & Nadeau 1998). Thus, information is needed about the burial history of the rock to model the temperature history. Rocks that have been subjected to uplift/erosion will display a more pronounced cementation than expected from rocks at the same depth/temperature that have not been subjected to uplift/erosion. It is assumed that there are no uplift effects in the real data analysis.

It is hard to obtain numerical values of some of the parameters in the cementation model. In this modelling the cement properties have been defined to lie between the properties of clay and quartz. The cement volume is calculated from the porosity losses for different quartz contents. But the

model is not very sensitive to different concentrations of the cement and the cement properties, as long as the fluid porosity is unchanged. Thus, these uncertainties are not crucial for model predictions. The shapes of the inclusions have a larger influence on the result.

Figure 7 illustrates the modelled effective properties of a cemented shale with 20% quartz, and the material properties as defined in Table 1. For the cementation model, the aspect ratio of the pores, cement and clay mineral vary, while only the shape of the clay mineral varies in the compaction model. This is because the compaction model expresses the pore aspect ratio as a function of mechanical compaction. Thus, the different approaches entail the discontinuities in the TZ. Figure 7 clearly shows that the degree of elongation of the constituents will have great influence on the vertical velocities and the degree of anisotropy in the rock. The cement and pores are considered to have the same shape as the clay minerals, while the quartz grains are approximated by spherical inclusions. The modelling indicates that the stiffnesses of a cemented shale are more dependent on the shape of the components, than a shale that has only been subjected to mechanical compaction.

x_c implicitly contains information about cement distribution. Figure 8 shows how the modelled anisotropy and vertical velocities will vary for different values of x_c in the TZ. The shale used in the modelling consists of 20% quartz in the matrix, and the component properties are given in Table 1. By

comparing the model to observed data, x_c can be found and analysed. The curves for the three lowest values of x_c in Figure 8, imply that a significant amount of the cement is precipitated in the pore space between the grain contacts. Thus, the cement will contribute little to the overall rock stiffnesses, until the cement concentration becomes so large that cement bridges the pores or starts to precipitate in the grain contacts. The curves with x_c values higher than one indicate that the concentration and distribution of the initial cement precipitated are capable of increasing the rock stiffnesses from the start of TZ. The effect of varying x_φ is much smaller, since the fluid porosity is the same, regardless of x_φ, and only the framework–cement ratio is affected.

An assumption has been made that the mechanical compaction is the only mechanism that enhances the alignment of framework grains for a given clay/quartz ratio. Pore geometry is considered constant with depth, and does not influence grain nor cement alignment in the cementation model. But cementation can influence the alignment in theory; if the dissolved materials are not aligned and precipitate on aligned grains, or vice versa, the cementation will affect the alignment. This effect is assumed to be very small, and negligible for the results.

Shales that are severely overpressured have anomalously high porosities when entering the TZ. They need more cement to stabilize the grain contacts than shales with lower porosities. This increases the TZ interval for the high porosity overpressured shale. The overpressure will not directly affect the precipitation rate, since cementation is practically independent of pressure (Bjørkum & Nadeau 1998). But uncemented fractures that result from overpressure will entail lower stiffnesses in the rock. The model does not include fracture effects and will thus predict too high rock stiffnesses where these occur.

CONCLUSIONS

A strategy has been presented to predict velocities and anisotropy for shales and silty shales from shallow to deep burial, in a basin with a given thermal history. Since the diagenetic processes vary according to burial depth and thermal history, the rock physics models must account for both mechanical and chemical compaction. A rock physics model that predicts effective properties of cemented shales has been suggested. The model is combined with an existing model for uncemented shales to cover the whole range of diagenetic changes from shallow to deep burial/high temperature.

During burial, the rock enters a depth/temperature interval (transition zone) where both chemical and mechanical compaction are active. Here, the shale compaction model and the shale cementation model are combined to produce effective rock properties in the transition zone.

The model showed consistent results when comparing vertical P- and S-wave velocities with logs from three wells. However, there are is no data control to evaluate the anisotropy–depth predictions. Results from the model can be applied readily in AVO and velocity analysis. The proposed strategy for estimating stiffnesses in the transition zone can be adopted easily in rock physics modelling of sandstones.

REFERENCES

Bethke, C.M., Harrison, W.J., Upson, C. & Altaner, S.P. 1988. Supercomputer analysis of sedimentary basins. *Science,* **239**, 261–267.

Bjørkum, P.A. & Nadeau, P.H. 1998. Temperature controlled porosity/permeabillity reduction, fluid migration and petroleum exploration in sedimentary basins. *Australian Petroleum Production and Exploration Association Journal,* **38**, 453–465.

Bjørlykke, K. & Aagaard, P. 1992. Clay minerals in North Sea sandstones. *In:* Houseknecht, D.W. & Pittman, E.D. (eds) *Origin, diagenesis, and petrophysics of clay minerals in sandstones.* SEPM Special Publication, **47**, 65–80.

Bjørlykke, K. & Høeg, K. 1997. Effect of burial diagenesis on stresses, compaction and fluid flow in sedimentary basins. *Marine and Petroleum Geology,* **14**, 267–276.

Chen, Q. & Nur, A. 1994. Critical concentration models for porous materials. *In:* Corapcioglu, M.Y. (ed.) *Advances in Porous Media,* **2**. Elsevier, Amsterdam, 169–308.

Cheng, C.H. 1978. *Seismic velocities in porous rocks: Direct and inverse problems.* PhD thesis. Massachusetts Institute of Technology, Cambridge, Massachusetts, USA.

Dvorkin, J. & Nur, A. 1996. Elasticity of high porosity sandstones: Theory for two North Sea data sets. *Geophysics,* **61**, 1363–1370.

Dvorkin, J., Mavko, G. & Hezhu, Y. 1994. Effective properties of cemented granular materials. *Mechanics of Materials,* **18**, 351–366.

Dvorkin, J., Berryman, J. & Nur, A. 1999. Elastic moduli of cemented sphere packs. *Mechanics of Materials,* **31**, 461–469.

Han, D., Nur, A. & Morgan, D. 1986. Effects of porosity and clay content on wave velocities in sandstones. *Geophysics,* **51**, 2093–2105.

Hill, R. 1952. The elastic behavior of crystalline aggregate. *Proceedings of the Physical Society of London,* **A65**, 349–354.

Hornby, B.E., Schwartz, L.M. & Hudson, J. 1994. Anisotropic effective-medium modelling of the elastic properties of shales. *Geophysics,* **59**, 1570–1583.

Jakobsen, M., Hudson, J.A., Minshull, T.A. & Singh, S.C. 2000. Elastic properties of hydrate-bearing sediments using effective medium theory. *Journal of Geophysical Research,* **105** (B1), 561–577.

Jakobsen, M., Johansen, T.A. & Ruud, B.O. 2001. Modelled velocity and reflectivity properties of anisotropic hydrated sediments. *Journal of Computational Acoustics,* **9**, 1507–1522.

Johansen, T.A., Drottning, A., Lecomte, I. & Gjøystdal, H. 2002. An approach to combined rock physics and seismic modelling of fluid substitution. *Geophysical Prospecting,* **50**, 119–137.

Johansen, T.A., Ruud, B.O. & Jakobsen, M. 2004. Effects of grain scale alignment on seismic anisotropy and reflectivity of shales. *Geophysical Prospecting,* **52**, 133–149.

Kuster, G.T. & Toksöz, M.N. 1974. Velocity and attenuation of seismic waves in two-phase media: Part I. Theoretical formulations. *Geophysics,* **39**, 587–606.

Morris, P.R. 1969. Averaging fourth-rank tensors with weight functions. *Journal of Applied Physics,* **40**, 447–448.

Nadeau, P.H., Peacor, D.R., Yan, J. & Hiller, S. 2002. I/S precipitation in pore space as the cause of geopressuring in Mesozoic mudstones, Egersund Basin, Norwegian Continental Shelf. *American Mineralogist,* **87**, 1580–1589.

Nishizawa, O. 1982. Seismic velocity anisotropy in a medium containing oriented cracks – transversely isotropic case. *Journal of Physics of the Earth,* **30**, 331–347.

Ramm, M. & Bjørlykke, K. 1994. Porosity/depth trends in reservoir sandstones: Assessing the quantitative effects of varying pore-pressure, temperature history and mineralogy, Norwegian Shelf data. *Clay minerals,* **29**, 475–490.

Ruud, B.O., Jakobsen, M. & Johansen, T.A. 2003. *Seismic properties of shales during compaction.* 73rd SEG Meeting, Expanded abstracts, Dallas, Texas, 1294–1297.

Sayers, C.M. 1994. The elastic anisotropy of shales. *Journal of Geophysical Research,* **99** (B1), 767–774.

Tosaya, C.A. 1982. *Acoustical properties of clay-bearing rocks.* PhD thesis. Stanford University, USA.

Voigt, W. 1928. *Lehrbuch der Kristallphysik.* Teubner, Leipzig.

Walderhaug, O. 1996. Kinetic modelling of quartz cementation and porosity loss in deeply buried sandstone reservoirs. *AAPG Bulletin,* **80**, 731–745.

Willis, J.R. 1977. Bounds and self-consistent estimates for the overall properties of anisotropic composites. *Journal of the Mechanics and Physics of Solids,* **25**, 185–202.

7 Paper 2

A strategy for modelling diagenetic evolution of seismic properties in sandstones

A strategy for modelling diagenetic evolution of seismic properties in sandstones

Anders Dræge[1,2], **Tor Arne Johansen**[1,2], **Ivar Brevik**[3] **and Camilla Thorsen Dræge**[4]

[1]*Department of Earth Science, Allegaten 41, 5007, University of Bergen, Norway*

[2]*Centre for Integrated Petroleum Research, Allegaten 41, 5007 Bergen, University of Bergen, Norway*

[3]*Statoil Research Centre, Rotvoll, 7005 Trondheim, Norway*

[4]*Norsar, Thormøhlensgate 49, 5006, Bergen, Norway*

(E-mail: Anders.Drage@geo.uib.no)

ABSTRACT: *The geometrical distribution of different components in a composite sandstone is decisive for the overall rock stiffness and velocities. Information about which constituents are e.g. loadbearing, dispersed in pore fluid or contact cementing is therefore necessary to perform a reliable modelling of the seismic properties. Based on thin section observations from a number of authors, a distribution classification for quartz cement, K-feldspar and some of the most common clay minerals in sandstones; illite, kaolinite, smectite and chlorite is suggested. This classification makes it possible to perform rock physics modelling as a function of concentrations of the different minerals in a rock. A composite rock physics model that accounts for various simultaneous combinations of mineral distributions has been developed. Different minerals tend to follow different and predictable paths during burial and temperature increase. Well known mineral reactions are used to make simple modelling of mineralogy versus temperature (depth) for different starting scenarios. The obtained mineralogy trends are further used as input to our rock physics model, to produce the diagenetic evolution of the seismic rock properties for different mineralogical starting points. This strategy is then used to estimate the effective rock properties of sandstones in a well log. The modelling enables considerations of possible mineralogies and distributions from seismic parameters. Finally, reflection coefficients that result from sands that have been subjected to various diagenetic processes are modelled and analysed. The modelling is able to discriminate between the reflections from a selection of common diagenetic scenarios.*

KEYWORDS: *sandstone, diagenesis, mineralogy, velocity, cementation, rock physics*

INTRODUCTION

Quartz is rarely the only solid component in sandstones, and Worden & Morad (2003) described several ways that clay minerals can be incorporated into sandstones. Amongst others, Anstey (1991), Dvorkin & Nur (1996), Gal et al. (1999) and Sams & Andrea (2001) stated that the elastic moduli of shaly sandstones strongly depend on both volume and position of clay. Thus two different sandstones with the same clay volume might have significantly stiffness differences, due to clay distribution. Sams & Andrea (2001) defined four different distributions of clay; between grain contacts, framework clay-rich grains (structural), in the pore space as dispersed clay (pore-filling or pore-lining), and clay lamination. They presented four distinct models for estimating the effects of

structural, dispersed and laminated clay on sandstones. They did not model contact cement explicitly, nor did they study the effects of more than one distribution of clay at the same time, like structural and dispersed. A rock physics model that aims to mimic a real sandstone with clay minerals, should include varieties of simultaneous clay distributions, to reflect the conditions in a real rock. A model for estimating effective anisotropic rock properties in shales during diagenesis is presented by Dræge et al. (2006).

In this paper, any mineral that is precipitated in the rock after deposition is termed cement. Precipitation of minerals is just chemical reactions which can be predicted, given the constituents and the environment. The mineral reactions follow certain chemical/physical laws, and stick to certain trends. Geologists and geochemists have recognized different temperature intervals where certain detrital (present at deposition) minerals dissolve and reprecipitate as authigenic (formed in situ during diagenesis) cementing minerals (e.g. Bjørlykke & Aagaard, 1992; Bjørkum, 1996; Ketzer et al., 2003; Worden & Morad, 2003). Thus they provide the constituents and their concentrations, but that is not sufficient for implementation into rock physics. Rock physicists also need to seek for patterns in distributions of constituents, because of the great influence it has on the overall stiffness. Thus a clay distribution classification for the most common clays in sandstones is suggested, based on thin section observations from a number of authors. The classification is combined with the geological knowledge of some of the most essential mineral reactions in sandstones. This enables us to make theoretical predictions of the evolution of the composition and distribution of a rock during diagenesis. Further, an attempt to create a rock physics model that incorporates the composite effect of the different types of mineral distributions is described. Micromechanical models like the ones applied, may in some cases have limited validity. But the essential part of this research

is the integration of geological processes and constraints with rock physics modelling, not the rock physics model itself. The obtained rock physics model allows us to make predictions of the diagenetic evolution of the seismic rock properties, given mineralogy and porosity during diagenesis. Hence, the quality of the mineralogy and porosity estimation influences the quality of the rock physics modelling. It should be emphasized that this paper presents a rock physics model and a modelling strategy, not a study in advanced geological modelling. Hence a simplified and insufficient porosity model has been used in the introductory examples. But when keeping the porosity-depth model constant for various mineralogy-depth scenarios, the differences that arise from porosities are excluded. When comparing the model with real data, well-log porosities are applied, to ensure realistic input to the rock physics model.

DISTRIBUTION TYPES AND ROCK PHYSICS MODELS

The distributions are defined for the solid constituents in the sandstone, except for framework quartz. Framework quartz is a "reference medium", which the distributions of other constituents are defined relative to. Four different distribution types are defined; **i)** cement that lies in the grain contacts, but not between grains, and stabilizes the contacts between framework grains, **ii)** pore-filling cement that contributes little to the overall rock stiffness until they become pore-bridging when presented at approximately 40 % or more in the pores, **iii)** graincoating and pore lining cement, that envelop the framework grains, but does not carry load in the framework grain-grain contacts, **iv a)** replacive clay or clay clasts which act as a part of the loadbearing framework and **iv b)** graincoating clay cement that prevent contact between the framework grains, and thus are loadbearing. Figure 1 illustrates the mineral distribution types. The text above each stage indicates the rock physics model applied in

the modelling. It is assumed that when cement content exceeds 50 % of the intergranular volume (i.e. the volume that is not occupied by the framework), the rock starts to become increasingly seismic impermeable until cement content exceeds 75 %, at which the rock is considered to have lost all its seismic permeability. Seismic permeability denotes the ability for fluid to move to neighbouring pores when a seismic wave travels through the rock, not permeability over longer time scales. Thus seismic isolated pores (seismic permeability = 0) should not be confused with completely isolated pores over geological time. The limits for seismic permeability changes can be adjusted, due to local differences in pore size. Small pores with narrow pore-throats are more prone to seismic isolation due to pore-filling cements than more spacious pores. Decreasing fluid mobility leads to enhanced rock rigidity (Wang, 2000). The rock physics models are chosen to reflect the increasingly seismic isolation of pores when pore space is reduced. In transitions from uncemented to cemented rock, and from seismic permeable to seismic impermeable rock, the Hill average (Hill, 1952) is applied between the different rock physics models shown in Figure 1, to obtain smooth transitions in the cement intervals 0-5 % and 50-75 % of the intergranular volume, respectively. The weighting function used when applying the Hill average is discussed in the appendix.
The DEM (Differential Effective Medium, Nishizawa, 1982) approach can be formulated by a set of differential equations where the physical analogue is that the inclusions are gradually embedded in or removed from the background medium. The procedure may be applied as follows (Johansen
et al., 2002): i) Start with a background medium with known properties, in our case framework quartz. ii) Embed or remove inclusions (e.g. pores or cement) to form a new composition. iii) Compute the effective properties which define the new background medium. Repeat ii) and iii) until the actual material composition is reached, at which the required elastic properties will be obtained.

New constituents that are added to the composite media using DEM will be added as unconnected seismic isolated inclusions. When using DEM for mixing framework quartz with isolated clay clasts and pores, quartz and clay is first mixed, and then the obtained effective framework is mixed with pores.

The CEMT (Combined Effective Medium Theory) model is applied to approach connected phases in a composite medium. The theory consists of two steps, where the first step makes use of the Self Consistent Approach (SCA) (Willis, 1977). The SCA model accounts for interactions between inclusions when a wave travels through the medium, by treating all constituents of the composite as embedded in a 'virtual' medium that has the required effective medium properties. The SCA solution occurs when the net (scattering) effect of all the inclusions is zero. The term 'self-consistent' means that the results do not depend on a selection of host medium to embed the remaining constituents, but do only depend on their volume fraction. If the concentrations of the constituents in a two phase medium are between approximately 40-60 %, the SCA solution will correspond to the effective properties of a two phase medium in which both phases constitute connected phases in the composite medium (Hornby et al. 1994; Jakobsen et al. 2000). The second step of the CEMT is utilizing DEM to estimate the effective properties of the two phase medium at the desired concentrations. The DEM model has the ability of preserving connectivity status when the concentrations of the constituents change. Thus connected phases will remain connected when the concentrations change, and vice versa for unconnected phases. CEMT is used to model connected cement/inclusion phases when the concentration of type **iii)** cement exceeds 50 % of intergranular volume.

Permeable rock with distribution type **ii)** and **iv a,b)** and uncemented rock is modelled with the combined theories of Hertz-Mindlin (HM) (Mindlin, 1949) and Hashin and Shtrikman (1963) (HS) lower

bound, like described in Dvorkin & Nur (1996). This combined model (HMHS) connects two end members; one has zero porosity and the modulus of the solid phase, and the other has critical porosity and a pressure dependent modulus as given by the Hertz-Mindlin theory.

The contact cementation theory (CCT) of Dvorkin et al. (1999) is applied to model the first stages of type **i)** cement. CCT provides the effective elastic properties of an aggregate of spheres, where the spheres are in direct point contact, and cement fills the space around the contacts. CCT cannot be used to estimate the elastic constants of an aggregate where cement fills the entire pore space or large portions of it (Dvorkin et al., 1999), therefore it is combined with DEM when the cement fills up more than 50 % of the intergranular volume.

The coated sphere (CS) model applied corresponds to the scheme 2 cement in Dvorkin & Nur (1996). This model treats the cement as evenly deposited on the grain surface, which lead to coated framework grains. The CS model is combined with CEMT to approximate connected phases of cement and framework when the cement concentration gets high.

If there are more than two types of loadbearing framework minerals, we first add the isolated (type **iv a)**) minerals by mixing the mineral 1 with framework quartz (DEM), and use the obtained result as framework in the next process where mineral 2 is mixed. Finally, if there is any grain enveloping cement, it is mixed with the framework by using CEMT, to obtain connectivity. Similarly, the Hill average is applied on the pore-filling cements to obtain the cement properties of an effective pore filling cement if more than one is present. In case of the presence of more than one type of coating sphere cement or contact cement, the effective rock properties is calculated for one cement type at a time, and then the Hill average is applied.

If more than one simultaneous distribution is present, the effective pore fluid stiffness is calculated with SCA, by mixing

fluid and type **ii)** minerals. The minerals with distribution types **iv a)** are considered as isolated framework grains, which contribute in the effective loadbearing framework. If distribution models **i)** and **iii)** both are present, the Hill (1952) average is applied between the modelling results for each inclusion type, like illustrated in Figure 2. Type **iv b)** cement is grain enveloping, and prevents precipitation of type **i)** and **iii)** cements in the areas it occurs. Thus in the case with type **i)**, **iii)**, and type **iv b)** all present, the Hill average is applied between the effective stiffness calculated for each distribution type, to obtain the overall effective rock moduli, as shown in Figure 2.

The fluid effects for seismic permeable sandstones without pore bridging cements are modelled with the Bound Averaging Method (BAM) (Marion & Nur, 1991) for all types of cement distributions. This model is an approximation to the Gassmann (1951) model for viscous fluids, and is applied as a consequence of the pore-filling cement being suspended in the fluid, making it more viscous. BAM relies on the assumption that the bulk modulus is a weighted average of the lower and upper limits for the given combination of grain modulus and fluid modulus, and that this weighting function is independent of the fluid. The weighting function can be found for the dry rock and then applied to find the modulus for the wet rock. We follow Sams & Andrea (2001) and apply the Reuss (1929) and Voigt (1928) averages for the lower and upper limits. Ideally the BAM and Gassmann models should coincide at the end points with no pore-filling cement and complete cementation, but Sams & Andrea (2001) found that the BAM model predicted slightly higher P-velocities for rocks with pure fluids.

In case of pore bridging cement (the effective fluid has positive shear stiffness), CEMT is used to model the mixture of framework and effective fluid in the seismic permeable rock. The DEM is applied for modelling the fluid effects in non-seismic permeable rocks for all distribution types. Brine is used as pore fluid in all modelling,

and mixed with pore-filling cement when present.

Figure 3 shows the bulk and shear moduli for the different distributions in a rock with 30 % intergranular volume. The rock loses its porosity exclusively by cementation. The figure demonstrates that the effective stiffness can vary significantly for equal cement concentrations, due to different distributions. In a rock with soft cement and rigid framework, the amount of loadbearing cement is decisive for the effective stiffness. Thus some of the curves for the different distributions do not converge when porosity approaches zero. The shear modulus of type **ii)** distribution is slightly increasing in the first stage of cementation. This increase is however not due to the cement, but an imposed linear porosity-pressure relationship which increases the moduli from the HMHS model. The bulk modulus will in addition to this, increase as a function of stiffer pore fluid, when the cementation proceeds. The rock physics models applied for isolated and connected loadbearing cement (type **iv a)** and **b)**) do not produce large differences, except for shear modulus with seismic isolated pores. Large changes in all stiffness gradients are observed when the pores starts to become seismic isolated at 15 % porosity, and when all pores are seismic isolated at 7.5 % porosity.

The K/µ-plot reveals three main trends with decreasing porosity; an initial sudden drop in the ratio (type **i)** and **ii)**), a smooth decrease (type **iv a)** and **b)**) and an initial little changed ratio, followed by a sudden drop (type **iii)**).

CLASSIFICATION

There are five dominant groups of clay minerals in sandstones (Worden & Morad, 2003); kaolinite, illite, chlorite, smectite and mixed layer varieties (e.g. illite-smectite (I/S) and chlorite-smectite (C/S)). In the following some important minerals in sandstones are studied, and classification of the minerals according to the four classes of distributions

is suggested, so that implementation to rock physics modelling becomes convenient. Normally a cemented sandstone will contain mixtures of these distributions, and when the cement concentrations reach certain levels, contact cement will turn into pore-filling, and pore-filling cement will further evolve to pore bridging. There are commonly additional minerals in sandstones than those considered in this paper, and correspondingly, a number of additional mineral reactions can occur. This paper focuses on a selection of essential and frequent clay mineral reactions, and neglect minerals that commonly play inferior roles in sandstones.

Kaolin minerals commonly have two occurrences; the vermicular booklet like kaolinite, which is progressively replaced by the well developed blocky crystals of dickite at temperatures between 90 - 130°C in open systems with good communication between pores (Cassagnabere, 1998; Worden & Morad, 2003), see Figure 4. Conversion of kaolinite to mixed-layer illite-smectite (I/S) and illite via diagenetic dissolution/precipitation reactions can occur at temperatures greater than 120°C (Ehrenberg & Nadeau, 1989). Mixtures of detrital kaolin and illite can perform as loadbearing clay clasts, like inclusion type **iv)**. Authigenic kaolin on the other hand, typically forms as pore-filling and pore-lining phases (Shaw & Conybeare, 2003), as also observed by e.g. Van Der Gaag (1997), Jolicoeur et al. (2000), Jones et al. (2000), Khidir & Catuneanu (2002), Thomas et al. (2002) and Marfil et al. (2003). Pore-filling kaolinite is not expected to generate continuous networks through the rock, and will not contribute much to the overall rock stiffness, until the concentration exceeds around 40 % of total pore space. Then the kaolinite starts to become pore- bridging. Authigenic and infiltrated kaolinite is a typical clay mineral of distribution type **ii)**.

The chlorite group is composed of several minerals with some variations in the content of aluminium, iron, lithium, magnesium, manganese, nickel, zinc and silicon. The chlorite composition suggested in

Worden & Morad (2003) is chosen for the different reactions in this paper that involve chlorite. The most common chlorite morphology is as graincoating boxwork, with the chlorite crystals attached perpendicular to the grain surface (Worden & Morad, 2003). Early authigenic chlorite coatings are commonly the products of chloritization of other less stable graincoating minerals. Ehrenberg (1993) and Grigsby (2001) concluded that synsedimentary Fe-rich clays is an important precursor for graincoating chlorite. The graincoating chlorite can prevent or inhibit precipitation of quartz on the grain surfaces, which can cause relatively high porosities even at large depths, as observed by e.g. Ehrenberg (1993), Anjos et al. (2003) and Rossi et al. (2003). Chlorite is generally graincoating, and acquires distribution type **iii)**.

The smectite group of minerals contains a variety of minerals which principally display variations in the calcium-, sodium-, aluminium-, magnesium-, iron-, zinc- and silicon content. The chemical composition of smectite is adopted from Worden & Morad (2003). Smectite usually occurs as flakes curling up from an attachment zone on the detrital sand grain surface (Worden & Morad, 2003). The grains are small, usually varying between 0.4-0.9 µm. In this study we divide smectite into detrital and authigenic. Detrital smectite is enveloping the framework grains before burial, and thus prevents direct contact between the framework grains. Graincoating authigenic smectite is deposited after the grain contacts in the framework are established, thus it is generally absent in the contacts. During diagenesis, smectite can be converted to chlorite or illite, see Figure 4. The conversion is gradual, and mixed illite-smectite (I/S) and chlorite-smectite (C/S) layers are the transition forms which get smectite poorer with increasing depth/temperature. As chlorite, authigenic smectite is a typical representative of type **iii)** distribution. Detrital smectite belongs to the **iv b)** inclusions, since it is loadbearing. But in contrast to load bearing clasts, detrital

smectite is considered to constitute a connected phase, since it covers grain surfaces, and prevent framework grain contacts. The intermediate forms of smectite, S/I and S/C, occur commonly as pore-lining or grain replacive clays (Ketzer et al., 2003).

Illite can occur as flakes, filaments or hair-like crystals (Worden & Morad, 2003). The thin, elongated crystals vary in length from < 1 µm to 7 µm, whereas the flakes are approximately 2 µm in diameter (Lemon & Cubitt, 2003). Illite morphology may cause a dramatic drop in permeability, because presence of illite increases specific surface of pore walls significantly. When the illite concentration increases, the illite lattice bridges the pores, reduces permeability, establishes communication between grains and strengthens the overall rock stiffness (e.g. Chuhan et al., 2001; Net, 2003), see Figure 5. Illite can evolve from precipitation from pore fluid and as a product from a number of precursor minerals, as illustrated in Figure 4. Graincoating and pore filling illite, absent in grain contacts, are observed and described by e.g. Ketzer (2002), Storvoll et al. (2002) and Patrier et al. (2003). Hence, illite is only considered to stiffen the pore fluid until it becomes pore bridging. These properties coincide with the inclusion type **ii)** criteria.

Bjørkum (1996) argued that dissolution of quartz in contact with mica or illitic clay surfaces is the most important quartz dissolution process in sandstones. The study suggested that pressure played a minor role for quartz dissolution; the quartz grains are only dependent on a certain minimum of effective pressure to stay in contact with the mica grains as the dissolution proceeds. The quartz cementation process consists of three sub processes; dissolution of quartz, transportation of aqueous silica and precipitation of quartz cement. The step that controls the rate of initial quartz cementation is the precipitation (Walderhaug, 1996). At reservoir temperatures of $80^{o}C$, the precipitation rate increases exponentially with further temperature increase, and the quartz cementation becomes effective. The mineralogy of the sandstone can influence the

cementation rate; pure quartz experiences a more rapid cementation than e.g. arcosic sand, and reduction of porosity has a tendency to be less severe if feldspar grains are present (Walderhaug, 1996). The surface area of quartz grains is decisive for the extent of cementation. Small quartz grains have larger surface area than larger grains, and are likely to produce more cement in otherwise similar conditions. Clay minerals or calcite cement covering the quartz surfaces reduces available surface area, and makes the quartz grains less susceptible to dissolution. Quartz cement commonly grows as a continuation of the original quartz grain. Together, the grain and cement form a single crystal, although the two parts of the crystal have different ages (Boggs, 1995). Continued increase in grain-contact area due to quartz precipitation during chemical compaction, was observed and described by Storvoll & Bjørlykke (2004). Contact cementing quartz has also been observed and studied by e.g. Avseth et al. (1998) and Florez-Niño & Mavko (2004). It is assumed that quartz cement preferentially precipitate near the grain contacts, until the cement volume exceeds 30 % of intergranular volume, after which the cement start to fill up the pore space. This corresponds to the definition of distribution type **i)**.

The last mineral considered in this paper is K-feldspar. When deposited, these grains are commonly a part of the loadbearing framework, as described by e.g. McKinley et al. (2003), and thus acquire type **iv a)** distribution. But if the mineral precipitates in situ, it is expected to be a coating sphere cement (e.g. Bjørlykke & Brendsdal, 1986), which qualifies for the type **iii)** distribution.

MINERAL REACTIONS

The mineral transitions considered in this paper are roughly illustrated in Figure 4, but both additional reactants and by-products are omitted. Large changes in mineral distributions occur from the various mineralogical processes shown. The relative volumes are calculated from stoichiometrically balanced (balanced due to number of atoms) mineral reactions by estimating the relative amount of moles for the different constituents, and then calculate their relative masses. Finally, the masses together with densities from Table 1 return relative volumes of the different constituents. Table 2 shows the volumetrically balanced mineral reactions. Aqueous anions and cations are omitted. The more complete stoichiometrically balanced reactions can be seen in Worden & Morad (2003). Diagenetic illite-smectite can also form from kaolinite and K-feldspar, like indicated by Nadeau et al. (2002) for shales from the Norwegian Continental Shelf. This pathway is however neglected in Figure 4 and in the simplified mineralogical modelling in this paper. Even if quartz is a product of reactions at temperatures lower than $80^{o}C$, it is not expected to precipitate until temperature exceeds $80^{o}C$. Thus, since the pore water is always supersaturated in respect of silica, the excess silica enters other diagenetic mineral reactions, like precipitation of feldspars. This connection is also not included in the modelling. The influence of chemical compaction on the total porosity due to dissolution of minerals in the transitions is also disregarded.

The mineral transitions in Table 2 will have significant effect on the overall rock stiffness, because they do not only entail new constituents with new properties, but the distributions and volumes of cement also change. In Figure 6, effective stiffness changes during the transitions from a starting mineral to the product mineral are modelled. The porosity is held constant at 20 % through all reactions, hence differences between reactant and product volumes are compensated with varying amounts of framework minerals. In all examples 25 % of the solid framework is clay clasts while the rest is detrital quartz. The pore-filling cements are all dispersed in the fluid, thus the total amount of solids become higher when this cement is present.

Effective moduli increase when authigenic smectite is replaced with illite and quartz cement. The increment is mainly due to quartz cement in the grain contacts, but the bulk modulus increases also due to stiffer pore fluid. Even if the volume of the products is less than the volume of reactants (Table 2), the contact cementing quartz together with increased cement stiffness increase the moduli. When modelling with detrital instead of authigenic smectite, the moduli have lower starting points, since the cement is load bearing, and prevents grain to grain contacts. But otherwise the trends are similar to authigenic smectite, and the curves converge when all the reactants are consumed.

When authigenic smectite converts to chlorite and quartz cement, both the effective bulk- and shear modulus increase smoothly although total cement volume decreases, as a consequence of the significantly higher stiffness of chlorite. Detrital smectite follow the same pattern, but as before, the moduli increase more because the starting point is lower.

The kaolinite to illite transition entails a small increase in effective bulk modulus, due to the higher stiffness of illite. The cements are bridging the pores, leading to positive shear modulus for the effective fluid. Hence, the rock shear modulus is also affected. It increases first, due to increased effective cement stiffness, since illite is stiffer than kaolinite. But when the reaction moves towards completion, the volume of pore-filling cement is reduced so much that shear modulus decreases slightly. Bulk modulus is less dependent on volume of pore-filling cements, and hence it increases through the whole reaction.

Illite and some quartz are produced when kaolinite and K-feldspar react. The quartz causes an initial stiffness increase due to stiffer framework contacts. The illite is not present in large enough concentrations to bridge the pores, and therefore plays a subordinate role in this example.

When moving from K-feldspar to illite and quartz cement, the contacts get stiffer from quartz cementing, and the fluid bulk modulus increases. The rock framework properties increase if the K-feldspar is softer than the other minerals in the framework. The sum of the products is less than the reactant volume, but the contact cement nevertheless dominates the moduli evolution, and increases both bulk- and shear modulus as the reaction proceeds.

When dispersed kaolinite reacts to produce pore lining chlorite, the bulk modulus increases significantly, because the chlorite contributes much to strengthen the grain contacts. The applied reaction also consumes water and ions that might origin from other minerals, and produces a higher volume than the original kaolinite volume. At the first stage of the reaction, two strong but opposite processes determine the effective rock stiffness. The kaolinite is pore-bridging, but the volume decreases as the reaction proceeds, hence the pore-bridging ceases and the moduli decrease. But the cementing chlorite counteracts this, and leads to a net stiffness increase relatively fast.

The K/μ-plot reveals large differences between the reactions. Except for the kaolinite to illite reaction, all reactions lead to a net decrease in the K/μ-ratio. Figure 6 also illustrates relative ratios of stiffness influence between various reactions when porosity changes are neglected.
If several reactions proceed simultaneously, some of them are likely to dominate the stiffness evolution more than others.

This kind of analysis can easily be performed for all kind of mineralogical reactions in rocks, as long as the stoichiometrically balanced equations and densities are known, and the minerals are classified due to distribution.

In real rocks the porosity will commonly not remain constant like in these examples. The rock will rather be subjected to chemical compaction, which means that when minerals dissolve, framework collapses and starts to occupy liberated space. To perform a realistic modelling of real rocks, the porosity should either be measured (e.g. from logs) or modelled consistently with mineral reactions and chemical compaction versus depth. Such

processes are not taken into consideration in the modelling of Figure 6.

COUPLED GEOLOGICAL AND ROCK PHYSICS MODELLING

CONSTRUCTED EXAMPLES

Three different scenarios are defined, and the diagenetic evolution of mineralogy and rock properties is modelled for each. When estimating reaction rates for the geochemical reactions, the "rule of thumb" from Worden & Burley (2003) is adopted, which assert that the rate doubles for every 10°C temperature increase. The linear effect of time is not accounted for in the mineral reactions in our modelling. Slow burial rates would result in higher degrees of mineral transformations at a given temperature, than high burial rates, since the latter has had less time to reach equilibrium. At 200 m depth, 10 % of the solids is framework clay clasts, 70 % is framework quartz, and the remaining 20 % is various other minerals. The apportionments of the minerals at 200 m depth are shown in Table 3 together with the mineral reactions involved in each case. The porosity-depth curve for all modelling is shown to the upper left in Figure 7. The porosity-depth relationship used in the modelling is from the porosity-depth model of Ramm & Bjørlykke (1994), which yields an exponential decreasing porosity with depth. Mineralogy dependent porosity evolution with depth is not a subject in this paper, thus the effect of specific minerals on porosity (e.g. the possible porosity preserving effect of chlorite) is disregarded when obtaining the porosity curve used in the following examples. By applying the same porosity curve for all cases, the velocities-depth curves are not realistic, but the rock physics modelling of the 3 cases can be compared solely on the basis of mineralogy and distribution differences. The concentrations off all minerals that are not involved in reactions increase with depth, due to increased concentration of solids when porosity decreases.

The temperatures are stippled in all curves in Figure 7. Case 1 produces no chlorite coating, but less quartz cement than case 2. Case 2 result in extensive quartz cementation, while the chlorite coating in case 3 inhibits precipitation of quartz cement, resulting in only small amount of quartz cementation. This is approximated by considering the amount of quartz cementation for case 1-3 to be 25 %, 50 % and 12.5 % of the total porosity loss after 80°C, respectively. All the pore-filling cement in case 1 and 2 result in pore bridging from ca 3.9 and 3.3 km respectively. In these cases the most dominant cement at large depths is pore-filling (distribution **ii)**), while in case 3 the coating chlorite (distribution **iii)**) dominates the cement. When the total amount of cement in Figure 7 exceeds 0.5 (50 % of intergranular volume), the rock starts to loose its seismic permeability, according to our models. This takes place at different stages for the three cases; 4 km, 3.5 km and 3.8 km for case 1-3 respectively. The type **iv a)** minerals are not included as a cement, when calculating total cement content due to the intergranular volume, since type **iv a)** minerals are a part of the effective loadbearing framework, and do not fill up space between framework grains.

Since the porosity, framework clay and initial framework quartz concentrations are the same in all cases, the velocity differences in Figure 8 are not very large, but large enough to easily distinguish the curves after incipient cementation. The circles around the curves reflect mineralogical and physical changes in the rock.

Five changes during depth characterize the case 1 velocity curves; initiation of quartz cementing at 2.5 km, incipient pore bridging at 3.96 km, all smectite is consumed at 4.0 km (125°C), incipient seismic isolation of pores at 4.1 km and all K-feldspar is consumed at 4.2 km. Not all these changes have the same impact on the velocity curves. Figure 3 and 6 give good indications about which of the mineralogical transformations that have the dominant

influence on the overall stiffness in case of simultaneous transformations. The first figure shows which distributions yield the highest stiffness, while the latter illustrates stiffness changes during the various mineral transformations. Case 1 had the highest smectite content, with equal amounts of detrital (type **iv b)**) and authigenic (type **iii)**) smectite, and it is clear that decreasing smectite content has a great influence on the velocities. The second factor that together with smectite exerts largest influence on velocities is the bridging of pores, which yields effective pore fluid with positive shear stiffness. Case 1-3 are all moderately influenced by the incipient seismic isolation of pores, while the other diagenetic changes play inferior roles in case 1.

A similar analysis for case 2, brings us to the conclusions that in addition to the two factors that dominated case 1, quartz cementation are more extensive in this case, and should be included as an important factor for the velocity evolution. Reaction **3)** and **4)** (Table 2) do only have minor influence on the velocities in this case.

Case 3 is dominated by the chlorite reactions (reaction **2)** and **7)**). Figure 6 shows that large effective stiffness increase from both reactions can be expected. Pronounced velocity gradient changes are also observed in Figure 8 when all smectite and kaolinite is consumed and chlorite production ceases, at 4.35 km and 4.5 km respectively.

The velocity differences between case 1-3 would have increased if we also had modelled the porosity as a function of volumetrically differences in the mineral reactions. Porosity evolution as a function of mineralogy and mineral transformations is however beyond the scope of this paper. The volumes in the mineral reactions from Table 2 are used to obtain the correct relative ratio between the different minerals at given porosities.

REAL WELL EXAMPLE

Figure 9 compares modelled velocities with well log velocities. The black dots in the three lower figures are well log velocities, which are the same in all the figures. The modelled velocities vary from case 1 - 3. The mineralogy concentrations for case 1 are shown in the upper plots. The temperature-depth gradient is 36.5^{o}C/km in the studied interval, and some of the mineral reactions do not run to completion at 4.4 km (ca. 120°C), see Figure 9. Thus the concentration of precipitated cements is too small to induce the same variations between the different models as observed in Figure 8. The relative concentrations of the minerals consumed in the reactions, do not necessarily exclusively decrease with depth, because porosity loss increase the relative concentrations of solids, and thereby the concentration of each mineral. The density, porosity, clay content, temperature and fluid properties from the well log are used in the velocity modelling. When it comes to estimation of mineral concentrations, the relative ratios between the minerals are calculated for case 1-3, and then normalized to the clay content from the log. At all depths, 10 % of the clay present is represented by clay clasts in the framework. The reactions involved in the different cases are shown in Table 3. In the shallow section of the log (depth<2.5 km) it is assumed that no type **i)** and **iii)** cement are present, since the log velocities are so low. However, authigenic smectite is introduced at depths greater than 2.5 km (T≈50°C). The mean deviations for V_p and V_s are ± 151.9 m/s and ± 132.5 m/s in case 1, ± 177.8 m/s and ± 174.4 m/s in case 2 and finally ± 147.3 and ± 115.5 m/s in case 3. All the modelled velocities in the deepest part of the well are too high. And although the deviations are pretty close, some considerations about the mineralogy can be performed:

Case 1 would have shown a better fit if there had been more loadbearing soft minerals. In Case 2, the quartz cement is responsible for the high velocities, thus lower concentrations of quartz cement would have decreased the gap between modelled and real velocities. Case 3 is barely closest to the real data, but although the amount of quartz cementation is

low, and chlorite cementation has not become extensive yet, the velocities are too high for the deep data. Higher portions of loadbearing or pore-filling clay instead of contact cementing clay minerals would have lowered the velocities. These considerations are off course limited by the simplified mineralogical modelling, but the methodology would be the same and the conclusions more nuanced with more advance geological modelling.

REFLECTIVITY OF DIAGENETIC PROCESSES

A hypothetical downgoing P-wave that reaches an interface between two different layers is considered. The reflected wave is split into a P- and S-wave due to impedance differences between the upper and lower layer. The layer properties used are shown in Table 4. Figure 10 shows the reflection coefficients versus angle for the reflected P- and S-waves, Rpp and Rps, respectively. The peaks in the curves represent the critical angles, where no P-wave is transmitted to the underlying layer. The Rpp should ideally be one for critical angels, but the curves are too steep and the sampling too coarse to capture the maximum values. At higher angles, the reflection coefficients consist of a real and an imaginary part. Only the real part is plotted, but the angles lower than critical angles are commonly the ones used in conventional seismic. Differences down to 0.02 in reflection coefficients should be identifiable in seismic data of good quality.
In the two plots above, the upper layer is an isotropic cemented shale with 3 % porosity modelled with the shale cementation model of Dræge et al. (2006), while the bottom layer vary between a pore-bridged, quartz cemented, quartz cemented with seismic isolated pores, uncemented and chlorite cemented sandstone, modelled with the theories presented in this paper. The sandstone porosity is 10 % in all but the chlorite cemented example. Ehrenberg (1993) observed 10 - 15 % higher porosity in chlorite cemented sandstones with inhibited quartz

cementing, hence porosity is set to 22.5 %. The figure shows that the quartz cemented sand with isolated pores stands out from the others by reaching the critical angle before the other sands. In addition this sand clearly has the highest P-wave reflectivity of the normal incident wave. The quartz cemented and pore-bridged sandstone differ most at low angles for the Rpp, and medium angles for the Rps, but can otherwise be hard to distinguish. A normal incident P-wave never returns reflected S-waves, so there must be a non-zero incident angle to separate the coefficients of S-wave reflections. The chlorite cemented sand has the largest critical angle of the studied sands, while the uncemented sand has an almost negligible S-wave reflection and a lower P-wave reflection for large incident angles than the other sands.

The two next plots show the evolution of the reflection coefficients versus angle with an overlying uncemented sand. The same patterns are seen, but the positive Rpp coefficients are somewhat higher in this example. All scenarios differ enough at subcritical angles to be separated in seismic.

The last reflection example is a chlorite cemented high porosity sandstone, overlying a quartz cemented sandstone. The coefficients are estimated when the underlying cemented sandstone is seismic permeable and seismic isolated, respectively. In the first case, the S-wave reflections are practically absent for all angles, while the P-wave reflections are pronounced, but considerably lower than in the case with seismic isolated pores at low angles. Hence, the two scenarios are easily separated by P-wave reflections alone. In addition the S-wave reflections differ considerably, and the critical angle differs with ca 20°. The modelling indicates that a high-porosity chlorite cemented layer can constitute a good reflector when overlying a quartz cemented sand with lower porosity. Further, seismic impermeable sands leave different signatures than seismic permeable sands, which should be recognized in seismic data.

Although the reflection coefficients some places indicate good reflections, there

are limits for how thin a layer can be, to still be detectable on seismic. This limit is dependent on the wavelength, which further depends on the frequency and velocity. Generally, a reflector that is thinner than 1/4 of the wavelength is considered to be beyond seismic resolution. In the chlorite cemented sandstone the wavelength for a 50 Hz wave will be 4343 m/s $/$ 50 s^{-1} = 86.9 m. Hence, the minimum thickness for this layer to be detectable in seismic should be ca 22 meters. Slower layers have shorter wavelengths for a given frequency, and hence better resolution.

DISCUSSION

Our model and strategy depend on knowledge about mineralogical properties of the minerals involved. Effective elastic properties of clay minerals have been derived by theoretical computations (Katahara, 1996), combined theoretical and experimental investigations on clay-epoxy mixtures (Wang et al., 2001), and direct measurements (Vanorio et al., 2003). In Figure 11 the mineral transitions from Figure 6 are reproduced with altered mineral properties. The alternative properties are listed in Table 5. The modelling shows that the changed kaolinite properties entail the largest changes, but even if the bulk and shear modulus increase with 433.6 % and 328.3 %, respectively, the "new" kaolinite only alter the corresponding effective rock moduli with 18.5 % and 31.8 % respectively. Alterations of the properties of the pore filling minerals induce smaller changes, unless they are pore-bridging. This is very well illustrated for the shear modulus with altered illite properties (blue curve) when kaolinite reacts to illite. The difference is large in the first part of reaction while there still is pore-bridging cement, but when the pore-bridging ceases, the curve coincide with the curve with original illite values (stippled brown). The increase of the properties of authigenic smectite results in a larger increase in the overall rock stiffness than for detrital smectite, because the latter is loadbearing and still softens the framework significantly. The new chlorite properties reduce the effective

shear modulus slightly. Figure 11 shows that the distribution type assigned to each mineral is more important for the overall rock stiffness than the mineral properties themselves. This also agrees with the conclusion of Dvorkin & Nur (1996), that reducing the stiffness of contact cement does not significantly reduce the stiffness of the cemented aggregate.

The chemical formulae used to calculate mineral molar masses, and further relative mineral volumes, are adopted from Worden & Morad (2003), and are not all unique. The composition of some clay minerals like illite, chlorite and smectite, might vary within certain limits, due to the chemical environment in which they are generated. The chemical formulae applied can bee viewed upon as an averaged mineral composition. The new mineral densities in Table 5 will also change the relative volumes in the reactions in Table 2. By normalizing the reactions to the reactants, the alternative illite density in reaction **1**) entails an illite-volume decrease of 2.8 %, and new smectite density result in a volume increase of 4.7 % for quartz and illite in the reaction. Similarly, new chlorite density in reaction **7**) leads to a reduction in chlorite volume in the reaction by 5.5 %, which is the same result as obtained when applying the kaolinite density from Table 5. Figure 11 does not account for changes in volumetrical relations between the constituents, only the stiffness changes. But the volumetrical changes also influence the overall rock stiffness through porosity and increased/decreased concentrations of compliant or stiff minerals.

Only a selection of diagenetic mineralogical transformations has been applied in this paper, while there exists numerous other more or less inferior transformations with local importance. Another aspect not considered in this paper, is the possibility of calcite cementing. Calcite is assumed to act in the same way as quartz, i.e. it will be distributed near the contacts like type **i**) cement. Thus calcite will occupy the same space as quartz cement. Calcite often precipitates at lower temperatures than quartz

(Bjørkum & Walderhaug, 1990), and might therefore prevent or reduce the extent of quartz cement precipitation.

It is assumed that all elongated components in the rock are randomly oriented, which lead to isotropic sands. Laminations of thin shales in the sands are not considered in this paper.

When comparing our models with real well log data, it is assumed that the depositional composition of minerals has been the same for all the sands in the time it has taken to deposit these sediments. This is probably a dubious assumption, but we can avoid the problem by decomposing the sand log into smaller intervals of similar depositional environment, and perform separate modelling on each fragment of the sand log.

A step to bring this strategy further is to include holistic and advanced geological modelling that includes the complicated interplay between various mineral reactions, and the related porosity evolution.

CONCLUSIONS

This paper has presented some new contributions to include geological and geochemical processes in rock physics modelling. The idea of classifying minerals due to distribution is the key for implementing mineralogical reactions into rock physics modelling. Further, the development of a rock physics model that allows multiple simultaneous distributions enables the modelling.

Together these two contributions introduce a new interdisciplinary workflow, where the first job should be an advanced geological modelling of mineralogy and porosity evolution, followed by rock physics modelling of seismic properties during diagenesis.

The rock physics modelling revealed significant differences between various diagenetic scenarios, when modelling reflection coefficients versus angle of incidence. High quality seismic can therefore be able to discriminate between well

developed diagenetic processes such as pore-bridging, quartz cementing, high porosity chlorite cemented sandstones and uncemented sandstones, when occurring in a sufficiently thick layer. Based on this, the presented strategy is considered a new and valuable rock physics tool in exploration purposes, which includes previously little used information. Combined with high quality geological input, this strategy can be inverted to make predictions about saturation, lithology, porosity and microstructures in the subsurface.

REFERENCES

Anjos, S. M. C., De Ros, L. F. & Silva, C. M. A. 2003. Chlorite authigenesis and porosity preservation in the Upper Cretaceous marine sandstones of the Santos Basin, offshore eastern Brazil. *International Association of Sedimentologists*, Special Publication, **34**, 291-316.

Anstey, N. A. 1991. Velocity in thin section. *First Break*, **10**, 449-457.

Avseth, P. A., Dvorkin, J., Mavko, G. & Rykkje, J. 1998. Diagnosing high porosity sands for reservoir characterization using sonic and seismic. *68th Conference SEG, Extended abstracts,* New Orleans, USA, 1024-1027.

Bjørkum, P. A. 1996. How important is pressure in causing dissolution of quartz in sandstones? *Journal of Sedimentary Research*, **A76**, 147-154.

Bjørkum, P. A. & Walderhaug, O. 1990. Geometrical arrangement of calcite cementation within shallow marine sandstones. *Earth Science Review*, **29**, 145-161.

Bjørlykke, K. & Aagaard, P. 1992. Clay minerals in North Sea sandstones. *In:* Houseknecht D. W., Pittman, E. D (eds), Origin, diagenesis, and petrophysics of clay minerals in sandstones, *Society of Economic Palaeontologists and Mineralogists*, Special Publication, **47**, 65-80.

Bjørlykke, K. & Brendsdal, A. 1986. Diagenesis of the Brent sandstone in the Statfjord Field, North Sea. *In:* D. L.Gautier (ed), Role of Organic Matter in Sediment Diagenesis, *Society of Economic Palaeontologists*

and Mineralogists, Special Publication, **38**, 157-166.

Boggs, S. (ed) 1995. *Principles of Sedimentology & Stratigraphy* (Second Ed). Prentice Hall, New Jersey.

Cassagnabere, A. 1998. *Caractèrisation et interprètation de la transition kaolinite-dickite dans les rèservoirs à hydrocarbures de Froy et Rind (Mer du Nord), Norvège*. PhD thesis, University of Poitiers, Poitiers, France.

Chuhan, F. A., Bjørlykke, K. and Lowrey, C. 2001. Closed-system burial diagenesis in reservoir sandstones: Examples from the Garn Formation at Haltenbanken area, offshore Mid-Norway. *Journal of Sedimentary Research*, **71** (1), 15-26.

Dræge, A., Jakobsen, M. & Johansen, T. A. 2006. Rock physics modelling of shale cementation. *Petroleum Geoscience*, **12**, 49-57.

Dvorkin, J. & Nur, A. 1996. Elasticity of high porosity sandstones: Theory for two North Sea data sets. *Geophysics,* **61** (5), 1363-1370.

Dvorkin, J., Berryman, J. & Nur, A. 1999. Elastic moduli of cemented sphere packs. *Mechanics of Materials*, **31**, 461-469.

Ehrenberg, S. N., Nadeau, P. H. 1989. Formation of diagenetic illite in sandstones of the Garn Formation, Haltenbanken area, Mid-Norwegian continental shelf. *Clay Minerals*, **24** (2), 233-253.

Ehrenberg, S. N. 1993. Preservation of Anomalously High Porosity in Deeply Buried Sandstones by Grain-Coating Chlorite: Examples from the Norwegian Continental Shelf. *The American Association of Petroleum Geologists Bulletin*, **77** (7), 1260-1285.

Florez-Niño, J. M. & Mavko, G. 2004. Pressure-solution and the rock physics diagenetic trend in quartzose sandstones. *74th Conference SEG, Extended abstracts,* 1702-1705.

Gal, D., Dvorkin, J. & Nur, A. 1999. Elastic-Wave Velocities in Sandstones with Non-Loadbearing Clay. *Geophysical Research Letters*, **26**, 939-942.

Gassmann, F. 1951. Über die Elastisität der pöröser medien. *Vierteljahrschrift der Naturforschenden Gesellshaft in Zürich*, **96**, 1-23.

Grigsby J. D. 2001. Origin and growth of authigenic chlorite in sandstones of the lower Vicksburg formation, South Texas. *Journal of Sedimentary Research*, **71** (1), 27-36.

Hashin, Z. & Shtrikman, S. 1963. A variational approach to the theory of the elastic behavior of multiphase materials. *Journal of the Mechanics and Physics of Solids*, **11**, 127-140.

Hill, R. 1952. The elastic behavior of crystalline aggregate. *Proceedings of the Physical Society of London*, **A65**, 349-354.

Hornby, B. E., Schwartz, L. M. & Hudson, J. 1994. Anisotropic effective-medium modelling of the elastic properties of shales. *Geophysics*, **59** (10), 1570-1583.

Jakobsen, M., Hudson, J. A., Minshull, T. A. & Singh, S. C. 2000. Elastic properties of hydrate-bearing sediments using effective medium theory. *Journal of Geophysical Research*, **105** (B1), 561-577.

Johansen, T. A., Drottning, A., Lecomte, I. & Gjøystdal, H. 2002. An approach to combined rock physics and seismic modelling of fluid substitution. *Geophysical Prospecting*, **50** (2), 119-137.

Jolicoeur, S., Ildefonse, P. & Bouchard, M. 2000. Kaolinite and Gibbsite Weathering of Biotite within Saprolites and Soils of Central Virginia. *Soil Science Society of America Journal*, **64**, 1118-1129.

Jones, B., Renaut, R. & Rosen, M. R. 2000. Stromatolites Forming in Acidic Hot-Spring Waters, North Island, New Zealand. *PALAIOS*, **15** (5), 450-475.

Katahara, K. W. 1996. Clay mineral elastic properties. 66th *Conference SEG, Extended abstracts*, Denver, USA, 1691-1694.

Ketzer, J. M., Morad, S. & Amorosi, A. 2003. Predictive diagenetic clay-mineral distribution in siliciclastic rocks with a sequence stratigraphic framework. *In:* Worden, R. H. & Morad, S. (eds), *Clay Mineral Cements in Sandstones*, International Association of Sedimentologists, Special Publication, **34**, Blackwell Publishing, Oxford, 43-61.

Ketzer, J. M. 2002. *Diagenesis & sequence stratigraphy* . PhD thesis, University of Uppsala, Uppsala, Sweden.

Khidir, A. & Catuneanu, O. 2002. Sedimentology and diagenesis of the Scollard sandstones in South Sentral Alberta. *Bulletin of Canadian Petroleum Geology,* **51**(1), 45-69.

Lemon, N. M. & Cubitt, C. J. 2003. Illite fluorescence microscopy: A new technique in the study of illite in the Merrimelia Formation, Cooper Basin, Australia. *In:* Worden, R. H. & Morad, S. (eds), *Clay Mineral Cements in Sandstones*, International Association of

Sedimentologists, Special Publication, **34**, Blackwell Publishing, Oxford, 411-424.

Marfil, R., Delgado, A., Rossi, C., La Iglesia, A. & Ramseyer, K. 2003. Origin and diagenetic evolution of kaolin in reservoir sandstones and assosiated shales of the Jurassic and Cretaceous, Salam Field, Western Desert (Egypt). *In:* Worden, R. H. & Morad, S. (eds), *Clay Mineral Cements in Sandstones*, International Association of Sedimentologists, Special Publication, **34**, Blackwell Publishing, Oxford, 319-342.

Marion D. & Nur, A. 1991. Pore-filling material and its effect on velocity in rocks. *Geophysics*, **56**, 225-230.

Mavko, G., Mukerji, T. & Dvorkin, J. 1998. *The Rock Physics Handbook: Tools for seismic analysis in porous media*. Cambridge University Press.

McKinley, J. M., Worden, R. H. and Ruffel, A. H. 2003. Smectite in sandstones: a review of the controls on occurrence and behaviour during diagenesis. *In:* Worden, R. H. & Morad, S. (eds), *Clay Mineral Cements in Sandstones*, International Association of Sedimentologists, Special Publication, **34**, Blackwell Publishing, Oxford, 109-128.

Mindlin, R. D. 1949. Compliance of elastic bodies in contact. *Journal of Applied Mechanics*, **16**, 259-268.

Nadeau, P. H., Peacor, D. R., Yan, J. and Hiller, S. 2002. I/S precipitation in pore space as the cause of geopressuring in Mesozoic mudstones, Egersund Basin, Norwegian Continental Shelf. *American Mineralogist*, **87**, 1580-1589.

Net, L. I. 2003. *Diagenesis and reservoir quality of the eolian nugget / Navajo sandstone (early Jurassic), Utah and Wyoming*. PhD thesis, University of Texas, Austin, USA.

Nishizawa, O. 1982. Seismic velocity anisotropy in a medium containing oriented cracks - transversely isotropic case. *Journal of Physics of the Earth*, **30**, 331-347.

Patrier, P. D. B., Laverett, E. & Bruneton, P. 2003. High-grade diagenetic dickite and 2M1 illite from the middle Proterozoic Kombolgie Formation (Northern Territory, Australia). *Clays and Clay Minerals*, **51** (1), 102-116.

Ramm, M. & Bjørlykke, K. 1994. Porosity/depth trends in reservoir sandstones: Assessing the quantitative effects of varying pore-pressure, temperature history and mineralogy, Norwegian Shelf data. *Clay minerals*, **29**, 475-490.

Reuss, A. 1929. Berechtungder fliessgrense von mischkristallen auf grund der Plastizitätbedingung für ein Kristalle. *Zeitschrift für Angewandte Mathematik aus Mechanik*, **9**, 49-58.

Rossi, C., Kalin, O., Arribas, J., La Iglesia, A. & Bartrina, T. 2003. Effect of Authigenic Grain-Coating Chlorite on the Resistivity and Reservoir Quality of the Lower Carboniferous RKF Sandstones (Rhourde El Krouf Field), Berkin Basin, Algeria. *2003 AAPG International Conference & Exhibition,* Barcelona, Spain, A81-A81.

Sams, M. S. & Andrea, M. 2001. The effect of clay distribution on the elastic properties of sandstones. *Geophysical Prospecting*, **49**, 128-150.

Shaw, H. F. & Conybeare, D. M. 2003. Patterns of clay mineral diagenesis in interbedded mudrocks and sandstones: An example from the Paleocene of the North Sea. *In:* Worden, R. H. & Morad, S. (eds), *Clay Mineral Cements in Sandstones*, International Association of sedimentologists, Special Publication, **34**, Blackwell Publishing, Oxford, 129-145.

Storvoll, V. & Bjørlykke, K. 2004. Sonic velocity and grain contact properties in reservoir sandstones. *Petroleum Geoscience*, **10** (3), 215-226.

Storvoll, V., Bjørlykke, K., Karlsen, D. & Saigal, G. 2002. Porosity preservation in reservoir sandstones due to grain coating illite: A study of the Jurassic Garn formation from the Kristin and Lavrans field, offshore Mid-Norway. *Marine and Petroleum Geology*, **19**(6), 767-781.

Thomas, M. B., McGillivray, P., Wong, R. & Hubbard, S. 2002. Bluesky/Ostracod Rock Properties-Peace River Tar Sands: Not a Simple 'Sand Tank' Model. *CSPG Convention, Calgary, Alberta, Canada.*

Tosaya, C. A. 1982. *Acoustical properties of clay-bearing rocks*. PhD thesis, Stanford University, USA.

Van Der Gaag, J. 1997. *Characterization of outburst channel sandstones in the Phalen Colliery, Cape Breton, Nova Scotia*. PhD thesis, Dalhouse University, Halifax, Canada.

Vanorio, T., Prashad, M. & Nur, A. 2003. Elastic properties of dry clay mineral aggregates, suspensions and sandstones. *Geophysical Journal International*, **155**, 319-326.

Voigt, W. (ed) 1928. *Lehrbuch der Kristallphysik*. Teubner, Leipzig.

Walderhaug, O. 1996. Kinetic modelling of quartz cementation and porosity loss in deeply buried sandstone reservoirs. *AAPG Bulletin*, **80**, 731-745.

Wang, Z. 2000. The Gassmann equation revisited: Comparing laboratory data with Gassmann's prediction. In: Wang, Z. and Nur, A. (eds), *Seismic and acoustic velocities in reservoir rocks*, (**3**): Recent developments: Society of Exploration Geophysicists, 8-23.

Wang, Z., Wang, H. & Cates, M. E. 2001. Elastic properties of solid clays. *Geophysics*, **66**, 428-440.

Willis, J. R. 1977. Bounds and self-consistent estimates for the overall properties of anisotropic composites. *Journal of the Mechanics and Physics of Solids*, **25**, 185-202.

Worden, R. H. & Burley, S. D. 2003. Sandstone diagenesis: the evolution of sand to stone. *In:* S. D. Burley and R. H. Worden (eds), *Sandstone Diagenesis - Recent and Ancient* . Shannon, Reprint Series, **4**, International Association of Sedimentologists, Blackwell Publishing, Oxford, 3-44.

Worden, R. H. and Morad, S. 2003. Clay minerals in sandstones: Controls on formation, distribution and evolution. *In:* Worden, R. H. & Morad, S. (eds), *Clay Mineral Cements in Sandstones*, International Association of Sedimentologists, Special Publication, **34**, Blackwell Publishing, Oxford, 3-41.

Mineral	k (GPa)	μ (GPa)	ρ (g/ccm)	Reference
Quartz	37	44	2.65	Mavko et al. (1998)
K-feldspar	37.5	15	2.62	Mavko et al. (1998)
Kaolinite	11	6	2.59	Vanorio et al. (2003)
Illite	62.2	25.7	2.706	Wang et al. (2001)
Chlorite	127.5	84.2	2.681	Wang et al. (2001)
Smectite	6	4	2.29	Vanorio et al. (2003)
Mixed clay	21.0	7.0	2.60	Tosaya (1982)

Table 1. Minerals and physical parameters used in the modelling. k, μ, and ρ denote the bulk modulus, shear modulus and density, respectively.

	Mineral reactions	Start	Completed
1)	S ➝ 0.201 Q + 0.354 I + 0.180 H$_2$0	65°C	125°C
2)	S + 0.035 H$_2$0 ➝ 0.303 Q + 0.545 C	70°C	135°C
3)	K ➝ D ➝ 0.943 I + 0.180 H$_2$0	70°C	160°C
4)	1.066 KF + K ➝ 0.455 Q + 1.414 I + 0.180 H$_2$0	70°C	110°C
5)	Q(framework) ➝ Q(cement)	80°C	-
6)	KF + 0.056 H$_2$0 ➝ 0.427 Q + 0.442 I	90°C	110°C
7)	K + 0.526 H$_2$0 ➝ 1.501 C	115°C	140°C

Table 2. Volumetrically balanced reactions, only including solids and water. The temperatures are used in this paper, but might vary due to permeability and accessibility of reactants. We do not apply any upper temperature limit for reaction **5)**.

Case nr	Q_o	K_o	KF_o	DS_o	AS_o	CL_o	Reactions involved
1	0.70	0.025	0.075	0.05	0.05	0.10	**1), 4), 5), 6)**
2	0.70	0.10	0.05	0.025	0.025	0.10	**1), 3), 4), 5)**
3	0.70	0.5	0.025	0.05	0.075	0.10	**2), 4), 5), 7)**

Table 3. The starting criteria for the different scenarios. The subscript "$_o$" indicates the relative concentration at deposition, normalized to the total volume of solids. Q and CL are framework quartz and clay clasts, respectively. The reactions are listed in Table 2.

	Shale	Q_{iso}	Q_{perm}	Porebridge	Chlorite	Uncemented
V_p (m/s)	3517	5330	4561	4545	4343	3462
V_s (m/s)	1832	3496	2883	2784	2770	2297
ρ (g/ccm)	2.56	2.48	2.48	2.33	2.29	2.48

Table 4. Velocities and densities for the layers used in Figure 10. Q_{iso} and Q_{perm} denote a quartz cemented sand with seismic isolated pores and permeable pores, respectively.

Mineral	K (GPa)	μ (GPa)	ρ (g/ccm)	Reference
Kaolinite	47.7	19.7	2.444	Wang et al. (2001)
Illite	61.4	41.8	2.79	Katahara (1996)
Chlorite	165.0	52.1	2.839	Wang et al. (2001)
Smectite	9.3	6.9	2.394	Wang et al. (2001)

Table 5. Alternative physical mineral properties used in Figure 11.
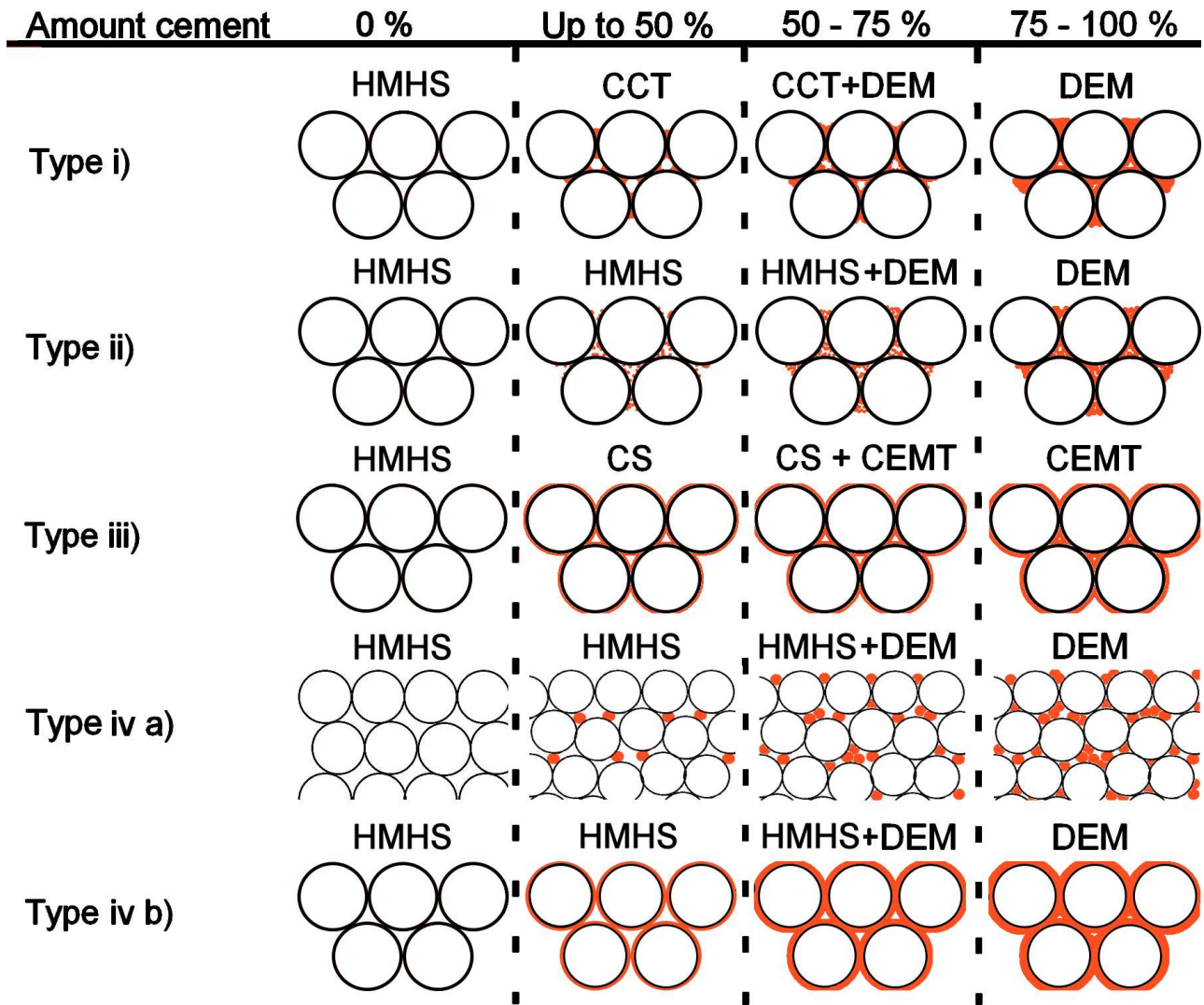
Figure 1. Modelling steps for the different distribution types. White circles are quartz framework grains, while orange colour represents other solid components in the sandstone. The models referred to above each step are discussed in the text. The cement volume is relative to intergranular volume. When the cement volume increases, the porosity decreases correspondingly.
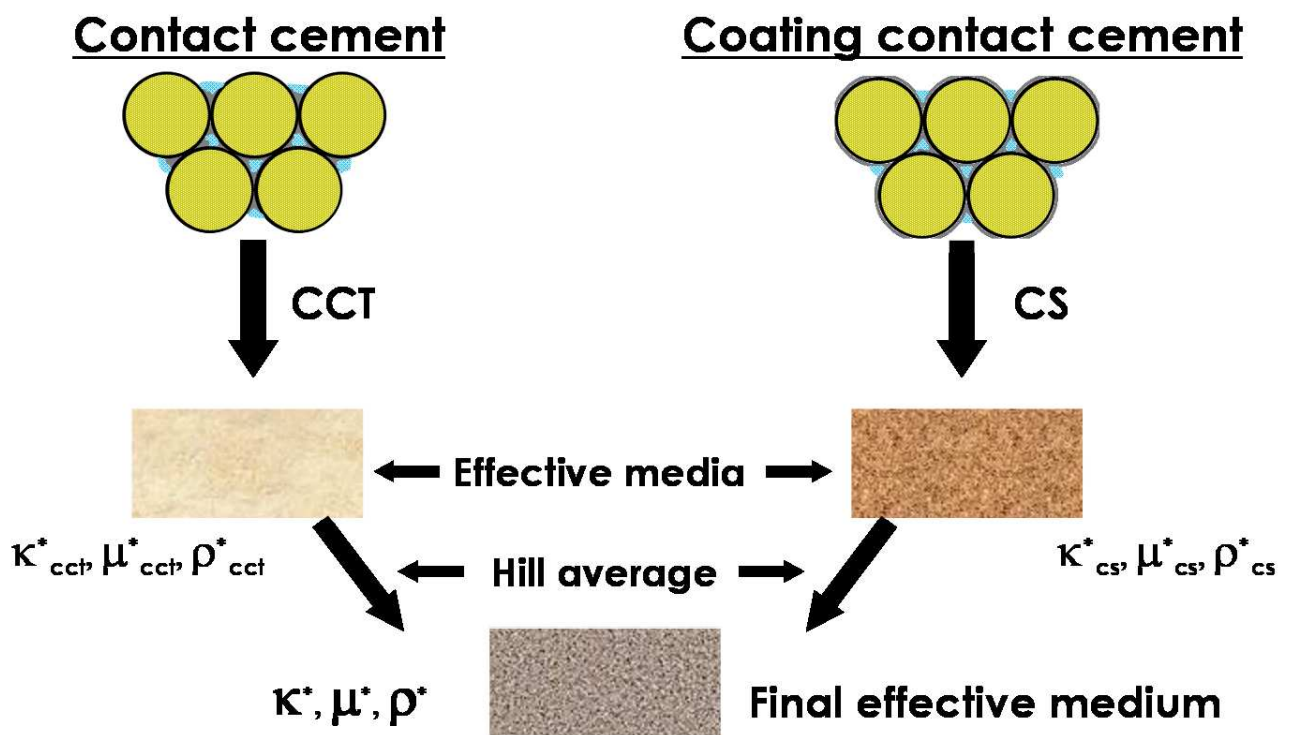
Figure 2. Distribution type **ii)** and the pore fluid constitute the effective pore fluid (blue), while distribution types **iv a,b)** together with the framework quartz constitute the effective framework (yellow). The effective medium properties are then calculated by the CCT- and CS models distinctively. Finally, a Hill average between the two results provides the modelled effective properties of the composite rock.
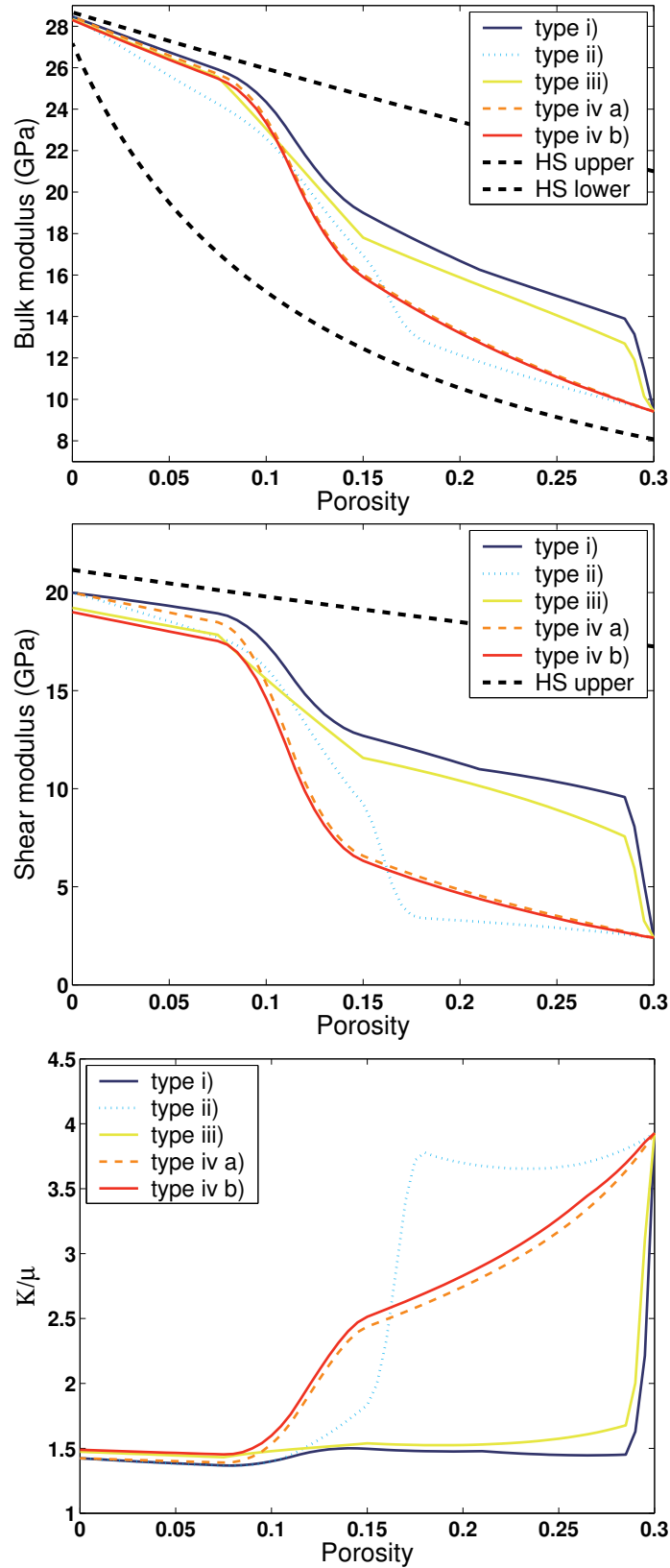
Figure 3. The modelled effect of different mineral distributions from uncemented (porosity = 0.3, cement = 0) to completely cemented (porosity = 0, cement = 0.3) rock is illustrated. The stippled black lines represent the Hashin & Shtrikman (1963) (HS) upper and lower bounds. K and μ denote bulk- and shear modulus, respectively. We have used mixed clay from Table 1 as cement in the modelling.
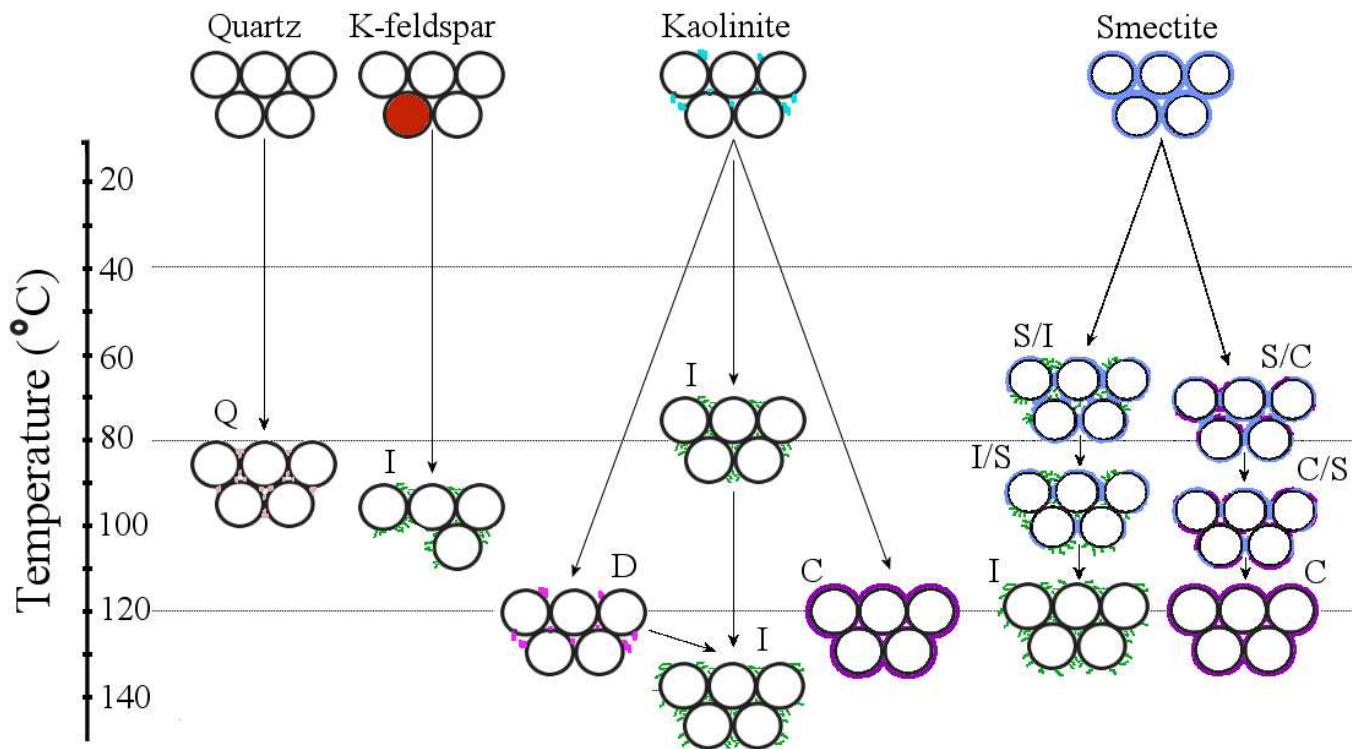
Figure 4. The clay reactions that occur at various temperatures are illustrated with mineral distributions. White circles are quartz framework grains, while the red circle is k-feldspar grain which dissolves at large temperatures. The top of each step indicates the temperatures at which the transitions start. Q, K, D, I, C, S denote the cementing minerals quartz, kaolinite, dickite, illite, chlorite and smectite respectively. The figure is based on data from Worden & Morad (2003).

Pore filling clay

Pore bridging clay

Framework grain
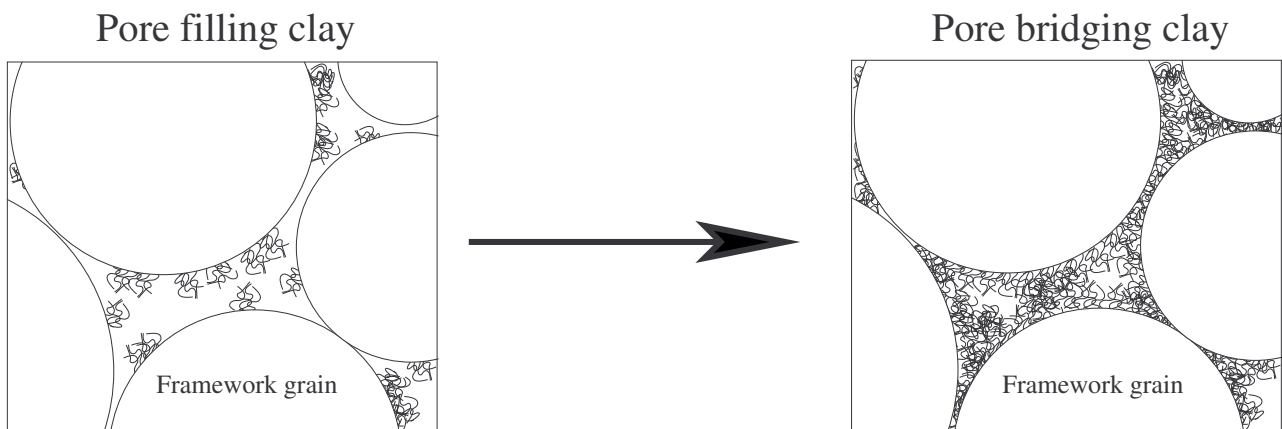
Framework grain

Figure 5. When the amount of pore-filling clay exceeds ca. 40 % of total pore space, the pore-fill establishes contact between the framework grains and increase the total rock stiffness.
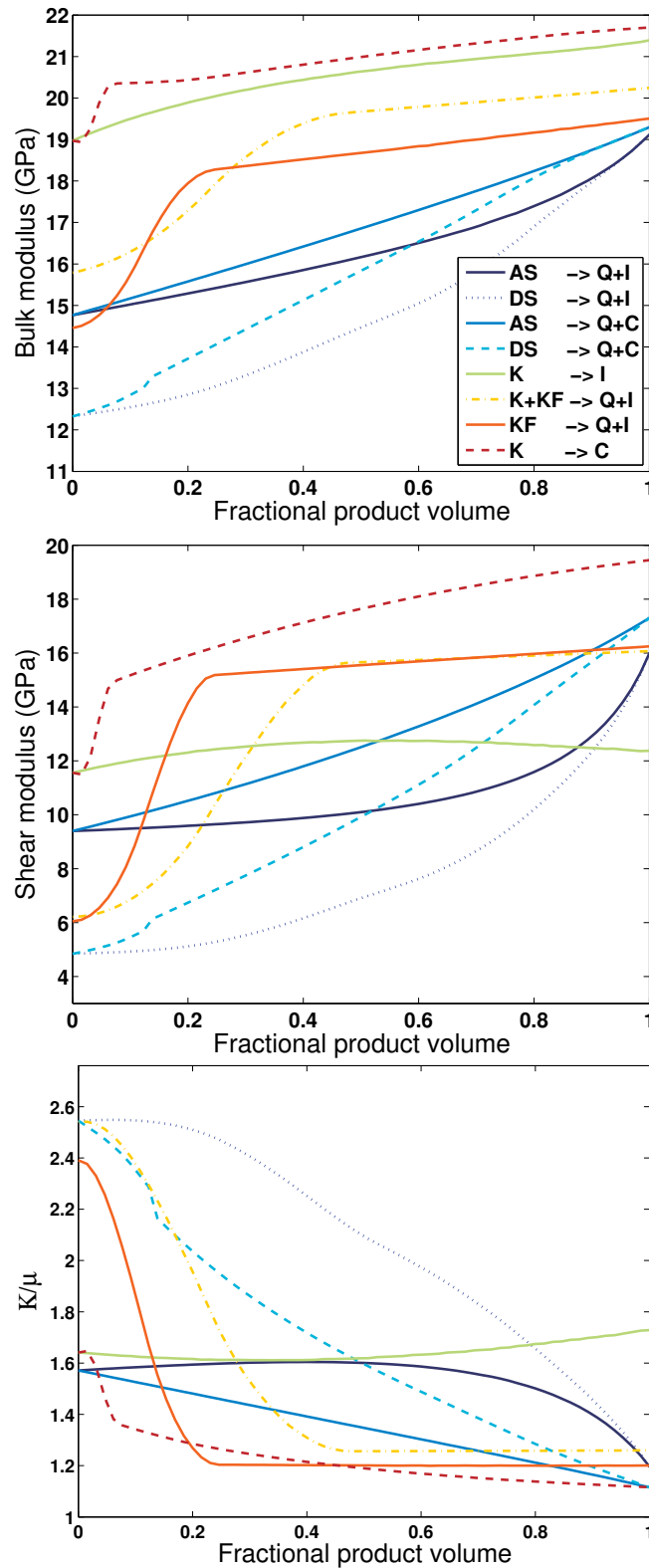
Figure 6. Modelled examples of how effective rock properties can vary due to diagenetic mineral reactions. AS and DS denote authigenic- and detrital smectite respectively. The reactants (to the left in the legend) constitute 100 % of the cement to the left in the graphs, and decrease when moving along the x-axis. When fractional product volume reaches one, all the reactants are consumed, and the cement is the product mineral of the reactions. Because the product volumes differ from the reactant volumes (see Table 2), the final cement volumes differ in the reactions.
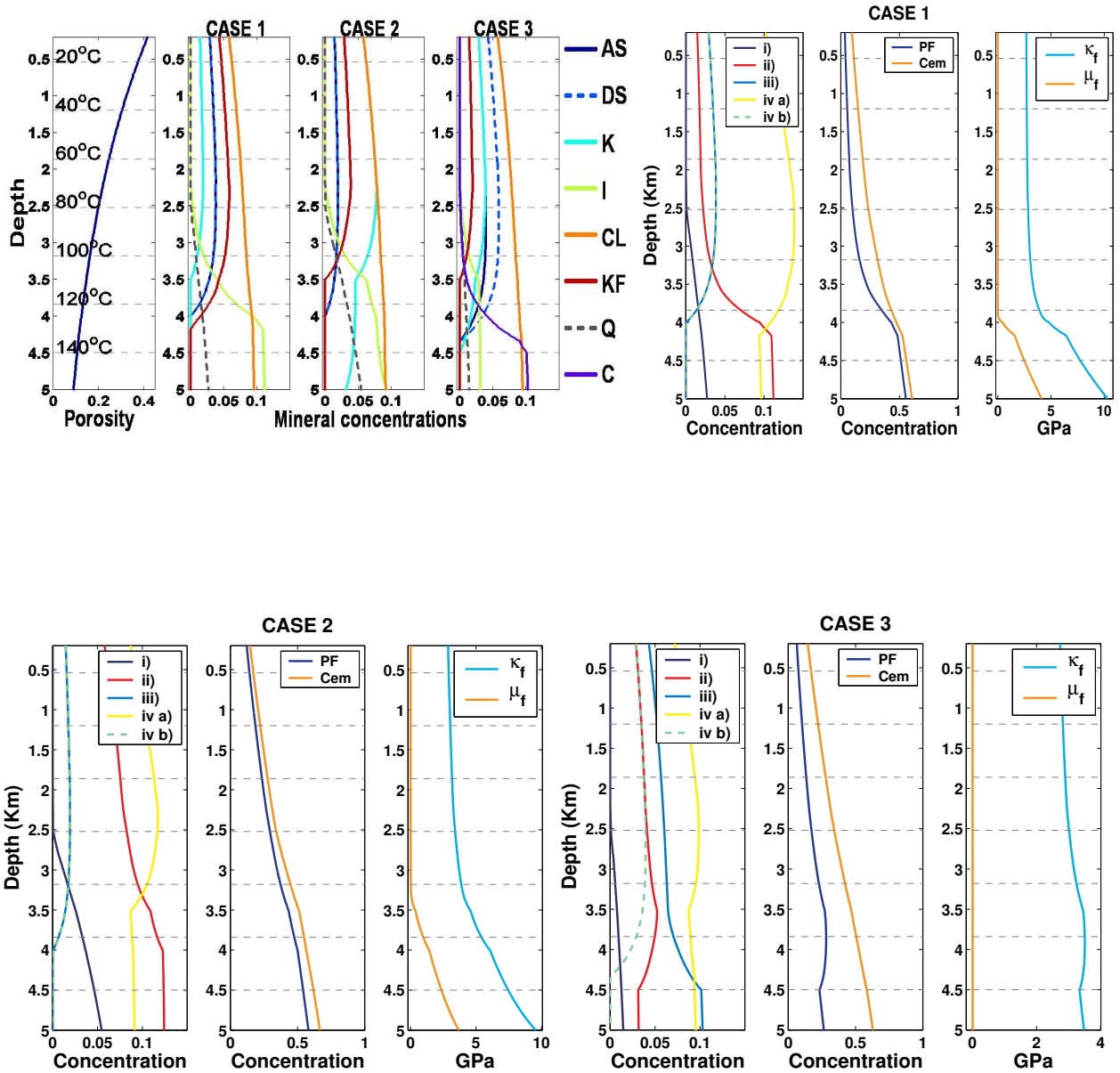
Figure 7. Above: The porosity-depth curve for all cases listed in Table 3 is shown to the left, together with stippled temperature lines. The modelled mineral evolutions are shown in the three next curves for case 1, 2 and 3 respectively. Concentrations of the different distributions, amount of pore-filling (PF) and total cement (Cem) relative to intergranular volume, fluid bulk modulus (κ_f) and shear modulus (μ_f) with depth are shown for case 1-3 in the other curves. Distribution **iv a)** is not included as a cement when calculating PF and Cem, since it constitutes a part of the effective framework, and do not fill up the space between framework grains.
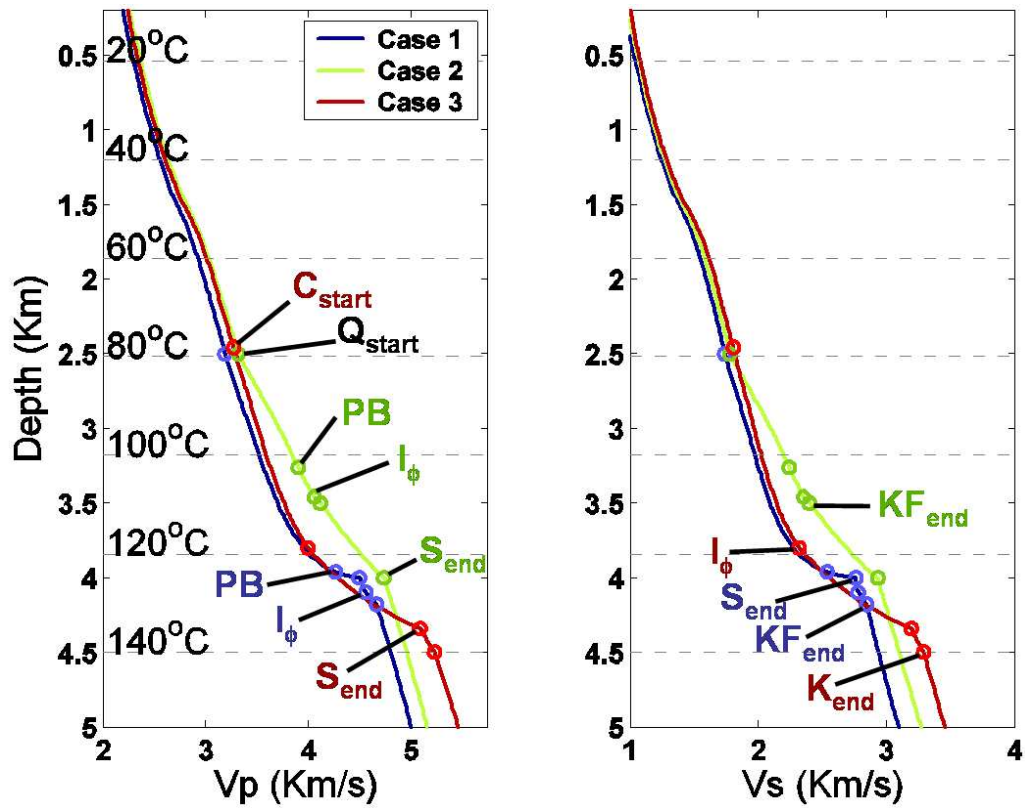
Figure 8. V_p and V_s versus depth are shown for the three cases. The coloured rings around the curves are related to mineralogical and physical changes in the rocks, and are discussed in the text. PB and I_ϕ denote incipient pore-bridging and seismic isolation of pores respectively. S, Q, K, KF and C are minerals, while start and end denote the start and end of the reaction in which the mineral is a part of.
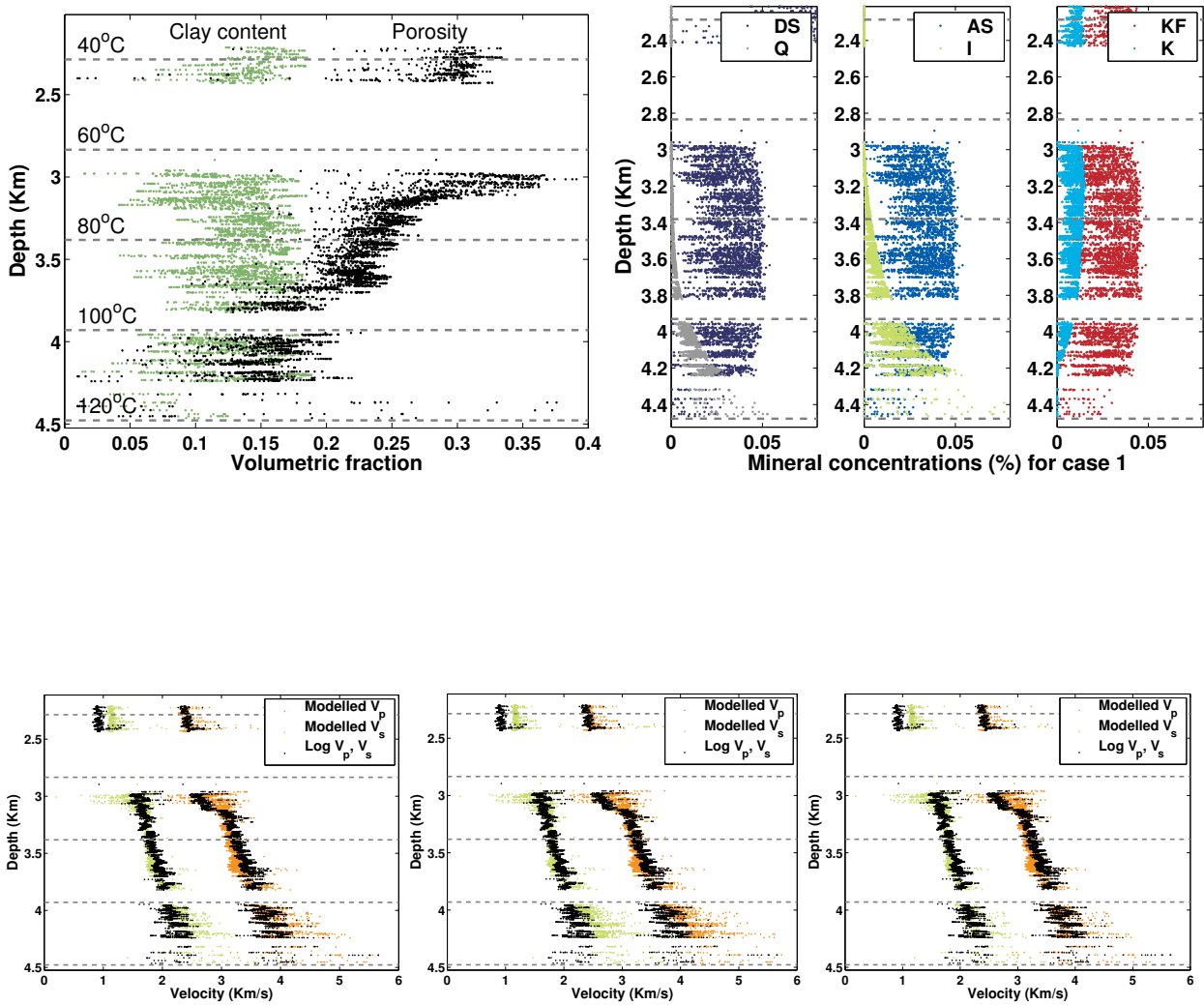
Figure 9. Above: The left plot shows the porosity and clay content from the well log. The right graphs show the modelled mineralogy for the case 1 model. The relative mineral concentrations are the same as for case 1 in the constructed example. Below: The modelled velocity curves for case 1-3 are shown together with the log velocities from left to right, respectively. All log points with more than 20 % clay in the solid part of the rock are excluded.
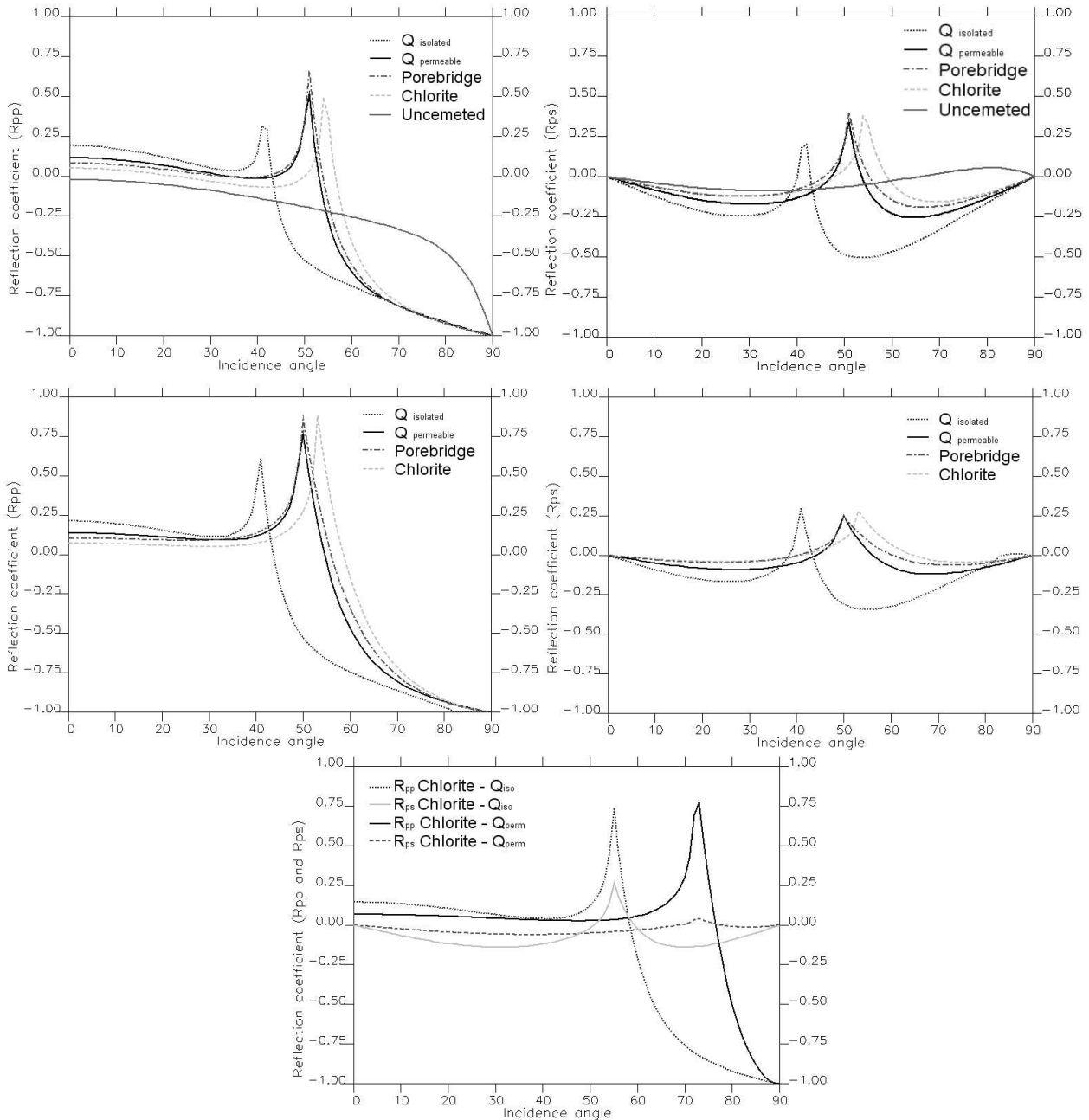
Figure 10. P- and S-wave reflectivity from an incident P-wave. The two upper plots shows an example with a shale overlaying a quartz cemented sand with seismic impermeable pores (Q_{iso}), a permeable quartz cemented sand (Q_{perm}), a pore-bridged, chlorite cemented and uncemented sand, respectively. The plots in the middle shows coefficients with an overlying uncemented sand, while the lower plot illustrates an example with a high porosity chlorite (22.5 %) overlying i) a quartz cemented and seismic impermeable sandstone and ii) a quartz cemented permeable sandstone, both with 10 % porosity. Layer properties are defined in Table 4.
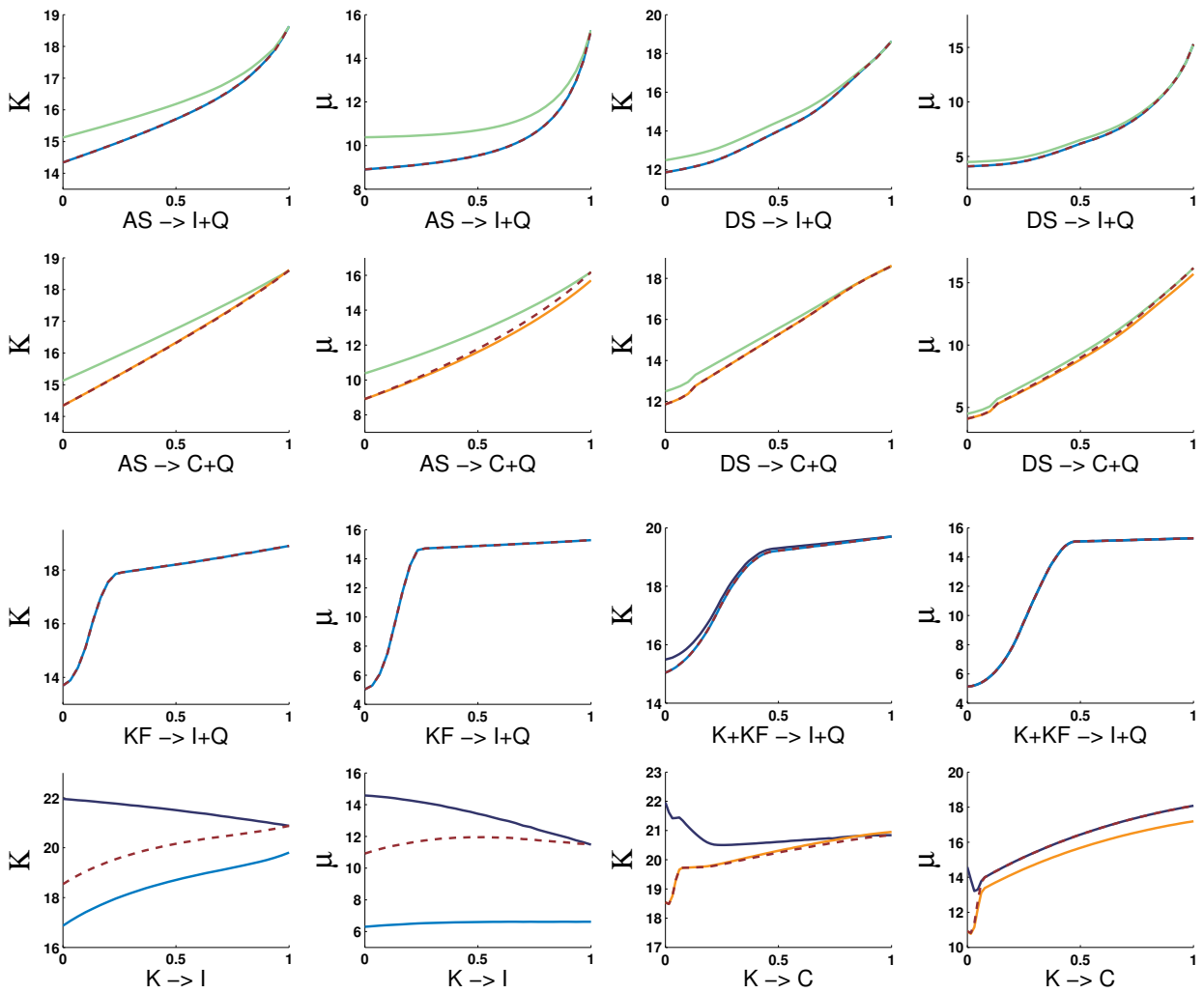
Figure 11. The figure shows the same mineral reactions as in Figure 6, but with new mineral properties. The brown stippled lines correspond to the original mineral properties, and are identical to the curves in Figure 6. Dark blue, light blue, orange and green are the colours of the curves with alternative kaolinite, illite, chlorite and smectite properties from Table 5, respectively.

APPENDIX

Bound averaging method (BAM)

The bound averaging method (Marion and Nur, 1991) is used to estimate effective bulk and shear modulus in a rock with pore-filling materials with non-zero shear stiffness. The model requires the same input as the Gassmann (1951) model:

$$K_{sat} = K_{dry} \frac{\left(1 - \frac{K_{dry}}{K_m} A\right)}{\frac{\phi}{K_f} + \frac{(1-\phi)}{K_m}}$$

and

$$\mu_{sat} = \mu_{dry}.$$

The subscripts *sat, dry, m* and *f* denote the properties for the saturated rock, dry rock, framework material and fluid, respectively. If the ratio K_f / K_m is assumed to be much smaller than one (typically on the order of 0.05), an approximate value for A is given by $A_{vr} \approx 1 + \phi$, when A is calculated by using the Voigt-Reuss bounds.

Weighting function when using Hill average

In this paper the Hill (1952) average is used to describe transitions from uncemented to cemented rock and from connected to isolated pores. The transition can be linear or non-linear, dependent on the weight used. The chosen weight applied is composed of two parts $W^{(1)}$ and $W^{(2)}$. $W^{(1)}$ is estimated as follows:

$$W^{(1,1)} = \frac{0^2}{n^2}\left(m - \frac{1}{2n}\right)$$

$$W^{(1,2)} = \frac{1^2}{n^2}\left(m - \frac{1}{2n}\right)$$

...

$$W^{(1,n-1)} = \frac{(n-1)^2}{n^2}\left(m - \frac{1}{2n}\right)$$

$$W^{(1,n)} = \frac{n^2}{n^2}\left(m - \frac{1}{2n}\right)$$

where 2n is the length of the weight and m is the mean value of the weight (commonly 0.5). This expression can be rewritten to:

$$W_r^{(1)} = \frac{r^2(2mn-1)}{2n^3},$$

where r = 0,1,…, n-1, n.
$W^{(2)}$ can now be written as:

$$W^{(2,1)} = 1 - W^{(1,n)}$$

$$W^{(2,2)} = 1 - W^{(1,n-1)}$$

...

$$W^{(2,n-1)} = 1 - W^{(1,2)}$$

$$W^{(2,n)} = 1 - W^{(1,1)}$$

which can be written:

$$W_r^{(2)} = 1 - \frac{(n+1-r)^2(2mn-1)}{2n^3}.$$

where r = n+1, n+2,…, 2n-1, 2n. The final weight then becomes $W = [W^{(1)}, W^{(2)}]$. The weight is shown in Figure 12. The shape of the weight reflects the assumption that the transitions are slowest near the terminal points (0 and 1). For the transition from uncemented to contact cemented rock (constant porosity) this implies that the very first contact cement (stage 1), only present in some of the contacts, can not contribute much to stiffen the whole rock. When all contacts approaches cemented however, the overall rock stiffness increases drastically (stage 2). But when the rock is pervasively contact cemented (stage 3), additional cementation does not contribute much to further stiffness increase, and the gradient of the weight decreases.
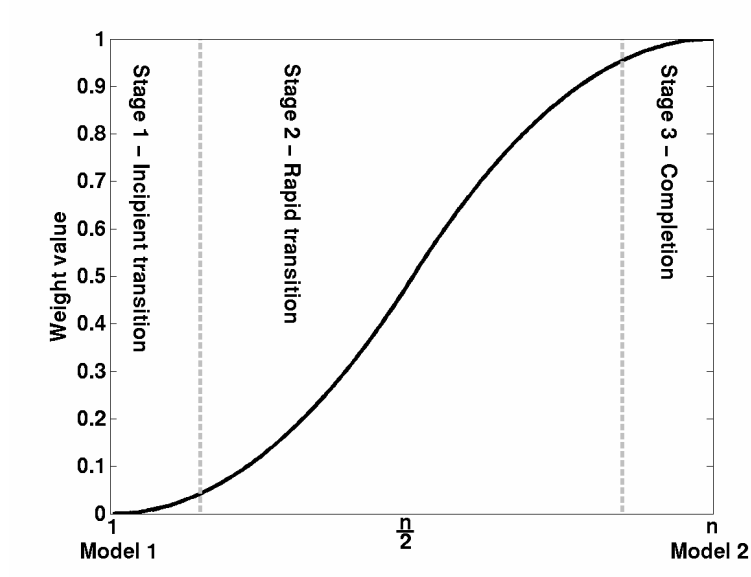
Figure 12. The non-linear symmetric weight of length n is applied in the transitions between different rock physics models. At the terminal points the transition speed is considered to be lower than in the stages between.

8   Paper 3

Interplay between mineralogy and velocity-depth trends during diagenesis in siliciclastic rocks

Interplay between mineralogy and velocity-depth trends during diagenesis in siliciclastic rocks

Anders Dræge[1,2]

[1]*Department of Earth Science, Allegaten 41, 5007, University of Bergen, Norway*
[2]*Centre for Integrated Petroleum Research, Allegaten 41, 5007 Bergen,University of Bergen, Norway*
(*E-mail: Anders.Drage@geo.uib.no*)

ABSTRACT: *The evolution of rock physical properties during diagenesis is in a great degree dependent on geological processes like dissolution and precipitation of various minerals. Diagenetic mineral reactions consume reactants and lead to precipitation of cements, and both these processes alter the composition of solids and potentially the distribution and volumes of solids. Therefore some mineral reactions influence the velocity-depth gradients when they occur. The reactions are mainly controlled by temperature and temperature-depth ratio. Geologists have constrained numerous mineralogical reactions to certain temperature intervals, which are used to guide the modelling in this paper. Simple geological modelling of mineralogy versus temperature (depth) is used for different successions of mineral reactions. A selection of depositional environments where these successions are prone to occur are also described. It is demonstrated that mineral transitions play important roles in diagenetic processes in rocks, such as cementation, pore-bridging, permeability and porosity loss. These parameters are the ones with largest influence on velocity-depth trends in the modelling. The combined development of these four parameters with depth differs between each modelled mineralogical scenario. Hence, unique velocity-depth trends for each scenario are modelled, that are products of the successions of mineral reactions involved. Finally the evolution of the velocity gradient versus depth is analysed, for different mineralogies, and qualitative seismic diagenetic fingerprints which differ for each succession of mineral reactions are derived.*

INTRODUCTION

Diagenesis comprises a broad spectrum of physical, chemical and biological post-depositional processes by which original sedimentary assemblages and their interstitial pore waters react in an attempt to reach textural and geochemical equilibrium with their environment. Temperature dependencies of mineral reactions are described by e.g. Bjørlykke & Brendsdal (1986), Walderhaug (1996), Bjørkum & Nadeau (1998), Morad et al. (2000) and Worden & Burley (2003). A consequence of the temperature dependency is that minerals stable with surface conditions can evolve into unstable minerals during burial/increased temperature. Conversely, unstable surface minerals can enter conditions where they are stable, during burial. Worden & Burley (2003) asserted that the gross depositional environment of a sand controls most eogenetic (T<70 $^{\circ}$C) processes and imparts a distinctive diagenetic 'fingerprint', or assemblage, on the sandstone. This fingerprint is related to the depositional

mineralogy of the rock, and how the mineralogy evolves during burial/increased temperature. But if there exist such a mineralogical diagenetic fingerprint, then it should be possible to reveal a seismic diagenetic fingerprint as well, given the mineralogical evolution versus depth. Seismic diagenetic fingerprint denotes the link between successions of mineralogical reactions versus depth (temperature), and evolution of seismic rock properties like P-wave velocities (V_p) and S-wave velocities (V_s) versus depth (temperature).

Mineral reactions influence the overall rock stiffness, and thereby the seismic velocities in several ways (Dræge et al., 2006b); reactants get consumed and 'new' minerals with new physical properties precipitate as cement, the volume of solids are likely to change, chemical compaction influence the porosity and the precipitated minerals can acquire different distributions than the reactants had. When trying to model realistic evolutions of seismic velocities during diagenesis, all these processes should be accounted for. The volume difference between reactants and products can be estimated, given the chemical formulae, stoichiometrically balanced (due to number of molecules) reactions, and the densities of the involved minerals. The porosity changes are modelled by a modified version of the clay dependent porosity-depth model for sands and shales (Ramm & Bjørlykke, 1994). The strategy of Dræge et al. (2006b) is adopted, and all minerals involved are classified due to four main classes of distribution for precipitated minerals (cement) and clasts; **i)** cement that lies in the grain contacts, but not between grains, and stabilizes the contacts between framework grains, **ii)** pore-filling cement that contributes little to the overall rock stiffness until they become pore-bridging when presented at approximately 40 % or more in the pores, **iii)** graincoating and pore lining cement, that envelop the framework grains, but does not carry load in the framework grain-grain contacts, **iv a)** replacive clay or clay clasts

which act as a part of the loadbearing framework and **iv b)** graincoating clay cement that prevent contact between the framework grains, and thus are loadbearing. The distribution types are illustrated in Figure 1. If fluid changes and deviating porosity trends (e.g. from overpressure) are disregarded, it is assumed that for a constant temperature/depth ratio, mineral reactions, pore-bridging and seismic isolation of pores can be held responsible for changes in seismic velocities versus depth. Seismic isolation means the inability of fluid to escape from high pressure areas to relaxed areas, when a seismic wave travels through the rock. These assumptions enable an analysis of velocity-depth (temperature) trends for various mineralogical settings.

Figure 2 is a principle sketch which illustrates how various diagenetic processes can influence velocity evolution with decreasing porosity (the porosity-depth curve is constant). The mechanical compaction line denotes a hypothetical rock with no cementation, and gives the lowest velocities for low porosities. The curve with pore-filling cement that evolves to pore-bridging initially shows lower velocities than the compaction line. That is a result of cement precipitating in the pore space, with no other rock stabilizing function than increasing the effective fluid bulk modulus. But when the concentration of pore-filling cement gets sufficiently high, the cement bridges the pores and an abrupt velocity increase is expected. Shallow contact cementation (e.g. calcite) rapidly increases velocities. Contact cement can precipitate at various diagenetic stages, and increases the velocities when it occurs. Dissolution of soft loadbearing minerals like various framework clays, increases the effective framework stiffness, and hence the velocities. Finally, incipient seismic isolation of pores increases velocities more than the compaction line, until all pores are isolated. Many of these processes are interrelated and rarely occur alone. The processes can occur at various stages of diagenesis, dependent on various

factors like mineralogy, temperature, permeability, pore fluid chemistry and availability of reactant minerals in general. The diagenetic processes in Figure 2 can also influence porosity in various ways, which is not considered in this principle sketch.

The paper starts with presenting the rock physics model involved in this study. Then a selection of mineralogical settings is described, and mineralogy evolution versus depth (temperature) is modelled for each setting. Instead of composing artificial mineral settings, the link between mineralogy compositions, succession of mineralogical reactions and depositional environments presented by Morad et al. (2000) is applied. Connections between mineralogy, diagenesis and depositional environments are also described by authors like Getti & Brigatti (1991), Hillier (1993), Ingles et al. (1998), Segall et al (2000), Worden & Morad (2003) and Worden & Burley (2003). The coupling with depositional environment is done both for the purpose of illustrating the application of the models, and to demonstrate that even though the variations can be large from place to place, some mineral reactions are prone to occur in certain depositional environments. The modelled mineralogies are used to estimate the evolution of seismic velocities versus depth for each mineralogical setting. The velocities are further analysed with special focus on the diagenetic processes in Figure 2, to study how mineralogy and diagenetic processes influence the different velocity curves. Finally, seismic diagenetic fingerprints are presented, which constitute a qualitative signature for each of the successions of mineral reactions. The differences between the fingerprints are a consequence of variations in diagenetic processes and at which stage they occur in the different scenarios studied, see Figure 2.

ROCK PHYSICS STRATEGY

The strategy presented by Dræge et al. (2006b) is used to model different mineral compositions in sandstones (clay content < 45 %). This strategy involves a classification of every mineral involved, due to four distribution classes which are illustrated in Figure 1. A selection of various rock physics models is used to account for different distributions. When simultaneous distributions occur, or in transitions from one model to another (e.g. from seismic permeable to seismic isolated), the problem is approached by estimating the elasticities for each case, and then apply the Hill (1952) average between the various models.

If pore-filling cement is present, self consistent approximation (SCA) (Willis, 1977) is applied to estimate the effective properties of the fluid-cement mixture. The estimated properties are used as fluid properties in further calculations, like shown in Figure 3. When the concentration of pore-filling cement exceeds approximately 40 % of intergranular volume, the SCA model returns effective fluid properties with positive shear stiffness. This is considered to approximate pore-bridging, and can increase the overall stiffness significantly.

The minerals with distribution types **iv a)** and **b)** are considered isolated and connected framework minerals, respectively. They contribute in the effective loadbearing framework, and differential effective medium (DEM) (Nishizawa, 1982) and combined effective medium theory (CEMT) (Hornby et al., 1994; Jakobsen et al., 2000) are applied to approximate the isolated and connected framework inclusions, respectively. The CEMT model is applied to approach connected phases in a composite medium when the rock consists of more than one connected phase. The model consists of two steps, where the first step make use of SCA to yield a mix of equal and connected volumes of two constituents. Secondly, the DEM is used to model the effective stiffness at desired concentrations.

Permeable rocks with distribution types **ii)** and **iv a,b)** are modelled with the combined theories of Hertz-Mindlin (HM) (Mindlin, 1949) and Hashin & Shtrikman (1963) (HS)

lower bound, like described in Dvorkin & Nur (1996). This combined model (HMHS) connects two end members; one has zero porosity and the modulus of the solid phase, and the other has critical porosity and a pressure dependent modulus as given by the Hertz-Mindlin theory.

The contact cement theory (CCT) of Dvorkin et al. (1999) is applied to model the first stages of type **i)** cement. CCT provides the effective elastic properties of an aggregate of spheres, where the spheres are in direct point contact, and cement fills the space around the contacts. CCT is combined with DEM for high cement concentrations. The DEM is used to approximate seismic isolated inclusions in the rock, like pores in a low-permeable rock.

The scheme 2 cement in Dvorkin & Nur (1996) is applied to model coated spheres (CS), distribution **iii)**. This model treats the cement as evenly deposited on the grain surface, which leads to coated framework grains. As for the CCT model it is combined with an effective medium model (CEMT) when the cement concentration gets high, to approximate a rock with two connected solid phases - cement and framework. If distribution models **i)** and **iii)** both are present, the Hill (1952) average is applied between the modelling results for each distribution to obtain the final effective medium properties. When several simultaneous distributions are present, the procedure in Figure 3 is followed.

The Bound Averaging Method (Marion & Nur, 1991) is applied to model the effects of fluid saturation in permeable sandstones. This model is meant to correspond with the Gassmann (1951) model, but for viscous fluids. The effective fluids might be viscous due to pore-filling cement. The DEM is applied for modelling the fluid effects in non-permeable rocks. In transitions from uncemented to cemented rock, and from permeable to impermeable rock, the Hill average between the different models is applied to obtain smooth transitions.

Following Dræge et al. (2006b), seismic isolation of pores is considered to start when the cement volume exceeds 50 % of intergranular volume. When the amount of cement reaches 75 % of intergranular volume, all pores are treated as seismic isolated. In the interval of 50 - 75 % cementation, the Hill (1952) average is applied between the models for connected pores and the models for seismic isolated pores, with increasingly weight on the latter. The limits for seismic isolation are adjustable parameters, and are expected to be influenced by pore-shape; narrow pores are easier blocked than spherical pores.

The seismic properties during mechanical and chemical compaction of shales (clay content > 55 %) are estimated by the shale compaction model of Ruud et al. (2003) and the shale cementation model of Dræge et al. (2006a), respectively. The shale compaction model is based on the Mori-Tanaka method (Mori & Tanaka, 1973) and SCA model. It also introduces theories for estimating clay mineral orientation, porosity, critical porosity and pore fluid shape as a function of only two parameters - compaction and/or silt content. Silt particles are considered as isolated inclusions while pores are connected.

The modelling with the shale cementation model is performed along a modified version of the three-step procedure formulated by Hornby et al. (1994); 1) Mix framework clay with cement at equal concentrations, by using SCA. 2) Use DEM to adjust constituent concentrations to desired levels. 3) Add fluid as isolated inclusions. 4) Apply an orientation distribution function, and use Voigt (1928) to average over the distributions. 5) Use DEM to add quartz as isolated inclusions. The grain orientation, pore and cement shape is considered constant with increasing depth/temperature. Pores and silt particles are considered isolated inclusions while cement constitutes a connected phase. Whenever the concentration of clay minerals is between 45 - 55 % of the solid rock, the Hill (1952)

average is applied between the appropriate shale model and the sand model, to obtain continuity in the stiffness estimation.

The porosity is estimated by a modified version of the depth and clay dependent porosity model of Ramm & Bjørlykke (1994):

$$\phi = \phi_0 e^{-(\alpha+(\beta*Cl))*Z} \quad , Cl > 0.2 \ \ or \ Z \leq Z',$$
$$\phi = \phi' - \gamma(Z - Z') \quad , Cl \leq 0.2 \ and \ Z > Z'.$$
(1)

Z, Cl, α, β and γ denote burial depth, the ratio of clay volume relative to total volume of stable framework, framework grain stability factor for clean sandstones (Cl=0), sensitivity towards increasing clay index (Cl) and porosity loss factor for quartz cemented rocks, respectively. The subscript 'o' denotes the parameter value at deposition, while marked parameters denote the parameter value at the initiation depth for quartz cementing. α and β are given the values 0.25 and 0.3 in the modelling, respectively, while the γ-values vary according to how much (if any) quartz cement is expected. The porosity model yields exponential decreasing porosity for non-quartz cemented rocks, and linear porosity loss for quartz cemented sandstones. The porosity loss in quartz cemented sandstones is higher than in more clay rich rocks without quartz cement. Although calcite cement can have large influence on porosity evolution with depth, it is not included as a parameter in the porosity-depth model. The model does also not incorporate grain sorting and grain surface area available for cementation, which can be important when estimating porosity during diagenesis.

MINERALOGY AND DIAGENESIS IN VARIOUS DEPOSITIONAL SETTINGS

The diagenesis is divided into three stages (Morad et al., 2000); eogenesis (temperature, T≤70°C), shallow mesogenesis (70°C < T < 100°C) and deep mesogenesis (T≥100°C). The focus in this paper is on successions of

mineral reactions that are common in fluvial and wave and storm dominated shelf depositional settings. These depositional settings are described in Morad et al. (2000), and Figure 4 - 5 are modifications of illustrations from that paper. The classification of minerals due to distributions is shown in Table 1, while the mineralogical reactions involved are shown in Table 2. Table 3 shows which mineral reactions and infiltrated minerals characterize the different hypothetical environments.

Fluvial depositional systems

Braided rivers commonly lie closer to the sediment source than do meandering rivers. Thus the sediments are expected to be more immature, and not degraded by weathering processes in the same way as further from the sediment source, where the environment has had more time to eliminate unstable minerals (McKinley et al., 2003). Smectite is a clay mineral that is expected to be abundant in braided rivers, and gradually decrease in concentration until it is practically absent at shore/foreshore deposits (McKinley et al., 2003; Worden & Morad, 2003). Infiltrated clay coats are common in braided river deposits, and braided rivers have thick dioctahedral smectite coatings that evolve to thick illite boxwork during mesogenesis (Morad et al., 2000). Worden & Morad (2003) asserted that the illitization of smectite is the dominating mineral reaction in braided rivers, which coincides with the observations of Lowey (2002). K-feldspar and albite transformation to smectite, illite and kaolinite is important in environments with extensive weathering (McKinley et al., 2003). Thus the concentrations of K-feldspar, albite and smectite in the river channel sands are considered to decrease with distance to source rock in fluvial systems. Plagioclase typically weathers faster than K-feldspar (Le Pera et al., 2001), so the plagioclase/K-feldspar ratio should decrease with distance to source rock.

Figure 4 illustrates four common fluvial environments together with the most common

dominating mineralogical processes during diagenesis and eogenesis. The modelled mineralogical and porosity evolution is shown below for braided river and each of the depositional environments in the illustration. The γ in equation 1 is set to 8 when estimating porosity for meandering rivers, due to quartz cement and quartz dominated framework. Other porosities are estimated with the equation for rocks with higher clay content.

Meandering rivers tend to be confined within a single major channel, characterized by cohesive banks that are difficult to erode. Weathering persists for a longer time interval than in braided rivers, and the sediment becomes more mature. The deposits include coarse bedload gravels and clasts of partly consolidated mud eroded from the channel wall. In proximal fluvial sediments, active percolation of undersaturated meteoric waters causes the dissolution of detrital silicates (primarily lithic grains, feldspar and mica) and precipitation of kaolinite (Morad et al., 2000; Segall et al., 2000; Bjørlykke, 2001). Kaolinite dominates in warm and wet environments, and some of the earliest reactions to occur are the replacement of albite and calcic plagioclase by kaolinite (Worden & Morad, 2003). Calcite concretions and cemented layers frequently occur in the eogenesis of channel sands (Morad et al., 2000). In the first stage of burial, kaolinite, mica and smectite get infiltrated into the sandstones (Morad et al., 2000; Segall et al., 2000). Precipitation of calcite cement and formation of kaolinite dominate the eogenesis of the river channel. Dickitization of kaolinite and illitization of smectite and quartz cementation are considered the dominant mesogenetic reactions in meandering rivers. Transformation of kaolinite to dickite can be aided by increasing acidity of formation water or decrease in the K^+(potassium ion)/H^+ (hydrogen ion) - ratio, which also triggers dissolution of framework silicates (e.g. feldspars) and carbonate cement precipitation (Worden & Morad, 2003).

Crevasse splay deposits may occur on floodplains where rising floodwaters breach natural levees. Sedimentation from traction and suspension occurs rapidly as water containing both coarse bedload sediment and suspended sediment debouches suddenly onto the plain, resulting in graded deposits that may resemble a Bouma turbidite sequence. Kaolinite formation can be of less importance in crevasse splay environment (Morad et al., 2000), but this is also dependent on climate. Warm, wet, typically verdant, subaerial eogenetic environments reduce ferric irons in the solid sediments to Fe^{2+} form by the redox processes, and often make it available for incorporation in siderite ($FeCO_3$). Siderite dominated eogenetic carbonates occur owing to local enrichment of iron in the system, resulting from the alteration of Fe-rich detrital clays. Small concentrations of siderite are therefore not uncommon during diagenesis of crevasse splay sediments, in addition to shallow vadose occurrences of calcrete and dolocrete. During mesogenesis, infiltrated clays become unstable, and transform to illite and/or chlorite. Small amounts of quartz cement are expected at large depths, see Figure 4.

Overbank flooding leads to deposition of fine silt and mud on the bank near the stream edge. Mud-rich surface water is prevalent in floodplain deposits (Worden & Morad, 2003). Siderite is a common, yet often minor diagenetic cement in siliciclastic fluvial overbank sediments (Morad et al., 2000), like floodplain deposits, oxbow lakes and crevasse splay. Vadose calcrete and dolocrete are introduced to the mudrock at shallow burial, while siderite cement is considered to precipitate from 10 - 70°C. Acidic (for instance from CO_2 in pore water) water favours dissolution of K-feldspar, and hence formation of kaolinite. Peat and coal deposits will enhance CO_2 production, and thereby increase formation of kaolinite. Illitization of kaolinite and K-feldspar are expected to characterize the high temperature mineralogical processes.

Oxbow lakes are the results of new river channels being cut, that bypass the old river and leave curved lakes behind. Oxbow lake deposits consist of fine silt and mud transported into the lakes from the main stream during overbank flooding (Boggs, 1995). Stagnant water leads to higher aqueous potassium and silica concentrations, and thus results in smectite growth (instead of kaolinite growth as under the main channel) or the growth of various 'green clays' like Fe-rich smectites (Worden & Burley, 2003). Siderite can occur in minor amounts during early diagenesis in oxbow lakes, while mesogenesis is commonly dominated by chloritization or illitization of smectite (Morad et al., 2000).

Wave and storm dominated shelf

Wave and storm dominated shelf settings are illustrated in Figure 5. The γ values 7 and 8 are assigned in the porosity estimation for the shoreface and backshore/foreshore environments respectively, while other porosities are estimated with the formula for higher clay content in equation 1. A coastal lagoon is a shallow stretch of seawater, near or communicating with the sea. It is partly or completely separated from the sea by a low, narrow, elongate strip of land, such as a reef, barrier island, sandbank or spit. Lagoons are predominantly areas of low water energy (Boggs, 1995), thus the sediments are mostly fine grained. Most or all of the sediments are from marine sources, since lagoons commonly do not receive freshwater discharge from rivers. According to Morad et al. (2000), the most important eogenetic processes in lagoons are precipitation of pyrite, siderite, dolomite, sulphates and K-feldspar. Anhydrite is used as a representative for sulphates, since anhydrite cement result from circulation of evaporite-related pore waters (Worden & Burley, 2003), which is typical for lagoonal environments with arid conditions (Boggs, 1995). When temperature exceeds $70^{\circ}C$, illitization of kaolinite and chloritization of smectite are considered to be the dominating mineralogical processes in the

rock, but albitization of detrital K-feldspar is also expected.

The foreshore represents the shore area most influenced by the high and low water marks and breaking waves, while backshore is submerged only during the highest tides and severest storms. Smectite and other syndepositional clay matrix, is typically absent or minor in continually high-energy environments, such as beaches, where the action of waves and ebb and flow tidal currents winnow out the fine-grained clays from the sand- and silt-grade material (McKinley et al., 2003). Thus relatively clean quartz-rich sands are expected. Some shallow calcite cementation can occur, but pervasive quartz cementation in the mesogenetic realm is expected in such clean sands.

Marine depositional environment often contains calcareous organisms (Bjørlykke, 2001; Worden & Burley, 2003), and their presence both in upper and lower shoreface is common. Upper shoreface refers to the portion of the seafloor that is shallow enough to be agitated by everyday wave action, while lower shoreface refers to the portion of the seafloor that lies below everyday wave base. The relative concentrations of minerals are likely to vary between sandstones from upper and lower shoreface, but according to Morad et al. (2000) the most important eogenetic and mesogenetic processes are: shallow dissolution of calcareous material, mainly shell fragments, followed by precipitation of calcite cement, and mesogenetic quartz cementation and illitization and chloritization of detrital clay coats.

The offshore sediments are likely to contain finer grains and mud, since the energy level is lower. Siderite in particular, is formed in a more distal extent of calcite and dolomite cemented lags, possibly because of the lower amounts of organic matter and thus prolonged suboxic diagenesis (Ketzer, 2002). Glaucony forms in the outer shelf, from suboxic marine pore waters that undergo nitrate reduction immediately below the seafloor (Morad et al.,

2000; Ketzer, 2002). In some cases the formation of glaucony are closely linked to the alteration of volcanic ash layers, as these layers release considerable amounts of Fe, Mg, K, Si and Al ions upon interaction with seawater. Graincoating apatite is used as a representative for eogenetic precipitated phosphates, since apatite is the most common phosphate mineral (White et al., 2004). Illitization of detrital smectite is considered to characterize the mesogenetic mineral transitions.

MODELLING OF ROCK PROPERTIES DURING DIAGENESIS

The parameters which influence velocity evolution most in the modelling are mineral distributions (e.g. amount of contact cementing or grain coating minerals), pore bridging, porosity and seismic isolation of pores. A distribution type is assigned to each mineral, see Table 1, so the concentration of a distribution is dependent on the sum of concentrations of minerals with that distribution. Incipient pore bridging occurs when the amount of pore filling cement (distribution **ii**)) exceeds approximately 40 % of the intergranular volume. Seismic isolation of pores increases from 0 - 100 % when cement concentration increases from 50 - 75 % of intergranular volume. The porosity is modelled with the clay dependent porosity - depth model in equation 1, and is shown together with mineralogies for the different scenarios in Figure 4 - 5. When the following analyses denote depths at where pores start to become seismic isolated or pore-filling cement become pore-bridging, the hypothetical modelled scenarios with given temperature/depth ratio are considered, not the behaviour of the mentioned depositional environments in general. In reality, both mineral composition and mineral reactions are likely to display some variations between similar depositional environments due to e.g. differences in climate or differences in source rock mineralogy. This will be discussed later.

Fluvial depositional systems

Figure 6 shows the modelled velocity evolution, distribution concentrations, fraction of total cement volume due to intergranular volume, fraction of pore-filling cement due to available pore space, and effective fluid properties versus depth for fluvial environments. The braided river example has high concentrations of detrital and infiltrated smectite, which transforms to pervasive pore-filling/bridging illite. This entails high effective fluid properties from ca 3.8 km depth (120°C), and is reflected in increasing velocity/depth gradient. The gradients for both V_p and V_s increase further when all grain coating (distribution **iv b**)) smectite get consumed when approaching 125°C, since smectite is a very compliant mineral. From ca 4.2 km the pores start to become increasingly seismic isolated, which together with small amounts of quartz cement contribute to high velocities at larger depths. The modelled effects of non-pore-filling cementation are generally largest before the cement gets pervasive. Hence, an increase in cement volume from 0 - 5 % generally affects the velocities considerably more than an increase from 10 - 15 %. The pore-filling cement has largest influence on velocities from incipient pore-bridging at approximately 40 % cementation. So even if cement continues to precipitate at large depths, a decline in the modelled velocity-depth ratio can often be observed when the rock is pervasively cemented.

The meandering river example displays a smooth velocity increase until quartz cementation initiates at 2.5 km. The velocity-depth ratio then increases somewhat. Incipient pore-bridging occurs at ca 3.8 km, illitization of soft loadbearing smectite moves towards completion at ca 4 km and at 4.2 km the pores start to get increasingly seismic isolated. The sum of these effects produces a steep velocity increase from 3.8 to 4.5 km. Deeper than 4.5 km, the rock is pervasively cemented and almost all pores are seismic

isolated, leading to less velocity increase with depth.

Due to precipitation of calcitic cements, the velocities are relatively high in the shallow part of the crevasse splay example. The early cementation makes the rock more rigid and less susceptible to large stiffness changes with depth. Pores start to get seismic isolated at around 4.4 km, but no pore-bridging is expected in the modelled interval. The velocity- depth changes are significantly less than the two previous examples.

The oxbow lake example produces some pore-filling type **ii)** cement, but due to high porosities, no pore-bridging is expected. The effect of consuming soft loadbearing smectite is not so great in rocks with clay dominated framework, because the stiffness difference is lower. But mesogenic precipitation of chlorite entails a pronounced velocity increase from 2.7 km. Seismic isolation of pores starts at 4.5 km, but at 5 km there is still communication between most of the pores. Precipitation of eogenic siderite (10 - 70°C) contributes to the shallow velocity increase.

As for the oxbow lake, eogenic siderite causes a shallow velocity increase in the floodplain example. Neither pore-bridging nor seismic isolation of pores occur, and together with modest amounts of cements it leads to low mesogenic velocity increase.

Wave and storm dominated shelf

The velocity and velocity-influencing parameters are shown in Figure 7 for shelfal depositional settings. The lagoonal example has relatively high concentrations of all distributions. The early precipitation of calcitic cements, sulphate and K-feldspar increases the velocity through the eogenesis. Chloritization of smectite from 2.5 km increases velocities in the shallow mesogenesis, while incipient pore-bridging at 3.5 km and seismic isolation of pores from approximately the same depth increase velocities during the deep mesogenesis. After

4.5 km most of the unstable minerals have transformed to more stable forms and cementation is reduced, thus velocities increase less with depth.

Clean quartz sands characterize the back/foreshore example. Shallow calcite cement entails high eogenetic velocities, and stabilizes the grain to grain contacts. This reduces the effect of the first quartz cement somewhat. A significant velocity increase is observed when more than 50 % of intergranular volume is cemented with quartz, and pores become increasingly seismic isolated, from ca 4.6 km. The velocity-depth ratio increases considerably faster due to seismic isolation of pores than in e.g. the lagoonal example. That is because the cementation rate is much higher in the back/foreshore example, leading to a more rapid isolation process.

Although the mineralogy and some of the mineral transitions differ from the back/foreshore example, the velocity trends for the shoreface/offshore example are quite similar. The velocities are somewhat lower though. The main difference in diagenetic mineral reactions, is the presence of clay coatings, which transform to pore-filling illite and coating chlorite from 2.5 km and deeper. Pore-bridging is important from 4.6 km and deeper. The quartz cementation rate is somewhat lower than in the back/foreshore example, entailing a less pronounced velocity increase.

The dominating cements in the offshore example are pore-filling and grain coating. In the eogenetic realm, especially shallow siderite cement leads to a relatively rapid velocity increase. All smectite is consumed at 4 km (125°C), leading to a minor local velocity increase. From 4.1 km the cement becomes pore-bridging, and the effective fluid stiffness increases.

Seismic diagenetic fingerprints

Even though the velocities are expected to vary between corresponding environments when relative mineral concentrations vary, it is assumed that the velocity gradient changes imposed by the mineral reactions will remain. The assumption is justified by considering a sandstone where incipient precipitation of quartz cement in the contacts is about to occur. The rock stiffness is likely to increase significantly when the first cement precipitates, regardless if it contains 5 % or 15 % clay materials in the framework, 5 % or 15 % non-contact cement or 20 % or 25 % porosity, even though the actual stiffness and cement amount might vary. The same reasoning would apply for other mineralogical reactions as well. Therefore a qualitative measure is needed to derive the seismic diagenetic fingerprint. This is obtained by approaching the velocity curves with polynomial curve-fitting, and estimate the first derivative with respect to depth for the resulting functions. The derivatives are averaged for each 100 meters, to avoid spikes and small anomalies. Negative derivatives in the uppermost and lowermost part of the fitted curve are set to zero when the velocity curves do not show any decrease. Deviations from the modelled velocities are commonly largest in the terminal points, but are always lower than 100 m/s. The first derivatives versus depth are plotted in Figure 8. The derivative is a qualitative parameter in the sense that it does not discriminate different velocities, as long as the velocity/depth - gradient changes are equal. Therefore it is suitable for relating changes in velocity gradients versus depth to the successions of mineralogical reactions with depth. The resulting graphs can be looked upon as bar codes or fingerprints, which can be related to each succession of mineral reactions. Each bar clearly defines where velocity is increasing much with depth (cyan to red colour) or where only small changes occur (dark blue). Figure 4 - 7 and the previous velocity-depth analyses explain the behaviour of each bar. Some mineralogical examples in

the modelling have large similarities in the fingerprints though, like shoreface and back/foreshore. In examples with similar qualitative behaviour, a quantitative analysis of the velocity plots might give some answers.

DISCUSSION

The velocities might vary in same types of depositional environments, due to variations of relative mineral concentrations, differences in source rock composition, different weathering processes or climate. Nevertheless, there are some minerals and mineralogical reactions which are prone to be present in certain depositional settings. Hence, to demonstrate application of the strategy, a link between mineralogy, reactions and depositional environment has been applied. Ideally, advanced geological modelling which incorporates any existing a priori knowledge about local and regional conditions should be performed, and used as input to the rock physics model. Variation of relative mineral concentrations might cause pore-bridging and seismic isolation of pores to take place at different depths and temperatures than shown, which can entail differences in the velocity curves, see Figure 9. In this figure the minerals are divided into two classes; i) coal and clay minerals and ii) non-clay minerals. The class i)/class ii) concentration-ratio is first increased with 20 %, then the class ii)/class i) concentration-ratio is increased with 20 %. The green curves are the original mineralogies used in the previous modelling. Some places the original velocities are lower than both of the other modelled velocities. This might happen if increased clay content increase the effect of pore-bridging and/or isolation, and increased content of quartz and calcitic minerals also enhance the velocity. In all examples, the velocities differ less than 200 m/s, and the main velocity-depths trends and gradient changes are preserved for all examples. This can also be seen in Figure 10, where the derivatives versus depth are shown for the

same examples. The environment with most significant differences in gradient is the lagoonal environment, when the clay content increases. This can be explained by increased amounts of authigenic clay cements, which stiffens the rock. This will have an impact on the deeper velocities as well. Figure 9 and 10 indicate that the modelling is fairly robust for fluctuations in the relative mineralogy, as long as the mineral reactions are unchanged. One case where mineralogical changes can have greater influence on the result, is when increased clay content alters the clay index in equation 1 from lower than 0.2 to higher. Then the porosity-depth curve will be somewhat different, which also will be pronounced in the velocity-depth curves. The opposite would be the case if increased quartz content altered the clay index to lower than 0.2. Hence, any a priori knowledge of regional or local geology and mineral compositions will improve the quality of the modelling of a real scenario.

The mineralogical modelling performed is constrained by temperatures, see Table 2. Thus, for different temperature-depth gradients, the velocity variations will occur at different depths, but the same temperatures, if other conditions are equal. Different authors have reported some variations in temperature intervals for mineralogical reactions, which can be due to variations in permeability (availability of reactants), pore fluid composition or composition of surrounding rocks. Control on the burial- and temperature history is crucial. Uplifted rocks with low present day temperature might be pervasive cemented from previous deep burial. Fast burial and low permeability might prevent mineralogical reactions to reach equilibrium, thus the rock can contain more unstable minerals than one should expect at a certain temperature. In addition to the mineral reactions considered, numerous other more or less inferior mineralogical reactions can be expected during diagenesis. In this paper, only common mineral transitions, and those considered relevant for the velocity evolution are included.

Due to lack of information about α and β in equation 1, these parameters are kept constant for all rocks. Hence, the porosity-depth model used in this study is only dependent on the clay index for uncemented sandstones and rocks with more than 20 % clay (the porosity evolution of cemented sandstones with <20 % clay is only dependent on γ), and does not differ between different clay minerals. Since different clay minerals might differ in distribution type and physical properties, they are likely to influence porosity differently. The applied porosity model is further ignorant with respect to porosity reduction due to calcite cementation and porosity enhancement due to chlorite cementation or overpressure. The porosity also has significant influence on velocities, which make this parameter to a dominant source of uncertainty in the estimations. Figure 11 shows that the velocity gradient changes can be recognized also when porosity is reduced with 10 % and 20 % of the original porosity. The velocity-gradient increase is shifted upwards, and the gradient change decreases, when porosity is reduced. The first effect is due to pore-bridging and seismic isolation of pores, which will occur at shallower depths when porosity is lower. This is most pronounced for the lagoonal example. The latter effect can be explained by higher initial velocities due to lower porosity, thus the velocity will not increase that much. Increased porosities are not studied, since it would lead to porosities larger than estimated critical velocities. The gradient changes in the lagoonal environment shift upwards when porosity decreases, but the relative change in gradient remains approximately the same. Larger deviations would occur if not the same systematic change in porosity was used for the whole depth interval. A porosity-depth model that responds differently on the presence of different minerals would probably be more accurate than the one applied.

The method presented can be used to analyse which mineralogical processes influence the velocity - depth trends for a given mineralogy. The modelling strategy can be

used on any composition of deposited siliciclastic sediment, if there exist knowledge or assumptions about the depositional mineralogy and mineral transformations during diagenesis. The strategy and obtained results presented can also be extended from the study of separated examples of depositional environments, to complex compositions of stacked environments. This could be used to generate a 3-D cube with both lateral and vertical variations in rock physics properties, easily comparable to seismic cubes. The strategy can be used in both forward and inverse modelling, to reveal subsurface properties.

CONCLUSION

This paper has introduced a composite rock physics model that is applicable for all siliciclastic rocks with various mineral distributions. The model uses mineralogy as input parameter, which enables it to analyse the effect of mineral transitions on the modelled velocities. Mineral transitions studied in this paper are linked to depositional environments, to relate the velocity-depth evolution to tangible scenarios, but all kind and combinations of mineral reactions can be included in the strategy. The modelled velocity curves and velocity-depth gradients versus depth, was directly linked to diagenetic mineralogical changes, porosity, pore-bridging and seismic isolation of pores. Each succession of mineralogical reactions was found to leave a seismic diagenetic fingerprint, found from the evolution of the velocity-depth gradient versus depth.

The modelling strategy is a valuable tool for understanding the interplay between mineralogical processes and seismic properties in lithologies that spans from pure sandstone to clean shale. The workflow requires geological as well as geophysical studies, and is therefore suitable for interdisciplinary collaboration. If there are assumptions about subsurface mineralogy, the method is suitable for forward modelling in

exploration purposes. It can also be used to identify depth intervals where the velocity-depth ratio is expected to change, and make predictions about how large the changes are. Inversion of the strategy can be useful to derive diagenetic processes and distributions from seismic properties, in addition to porosity, lithology and fluid properties.

Acknowledgement

REFERENCES

Bjørkum, P. A. & Nadeau, P. H. 1998. Temperature controlled porosity/permeability reduction, fluid migration and petroleum exploration in sedimentary basins. *Australian Petroleum Production and Exploration Association, 38*, 453-465.

Bjørlykke, K. (ed) 2001. *Sedimentologi og petroleumsgeologi* (Second edition). Gyldendal.

Bjørlykke, K. & Brendsdal, A. 1986. Diagenesis of the Brent sandstone in the Statfjord Field, North Sea. *In:* D. L.Gautier (ed) Role of Organic Matter in Sediment Diagenesis, *Society of Economic Palaeontologists and Mineralogists*, Special Publication, **38**, 157-166.

Boggs, S. (ed) 1995. *Principles of Sedimentology & Stratigraphy* (Second edition). Prentice Hall, New Jersey.

Dræge, A., Jakobsen, M. & Johansen, T. A. 2006a. Rock physics modelling of shale diagenesis. *Petroleum Geoscience*, **12**, 49-57.

Dræge, A., Johansen, T. A., Brevik, I. & Dræge, C. T. 2006b. A strategy for modelling diagenetic evolution of seismic properties in sandstones. *Accepted for publication in Petroleum Geoscience.*

Dvorkin, J. & Nur, A. 1996. Elasticity of high porosity sandstones: Theory for two North Sea data sets. *Geophysics*, **61**(5), 1363-1370.

Dvorkin, J., Berryman, J. & Nur, A. 1999. Elastic moduli of cemented sphere packs. *Mechanics of Materials*, **31**, 461-469.

Gassmann, F. 1951. Über die Elastisität der poröser medien. *Vierteljahrschrift der Naturforschenden Gesellshaft in Zürich*, **96**, 1-23.

Ghetti, S. & Brigatti, M. F. 1991. Mineralogy of Cretaceous green clay levels, Friuli Platform, Southern Alps, Italy: relationships to the depositional environment. *Neues Jahrbuch für Geologie und Palaeontologies*. Monatshefte, 489-501.

Hashin, Z. & Shtrikman, S. 1963. A variational approach to the theory of the elastic behavior of multiphase materials. *Journal of the Mechanics and Physics of Solids*, **11**, 127-140.

Hill, R. 1952. The elastic behavior of crystalline aggregate. *Proceedings of the Physical Society of London*, **A65**, 349-354.

Hillier, S. 1993. Origin, diagenesis and mineralogy of chlorithe minerals in Devonian lacustrine mudrocks, Orcadian basin, Scotland. *Clays and Clay Minerals*, **41**, 240-259.

Hornby, B. E., Schwartz, L. M. and Hudson, J. 1994. Anisotropic effective-medium modelling of the elastic properties of shales. *Geophysics*, **59**(10), 1570-1583.

Ingles, M., Salvany, J. M., Munoz, A. & Perez, A. 1998. Relationship of mineralogy to depositional environments in the non-marine Tertiary mudstones of the southwestern Ebron Basin (Spain). *Sedimentary Geology*, **116**, 159-176.

Jakobsen, M., Hudson, J. A., Minshull, T. A. & Singh, S. C. 2000. Elastic properties of hydrate-bearing sediments using effective medium theory. *Journal of Geophysical Research*, **105**(B1), 561-577.

Ketzer, J. M. 2002. *Diagenesis & sequence stratigraphy* . PhD thesis, University of Uppsala, Uppsala, Sweden.

Le Pera, E., Arribas, J., Critelli, S. & Tortosa A. 2001. The effects of source rocks and chemical weathering on the petrogenesis of siliciclastic sand from the Neto River (Calabria, Italy); Implications for provenance studies. *Sedimentology,* **48**(2), 357-378.

Lowey, G. W. 2002. White Channel Gravel alteration revisited. In: *Yukon Exploration and Geology 2001*, D.S. Emond and L.H. Weston (eds), Exploration and Geological Services Division, Yukon, Indian and Northern Affairs Canada, 147-162.

Marion D. & Nur, A. 1991. Pore-filling material and its effect on velocity in rocks. *Geophysics*, **56**, 225-230.

McKinley, J. M., Worden, R. H. and Ruffel, A. H. 2003. Smectite in sandstones: a review of the controls on occurrence and behaviour during diagenesis. *In:* Worden, R. H. & Morad, S. (eds), *Clay Mineral Cements in Sandstones*, International Association of

Sedimentologists, Special Publication, **34**, Blackwell Publishing, Oxford, 109-128.

Mindlin, R. D. 1949. Compliance of elastic bodies in contact. *Journal of Applied Mechanics*, **16**, 259-268.

Morad, S., Ketzer, J. M. & De Ros, L. F. 2000. Spatial and temporal distribution of diagenetic alterations in siliciclastic rocks: implications for mass transfer in sedimentary basins. *Sedimentology*, **47**, 95-120.

Mori, T. & Tanaka, K. 1973. Average stress in matrix and average elastic energy in materials with misfitting inclusions. *Acta Metal*, **21**, 571-574.

Nishizawa, O. 1982. Seismic velocity anisotropy in a medium containing oriented cracks - transversely isotropic case. *Journal of Physics of the Earth*, **30**, 331-347.

Ramm, M. & Bjørlykke, K. 1994. Porosity/depth trends in reservoir sandstones: Assessing the quantitative effects of varying pore-pressure, temperature history and mineralogy, Norwegian Shelf data. *Clay minerals*, **29**, 475-490.

Ruud, B. O., Jakobsen, M. & Johansen, T. A. 2003. Seismic properties of shales during compaction. *73rd SEG Conference*, Dallas, USA, Expanded Abstracts, 1294-1297.

Segall, M. P., Siron, D. L. & Colquhoun, D. J. 2000. Depositional and diagenetic signatures of Late Eocene-Oligocene sediments, *South California Sedimentary Geology*, **134**, 27-47.

Voigt, W. (ed) 1928. *Lehrbuch der Kristallphysik*. Teubner, Leipzig.

Walderhaug, O. 1996. Kinetic modelling of quartz cementation and porosity loss in deeply buried sandstone reservoirs. *AAPG Bulletin*, **80**, 731-745.

White, T., Ferraris, C., Kim, J. & Srinivasan, M. 2004. Apatite - An adaptive framework structure. *Conference: Micro- and Mesoporous Mineral Phases, Mineralogical, Crystallographic and Technological aspects*, 6-7 December 2004, Rome, Italy.

Willis, J. R. 1977. Bounds and self-consistent estimates for the overall properties of anisotropic composites. *Journal of the Mechanics and Physics of Solids*, **25**, 185-202.

Worden, R. H. & Burley, S. D. 2003. Sandstone diagenesis: the evolution of sand to stone. *In:* S. D. Burley and R. H. Worden (eds), *Sandstone Diagenesis - Recent and Ancient* . Shannon, Reprint Series, **4**, International Association of Sedimentologists, Blackwell Publishing, Oxford, 3-44.

Worden, R. H. & Morad, S. 2003. Clay minerals in sandstones: Controls on formation, distribution and evolution. *In:* Worden, R. H. & Morad, S. (eds), *Clay Mineral Cements in Sandstones*, International Association of Sedimentologists, Special Publication, **34**, Blackwell Publishing, Oxford, 3-41.

Distribution	Minerals
Distribution **i)**	Aalbite (Al), anhydrite (Anh), apatite (Apa)
	Asmectite (AS), AK-feldspar (AKF), chlorite (Ch)
Distribution **ii)**	Illite (I), kaolinite (K), pyrite (Py)
Distribution **iii)**	Calcite$_{cem}$ (Ca),dolomite (Do), quartz $_{cem}$ (Q), siderite (Si)
Distribution **iv a)**	DAlbite (Al), anorthite/plagioclase (Ano/P), Calcite$_{fw}$ (Cfw), coal (Co)
	DK-feldspar (DKF), mixed clay$_{fw}$(Clfw), Quartz$_{fw}$ (Qfw), glauconite (Gl)
Distribution **iv b)**	Claycoats (Clct), Dsmectite (DS)

Table 1. Classification of minerals due to different distribution classes. Illustration of the different distributions can be seen in Figure 1. 'A' or 'D' in front of the mineral name denote authigenic (precipitated in situ, after deposition) and detrital (present at deposition), respectively. The subscripts 'cem' and 'fw' denote precipitated cement and framework, respectively. The mineral abbreviations written in parenthesis are used in Table 2 - 3 and Figure 4 - 5.

	Mineral reactions	Temperature
1)	$Al + 0.180\ H_2O \rightarrow 0.500\ K + 0.455\ Q(aq)$	$10\text{-}25^{\circ}C$
2)	$Ano + 0.179\ H_2O \rightarrow 0.992\ K$	$10\text{-}25^{\circ}C$
3)	$KF + 0.081 H_2O \rightarrow 0.451\ K + 0.411\ Q(aq)$	$10\text{-}50^{\circ}C$
4)	$Cl_{fw} + 0.318\ Q(aq) \rightarrow 0.744\ KF + 0.698\ K$	$10\text{-}50^{\circ}C$
5)	$S \rightarrow 0.201\ Q + 0.354\ I + 0.180\ H_2O$	$65\text{-}125^{\circ}C$
6)	$1.066\ KF + K \rightarrow 0.455\ Q + 1.414\ I + 0.180\ H_2O$	$70\text{-}110^{\circ}C$
7)	$K \rightarrow D \rightarrow 0.943\ I + 0.180\ H_2O$	$70\text{-}160^{\circ}C$
8)	$S + 0.035\ H_2O \rightarrow 0.303\ Q + 0.545\ Ch$	$70\text{-}135^{\circ}C$
9)	$KF + 0.056\ H_2O \rightarrow 0.427\ Q + 0.442\ I$	$110\text{-}130^{\circ}C$
10)	$KF \xrightarrow{*} Al$	$15^{\circ}C\ \text{-} \rightarrow$
11)	$Q_{fw} \xrightarrow{*} Q_{cem}$	$80^{\circ}C\ \text{-} \rightarrow$
12)	$C_{fw} \xrightarrow{*} Ca_{cem}$	$10\text{-}50^{\circ}C$
13)	$Cl_{fw} \xrightarrow{*} 0.201\ Q + 0.354\ I$	$65\text{-}125^{\circ}C$
14)	$Cl_{fw} \xrightarrow{*} 0.303\ Q + 0.545\ Ch$	$65\text{-}125^{\circ}C$

Table 2. Volumetrically balanced reactions involved in the mineralogical modelling. Mineral abbreviations are explained in Table 1. The Cl_{fw} in reaction **4)** is muscovite. A star above some of the arrows means that the volumes in the reaction are assigned rather than calculated. In reaction 13 and 14, the volumes from reaction 5 and 8 were applied, respectively, while reactions 10-12 are considered to be one-to-one reactions. The temperature intervals to the right are indicative and not absolute. The right arrows in reactions 10 and 11 means that there is no upper temperature limit in the temperature intervals studied ($10\text{-}160^{\circ}C$).

Environment	Reactions involved	Infiltrated minerals
Braided river	1, 2, 3, 4, 5, 6, 7, 11	AS
Meandering river	1, 2, 3, 4, 5, 6, 7, 11	AS, Ca, K
Floodplain	3, 6, 7, 13	Ca, Do, Si
Crevasse splay	1, 2, 3, 4, 5, 6, 7, 8, 11	AS, Ca, Do, K, Si
Oxbow lake	5, 6, 8, 9, 13, 14	Si
Lagoon	6, 7, 8, 10	AS, Anh, Do, KF, Py, Si
Shoreface/offshore	11, 12, 13, 14	
Backshore/foreshore	11	Ca
Offshore	5	Apa, Gla, Py, Si

Table 3. Overview of mineralogical reactions and infiltrated minerals that are assumed to dominate the diagenesis of the different depositional environments. Mineral abbreviations are explained in Table 1, while reactions are defined in Table 2.
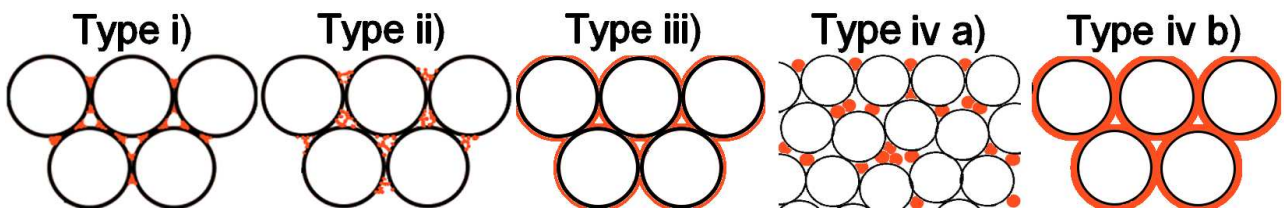
Figure 1. Four classes of mineral distributions. The class number is written above each illustration. Both **iv a)** and **b)** are loadbearing, but only **b)** constitute a connected phase. White grains are framework quartz, while orange represent cement or loadbearing inclusions. See text for further details.
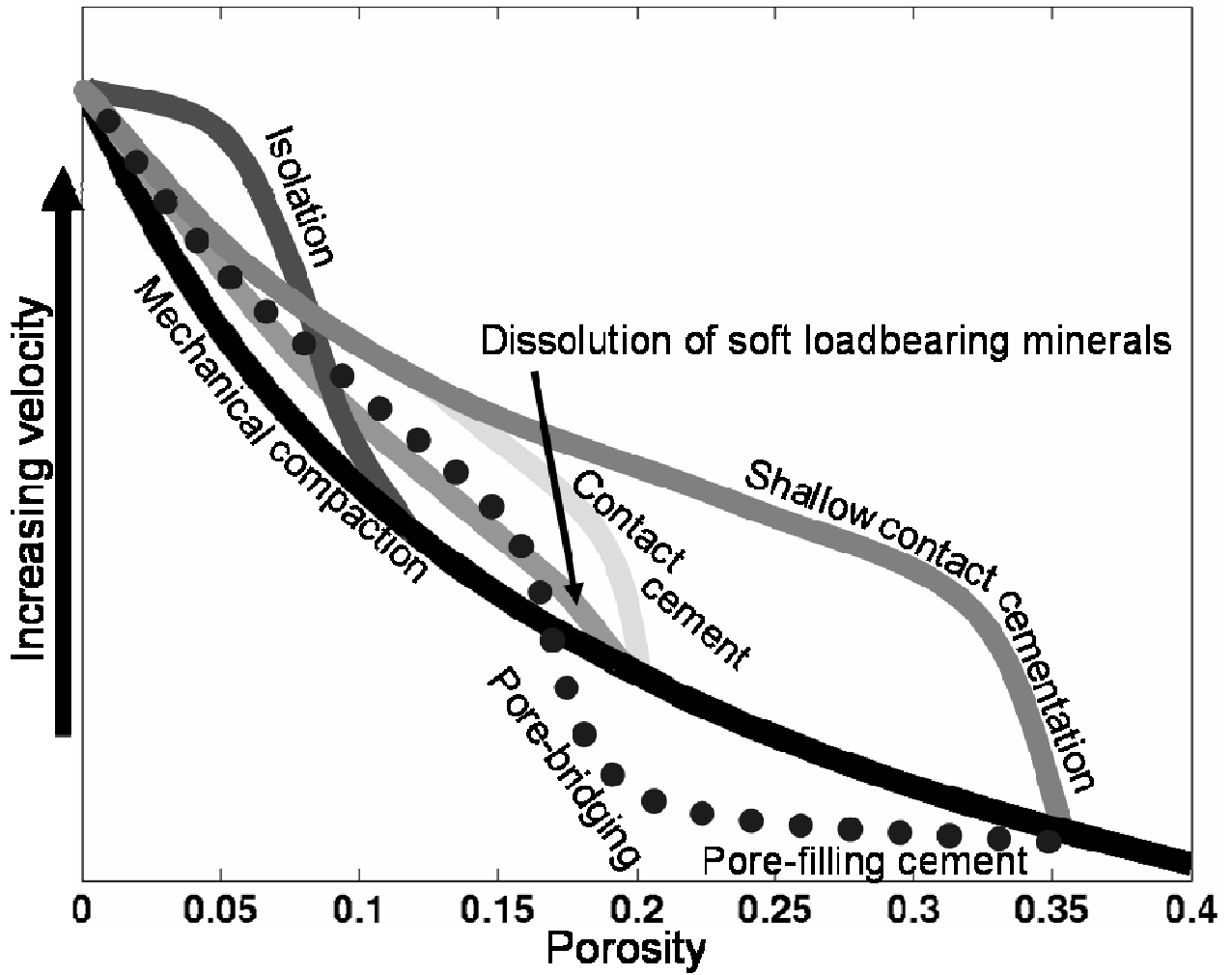
Figure 2. Principle sketch of some important diagenetic processes and how they can influence rock velocity. The relative differences in velocity increase can vary. Different processes can occur in combination, and at various stages of the diagenesis.
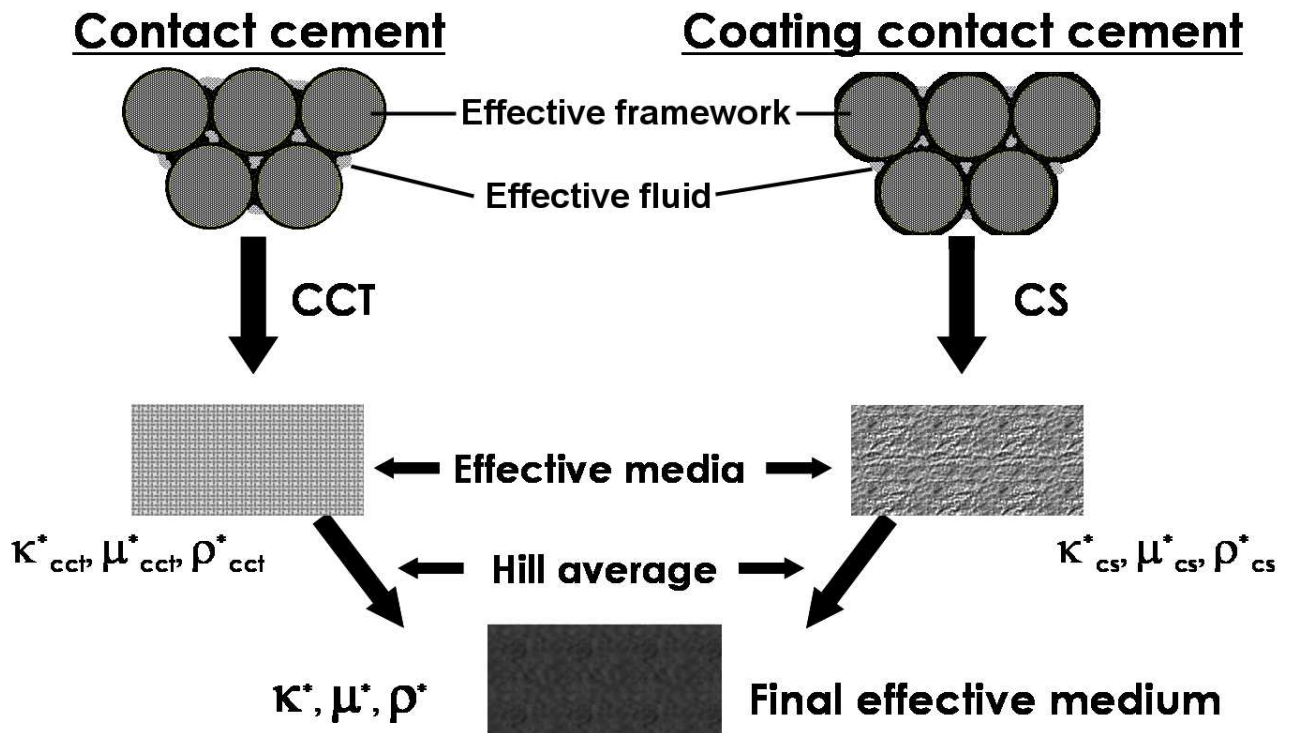
Figure 3. Modelling procedure for cemented sandstones. Distribution type **ii)** and the pore fluid constitute the effective pore fluid, while the distribution types **iv a,b)** and the quartz framework constitute effective framework. The effective properties are calculated for the contact cemented and coated contact cemented case distinctively. Finally, the Hill average is applied between the results, and the effective properties of the composite cemented rock is obtained.
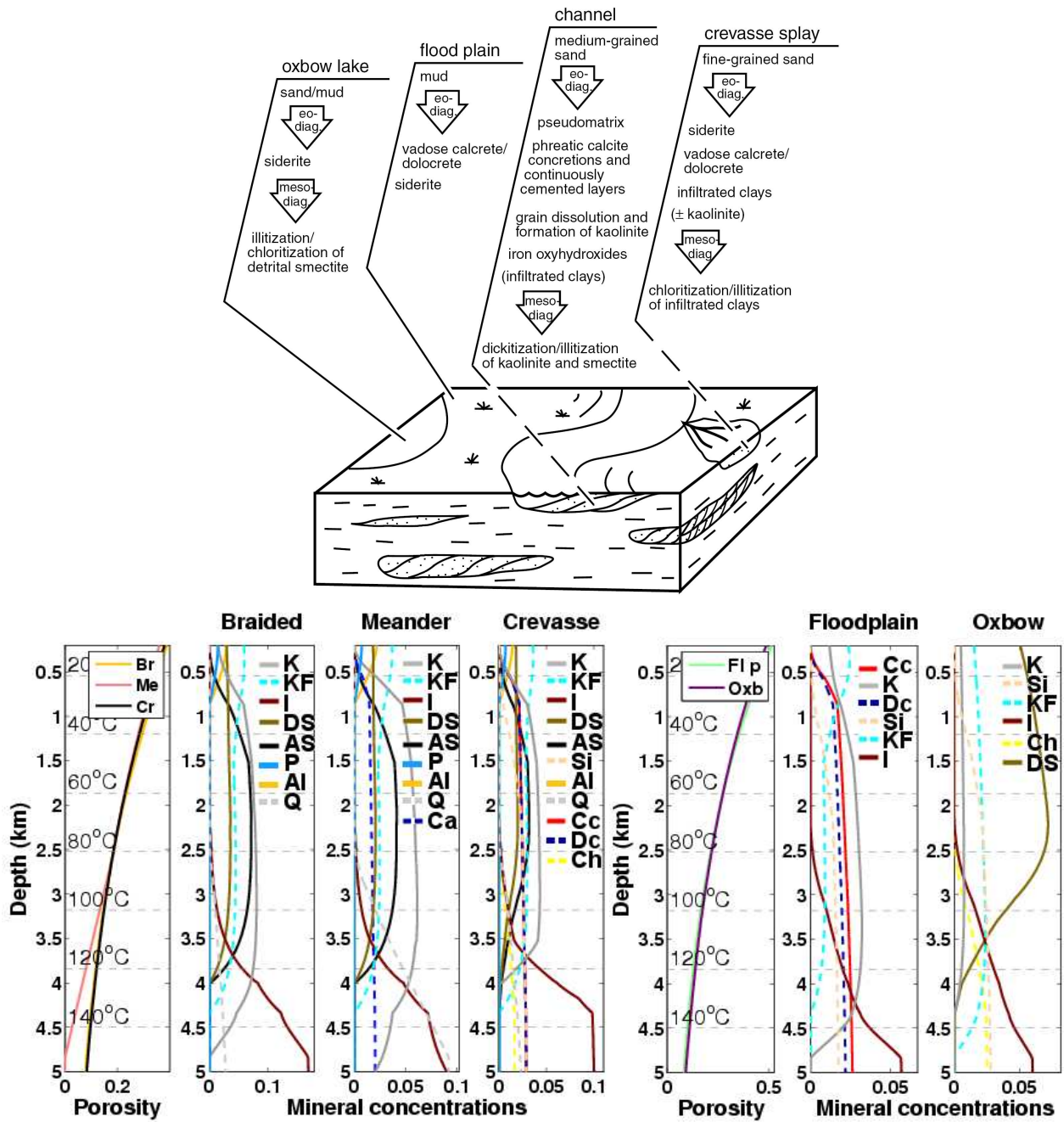
Figure 4. Above: Illustration of four different fluvial depositional environments. Below: Modelled mineralogical evolution with depth for braided river together with the illustrated environments. The curves for framework quartz and clay are left out. The upper illustration is modified from Morad et al. (2000). Mineral abbreviations in the legends are explained in Table 1.
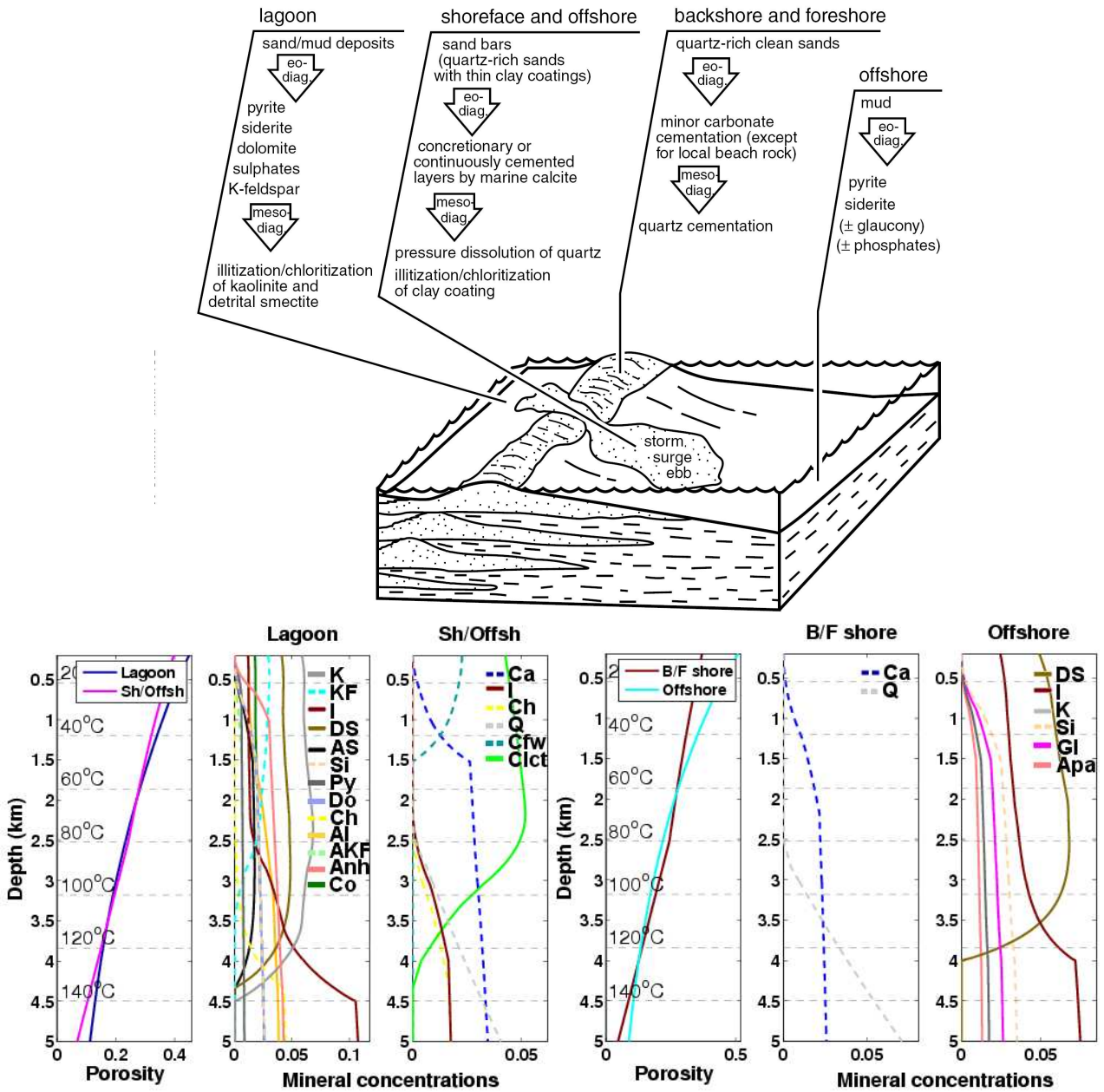
Figure 5. Illustration of four different depositional environments in a wave- and storm dominated shelf, together with modelled porosity mineralogical depth trends for each environment. The curves for framework quartz and clay are left out. The upper illustration is modified from Morad et al. (2000). Mineral abbreviations in the legends are explained in Table 1.
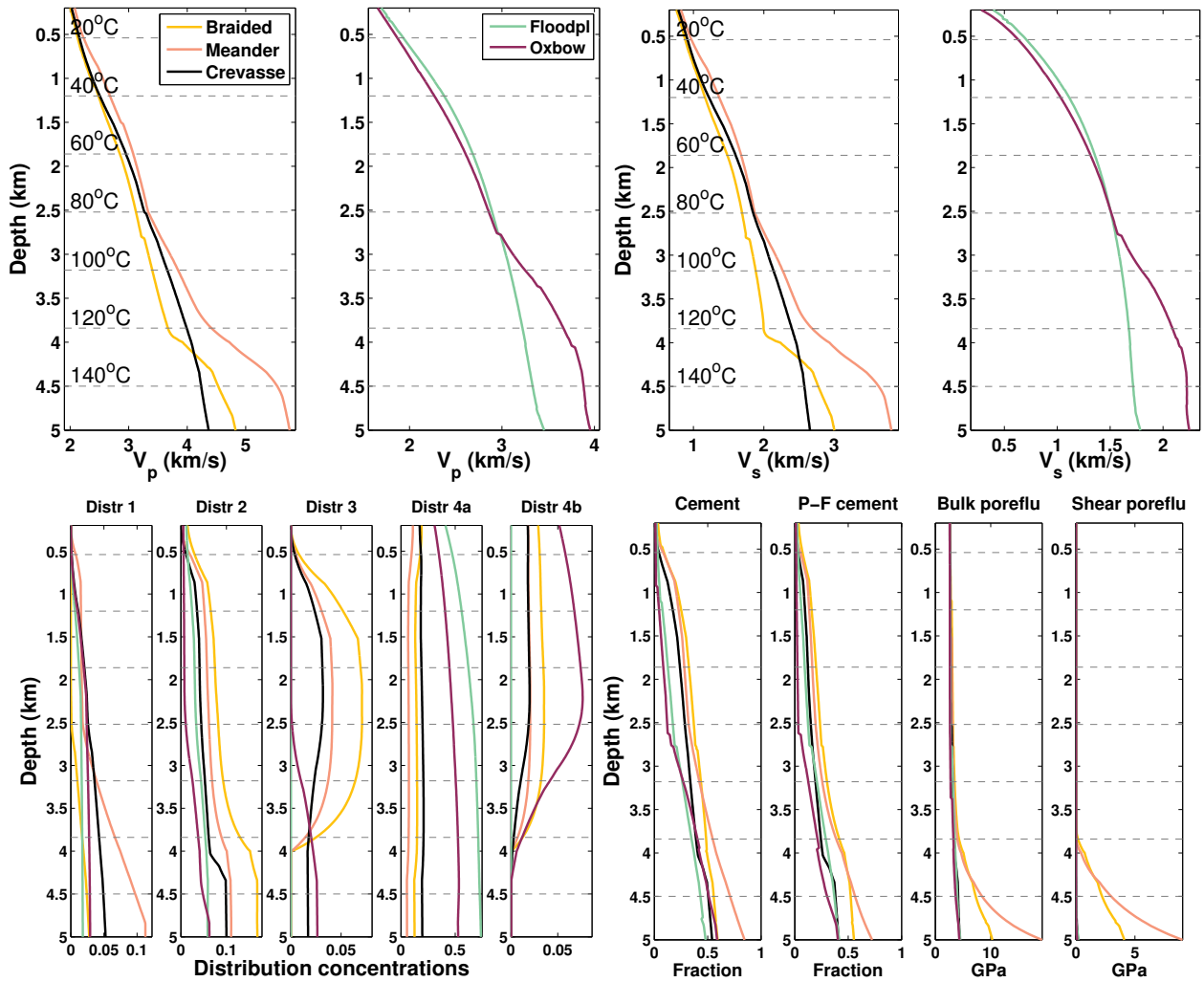
Figure 6. Above: Modelled velocities in fluvial depositional settings. Below: Concentrations of the different mineral distributions are shown to the left. The right curves show fraction of intergranular volume that is filled with cement, fraction of pore volume that is filled with pore-filling cement, and effective bulk- and shear modulus for the mixture of pore-filling cement and pore fluid. Framework quartz and clay are left out in the distribution plots. Each environment has the same colour in every plot.
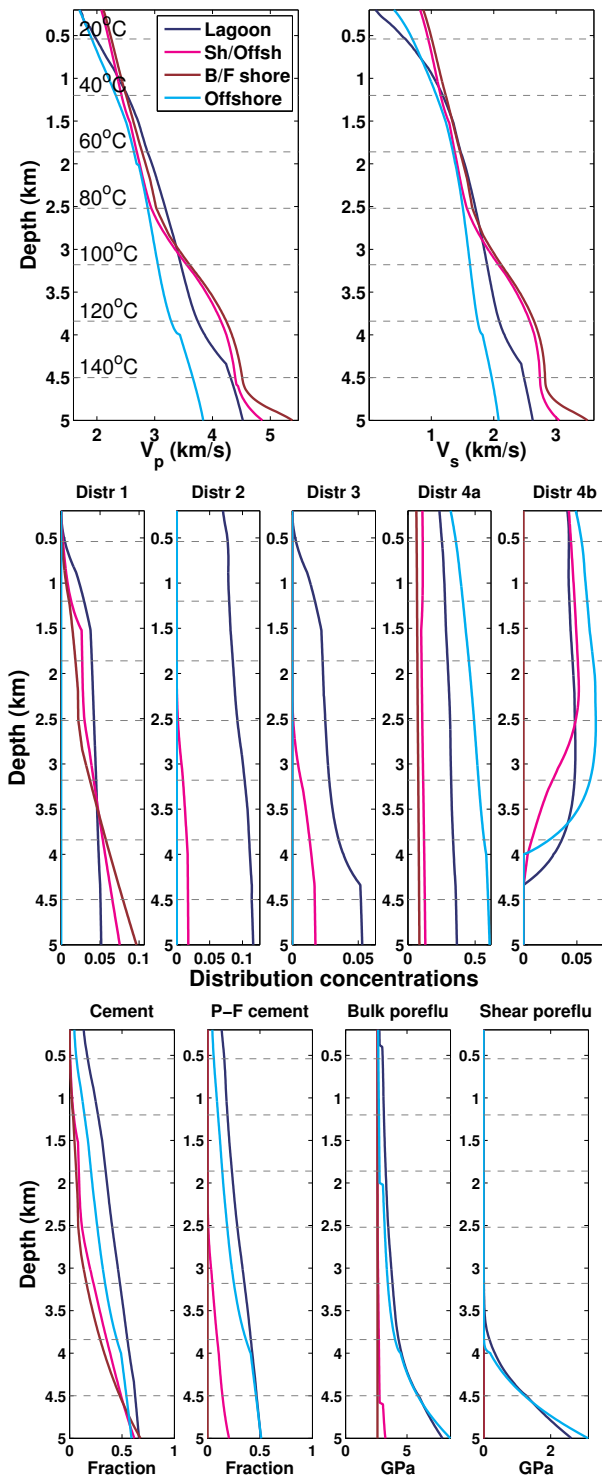
Figure 7. Above: Modelled velocities in shelfal depositional settings. Middle: Concentrations of the different mineral distributions. Below: Fraction of intergranular volume that is filled with cement, fraction of intergranular volume that is filled with pore-filling cement, and effective bulk- and shear modulus for the mixture of pore-filling cement and pore fluid. Framework quartz and clay are left out in the distribution plots. Each environment has the same colour in every plot.
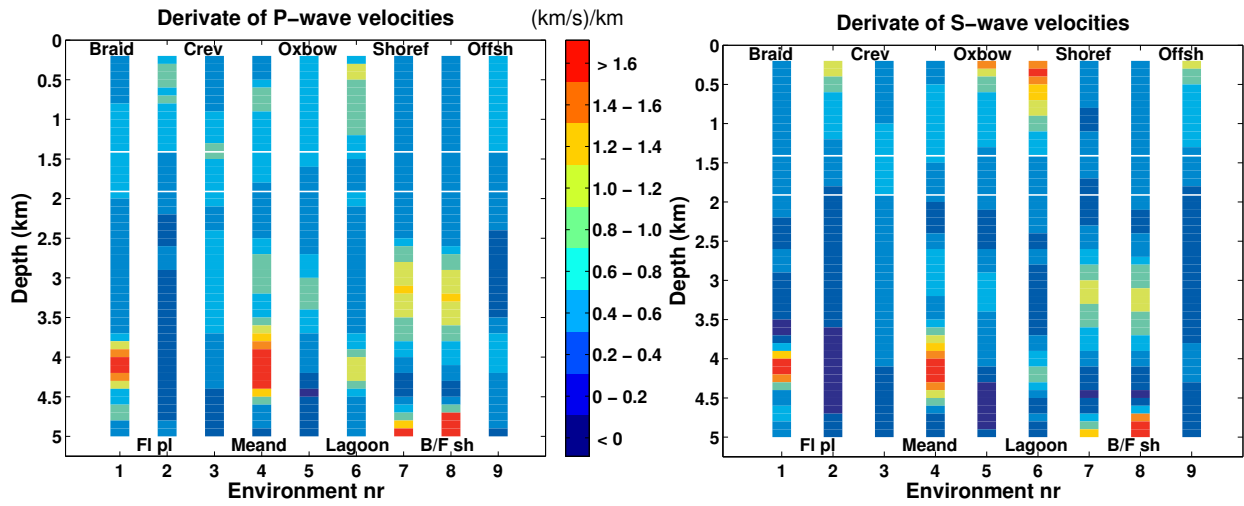
Figure 8. The environments from number 1 to 9 are shown in the same order as in Figure 4 - 5. The colour bar indicates the velocity gradients, averaged over 100 meters of depth.
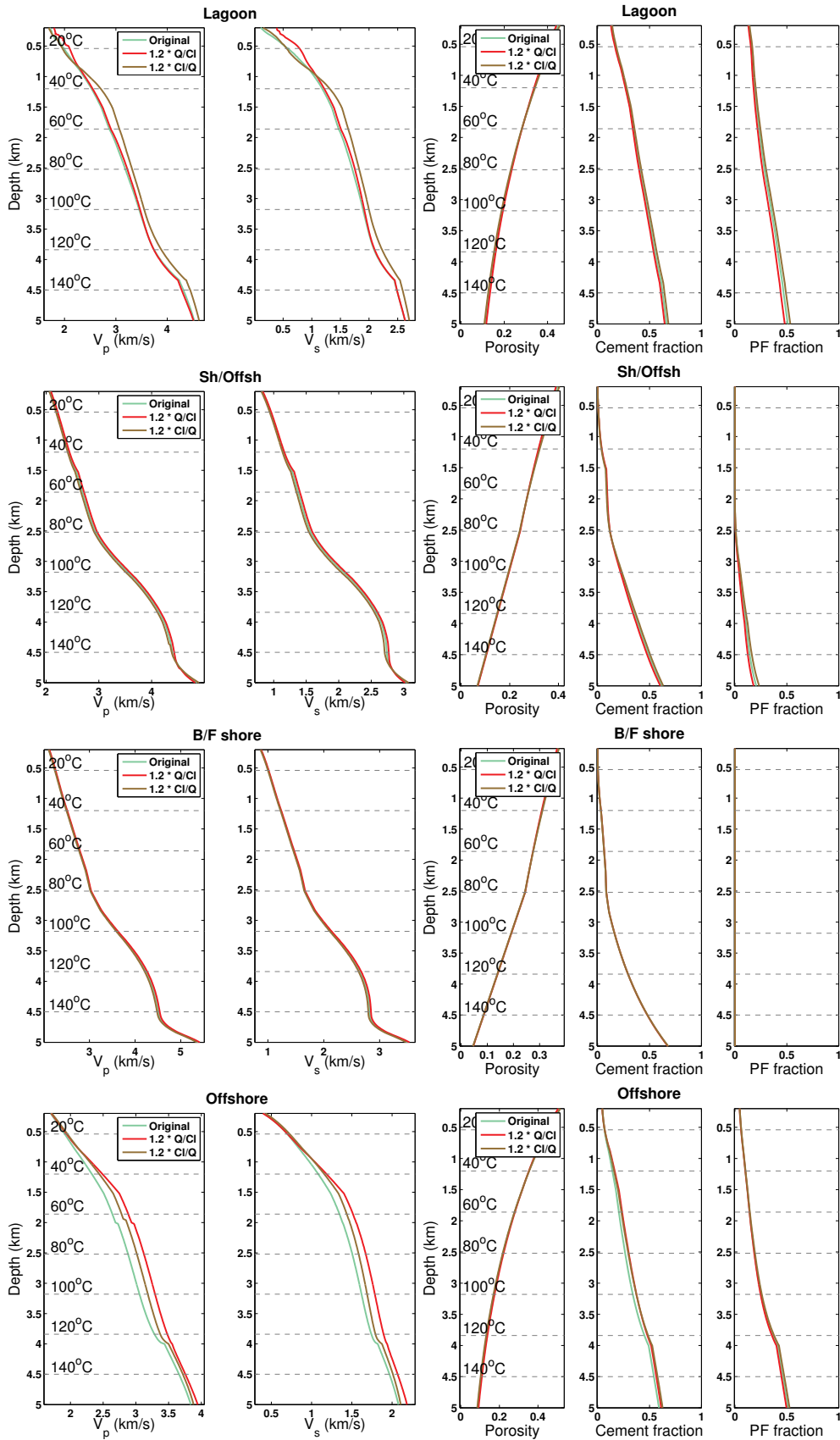
Figure 9. The velocities and relevant parameters for four wave- and storm dominated shelf environments with original mineralogy (green), increased non-clay/clay ratio (red) and increased clay/non-clay ratio (brown).
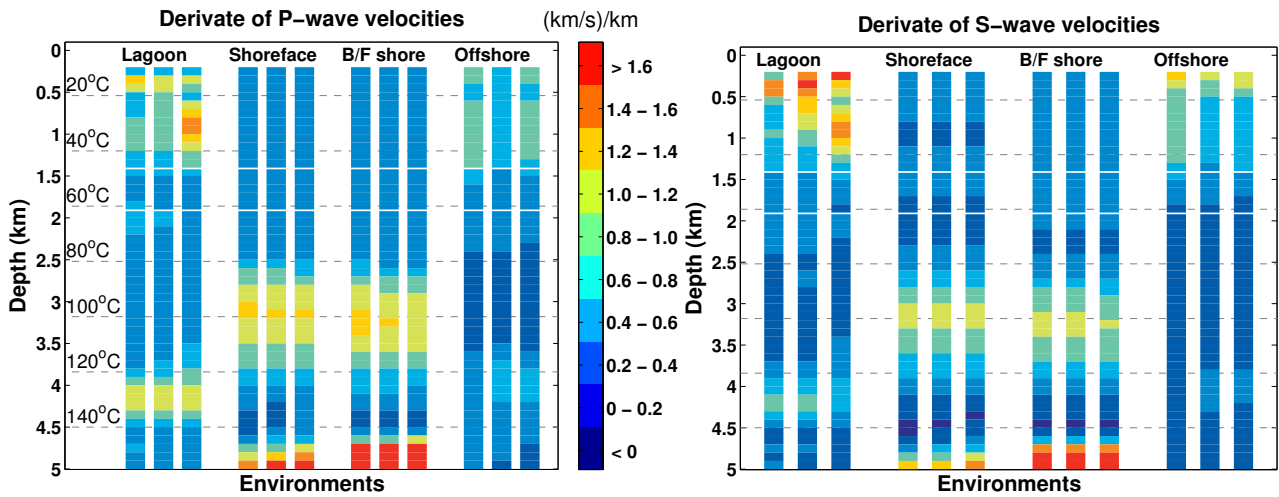
Figure 10. Derivative of velocity versus depth for four environments with varying mineralogy. The non-clay/clay ratio is increased to the left, original non-clay/clay ratio is in the middle, and increased clay/non-clay ratio to the right for each environment.
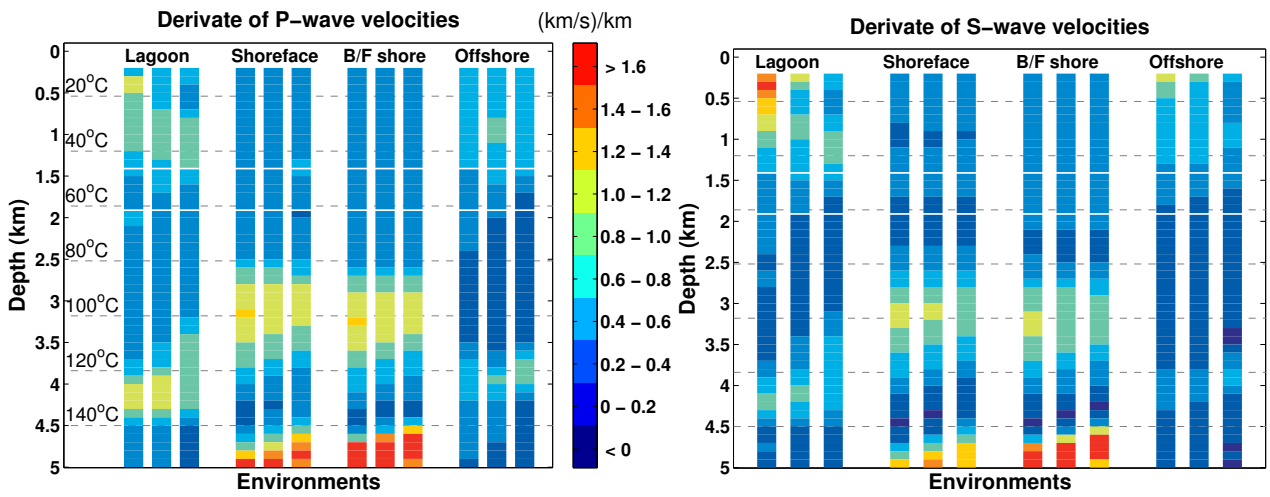
Figure 11. Derivative of velocity versus depth for four environments with varying porosity. The original porosity is used in the left curves, the porosity reduced with 10 % and 20 % of the original porosity is shown in the middle and to the right, respectively, for each environment.

7   Paper 4

Diagnostic of PLF parameters and microstructure of siliciclastic rocks from borehole acoustic data

Diagnostic of PLF parameters and microstructure of siliciclastic rocks from borehole acoustic data

Anders Dræge[1,2] **and Tor Arne Johansen**[1,2]

[1]*Department of Earth Science, Allegaten 41, 5007, University of Bergen, Norway*

[2]*Centre for Integrated Petroleum Research, Allegaten 41, 5007 Bergen, University of Bergen, Norway*
(E-mail: Anders.Drage@geo.uib.no)

ABSTRACT: *When characterizing hydrocarbon reservoirs, estimating reserves or developing reservoir models, the porosity (P), lithology (L) and pore fluid (F) are key reservoir parameters. These parameters also have great impact on seismic properties (velocities and density) in rocks, and are then used as model parameters in most rock physics models which aim to estimate seismic rock properties. We here outline how to use and evaluate various rock physics models for estimation of PLF parameters from seismic velocities and density. The method is founded on use of so called constraint cubes, which numerically relates the two data domains. The estimation procedure is formulated to also reveal non-unique solution sets, and it is flexible to the amount of data parameters available. Estimated PLF parameters are consistent with all input data parameters, and the method therefore points to (rock) physics models that are suitable for describing the input data. This potentially opens up for also revealing the rock microstructure in addition to PLF parameters, since almost any forward rock physics model is founded on an idea of the microstructure. The method is applied to both synthetic and real data.*

KEYWORDS: *inversion, rock physics, cement distribution, porosity, lithology, pore fluid*

INTRODUCTION

Estimation of reservoir quality from seismic parameters is a crucial task in seismic reservoir characterization. Reservoir quality is related to porosity - P, lithology – L and the type of pore fluid - F. While porosity (ϕ) directly indicates the reservoir capacity, the knowledge of lithology is, first and foremost, important for revealing the reservoir architecture; i.e. to identify the source rock, reservoir rock and (reservoir) sealing rock. From a geological point of view lithology is generally not associated with a number; it is either sandstone, shale, or carbonate, et cetera. However, the lithology can for siliciclastic rocks be quantified by the shale ratio c, which is the fraction of the volume of clay minerals to the total volume of the solid particles within a representative volume of the rock. Hence, $c = 0$ for a clean sandstone and $c = 1$ for a pure shale. For low values of c we have clayey sands, and for large values we have sandy shales. A similar quantification can be applied for describing the pore fluid if we consider it to represent a mixture of, say, gas and water, and define a saturation parameter s as the volume fraction of gas or water to the total volume of the pore fluid.

The reservoir quality of siliciclastic rocks is related to c, as a low value indicates small amounts of clay and better chances for good pore-to-pore connections, and, thus, high permeability. The presence of

129

clay often gives reduced porosity, increased number of narrow pore throats and reduced permeability. The knowledge of the lithological composition is furthermore important for deriving the elastic properties of the dry rock and grains, which is needed for estimation of fluid saturation effects on seismic properties using the model of Gassmann (1951).

One fundamental problem in estimation of PLF parameters from seismic parameters, is due to the non-unique relationships between the two parameter domains. For instance, the effects of clay on the P-wave velocity (V_p) and S-wave velocity (V_s) are not only related to its volume fraction, but also to how it is distributed within the rock. Clay minerals can for example occur as pore-filling, grain coating, grain cementing, framework structural, or combinations of these. The choice of rock physics theory for relating the PLF parameters to seismic parameters, or vice versa, usually implies a model for the microscopic mineral distribution. This is, for instance, the case for Hashin-Shtrikman models (upper and lower boundaries) (Hashin-Sthrikman; 1963), Contact Cementation models (Dvorkin; 1999) and inclusion based models (Xu and White, 1995) and several others. However, the density (ρ) does not distinguish between such micro-structural variations. Furthermore, V_p and V_s as functions of porosity and pore fluid do also depend on the pore structure, as, for instance, the amount of compliant (flat) pores and the connectivity of the pore system. Thus, information about how the rock was formed, and the corresponding implication to its microstructure may be of severe importance for finding the optimum rock-to-velocity transformation model to apply in the inversion for PLF parameters. The rock physics model(s) used for inversion should therefore to a wider extent relate to the processes forming the small scale texture of the rock. These processes can to

some degree be deduced from a history of the mechanical and chemical compaction (pressure, temperature). Previous work on deriving PLF parameters from seismic parameters includes Avseth et al. (2005), which use so called rock physics templates, Saltzer et al. (2005) which describe a two-step inversion method for estimating the volume of shale and porosity from seismic reflection data, and Li et al. (2005) which focus on deriving saturation and porosity from seismic AVO.

The scope of this study is to discuss how model based inversion of seismic parameters to PLF parameters also can provide information about the small scale features of the rock. The outline of this paper is as follows: First we review how to make rock physics constraints adapting small scale microstructure. Then we discuss the inversion strategy, non-uniqueness of solutions and applications to both synthetic and real well log data.

ROCK PHYSICS MODELS AND MICROSTRUCTURE

Rock physics models can be used in a forward manner to estimate seismic properties from PLF parameters, given constituent properties and knowledge about geometrical arrangements. Some models are tailored for special scenarios, like a rock with round grains (approximation for quartz grains) without cement, or with a specified cement type like pore-filling cement or contact cement. The pore-filling and contact cement distribution and corresponding rock physics models were discussed by Dræge et al. (2006a), and will be the focus on the first part of the modelling in this paper. The rock physics model used for pore-filling cement is denoted PF model, while the model that accounts for contact cemented rocks is denoted CT model. The PF model is illustrated in Figure 1. All constituent properties used in this study are given in Table 1. When pore-filling cement precipitates, the immediate effect is not

very pronounced. The cement only stiffens the pore fluid, and hence the effective bulk modulus, in addition to increasing the bulk density. At higher concentrations (> 40 % of intergranular volume), the cement starts to create contacts across pores, and incipient pore-bridging occurs. This process significantly strengthens the rock, and especially the effective shear modulus increase when pore-bridging becomes effective. A limit is applied for how high concentrations of cement are needed to inhibit fluid flow, since the overall rock stiffness is expected to increase as the fluid mobility decrease (Wang, 2000). This limit can be adjusted to fit local conditions/lithologies. In this paper it is assumed that when cement content exceeds 50 % of the intergranular volume (e.g. the volume that is not occupied by the framework), pore connectivity starts to decrease until cement content exceeds 75 %. Then all pores are treated as isolated and appropriate rock physics models are used for the modelling.

The CT model is illustrated in Figure 2. A gradual transition from a rock physics model that treats the rock as completely uncemented to a rock physics model for pervasive cementation in all contacts is modelled by the Hill (1952) average in the interval 0 – 30 % cement of the intergranular volume. The isolation of the pores is set to follow the same limits as the PF model, and the process leads to increased stiffness in the CT model as well. Density versus porosity and clay content is shown in Figure 3. Densities are solely dependent on constituent densities and concentrations, and are therefore equal for the PF and CT model, as seen in Figure 1 and 2.

Permeable rocks with pore-filling cement (PF model), and uncemented rocks are modelled with the combined theories of Hertz-Mindlin (HM) (Mindlin, 1949) and Hashin and Shtrikman (1963) (HS) lower bound, like described in Dvorkin & Nur

(1996). This combined model (HMHS) connects two end members; one has zero porosity and the moduli of the solid phase, and the other has critical porosity and a pressure dependent modulus as given by the Hertz-Mindlin theory. The formulas for the applied theories are given in the appendix.

The contact cement theory (CCT) of Dvorkin et al. (1999) is applied to model the first stages of contact cementing in the CT model. CCT provides the effective elastic properties of an aggregate of spheres, where the spheres are in direct point contact, and cement fills the space around the contacts. CCT cannot be used to estimate the elastic constants of an aggregate where cement fills the entire pore space or large portions of it (Dvorkin et al., 1999), therefore it is combined with DEM when the cement fills up more than 50 % of the intergranular volume.

The DEM (Differential Effective Medium, Berrymann, 1992) approach can be formulated by a set of differential equations where the physical analogue is that the inclusions are gradually embedded in or removed from the background medium. The procedure may be applied as follows (Johansen et al., 2002): i) Start with a background medium with known properties, in our case framework quartz. ii) Embed or remove inclusions (e.g. pores or cement) to form a new composition. iii) Compute the effective properties which define the new background medium. Repeat ii) and iii) until the actual material composition is reached, at which the required elastic properties will be obtained. New constituents that are added to the composite media using DEM will be added as unconnected isolated inclusions. This is used to estimate the effective rock properties with isolated pores at cement concentrations higher than 50 % of intergranular volume for both the PF and CT model. When using DEM for mixing framework quartz with isolated clay clasts

and pores, quartz and clay are first mixed, and then the obtained effective framework is mixed with pores.

The fluid effects for permeable rocks without porebridging cements are modelled with the Bound Averaging Method (BAM) (Marion & Nur, 1991) for both types of cement distributions. This model is an approximation to the Gassmann (1951) model for viscous fluids, and is applied as a consequence of the pore-filling cement being suspended in the fluid, making it more viscous. BAM relies on the assumption that the bulk modulus is a weighted average of the lower and upper limits for the given combination of grain modulus and fluid modulus, and that this weighting function is independent of the fluid. The weighting function can be found for the dry rock and then applied to find the modulus for the saturated rock. The approach of Sams & Andrea (2001) is adopted, and the Reuss (1929) and Voigt (1928) averages are applied for the lower and upper limits. Ideally the BAM and Gassmann models should coincide at the end points with no pore-filling cement and complete cementation, but Sams & Andrea (2001) found that the BAM model predicted slightly higher P-velocities for rocks with pure fluids.

When pore-filling cement is present, self consistent approximation (SCA), (Berrymann, 1995) is used to calculate the effective fluid properties as a mixture between pore-filling cement and fluid. The SCA model accounts for interactions between inclusions when a wave travels through the medium, by treating all constituents of the composite as embedded in a 'virtual' medium that has the required effective medium properties. The SCA solution occurs when the net (scattering) effect of all the inclusions is zero. The term 'self-consistent' means that the results do not depend on a selection of host medium to embed the remaining constituents, but do only depend on their volume fraction. If the concentrations of the constituents in a two phase medium are between approximately 40-60 %, the SCA solution will correspond to the effective properties of a two phase medium in which both phases constitute connected phases in the composite medium (Hornby et al. 1994; Jakobsen et al. 2000).

In case of porebridging cement (the effective fluid has positive shear stiffness), combined effective medium theory (CEMT) is used to model the mixture of framework and effective fluid in the permeable rock. The theory consists of two steps, where the first step make use of SCA to mix two constituents of equal concentrations, to approximate connected phases. The second step of the CEMT is utilizing DEM to estimate the effective properties of the two phase medium at the desired concentrations. The DEM model is considered to preserve the connectivity of the constituents when the concentrations are altered. Thus connected phases remain connected when the concentrations change, and vice versa for unconnected phases.

The DEM is applied for modelling the fluid effects in non-permeable rocks for both the PF and CT models. Brine and gas are representative for pore fluid in all our modelling, mixed with pore-filling cement when present.

The PF and CT models have different assumptions about the rock microstructure and cementing processes. In the next section, it will be shown how such process defined rock physics models may be evaluated and be used for estimation of PLF parameters from seismic parameters.

ESTIMATION OF PLF PARAMETERS

In the following we adapt the procedure for estimation of PLF parameters as was outlined by Johansen et al. (2004) and Johansen and Ruud (2006). Well log data

often provide measurements of both V_p, V_s and ρ, which, when assuming isotropic rocks, provide the bulk modulus (K) and shear modulus (μ) from

$$K = \rho\left(V_p^{\,2} - 4V_s^{\,2}/3\right),$$
$$\mu = \rho V_s^{\,2}. \quad (1)$$

We now apply various rock physics models (see appendix) to define the elastic properties (K and μ) and the density (ρ) as functions of porosity, lithology and fluid saturation. Hence, on selected values for porosity ϕ_i, $i=1,N$, lithology c_j, $j=1,M$, and saturation s_k, $k=1,L$ tabulated functions for $K(\phi_i, c_j, s_k)$, $\mu(\phi_i, c_j, s_k)$ and $\rho(\phi_i, c_j, s_k)$ are established. Since they are functions of three parameters, we hereafter denote these as the bulk, shear or density constraint cubes. The node values for each axis are defined at equidistant intervals so that $\phi_i = i\Delta\phi$ with $\Delta\phi=\phi_{max}/(N-1)$, $c_j=(j-1)\,\Delta c$ with $\Delta c=1/(M-1)$ and $s_k=(k-1)\Delta s$ with $\Delta s=1/(L-1)$. In the following we use $\phi_{max}=0.4$, implying the constraint cubes to be defined for $0\leq\phi\leq0.4$, $0\leq c\leq1$ and $0\leq s\leq1$.

The constraint cubes can now be realizations of various rock physics models, or, they can be made to mimic compaction and sedimentation processes as discussed in the previous section. Our task is essentially to establish inverse functions f_1, f_2 and f_3, so that we from a set of measured data, for instance, K^*, μ^* and ρ^* can find the PLF parameters, e.g.

$$\phi = f_1(K^*,\mu^*,\rho^*),$$
$$c = f_2(K^*,\mu^*,\rho^*), \quad (2)$$
$$s = f_3(K^*,\mu^*,\rho^*).$$

From Figure 1 and 2, we see that the functional relationships between the PLF parameters and the seismic parameters are strongly non-linear and different for the two models displayed (PF and CT). Furthermore, in these approaches there are no analytical models that describe the

relationships, since the forward models merge different rock physics models. Therefore the inversion has to be made by numerical procedures. In the approach of Johansen et al. (2004) the inversion strategy is as follows: First, seek for correlations between the PLF parameters ϕ, c and s for each bulk modulus K_l for M_K K-values ($K_1,\ldots K_{MK}$) where $K_1=\mathrm{MIN}[K(\phi_i, c_j, s_k)] < K_2, < \ldots < K_{MK-1} < K_{MK}=\mathrm{MAX}[K(\phi_i, c_j, s_k)]$. The solution for each K-value can be viewed as a subspace of a model space spanned by the coordinate axes ϕ, c and s. As will be shown later, this subspace is usually a 3-dimensional surface; hence, every point (ϕ, c, s) on this surface corresponds to a possible set of PLF parameters for this specific K-value. We denote a subset (e.g. usually a 3D surface) corresponding to a specific value K_l by $(\phi, c, s)_{(K)}$. Numerically this subset is represented by a set of correlation functions (2D contours), one for each saturation s_k with $k=1$, L, i.e. from water saturated to gas saturated. For each saturation s_k, the coordinate pairs (ϕ, c) (correlation function (ϕ, c) $_{(Sk)}$) is re-sampled along a constant K-value (K_l) within the bulk constraint cube $K(\phi_i, c_j, s_k)$ using cubic spline interpolations. The procedure is schematically illustrated in Figure 4, where two 2D contours for (ϕ, c) are shown for gas and water saturated cases and for two different K-values (10 and 20 GPa). The contour for (ϕ, c)$_{Sk}$ is represented by the same number of points for any K, which means that by "drawing curves" through points of the same index number of every contour (ϕ, c) $_{(Sk)}$, k=1,L we may by interpolation obtain the contour (ϕ, c)$_{(s)}$ for any saturation s which is not represented by the set s_1, $s_2,\ldots s_L$ used to generate the constraint cube.

Correspondingly, we can establish the subspace (ϕ, c, s) $_{(\mu m)}$ for each shear modulus value (μ_m) from the shear modulus constraint cube $\mu(\phi_i, c_j, s_k)$ for M_μ values ($\mu_1,\ldots \mu_{M\mu}$), where $\mu_1=\mathrm{MIN}[\mu(\phi_i, c_j,$

$s_k)$])] $< \mu_2 < \ldots < \mu_{M\mu-1} < \mu_{M\mu}$ =MAX[$\mu(\phi_i, c_j, s_k)$]. In a similar way the subspace $(\phi, c, s)_{(\rho n)}$ is obtained for each density value (ρ_n) from the density constraint cube $\rho(\phi_i, c_j, s_k)$ using M_ρ ρ−values, where ρ_1=MIN[$\rho(\phi_i, c_j, s_k)$] $< \rho_2$ $< \ldots < \rho_{M\rho-1} < \rho_{M\rho}$ =MAX[$\rho(\phi_i, c_j, s_k)$]. Figure 5 shows contours for $(\phi, c)_{(s=1)}$ lines obtained for various values of K, μ and ρ.

Along the same lines as described above, the correlation $(\phi, c, s)_{(K*)}$ for an arbitrary bulk modulus $K*$ may subsequently be estimated by interpolation along curves drawn through points of corresponding indices within the set $\{(\phi, c, s)_{(K1)} (\phi, c, s)_{(K2),\ldots} (\phi, c, s)_{(KMK)}\}$. In our case this is made using cubic spline functions. Furthermore, we can obtain $(\phi, c, s)_{(\mu*)}$ consistent to the shear modulus $\mu*$, and $(\phi, c, s)_{(\rho*)}$ consistent to the density $\rho*$. Using this technique, we can easily explore how the solution space changes with the kind of input data available. Say we know the data parameters $K*$ and $\mu*$, then the solution $(\phi, c, s)_{(K*\wedge\mu*)}$ are found by the intersection of $(\phi, c, s)_{(K*)}$ and $(\phi, c, s)_{(\mu*)}$, i.e

$$(\phi,c,s)_{(K*\wedge\mu*)} = (\phi,c,s)_{(K*)} \cap (\phi,c,s)_{(\mu*)}.$$
(3)

If $K*$ and $\rho*$ are the known data parameters, the solution $(\phi, c, s)_{(K*\wedge\rho*)}$ is

$$(\phi,c,s)_{(K*\wedge\rho*)} = (\phi,c,s)_{(K*)} \cap (\phi,c,s)_{(\rho*)}.$$
(4)

And if $K*$, $\mu*$ and $\rho*$ are all known, the solution $(\phi, c, s)_{(K*\wedge\mu*\wedge\rho*)}$ is found from intersection of the solution sets obtained for $K*$ and $\mu*$ and $K*$ and $\rho*$, i.e.

$$(\phi,c,s)_{(K*\wedge\mu*\wedge\rho*)} = (\phi,c,s)_{(K*\wedge\mu*)} \cap (\phi,c,s)_{(K*\wedge\rho*)}.$$
(5)

Alternatively, the solutions can have been found by intersection of the solution sets

$K*$ and $\rho*$ and $\mu*$ and $\rho*$, or $K*$ and $\mu*$ and $\mu*$ and $\rho*$.

SYNTHETIC EXAMPLES

Under determined example – using two data parameters (K and μ)

The purpose of this section is to find possible solutions (ϕ,s,c) from K and μ, i.e. density data is not used. Lack of knowledge about density data or any other parameter might lead to an under determined inversion problem. The problem of finding the combinations of ϕ, s and c values that give a consistent solution for the different models, is approached to by studying the 3D (ϕ,s,c) solution planes given by $(\phi,c,s)_{(K*\wedge\mu*)}$ obtained from (3).

First an example is shown in Figure 6 for two sets of K and μ resulting from forward modelling of the PF and CT models, which are further referred to as set 1 (K=7.47 GPa, μ=2.60 GPa) and set 2 (K=18.43 GPa, μ=13.52 GPa), respectively. The figure shows that the PF- and CT models return completely different solutions for $(\phi,c,s)_{(K*\wedge\mu*)}$. If the CT model returns parameter values that coincide with observed values, this points to a rock model indicating contact cementation. Conversely, if the PF model gives consistency with observed data, this points to a rock assumed to have pore-filling cementation. The intersection lines between the different planes of solutions in Figure 6, i.e. $(\phi,c,s)_{(K*\wedge\mu*)}$, are more pronounced in Figure 7. As seen, the PF model gives a set of PLF parameters for set 1, while the CT model only provides a solution in case of full water saturation (s=1). Both models returns possible solutions for set 2, but the CT model has larger variations in solution parameters. Hence, if the shallow set is a rock with pore-filling cement, the alternative

solutions for ϕ, c and s are expected to lie on the PF- solution line defined by $(\phi,c,s)_{(K*\Lambda\mu*)PF}$. Similarly if the deeper rock is contact cemented, the solution should be found on the CT- solution line defined by $(\phi,c,s)_{(K*\Lambda\mu*)CT}$.

Figure 8 shows synthetic logs of K, μ and ρ made from forward modelling using the PF- and CT models with model parameters ϕ, c, and s. The shallow data comes from the PF model, the interval 1.5 – 2.5 km is a transition from the PF to CT model, where increasingly weight is put on the CT values. From 2.5 km, the log values are made using the CT model only. In the following, the log will be used to demonstrate the estimation strategy. Figure 9 shows estimated PLF parameters obtained from K and μ, given in Figure 8. Now both the PF and CT constraint cubes are used to estimate the solutions of $(\phi,c,s)_{(K*\Lambda\mu*)}$ for each depth. The synthetic data are made with full water saturation. Each saturation level in the solutions is given a colour from dark blue ($s=0$) to dark red ($s=1$). The colour is also used when displaying the ϕ and c solutions. The PF model predicts solutions consistent with the log parameters down to 1.5 km, and from 4 km and deeper. The CT model does not predict solutions that agree with both c and ϕ at depths shallower than 2 km, and for some depths it has no solutions at all. But from 2 km, the model predicts solutions consistent with log values for s, c and ϕ at all depths. The spread of the PLF solutions are large at depths shallower than 3 km ($\phi>0.15$), which makes it difficult to extract useful information. But when ϕ decreases below 0.15, the spread in ϕ and c decreases, and can be constrained within small intervals. Fluid prediction is hard to perform without having density information. Figure 9 further indicates that the likely distributions are pore-filling cement in the shallow part of the log, contact cement from 2-4 km and

possibilities of both cement distributions in the deepest part.

Three data parameters (K, μ and ρ)

If there is information about all the three parameters that defines the seismic properties of an isotropic rock, K, μ and ρ, respectively, the inversion problem can potentially be solved uniquely with respect to s, ϕ and c, as shown in (5). Figure 10 shows where the three planes defined by $(\phi,c,s)_{(K*\Lambda\mu*\Lambda\rho*)}$ intersect, for set 1 and 2. Now there are no intersection lines with sets of solutions, but rather one or more points in the 3-D s, ϕ and c coordinate system for each depth. The points are where the solution lines cross according to (5). This procedure can be applied on whole logs where the seismic parameters have been measured. In Figure 11 all the consistent solutions are shown, when inverting the log in Figure 8. At the shallow depths, the inversion of the PF model gives unique solutions. But for larger depths, the inversion of the CT model does not only provide the correct solutions, it also gives alternative solutions also consistent with the model. The interval of solutions for ϕ and c are mostly small, while the saturation changes are significant, when several solutions occur. This is due to the stiff rock resulting from low porosity, which make the overall rock stiffness much less dependent on fluid properties. Hence, to compensate for a small change in porosity and/or clay content, the saturation must change much to produce the same seismic parameters. Saturation is therefore considered the most sensitive PLF parameter in this modelling.

REAL DATA EXAMPLE

The strategy presented can easily be applied to well logs of velocities and density, to estimate the porosity, saturation and lithology provided there is a model relating elasticity and density to PLF

parameters. The model(s) found to give reliable solutions may further provide information about the rock composition/structure (e.g. contact vs pore-filling cement). Figure 12 displays data logs from a well A. Due to the large size of the log, only 984 samples are extracted from the log at different depths. Half of the log depths are randomly picked, and the other half is depths found from iterative modelling, which extracted some sets of parameters that coincide with our models. The inversion results are shown in Figure 13, using both PF and CT constraint cubes. The constraints provide solutions consistent with K, μ and ρ only for some depths, while at other depths there is no space spanned by both $(\phi, c, s)_{(K^* \wedge \mu^*)}$ and $(\phi, c, s)_{(K^* \wedge \rho^*)}$ in (5), and no solutions are given. In some places there are multiple solutions for the PLF parameters, some consistent with the well log, some not. Hence, a priori information e.g. about saturation will be helpful to perform a probability analysis of the inversion results. The best sets of solutions are plotted with a coloured hexagon, at depths where solutions exist. In Figure 13 both the PF and CT models return consistent solutions for many depths. However the CT constraints do not imply correct clay contents, while the porosity values are close to measured. This indicates that in this example, the PF model is better than the CT model for describing the link between PLF parameters and seismic parameters.

Along the same procedure, we now apply a more extended set of rock physics constraint cubes, as defined by Dræge et al. (2006a). Here three additional distributions for clasts and cements in siliciclastic rocks are discussed; graincoating and pore-lining cement that envelop the framework grains, stabilizing grain contacts, but does not carry load in the grain-grain contacts (CS), replace clay or clay clasts which act as a part of the loadbearing framework (FW),

and graincoating clay cement that prevent contact between the framework grains, and thus are loadbearing (GC). The constraint cubes are modelled with various rock physics models described in detail by Dræge et al. (2006a). Illustrations of all distributions considered are shown in the upper part of Figure 15. A connection between concentration of the cement and porosity has been implied so that the porosity is exclusively reduced by cementation. Hence, low porosities mean high concentrations of cement. An alternative way is to impose other relationships than the one-to-one between cement content and porosity loss and apply the same rock physics models. This is also performed for another set of constraint cubes. This set is denoted by appending the number 2 on the rock physics model applied (e.g. CT2). For these cubes mechanical compaction is responsible for porosity loss down to 25 % porosity, and for lower porosities cement content is set to increase with ¼ of the further porosity loss. In Figure 14 seven different constraint cubes are used in the inversion, and the results are compared with the well A log. Only the best predictions are kept from each model at one depth. Now there are many depths with log-consistent PLF parameters, given by $(\phi, c, s)_{(K^* \wedge \mu^* \wedge \rho^*)}$. Especially the CT2, CS2 and GC2 models fit the data well, and predict fairly accurate clay content in most cases, while the porosity and saturation predictions are very good for all models. Figure 15 sums up the inversion of well A by showing the solutions versus depth for all models involved. Only solutions with accumulated deviation (sum of deviations in s, ϕ and c) less than 0.1 are included, so that the microstructure associated with the various rock physics models can explain the rock texture. The figure shows that one or more distributions dominate certain intervals, while the microstructure of other intervals is more ambiguous and harder to identify. All distributions are predicted to be present at various depths in the upper sand (down

to 3.8 km). The CS and GC models and corresponding microstructure seem to best describe the upper shale and the following shaly sandstone. The shale from ca 4.25 - 4.3 km is predicted to be cemented by contact cement (CT) and coating contact cement (CS), while the sand below contains grain coating cement (GC) in addition to CT and CS. An interval of the deepest shale (from ca 4.45 km) is predicted to consist of pore-filling cement. At low porosities (< 3%) some of the models tend to coincide, and the cement distributions are more difficult to reveal by this technique. This is because the rock approaches a two phase (quartz and clay) material with less range of elasticity differences than in the more porous three phase rock.

DISCUSSION

The rock physics models applied in this paper requires some assumptions about the input parameters, like number of grain contacts, critical porosity and density and elasticity of the constituents. To construct appropriate constraint cubes, iteratively modelling can be performed to find proper values for these parameters. One way to condition the PLF problem can be to calibrate a forward model to a known dataset, and then use this model to create constraint cubes to be applied in the inversion. If there are no data to calibrate our models with, a library of constraint cubes can be applied, and the inversion results can be evaluated. By systematically varying the input parameters and create a larger number of model cubes, the applied models are likely to be capable of predicting the microstructure of even larger parts of the logs.

One drawback of creating constraint cubes is that some of the parameters need to be correlated, which might be incorrect in some cases. When constructing a constraint cube associated with a cementation model (e.g. CT or CS), an

expression for the cement content is necessary. Two approaches are used in this paper; a one-to-one connection between cement and clay content, which means that the sum of porosity and cement is 0.4 at all porosities. Secondly cementation is considered to initiate from 25 % porosity, and further increase with ¼ of the porosity loss. Empirical studies and knowledge about local conditions can help choosing the right relations between those parameters. Empirical rock physics models can also be used to create constraint cubes, but then the information about the microstructure will not be revealed to the same extent (dependent on model).

The rocks in this paper are considered to be isotropic, even pure shales. Unless all elongated constituents are completely randomly orientated, this assumption is not quite met. Some of the rock physics models applied, are further constructed for spherical grains, which is commonly not the case in shaly rocks. But the inversion procedure is model independent in the sense that all rock physics models can be used to make constraint cubes for further inversion. Therefore a shale model like the one of Hornby et al. (1994) or Dræge et al. (2006b) for transversely isotropic shales, can be used in the inversion. The PLF parameters then becomes function of density and 5 elastic parameters: $(\phi, c, s)_{(c_{11} \wedge c_{12} \wedge c_{13} \wedge c_{33} \wedge c_{44} \wedge \rho)}$, where c_{11}, c_{12},… are elastic parameters that describe the elasticity in a transversely isotropic material.

There are always some uncertainties in the data parameters used. An indication on the importance of accurate log measurements, and which parameters are most important are obtained by inflicting an uncertainty on K, μ and ρ respectively, and studying the corresponding inversion results. Figure 16 corresponds with the plot using the PF model in Figure 13, but with an uncertainty of ± 2 % on the log data. By comparing the figures, it can be seen that the numbers of

solutions at each depth generally increase. But the effect of imposing an uncertainty on density is more pronounced than on the elastic parameters. Both number of solutions and accuracy of the solutions increase when densities are allowed to vary with ± 2 %. The predicted saturation values are most exposed to perturbations when input parameters have uncertainties, and saturation is therefore considered the most sensitive parameter in the modelling. The similar results were found using the CT model. This example shows the importance of having accurate log data, in order to extract the correct PLF parameters.

Figure 13 illustrates moreover that one model can provide multiple solutions at one depth, and Figure 15 also shows that more than one model can predict solutions at a given depth. Then a priori knowledge either about the rock texture or of ϕ, s or c can help choosing the correct solution. The latter figure also indicate that there can be more than one model with log-consistent, and almost identically parameter predictions. This is often the case when porosity is low, and the rock approaches a two phase composite. Then many of the models approach the same stiffness values (the densities are equal regardless of models), and the system is less sensitive to the fluid properties.

CONCLUSIONS

A method for mapping porosity (P), lithology (L) and pore fluid (F) from seismic parameters has been outlined. Essentially any forward rock physics model may be used as constraints for the estimation of the PLF parameters. The estimation procedure reveals non-unique solution sets, and it is flexible to the number of input parameters (V_p, V_s, ρ) at each position. The inversion method establish correlations between rock parameters also when the problem is under determined. The method gives the

possibility of evaluating the relevance of a given rock physics model to describe the measured data. If V_p, V_s and ρ are available, this opens up for estimation of the microstructure in addition to the PLF parameters, since any rock physics model implies an assumption of the rock microstructure.

Acknowledgement

REFERENCES

Avseth, P. A., Mukerji, T. and Mavko, G. (2005). *Quantitative Seismic Interpretation: Applying Rock Physics Tools to Reduce Interpretation Risk* (First edition). Cambridge University Press, Cambridge, UK.

Berrymann, J. G. 1992. Single-scattering approximaitons for coefficients in Biot's equations of poroelasticity. *The Journal of the Acoustical Society of America,* **91**, 551-571.

Berrymann, J. G. 1995. Mixture theories for rock properties. *In:* Ahrens, T. J. (ed), *A handbook of physical constants,* American Geophysical Union, Washington, D. C., 205-208.

Dræge, A., Jakobsen, M. & Johansen, T. A. 2006a. Rock physics modelling of shale diagenesis. *Petroleum Geoscience*, **12**, 49-57.

Dræge, A., Johansen, T. A., Brevik, I. & Dræge, C. T. 2006b. A strategy for modelling diagenetic evolution of seismic properties in sandstones. *Accepted for publication in Petroleum Geoscience*.

Dvorkin, J. & Nur, A. 1996. Elasticity of high porosity sandstones: Theory for two North Sea data sets. *Geophysics*, **61**(5), 1363-1370.

Dvorkin, J., Berryman, J. & Nur, A. 1999. Elastic moduli of cemented sphere packs. *Mechanics of Materials*, **31**, 461-469.

Gassmann, F. 1951. Über die Elastisität der poröser medien. *Vierteljahrschrift der Naturforschenden Gesellshaft in Zürich*, **96**, 1-23.

Hashin, Z. & Shtrikman, S. 1963. A variational approach to the theory of the elastic behavior of

multiphase materials. *Journal of the Mechanics and Physics of Solids*, **11**, 127-140.

Hill, R. 1952. The elastic behavior of crystalline aggregate. *Proceedings of the Physical Society of London*, **A65**, 349-354.

Hornby, B. E., Schwartz, L. M. & Hudson, J. 1994. Anisotropic effective-medium modelling of the elastic properties of shales. *Geophysics*, **59**(10), 1570-1583.

Jakobsen, M., Hudson, J. A., Minshull, T. A. & Singh, S. C. 2000. Elastic properties of hydrate-bearing sediments using effective medium theory. *Journal of Geophysical Research*, **105**(B1), 561-577.

Johansen, T. A., Drottning, A., Lecomte, I. & Gjøystdal, H. 2002. An approach to combined rock physics and seismic modelling of fluid substitution. *Geophysical Prospecting*, 50(2), 119-137.

Johansen, T. A., Spikes, K. & Dvorkin, J. 2004. *Strategy for estimation of lithology and reservoir properties from seismic velocities and density.* 74th SEG meeting, Expanded abstracts, Denver, Colorado, USA. 1726-1729.

Johansen, T. A., Ruud, B. O. 2006. Rock physics processing for reservoir properties from seismic parameters. In preparation for submission to the 76th SEG meeting, New Orleans, Louisiana, USA.

Li, X. G., Han, D. H., Liu, J. and McGuire, D. 2005. *Inversion of Sw and porosity from seismic AVO.* 75th SEG meeting, Expanded abstracts, Houston, Texas, USA. 1307-1310.

Marion D. & Nur, A. 1991. Pore-filling material and its effect on velocity in rocks. *Geophysics*, **56**, 225-230.

Mindlin, R. D. 1949. Compliance of elastic bodies in contact. *Journal of Applied Mechanics*, **16**, 259-268.

Reuss, A. 1929. Berechtungder fliessgrense von mischkristallen auf grund der Plastizitätbedingung für ein Kristalle. *Zeitschrift für Angewandte Mathematik aus Mechanik*, **9**, 49-58.

Sams, M. S. & Andrea, M. 2001. The effect of clay distribution on the elastic properties of sandstones. *Geophysical Prospecting*, **49**, 128-150.

Saltzer, R., Finn, S. and Burtz, O. 2005. Predicting V_{shale} and porosity using cascaded seismic and rock physics inversion. The Leading Edge, **24**, 732-736.

Voigt, W. (ed) 1928. Lehrbuch der Kristallphysik. Teubner, Leipzig.

Wang, Z. 2000. The Gassmann equation revisited: Comparing laboratory data with Gassmann's prediction. In: Wang, Z. and Nur, A. (eds), *Seismic and acoustic velocities in reservoir rocks*, **3**: Recent developments: Society of Exploration Geophysicists, 8-23.

Xu, S. and White, R. E. 1995. A new velocity model for clay-sand mixtures. *Geophysical Prospecting*, **43**, 91-118.

	k (GPa)	μ (GPa)	ρ (g/ccm)	α
Quartz	37.0	44.0	2.65	1.00
Clay	21.0	7.0	2.60	0.15
Brine	2.96	0.00	1.03	-
Gas	0.06	0.00	0.15	-

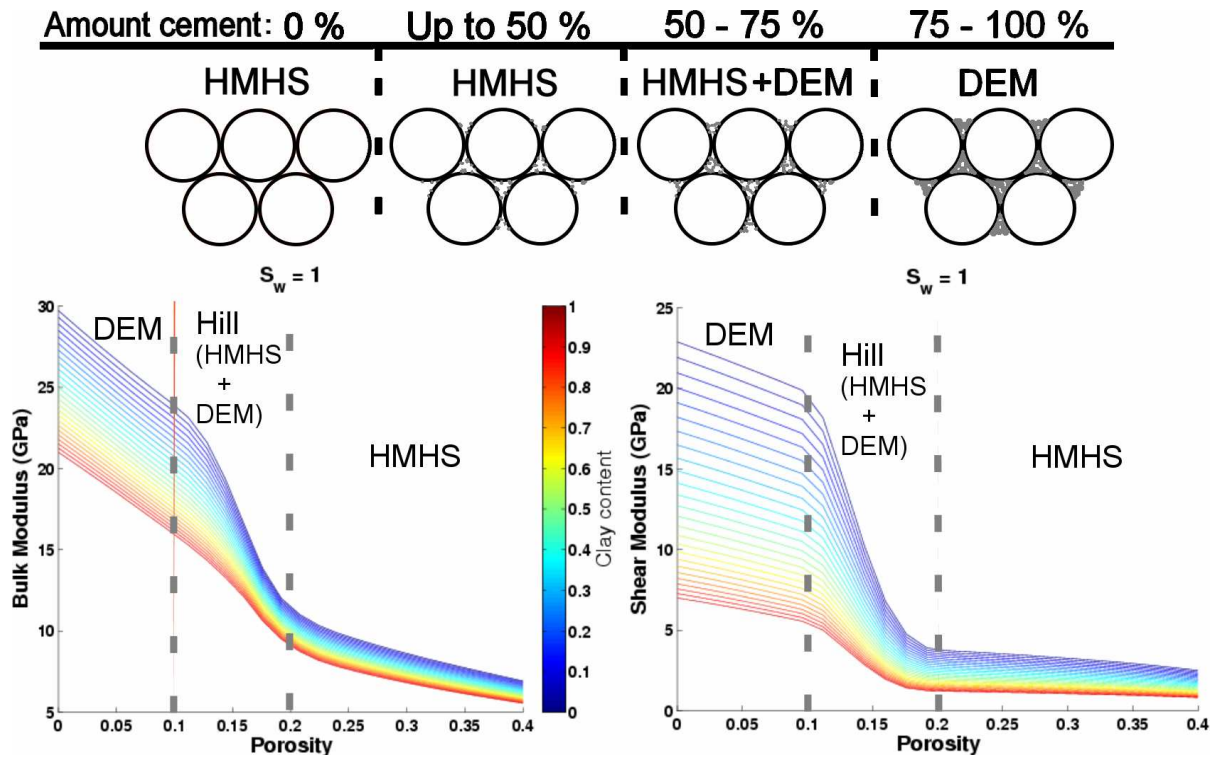**Table 1**. Physical properties of the constituents used in the modelling. Cement has the same properties as clay.

Figure 1. Above: modelling procedure for the PF model. White circles are framework grains (quartz or clay), while grey colour indicates precipitated pore-filling cements. The text above each stage of cementation indicates the rock physics model applied in the modelling, and is dependent on cement volume. The bulk- and shear modulus for the PF model are shown below as a function of porosity and clay content for a water saturated rock. The colour bar in the middle indicates the amount of framework clay. The rock physics models are discussed in the text. Cement volume is relative to the intergranular volume.
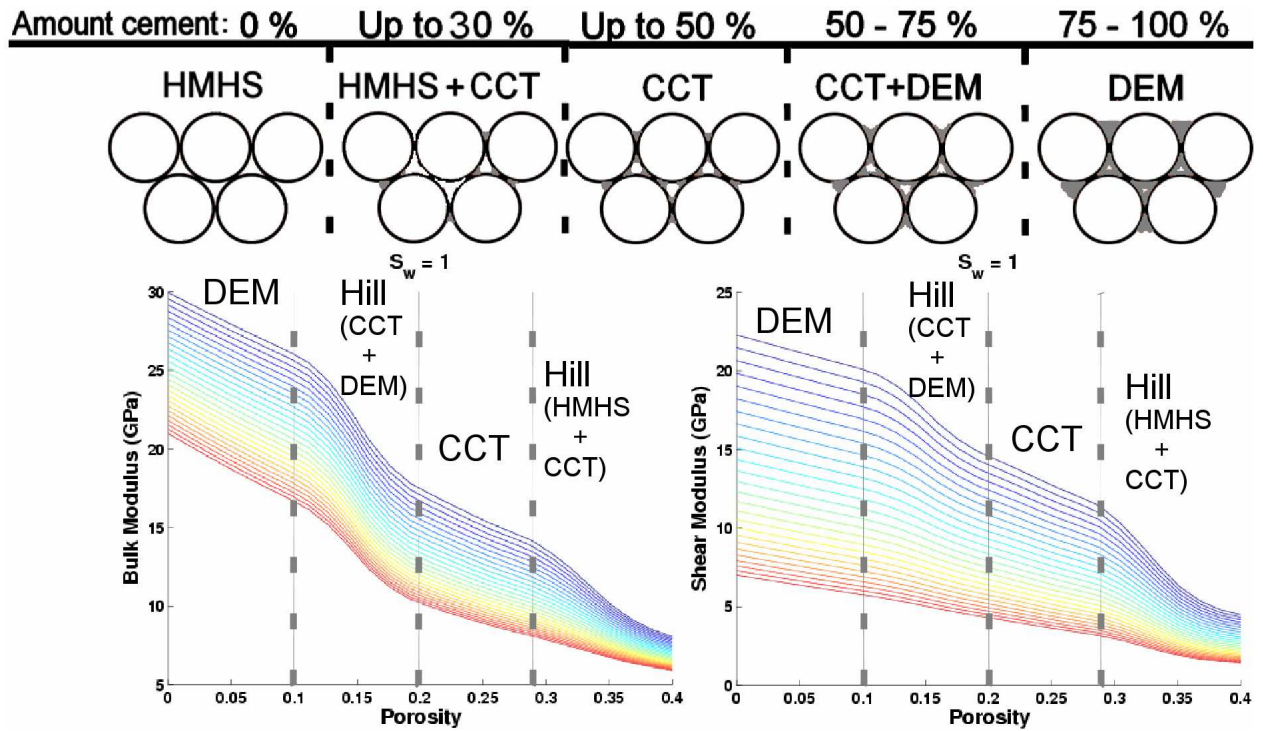
Figure 2. Above: modelling procedure for the CT model. White circles are framework grains (quartz or clay), while grey colour indicates precipitated contact cement. The text above each stage of cementation indicates the rock physics model applied in the modelling, and is dependent on cement volume. The elastic parameters for the CT model are shown below as a function of porosity and clay content for a water saturated rock. The colour code for framework clay is the same as in Figure 1. The rock physics models are discussed in the text. Cement volume is relative to the intergranular volume.
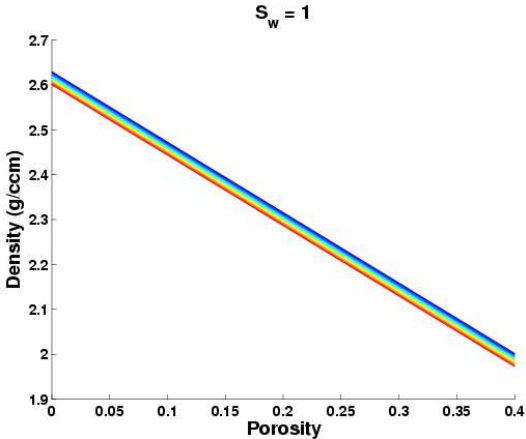
Figure 3. Density versus clay content and porosity for a water saturated rock. Since densities are independent on cement distribution, they are common for both PF and CT model. The clay content varies due to the colour bar in Figure 1.
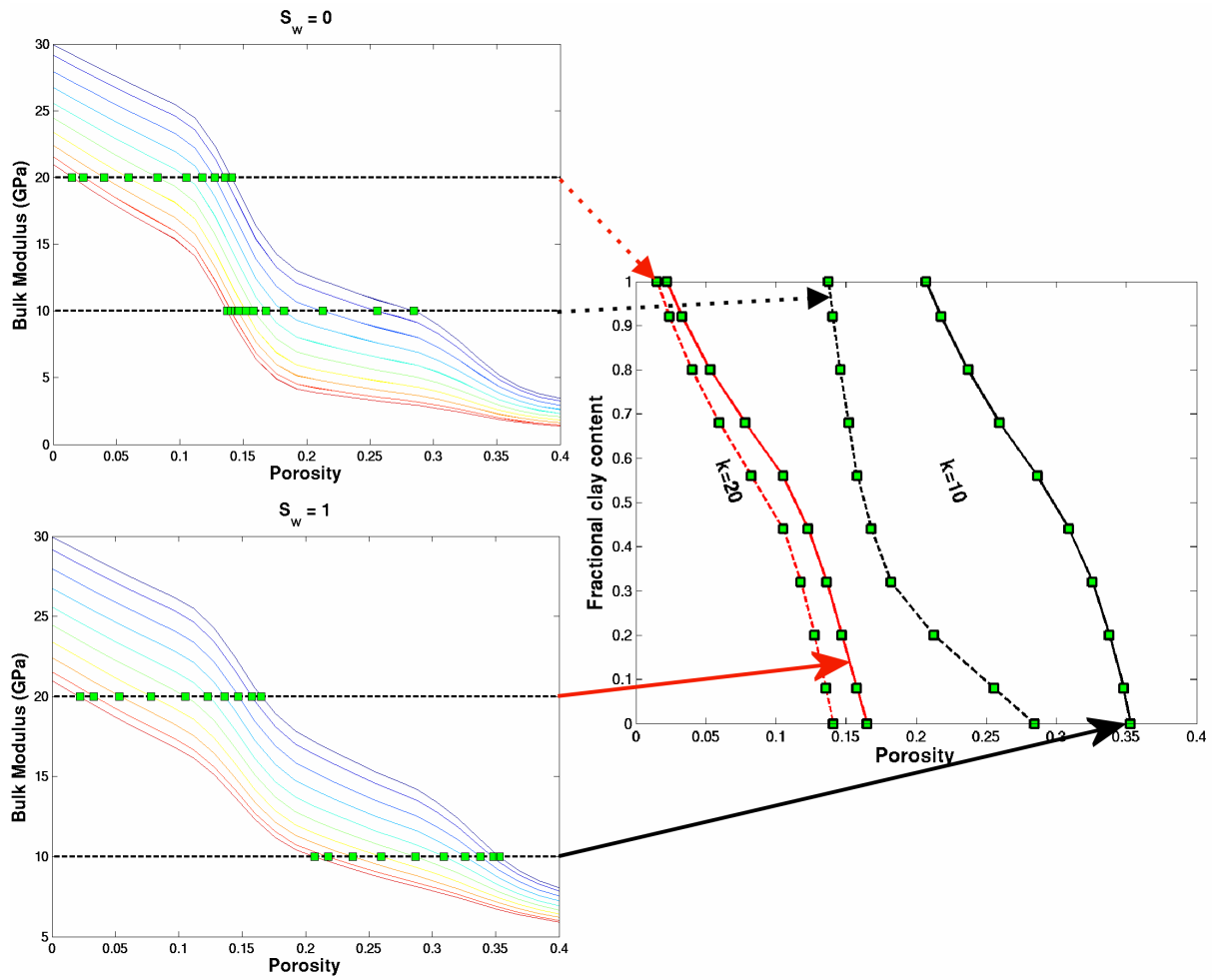
Figure 4. Example of resampling of bulk cubes with gas saturation (*s*=0) and brine saturation (*s*=1) for 2 bulk modulus values, using both the PF (above) and CT (below) model. All porosity and clay values are found for each value of bulk modulus (here 10 GPa and 20 GPa), and plotted in the $\phi - c$ plane. The stippled lines in the right plot denote gas saturated rock, while the continuous lines denote brine saturated rock. The green squares in the left plots correspond with the green squares in the right plot.
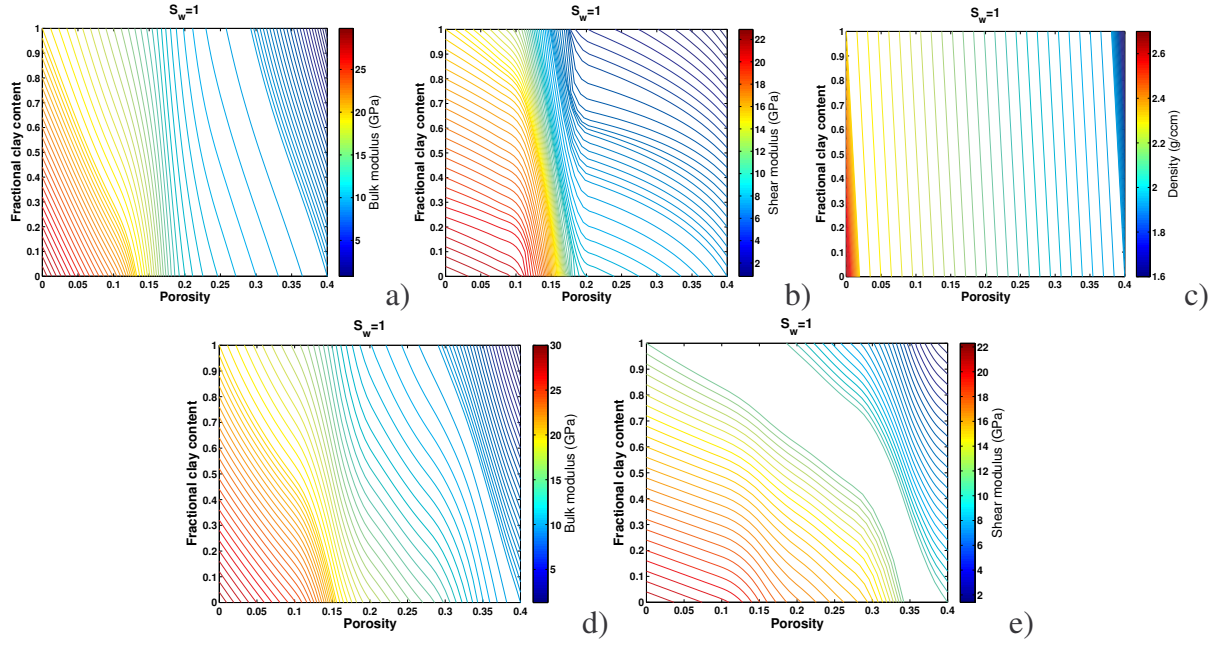
Figure 5. The plots show examples of contours resulting from resampling of the constraint cubes for water saturated case. Each bulk modulus curve is defined by $(\phi, c, s)_{(K_i)}$, where K_i is a constant bulk modulus value for each contour. In the same way $(\phi, c, s)_{(\mu_i)}$ and $(\phi, c, s)_{(\rho_i)}$ define the contour lines for constant values of shear modulus and density. Hence, each contour shows all possible combinations of ϕ and c for a given K, μ or ρ and saturation. a) and b) show elastic moduli for the PF model, while d) and e) shows the corresponding plots for the CT model. The density plot in c) is common for both models.
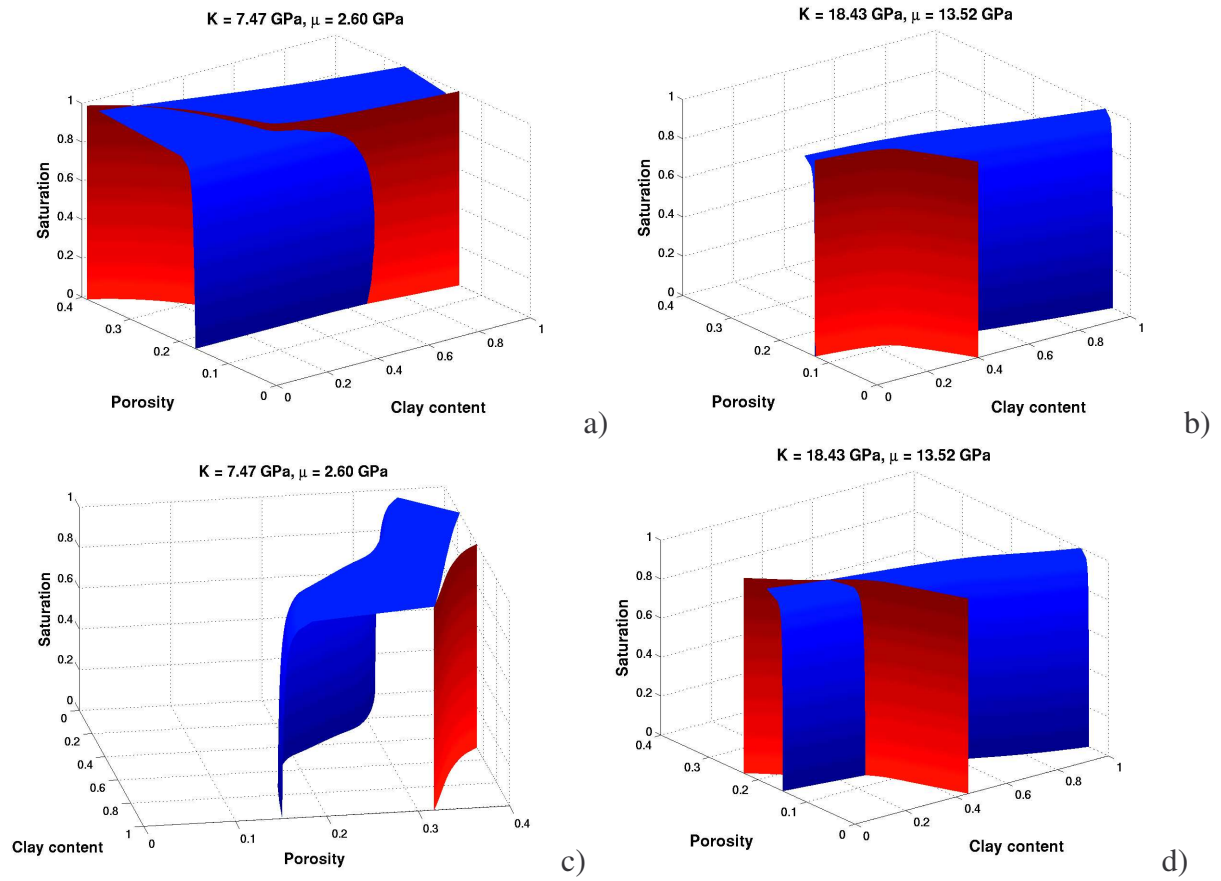
Figure 6. Different solution planes of $(\phi, c, s)_{(K*)}$ and $(\phi, c, s)_{(\mu*)}$ for the two different rock physics models. The bulk-modulus plane is blue, while shear modulus is red. a) and b) shows the solutions for the PF model, while c) and d) shows solutions for the CT model. a) and c) is for an uncemented rock with low stiffness (set 1), and b) and d) is for a contact cemented rock (set 2).
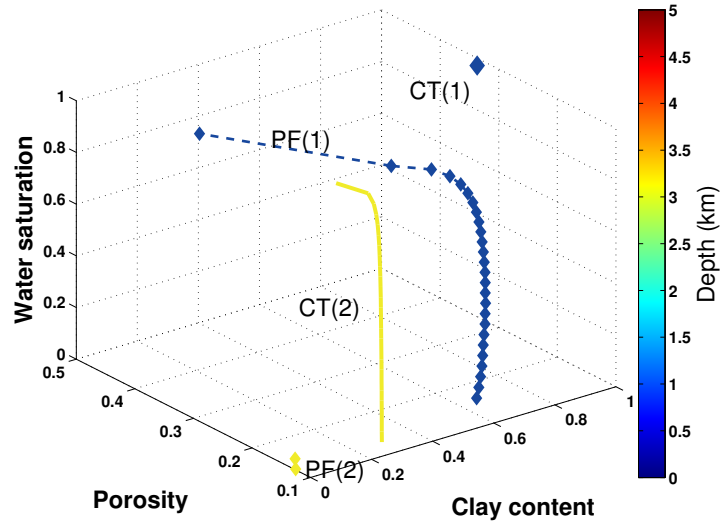
Figure 7. The solution lines for the PF- and CT model are given by $(\phi,c,s)_{(K^*\Lambda\mu^*)}$ and correspond with the intersections of the planes in Figure 6. The shallow solutions correspond with set 1, and the deep solutions with set 2, as indicated in the parenthesis.
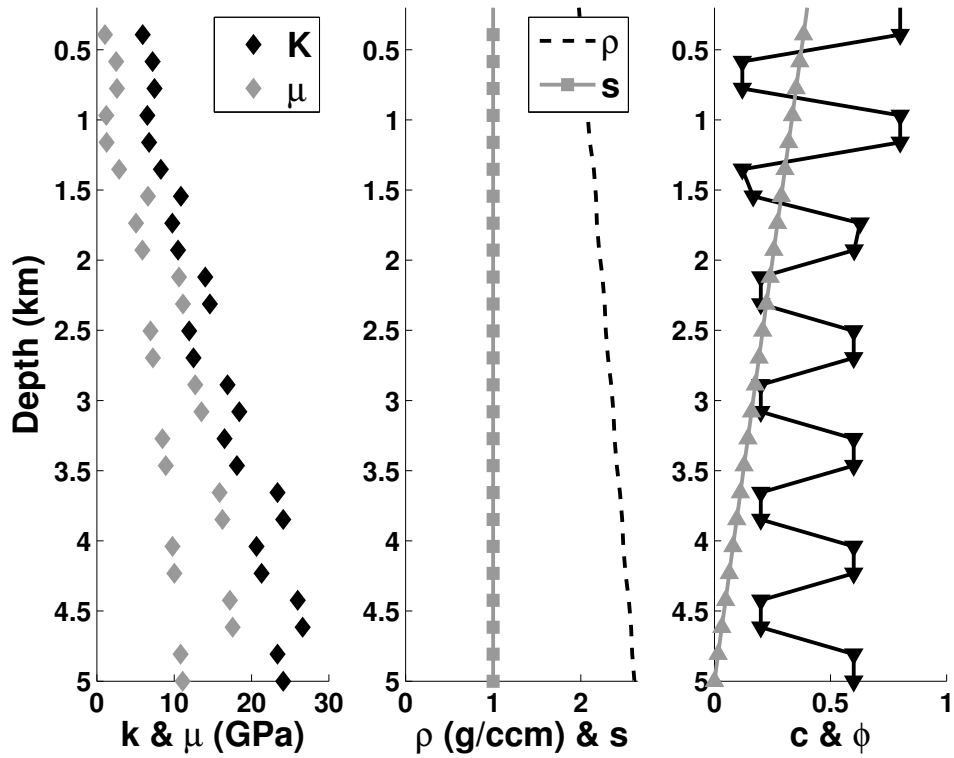
Figure 8. The synthetic log is made from the PF and CT models, and applied in the modelling of Figure 9 and 11. The unitless parameters are fractions of the total pore volume (*s*), total volume of solids (*c*) and total rock volume (*ϕ*) respectively. *c* is black and *ϕ* is grey in the right plot.
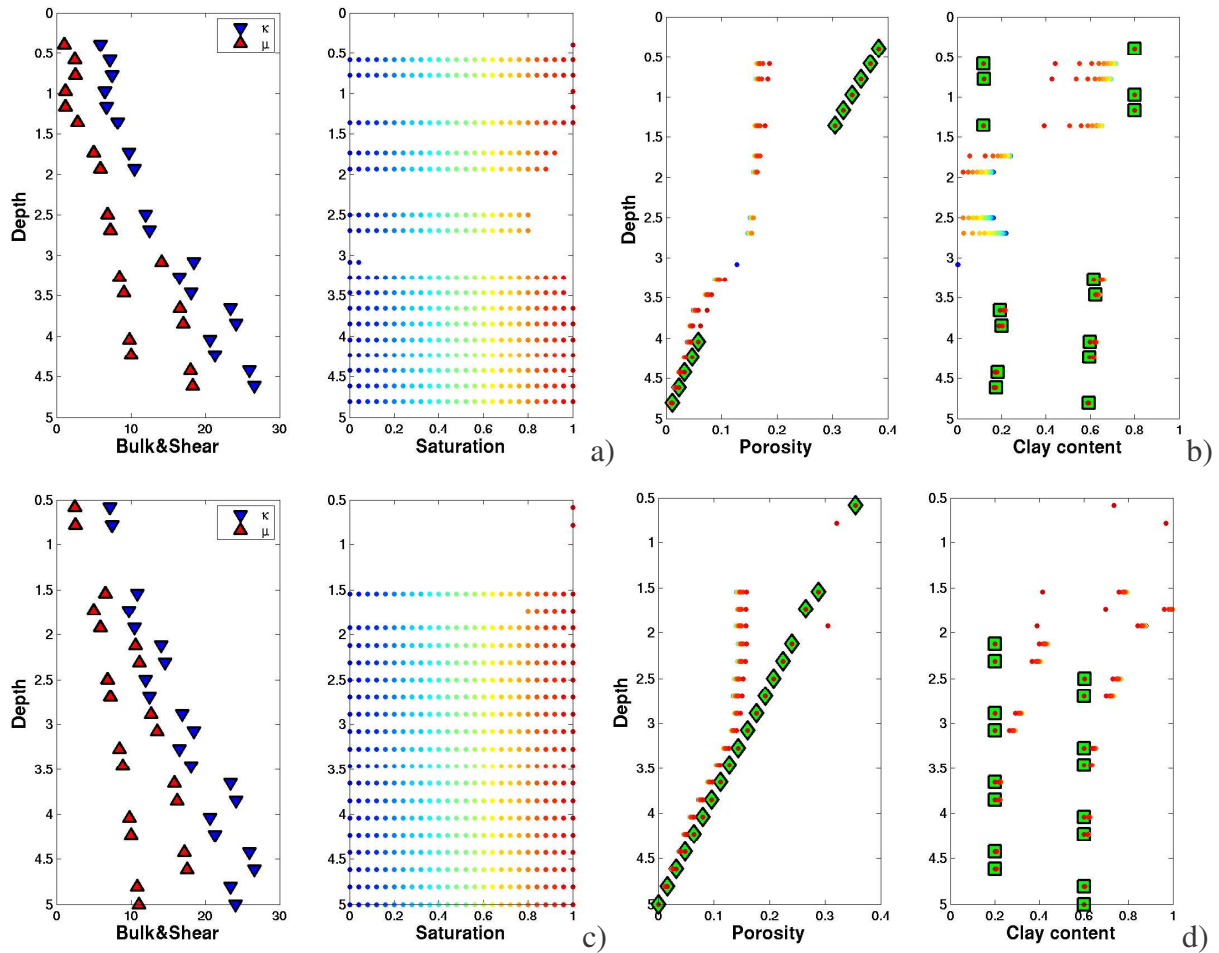
Figure 9. The solutions defined by $(\phi, c, s)_{(K*\Lambda\mu*)}$ for the PF model are shown in a) and b) for the whole log, while the corresponding results for the CT model are shown in c) and d). The K and μ values are shown to the left in each case. Different saturations from zero (dark blue) to one (dark red) that give solutions for given K and μ values, are shown in a) and c). The porosity and clay content are given in b) and d), with dot-colour that corresponds with the saturation level. The green diamonds indicate where the porosity prediction matches the correct log porosity within 2.5 % error. Similarly, green squares indicate where the clay content predictions deviate with less than 5 %.
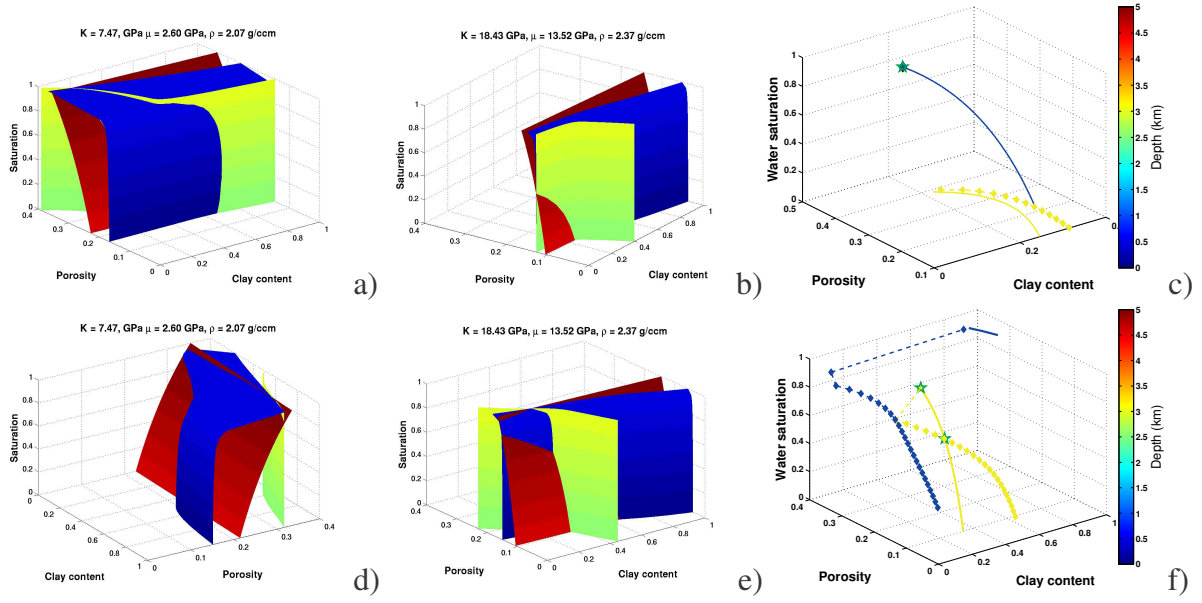
Figure 10. The solution planes defined by $(\phi, c, s)_{(K^*)}$, $(\phi, c, s)_{(\mu^*)}$ and $(\phi, c, s)_{(\rho^*)}$ for the PF model are shown in a) and b), while the planes for the CT model is in d) and e). The three solution planes for set 1 are shown in a) (PF) and d) (CT), set 2 in b) (PF) and e) (CT). The bulk modulus plane is blue, shear modulus red and density green. c) and f) show the intersection curves where $(\phi, c, s)_{(K^* \wedge \rho^*)}$ (diamonds on stippled line) and $(\phi, c, s)_{(\mu^* \wedge \rho^*)}$ (solid line) give solutions for the PF and CT model, respectively. The solutions are given in the intersections, where $(\phi, c, s)_{(K^* \wedge \rho^*)} = (\phi, c, s)_{(\mu^* \wedge \rho^*)}$, and are marked with green stars.
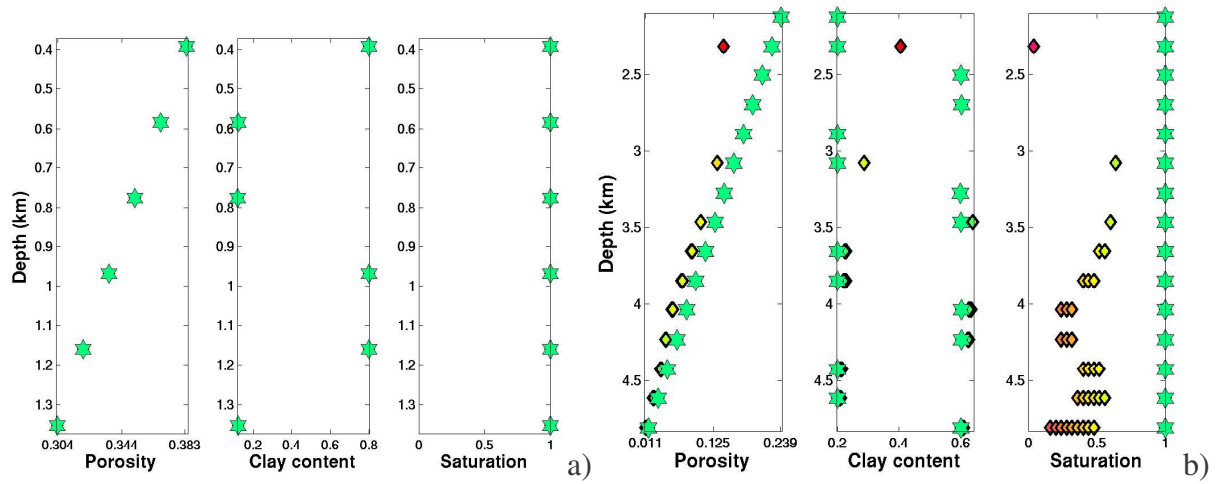
Figure 11. The inversion solutions from inverting the log in Figure 8, using the a) PF and b) CT model. All consistent solutions are shown, but the ones that agrees with the log values are shown in green. The colour moves from green via yellow to red when the deviation increases from 0 to 0.05, 0.10 and 1.0 for ϕ, c and s, respectively. Deviations that exceed these values are red.
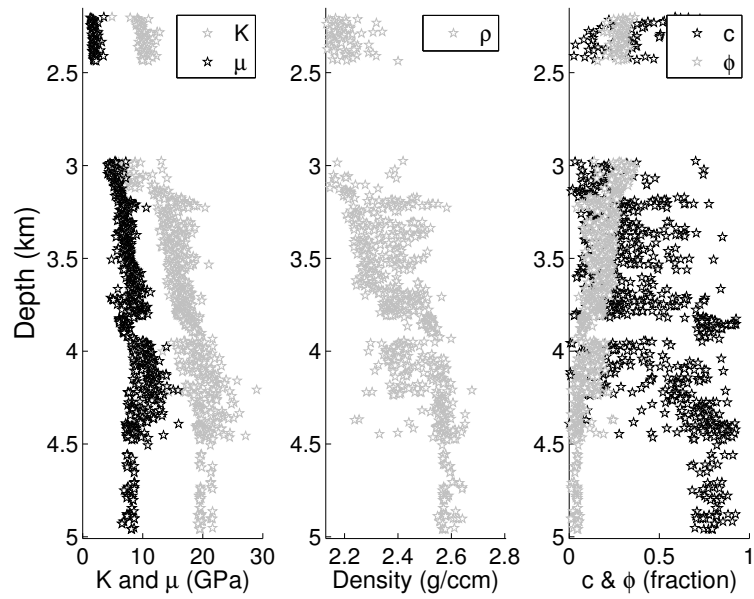
Figure 12. The log values used from well A. The fluid bulk modulus was approximately 2.5 GPa for all depths, which indicates water saturated rock.
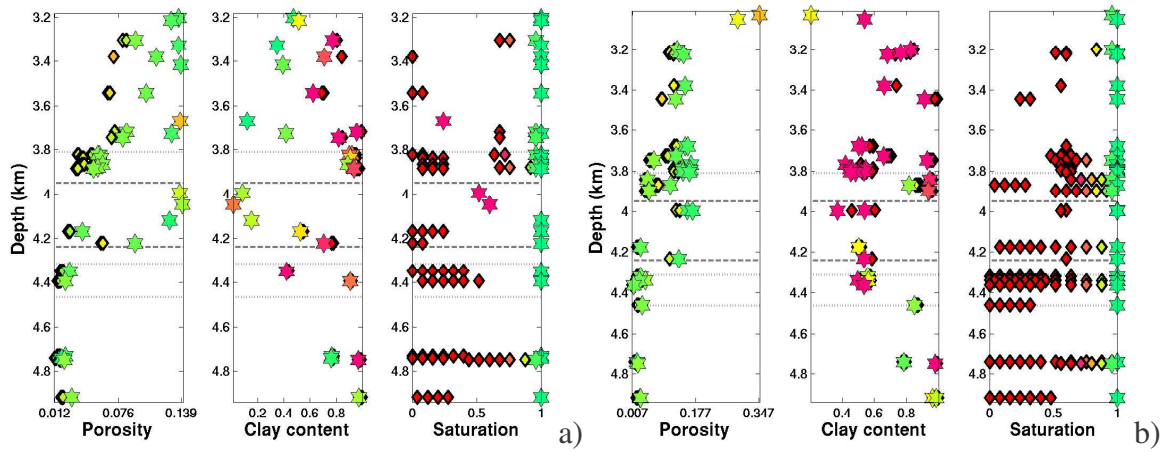
Figure 13. Inversion of well A from rock elasticity and density given by the well A log. The best set of solution parameters from each depth is plotted as a hexagon for the PF model in a) and the CT model in b). The colours indicate the precision of the solutions; green is consistent with well log, yellow is deviation of 5%, 10% and 15% for ϕ, c and s respectively, and red is for the doubled values and worse. The intervals between similar horizontal lines are sandstones and shaly sands, while the intervals between stippled and dotted lines are shales. The depths are not equal in both plots, since the PF model has solutions that lie shallower than the CT model.
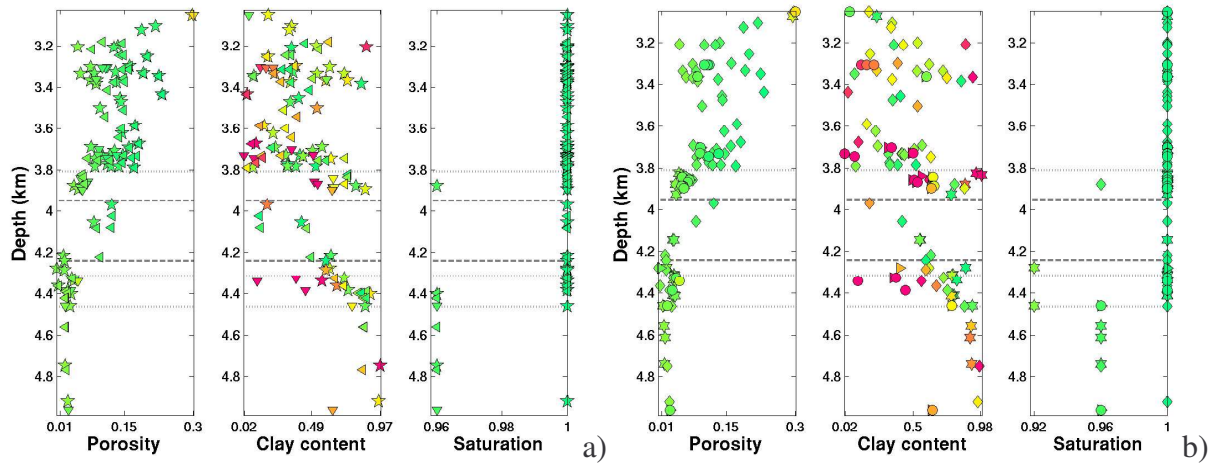
Figure 14. Inversion of parameters from the well A log The intervals between similar horizontal lines are primarily sandstones and shaly sands, while the intervals between stippled and dotted lines are shales. Seven different rock physics models are applied; each is represented by a unique marker. a): pentagon (CS2), down triangle (FW2), left triangle (GC2). b): hexagon (CS), diamond (CT2), right triangle (GC), circle (FW). The models in the parentheses are explained in the text. The colour code is similar to Figure 13.
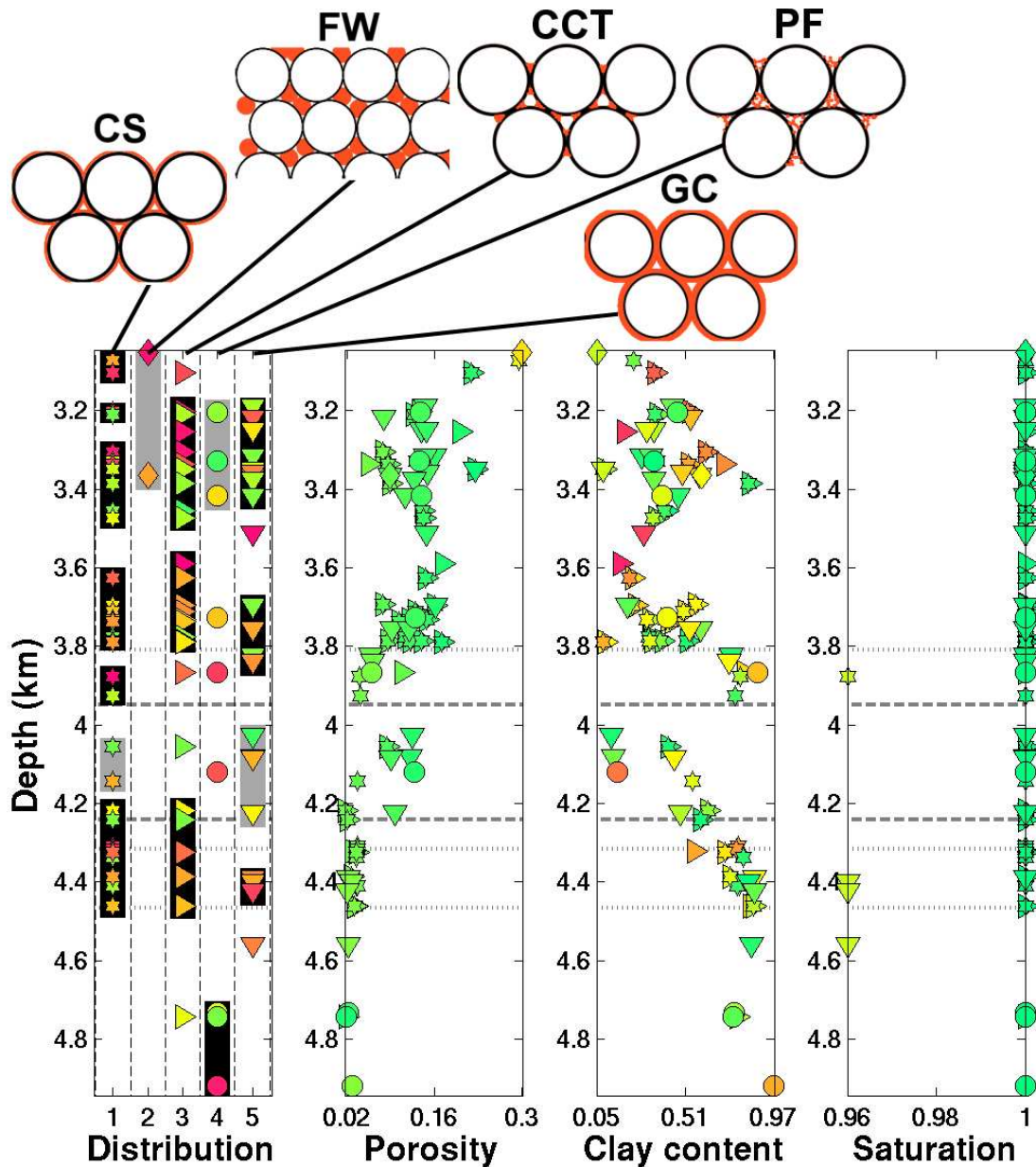
Figure 15. Comparison of the solutions and accuracy of the different models versus depth. The intervals between similar horizontal lines are primarily sandstones and shaly sands, while the intervals between stippled and dotted lines are shales. The black and grey background colour in the distribution plot, indicate log-depths where a distribution is likely to occur, and depths where the predictions are possible but more uncertain, respectively. No background colour (white), means that according to the models, the distribution is not expected at that depth. The distribution numbers in the plot are defined as follows: 1: CS, 2: FW, 3: CCT, 4: PF and 5: GC. The distributions include the 2-models as well, since the cement distribution is equal in e.g. the CT and CT2 model. The marker colours from green to red indicate the precision of the predictions. Perfect match is green, while 10 % deviation is red. In the distribution plot, the accumulated deviations from the other plots are indicated (sum of 10 % corresponds with red). Only solutions with 10 % or less accumulated deviation are included.
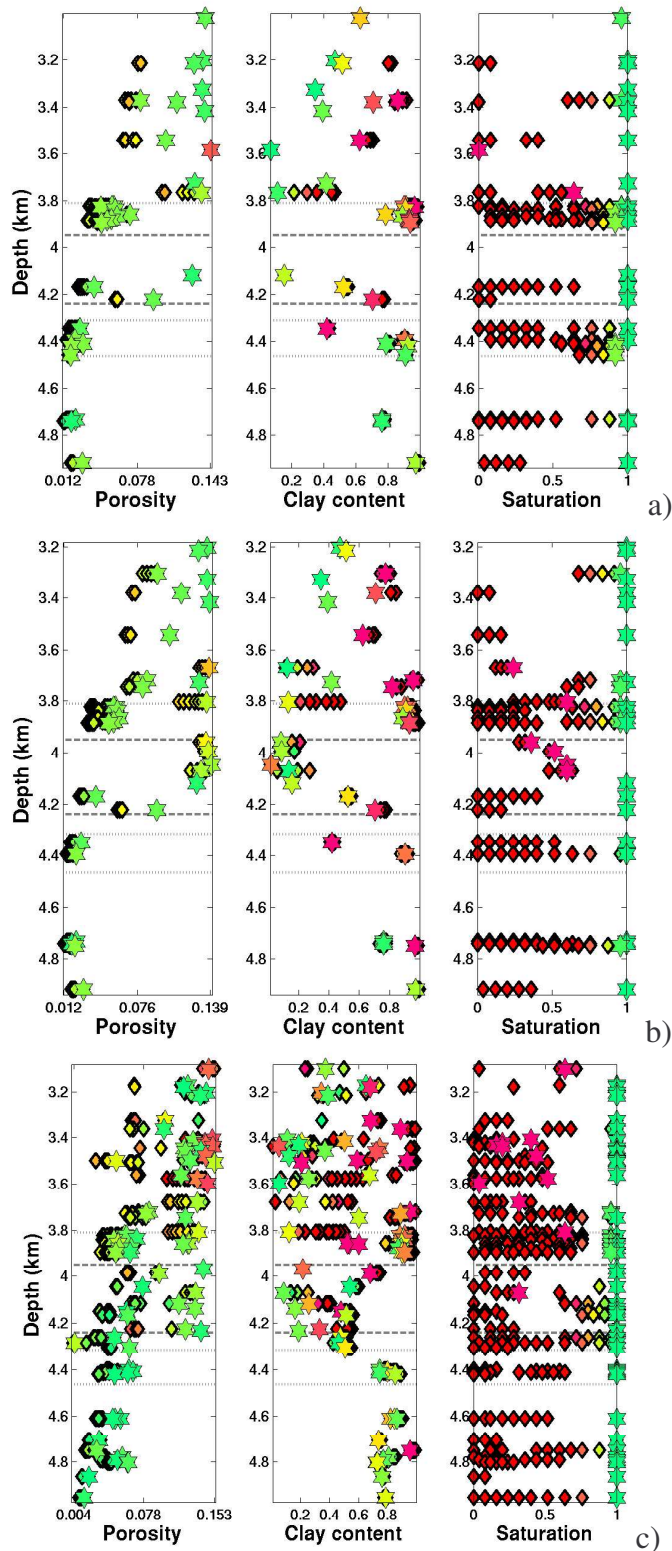
Figure 16. The plots correspond with the PF model in Figure 13, but now with an inflicted uncertainty of ± 2% in a) bulk modulus, b) shear modulus, and c) density. The colours indicate the precision of the solutions; green is consistent with well log, yellow is deviation of 5%, 10% and 15% for ϕ , c and s respectively, and red is for the doubled values and worse. The intervals between similar horizontal lines are sandstones and shaly sands, while the intervals between stippled and dotted lines are shales.

APPENDIX

Hertz-Mindlin – Hashin-Shtrikman (HMHS) model

The combined Hertz-Mindlin Hashin-Shtrikman model is applied for permeable rocks without contact cement. The formula for bulk and shear modulus are first estimated by the Hertz-Mindlin (HM) model as in Dvorkin and Nur (1996):

$$K_{HM} = \left[\frac{n^2(1-\phi_0)^2 \mu^2}{18\pi^2(1-v)^2} P \right]^{\frac{1}{3}}, \quad \mu_{HM} = \frac{5-4v}{5(2-v)} \left[\frac{3n^2(1-\phi_0)^2 \mu^2}{2\pi^2(1-v)^2} P \right]^{\frac{1}{3}},$$

where ϕ_0, n, μ and v denote critical porosity, number of grain contacts and shear modulus and Poisson's ratio of the framework grains respectively. These results are further combined with the Hashin-Shtrikman model, which yields (Dvorkin and Nur, 1996):

$$K_{HMHS} = \left[\frac{\phi/\phi_0}{K_{HM} + \frac{4}{3}\mu_{HM}} + \frac{1-\phi/\phi_0}{K_{HM} + \frac{4}{3}\mu_{HM}} \right]^{-1} - \frac{4}{3}\mu_{HM},$$

$$\mu_{HMHS} = \left[\frac{\phi/\phi_0}{\mu_{HM} + Z} + \frac{1-\phi/\phi_0}{\mu + Z} \right]^{-1} - Z\mu_{HM}.$$

ϕ is porosity, and Z is expressed by:

$$Z = \frac{\mu_{HM}}{6} \left(\frac{9K_{HM} + 8\mu_{HM}}{K_{HM} + 2\mu_{HM}} \right).$$

Differential effective medium model (DEM)

When pores get increasingly isolated, the Differential effective medium model is applied. This model treats inclusions as unconnected. For an isotropic rock, the coupled system of ordinary differential equations for the effective bulk and shear moduli can be written (Berrymann, 1992):

$$(1-y)\frac{d}{dy}[K_{eff}(y)] = (K_2 - K_{eff})P_{*2}(y)$$

$$(1-y)\frac{d}{dy}[\mu_{eff}(y)] = (\mu_2 - \mu_{eff})Q_{*2}(y) \quad,$$

with initial conditions $K_{eff}(0) = K_1$ and $\mu_{eff}(0) = \mu_1$, where 1 and 2 denote the initial host material and the inclusion material, respectively. y is concentration of phase 2. P and Q are tensors that depend on the elastic properties of the inclusion material and the background medium. The subscript $_{*2}$ indicates that the tensors are estimated for an inclusion material 2 in a background medium with effective moduli K_{eff} and μ_{eff}.

Self consistent approximation (SCA)

In this model the interactions of inclusions is approximated by replacing the background material with the as-yet-unknown effective medium. The SCA solution occurs when the net (scattering) effect of all the inclusions is zero. The term 'self-consistent' means that the results do not depend on a selection of host medium to embed the remaining constituents, but do only depend on their volume fraction. Berrymann (1995) gives a general form of the self-consistent approximation for N-phase composites:

$$\sum_{i=1}^{N} x_i (K_i - K_{SCA}^*) P_i = 0$$

$$\sum_{i=1}^{N} x_i (\mu_i - \mu_{SCA}^*) Q_i = 0,$$

where i refers to the i*th* material, x_i is its volume fraction, P and Q are tensors that depend on the elastic properties of the i*th* material and the background medium.

Contact cementation theory (CCT)

For permeable rocks with contact cement, the contact cement of Dvorkin et al. (1999) is applied. The expressions are written:

$$K_{CCT} = \frac{n(1-\phi_0)}{6}\left[\frac{4}{3}\mu_c + K_c\right]S_n \text{ and } \mu_{CCT} = \frac{3}{5}K_{cct} + \frac{3n(1-\phi_0)}{20}\mu_c S_\tau,$$

where S_n and S_τ are the normal and tangential stiffness of a two sphere combination, and is given in Dvorkin et al. (1999). If the moduli K_s and μ_s of the unknown matrix material were known, the self consistent approximation for spherical inclusions of void with concentration ϕ predicts that K_{cct} and μ_{cct} are given by the coupled equations:

$$\frac{1}{K_{CCT} + \frac{4}{3}\mu_{CCT}} = \frac{1-\phi}{K_S + \frac{4}{3}\mu_{CCT}} + \frac{\phi}{\frac{4}{3}\mu_{CCT}}$$

and

$$\frac{1}{\mu_{CCT} + Z} = \frac{1-\phi}{\mu_S + Z} + \frac{\phi}{Z},$$

where Z is the same as previously defined. The moduli K_{fill} and μ_{fill} of the matrix where all inclusions (of concentration ϕ) are filled with the cement can be found from the equations:

$$(1-\phi_0)(K_s - K_{fill})P_s + \phi(K_c - K_{fill})P_c = 0$$

$$(1-\phi_0)(\mu_s - K_{fill})Q_s + \phi(\mu_c - K_{fill})Q_c = 0,$$

where P_i and Q_i (i=s, c) are tensors that depend on the elastic properties of the host- (s) and inclusion (c) material respectively. Now the effective moduli (K_{eff} and μ_{eff}) of the rock with some inclusions filled with cement, and some empty can be calculated. If the concentration of

empty inclusions is ϕ_e the concentration of cemented inclusions is $\phi - \phi_e$ because the volumetric fraction of the matrix is still *1-ϕ*. K_{eff} and μ_{eff} are found from:

$$(1-\phi)(K_s - K_{eff})P_s + (\phi - \phi_e)(K_c - K_{eff})P_c - \phi_e K_{eff}P_0 = 0$$
$$(1-\phi)(\mu_s - \mu_{eff})Q_s + (\phi - \phi_e)(\mu_c - \mu_{eff})Q_c - \phi_e \mu_{eff}Q_0 = 0.$$

Bound averaging method (BAM)

The bound averaging method is used to estimate effective bulk and shear modulus in a rock with pore-filling materials with non-zero shear stiffness (Marion and Nur, 1991). The model requires the same input as the Gassmann (1951) model:

$$K_{sat} = K_{dry} \frac{\left(1 - \dfrac{K_{dry}}{K_m}A\right)}{\dfrac{\phi}{K_f} + \dfrac{(1-\phi)}{K_m}}$$

and

$$\mu_{sat} = \mu_{dry}.$$

The subscripts *sat, dry, m* and *f* denote the properties for the saturated rock, dry rock, framework material and fluid, respectively. If the ratio K_f / K_m is assumed to be much smaller than one (typically on the order of 0.05), an approximate value for A is given by $A_{vr} \approx 1 + \phi$, when A is calculated by using the Voigt-Reuss bounds.

Wood's formula for calculating fluid properties

In a fluid suspension or a mixture, where the heterogeneities are small compared with a wavelength, the effective bulk modulus (K_f) is given by the Wood (1955) relation:

$$\frac{1}{K_f} = \sum_{i=1}^{N} \frac{f_i}{K_i},$$

and effective density (ρ) becomes:

$$\rho = \sum_{i=1}^{N} f_i \rho_i ,$$

where f_i, K_i and ρ_i are the volume fractions, bulk moduli and densities of the different phases, respectively. The density estimation is independent of the aggregate condition of the constituents, hence this estimation is used to estimate the bulk density of the rock.

Weighting function when using Hill average

In this paper the Hill (1952) average is used to describe transitions from uncemented to cemented rock and from connected to isolated pores. The transition can be linear or non-

linear, dependent on the weight used. The chosen weight applied is composed of two parts $W^{(1)}$ and $W^{(2)}$. $W^{(1)}$ is estimated as follows:

$$W^{(1,1)} = \frac{0^2}{n^2}\left(m - \frac{1}{2n}\right)$$

$$W^{(1,2)} = \frac{1^2}{n^2}\left(m - \frac{1}{2n}\right)$$

...

$$W^{(1,n-1)} = \frac{(n-1)^2}{n^2}\left(m - \frac{1}{2n}\right)$$

$$W^{(1,n)} = \frac{n^2}{n^2}\left(m - \frac{1}{2n}\right)$$

where 2n is the length of the weight and m is the mean value of the weight (commonly 0.5). This expression can be rewritten to:

$$W_r^{(1)} = \frac{r^2(2mn-1)}{2n^3},$$

where r = 0,1,…, n-1, n. $W^{(2)}$ can now be written as:

$$W^{(2,1)} = 1 - W^{(1,n)}$$

$$W^{(2,2)} = 1 - W^{(1,n-1)}$$

...

$$W^{(2,n-1)} = 1 - W^{(1,2)}$$

$$W^{(2,n)} = 1 - W^{(1,1)}$$

which can be written:

$$W_r^{(2)} = 1 - \frac{(n+1-r)^2(2mn-1)}{2n^3}.$$

where r =n+1,n+2,…, 2n-1, 2n. The final weight then becomes $W = [W^{(1)}, W^{(2)}]$. The weight is shown in Figure 17. The shape of the weight reflects the assumption that the transitions are slowest near the terminal points (0 and 1). For the transition from uncemented to contact cemented rock (constant porosity) this implies that the very first contact cement (stage 1), only present in some of the contacts, can not contribute much to stiffen the whole rock. When all contacts approaches cemented however, the overall rock stiffness increases drastically (stage 2). But when the rock is pervasively contact cemented (stage 3), additional cementation does not contribute much to further stiffness increase, and the gradient of the weight decreases.
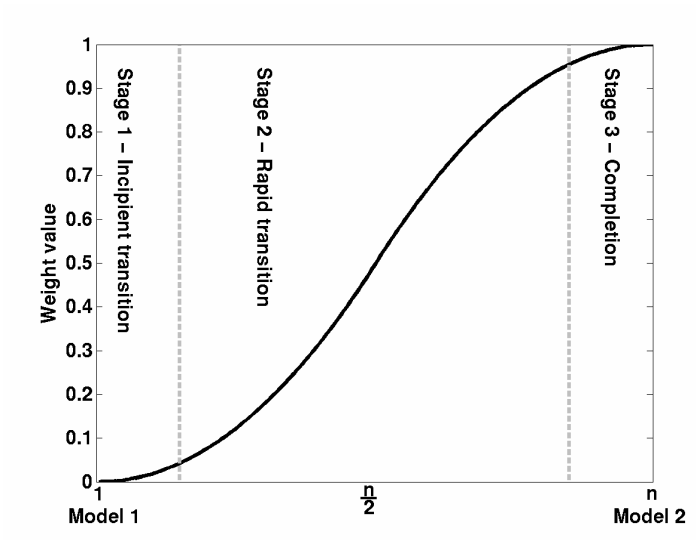
Figure 17. The non-linear symmetric weight of length n is applied in the transitions between different rock physics models. At the terminal points the transition speed is considered to be lower than in the stages between.

10 Summary and perspectives

The purpose of this thesis was to find ways of relating rock physics and seismic properties to geology and geological processes during diagenesis. The approach was to study mineralogical processes commonly found with increasing depth and temperature in siliciclastic rocks. Because rock rigidity is dependent on how the constituents are arranged, a distribution classification for minerals involved in the modelling was suggested. Distribution changes during diagenesis could then be incorporated in the modelling.

There are large differences in the rock physics of shales and sandstones at deposition, and during diagenesis. Therefore one strategy for shale diagenesis (paper 1) and one for sandstone diagenesis (paper 2) were developed. In the border area between shaly sands and silty shales (45%<quartz<55%), the models were combined (paper 3). Paper 3 discussed how diagenesis caused variations in the velocity depth trends for various successions of mineralogical reactions, which were coupled to depositional environments. By inverting the rock physics models of paper 2, the rock micro structure (mineral distribution) can be revealed, in addition to porosity, lithology and fluid parameters. This was shown in paper 4, together with an evaluation of how uncertainties in seismic parameters can influence the inversion results.

The predictions of the shale model in paper 1 showed good correlations with well log velocities. Evaluation of the models of paper 2 and 3 against real data with known mineralogy remains to be performed, except for some comparison with dry core-plugs shown in Appendix F.

The sandstone modelling performed required a very comprehensive rock physics model, to account for variations of simultaneous distributions, increasingly isolation of pores, pore-bridging and porosity variations from deposition to deep burial. The solution to the problem was to combine rock physics models that have validity only for certain rock conditions, like uncemented rocks, contact cemented rocks or rocks with graincoating contact cement. In cases with simultaneous cement distributions, the Hill average was applied between rock physics models for the different distributions, without any scientific evidence of validity. Further, the expected stiffness-increase in rocks with incipient isolation of pores is modelled as transitions from one rock physics model to another. Hence, the validity areas and assumptions of the applied models are changed. An optimal use of the modelling strategy for sandstones would be if there existed one single "unified rock physics model" that accounted for all diagenetic effects, instead of mixing various models with varying validities. To the author's knowledge, such a model does not currently exist.

Another potential for improvements in further studies, is the quality of geological input. The modelling presented is a product of both geological and geophysical efforts. A combined geological/geophysical diagenesis study, where the mineralogy is thoroughly examined, could be a good way of evaluating the geophysical models. After testing the models, the validity areas and need for calibration from area to area can be discussed.

Errata for "Impact of diagenesis on seismic properties of siliciclastic rocks"

Changes from the first delivery to the final print are listed below:

- Content list, page 2, line 23: The page number is changed to 162, due to modifications of the appendix of paper 4.
- Content list, page 2, line 24: The errata is included in the content list.
- Chapter 4, page 13, line 8: The reference is corrected to "Dvorkin and Nur (1993)."
- Chapter 4, page 15, line 9: The "**?**)" is replaced with "Hill (1952)".
- Chapter 4, page 15, line 16: The words "shale concentration" are replaced with "clay mineral concentration".
- References, page 48, line 10: The authors are corrected to "Dvorkin, J. and Nur, A."
- Paper 2, page 66, line 2, column 1 and line 1-2, column 2: The sentence in column 1 should sound: "They did not model contact cement explicitly, nor did they study the effects of more than one distribution of clay at the same time, like structural and dispersed." The two upper lines in column 2 are hence moved to column 1.
- Paper 2, page 68, column 2, lines 19-20 and paper 3, page 103, column 1, line 35: Bound Averaging Method is the correct name on the theories of Marion and Nur (1991).
- Paper 2, page 74, column 2, line 46: Unintended line break from document formatting is removed. This is also the case in page 76, column 1, line 33, and page 76, column 2, line 10.
- Paper 2, page 79, column 1 and Paper 3, page 112, column 1: The reference McKinley et al. (1999) is wrong, and is corrected to:
  McKinley, J. M., Worden, R. H. and Ruffel, A. H. 2003. Smectite in sandstones: a review of the controls on occurrence and behaviour during diagenesis. *In*: Worden, R. H. & Morad, S. (eds), *Clay Mineral Cements in Sandstones*, International Association of Sedimentologists, Special Publication, **34**, Blackwell Publishing, Oxford, 109-128.
- Paper 2, page 97, column 2, line 5: The equation has been altered. Every single number in the weight should be squared instead of the whole weight. The notation is also altered, and the equation is rewritten in a simpler form.
- Paper 2, page 97, column 2, line 7: The equation is not correct, and is rewritten with new notation.
- Paper 2, page 98, figure 12: The figure is modified, the text "Model 2" is shifted to the right to avoid confusion, and the length of the weight is included on the x-axis. Changes on page 97-98 is also performed in paper 4, page 160.
- Paper 3, page 109, column 1, line 23: The word "derivate" is replaced with "derivative".
- Paper 4, page 133, column 1, equation 1: Correct upper equation is: "$K=\rho(V_p^2-4\ V_s^2/3)$"
- Paper 4, page 159, line 23: The words "if the constituents are solid, fluid or gas" are replaced with "the aggregate condition of the constituents".